Stony Brook University

SUBMARINE GROUNDWATER DISCHARGE (SGD) AND DISSOLVED TRACE METAL CYCLING IN THE SUBTERRANEAN ESTUARY AND COASTAL OCEAN

A Dissertation Presented

by

Aaron Joseph Beck

to

The Graduate School

in Partial fulfillment of the

Requirements

for the degree of

Doctor of Philosophy

in

Marine and Atmospheric Science

Stony Brook University

May 2007

Stony Brook University

The Graduate School

Aaron Joseph Beck

We, the dissertation committee for the above candidate for the

Doctor of Philosophy degree, hereby recommend

acceptance of this dissertation.

J. Kirk Cochran - Dissertation Co-advisor
Professor, Marine Sciences Research Center, Stony Brook University

Sergio A. Sañudo-Wilhelmy - Dissertation Co-advisor
Associate Professor, Marine Sciences Research Center, Stony Brook University

Henry J. Bokuniewicz - Chairperson of Defense
Professor, Marine Sciences Research Center, Stony Brook University

Gilbert N. Hanson, Distinguished Service Professor
Department of Geosciences, Stony Brook University

Matthew A. Charette, Associate Scientist
Department of Marine Chemistry and Geochemistry,
Woods Hole Oceanographic Institution

This dissertation is accepted by the Graduate School

Lawrence Martin
Dean of the Graduate School

Abstract of the Dissertation

Submarine groundwater discharge (SGD) and dissolved trace metal cycling in the subterranean estuary and coastal ocean

by

Aaron Joseph Beck

Doctor of Philosophy

in

Marine and Atmospheric Science

Stony Brook University

2007

During the past quarter century, submarine groundwater discharge (SGD) has gained increasing recognition as a major contributor to chemical budgets in the coastal ocean. Advection of groundwater through permeable sediments is now accepted to be large and generally ubiquitous in the coastal marine environment. Rapid organic matter remineralization couples with high fluid exchange rates in these sediments to make them very active zones of geochemical cycling. However, little is known about the distribution and speciation of trace metals in the subsurface mixing zone of fresh and saline groundwaters, and how geochemical cycling in permeable sediment porewater affects trace metal fluxes via SGD. The purpose of this dissertation is to examine these two issues. In two Long Island, NY, estuaries – Jamaica Bay and Great South Bay – mass balance calculations for the suite of Ra isotopes indicated an SGD flux for each

embayment of 1 to 10 billions of liters per day. A seasonal trend in Ra-derived SGD estimates was reflected in dissolved Mo levels in the water column, as increased recirculation of seawater through permeable sediments apparently resulted in Mo removal. Conversely, positive correlation between ^{223}Ra and dissolved Fe, Co, Zn, and Ni in bottom waters indicated that SGD was a source of these metals to the Jamaica Bay water column. In Great South Bay, the spatial distribution of Ra matched previous reports of regions enriched with dissolved trace metals. Shallow, high-resolution depth profiles were collected in Great South Bay permeable sediments to examine dissolved metal cycling and speciation in the subterranean estuary. Geochemical cycling of trace metals in shallow porewater resulted in order-of-magnitude enrichments over surface waters. A major portion of the total dissolved pool for many metals comprised kinetically-labile species. Although metal-oxide cycling at the sediment-water interface probably prevents release of most metals from the sediments, evidence for preferential conduits of vertical flow may allow substantial dissolved metal transport by SGD. Thus, SGD can represent a significant source or sink for different trace metals in coastal waters, and geochemical cycling in surficial porewater and the subterranean estuary is vastly important in determining the trace metal composition of submarine groundwater.

To my parents, Michael J. Beck and Alma T. Beck,
for teaching me to love the natural world and to play science;
and for, with your unfailing love and support, giving my dreams freedom
to go wherever those fickle winds direct.

TABLE OF CONTENTS

TABLE OF CONTENTS – Continued

TABLE OF CONTENTS – Continued

TABLE OF CONTENTS – Continued

TABLE OF CONTENTS – Continued

LIST OF TABLES

LIST OF FIGURES

LIST OF FIGURES -- Continued

LIST OF FIGURES -- Continued

Acknowledgements

My first and most heartfelt thanks go to my co-advisors, Drs. J. Kirk Cochran and Sergio A. Sañudo-Wilhelmy. During my time at MSRC, I was given constant opportunities to travel and expand my scientific knowledge; I was always well-supported financially; and the turbulence of my entering the academic world was constantly smoothed and made easier by the generous attention and genuine friendship of both my advisors. I was generally allowed to explore my research with autonomy, but Kirk and Sergio were always ready with encouragement, criticism, and advice; without their patient and careful guidance, I would not have had such an enjoyable graduate career, nor would I have been able to produce what is in the Reader's hands now. For Kirk and Sergio I have overwhelming gratitude that extends far beyond the achievement of an academic degree; were that debt and appreciation written in full, it would extend farther than the pages of this dissertation.

Similar acknowledgement is due Dr. Henry J. Bokuniewicz. Nominally only a dissertation committee member, Henry was in fact the hidden member of my tripartite group of advisors. Through funding and travel opportunities, endless scientific writing instruction, and lively data discussions, I am indebted to Henry for making my time at MSRC happier, more productive, and more educational.

I also greatly appreciate the contributions of my committee members, Drs. Gil N. Hanson and Matt A. Charette. They generously gave time, energy, and insight throughout a number of exams, as well as the reading of this dissertation; this final work was much improved by their careful scrutiny and suggestions.

I am endlessly grateful to fellow student John "Stegosaurus" Rapaglia for more than can be described here. He participated in every field campaign described in this dissertation, and most of the samples would never have been born without his tireless dedication to hard work in the worst of conditions. Better, his voracious devotion to enjoying life followed our work around the world, and adventure and excitement permeated to the very core of everything we did together.

Many staff members at MSRC deserve thanks for their help, and my interactions with a few warrant particular mention:

Few, if any, of the data in this dissertation were unaffected by the influence of David Hirschberg. A magician with capricious laboratory equipment, and a critical and demanding analytical chemist, David taught me to examine my research and techniques at the most fundamental level. His patient instruction and friendship made my labwork more pleasurable, and has made me a more capable and thorough scientist.

There is endless scaffolding and machinery hidden beneath my time at MSRC, and it's smooth and pleasant function was almost entirely due to the expert assistance of Eileen Goldsmith. More simply, and probably more importantly, although Stony Brook is often cold, Eileen made it warm and joyful in any season.

Cliff Jones ingenuously and effortlessly solved innumerable small and constant worries that would have otherwise been agonizing impediments to my

progress. His kindness, willingness to help on short notice, and friendship played no small part in my finishing this work painlessly and happily.

I am grateful for the assistance of Bob Slavonik, who was critical to producing many of the sampling devices that provided the data in this dissertation. He is an artist with machining tools, and was a very able and willing teacher as I fumbled my way though making my equipment.

Finally, there are endless others who have contributed to making my time at MSRC the most happy and intellectually satisfying years of my life. Too innumerable to list in full, I am profoundly grateful to many MSRC faculty and staff, and to my fellow students.

I probably stole more than a fair share of time from several professors who willingly and generously contributed to my academic growth; in particular, these include Drs. R. Aller, C. Lee, M. Scranton, N. Fisher, B. Brownawell, R. Wilson, C. Gobler, and A. Dove.

I am unable to describe the appreciation I have for friends who have elevated ideas and beers alike over the past four years, especially: Dane, Mark S., Michael F., Lora, Owen, Travis and Katie, and Mark B.

Lastly, it is too easy to become overwhelmed and suffocated by four years of such intense work; much of my survival is owed to Caterina Panzeca, who always strove to keep my head close to reality. I am grateful for her love, support, and friendship, and for great times from the Atlantic to the Pacific.

CHAPTER I:

Introduction and a brief background

Submarine Groundwater Discharge

An increasing volume of literature published during the past quarter century reflects increasing awareness of the ecological and geochemical significance of direct groundwater discharge to the ocean. The novelty of the subject matter derives in part from the difficulty in observing and quantifying the discharge, both of which are becoming simpler with the development of new tracer and direct measurement techniques. However, much of the recent understanding has begun simply by defining the phenomenon that is desired to study. Submarine groundwater discharge (SGD) has been defined by Burnett et al. (2003, p. 6) as "as any and all flow of water on continental margins from the seabed to the coastal ocean, regardless of fluid composition or driving force. We thus define SGD without regard to its composition (e.g., salinity), origin, or phenomena driving the flow." Fundamentally, this is a broad and nebulous definition. In terms of chemical composition, it is not difficult to appreciate that SGD should include both fresh, meteoric groundwater discharge, as well as saline fluids in submarine surficial aquifers. However, mechanisms of flow span enormous scales of space and time.

From large- to fine-scale, examples of SGD include massive (though perhaps rare) submarine springs (Zektzer et al., 1973), meteoric groundwater flow driven by a terrestrial hydraulic gradient (Zektzer et al., 1973; Freeze and Cherry, 1979; Lewis, 1987; Oberdorfer et al., 1990; Buddemeier, 1996; Younger, 1996; Cambareri and Eichner, 1998; Portnoy et al., 1998; Alley et al., 2002; Michael et al., 2005), tidal pumping

(Nielsen, 1990; Church, 1996; Li et al., 1999; Michael et al., 2003; Martin et al., 2004; Robinson et al., 2006; Billerbeck et al., 2006), wave setup and pumping/stirring (Riedl et al., 1972; Li et al., 1999; Haberstroh and Sansone, 1999; Falter and Sansone, 2000; Martin et al., 2004; Robinson et al., 2006; Billerbeck et al., 2006), pressure gradients resulting from flow over rough sediment surfaces (Huettel and Gust, 1992; Shum, 1992, 1993; Shum and Sundby, 1996; Huettel et al., 1998; Huettel et al., 2003; Riemers et al., 2004), salt fingering (Seplow, 1991; Bokuniewicz et al., 2004), and bioirrigation (Emerson et al., 1984; Boudreau and Marinelli, 1994; Aller, 2001; Martin et al., 2004; D'Andrea et al., 2004; Waldbusser and Marinelli, 2006). Figure I-1 shows a cartoon of these different mechanisms of flow. These processes are alike in that they all identify processes of porewater advection, but they are fundamentally different in terms of how temporal and spatial scales affect their chemical composition.

Both seepage meters (Lee, 1977; Bokuniewicz, 1980; Michael et al., 2003), and tracer techniques (Cable et al., 1996; Moore, 1996; Cai and Wang, 1998; Bugna et al., 1996; Kim and Hwang, 2002; Kim et al., 2005; Charette et al., 2003) estimate the average advection represented by these various processes, but each has limitations which will tend to under- or over-estimate different contributions to the total flux. For example, seepage meters may be too small to capture flow from submarine springs (e.g. Bokuniewicz et al., submitted) or too large to observe discharge due to salt fingering and bioirrigation. Tracer techniques can capture flow from springs, but may not account for the rapid flushing and recirculation due to water flow over rough sediment surfaces. Consequently, there is a need for examining advective processes on both grand (Moore, 1996) and fine (Huettel et al., 1998) scales.

If the general difficulty in defining and measuring SGD can be momentarily overlooked, there is a substantial body of literature showing that advective porewater flow is a major geophysical process occurring in coastal zones (e.g. Bokuniewicz, 1980; Moore, 1996; Huettel et al., 1998; Martin et al., 2004). Fresh SGD is generally shown to be about 10% of the total SGD (Li et al., 1999), and is often not insignificant in coastal water budgets (Church, 1996; Cambareri and Eichner; 1998; Alley et al., 2002). However, both saline and fresh SGD have unique and very important chemical signatures. Advective transport of porewater, irrespective of salinity, is enormously important for the transport of dissolved chemical constituents such as nutrients (Oberdorfer et al., 1990; Haberstroh and Sansone, 1999; Billerbeck et al., 2006), non-metal trace elements (Bugna et al., 1996; Shaw et al., 1998; Charette and Sholkovitz, 2006), and trace metals (Windom and Niencheski, 2003; Charette and Sholkovitz, 2006; Windom et al., 2006; Bone et al., 2006, submitted; Laurier et al., 2006; Beck et al., 2007).

Biogeochemistry of permeable sediments

One of the main reasons that advective chemical input to the coastal ocean has been overlooked (Boudreau et al., 2001) is the fact that permeable sediments typically have very low organic matter (<0.1%; Bergamaschi et al., 1997; D'Andrea et al., 2002; Rusch et al., 2003; Riemers et al., 2004; Charette et al., 2005; Billerbeck et al., 2006). Thus, the apparently low inventory of available reductant implies a low reactivity of sandy sediments. However, measurements of oxygen consumption (as analogy for organic matter decomposition) in organic-poor permeable sediments show similar rates to organic-rich sedimentary environments (Rowe et al., 1988; Grant et al., 1991; Archer and

Devol, 1992; Devol and Christensen, 1993; de Beer et al., 2005). The review of Shum and Sundby (1996) shows clearly that organic matter cycling in permeable sediments is in fact a major process, primarily because porewater recirculation delivers both organic matter and oxygen to bacteria-laden sediments (Rusch et al., 2001). Organic matter cycling in permeable sediments is summarized eloquently by Huettel et al. (2003, p. 235): "A low content of reactive materials in such beds, thus, cannot be interpreted as low metabolic activity but rather is the consequence of rapid turnover and high exchange rates."

The implications for SGD-derived chemical flux are clear: substantial organic matter decomposition and accelerated diagenetic cycling (Shaw, 2001) will likely have a profound effect on dissolved chemical constituents in the porewaters (Shaw et al., 1990; Froelich et al., 1979). Indeed, studies of nutrient input due to SGD have shown that advective transport can be responsible for major fluxes of nitrogen species (Lewis, 1987; Portnoy et al., 1998; Charette et al., 2001; Crusius et al., 2005), phosphate (Zimmermann et al., 1985), and silicate (Kim et al., 2005), or all of these together (Kelly and Moran, 2002; Crotwell and Moore, 2003; Jahnke et al., 2003; Ullman et al., 2003; Charette and Buessler, 2004; Slomp and Van Cappellen, 2004; Hwang et al., 2005). In fact, SGD-associated input of nutrients has been argued to be vital for the sustenance of primary production in coral reefs, estuaries, and other shelf communities (Johannes, 1980; D'Elia et al., 1981; Johannes and Hearn, 1985; Bussmann et al., 1999; Krest et al., 2000), although such observations are not ubiquitous (Rutkowski et al., 1999).

Estimating chemical fluxes due to SGD

However, estimating SGD-derived nutrient input (as is often done) by assuming that nutrient concentrations measured in groundwater are representative of the fluid actually crossing the sediment-water interface may not be accurate. Nutrient enrichment due to organic matter remineralization in surface sediments may increase the flux (Rusch et al., 2000; Jahnke et al., 2003), while removal through processes such as sorption and denitrification will decrease the flux (Capone and Slater, 1990; Talbot et al., 2003; Addy et al., 2005). Certainly, processes occurring in the subsurface environment regulate the ultimate nutrient ratios in the discharging porewater and may thus cause differential nutrient limitation (Paerl, 1997; Valiela et al., 1990; Slomp and Van Cappellen, 2004) and affect primary production differently (LaRoche et al., 1997; Gobler and Sañudo-Wilhelmy, 2001; Gobler and Boneillo, 2003).

Our understanding of trace element transport by porewater advection is far less well-understood. Discharge of trace constituents is implicit in the use of such geochemical tracers as Ra isotopes to estimate SGD volume flux (e.g. Moore, 1996, 1999), and Zektzer et al. (1973) even argued for the utility of dissolved Mn and Fe as tracers of SGD. Some previous estimates of metal discharge due to SGD have relied on the same tenuous procedure as that mentioned for estimation of nutrient flux (e.g. Moore, 1997; Shaw et al., 1998; Montlucon and Sañudo-Wilhelmy, 2001; Basu et al., 2001; Charette and Buesseler, 2004). Some recent studies have improved on this method by calculating an effective SGD endmember based on the element behavior with respect to salinity in the subterranean estuary (Charette and Sholkovitz, 2006; Beck et al., 2007; Bone et al., in press). Alternatively, the best approach may be the direct observation of

SGD-derived metals in the actual water column (Windom et al., 2006; Laurier et al., 2006).

[There is a large body of work published by M. Huettel and co-workers examining trace metal transport by topography-induced flow at the surface of permeable sediments. Considering the earlier discussion of the definition of SGD, their work should probably be included in this section; inasmuch as most studies of SGD have focused on greater sediment depths, and because the subterranean estuary is probably not subject to the flow-forcing mechanisms examined by the Huettel group, their very sophisticated and elegant work has been omitted from this section.]

Fresh vs. saline groundwater, and the subterranean estuary

One of the major gaps in our understanding of SGD chemical flux, as noted by Lewis (1987), is due to the black box represented by the sub-surface, fresh-saline mixing zone, the so-called "subterranean estuary" (Moore, 1999). Classical estimates of SGD chemical flux have been calculated by measuring constituent concentrations in monitoring wells or other inland groundwater sources, and assuming that material flux is simply the product of water flux and chemical concentration (Oberdorfer et al., 1990; Charette et al., 2001; Montlucon and Sañudo-Wilhelmy, 2001). Moore (1996) found that such a perspective could not account for the observed Ra enrichment off the South Carolina coast, and instead required an input of brackish, chemically-modified and enriched porewater. Subsequent studies of groundwater flux to the ocean have begun incorporating saline porewater considerations into estimates of chemical transport (Shaw et al., 1998; Charette and Buesseler, 2004).

The subterranean estuary is defined simply as the mixing zone of fresh, terrestrial, meteoric groundwater and interstitial seawater in permeable sediments (Moore, 1999; Burnett et al., 2003). Schematic representations of the meeting of fresh and saline water in coastal aquifers tend to be restricted to the stable situation of a saline wedge underlying a fresh wedge (e.g. Burnett et al., 2006; see also Burnett et al., 2003, for a detailed discussion). This theoretical interface is consistent with the observations of Charette and Sholkovitz (2006) and the example of Appelo and Willemsen (1987). However, it may be argued that there are in fact a minimum of two subterranean estuaries at any given coastal site: (1) a deep mixing zone along the interface of the salt wedge (as shown by Burnett et al., 2006), and (2) a shallow mixing zone that exists due to mixing and dispersion processes occurring at the sediment-water interface (Fig. I-2). This situation has been shown by Magaritz and Luzier (1985), although their surface mixing zone extends to a depth of 10-20 m. Robinson et al. (2006) show a surficial mixing zone on the order of 2-6 m, and although their profiles do not extend deeper, their model shows a suggestion of a deeper mixing zone as well. Charette and Sholkovitz (2006) sampled a series of high resolution profiles thorough the deep mixing zone (2-8 m, in Waquoit Bay, MA). They also observed a reverse salinity gradient at the surface of several profiles, but attributed it to "transient features which result from tidally-pumped seawater into the upper ~1 m of the sediment column during high tides" (Charette and Sholkovitz, 2006, p. 819). It is possible that this surface mixing zone is not, in fact, a transient feature, but is instead a dynamically stable and necessary situation arising from upward flux of meteoric groundwater and downward dispersion of saltwater.

Bokuniewicz (1992) and Bokuniewicz et al. (2004) have shown that salt fingering and wave-driven dispersion can account for the observed saltwater intrusion.

The thickness of the mixing zone will thus be set by the rate of freshwater advection versus the strength of the dispersive processes. Certainly, a mixing zone must exist wherever fresh groundwater discharges to coastal waters. In some rare cases, such as springs or so-called "wonky holes," fresh discharge sufficiently overwhelms dispersive processes such that the mixing zone is actually in the overlying water column (e.g. Stieglitz, 2005). Where discharge rates are lower, salt penetration into the surface sediments is to be expected, and has been documented (Capone and Bautista, 1985; Seplow, 1991; Bokuniewicz et al., 2004; Burnett et al., 2006; Robinson et al., 2006). It is worth noting that we have observed salt intrusion to tens of centimeters, even in the face of SGD rates exceeding 200 cm d^{-1}, and the salinity of the discharging water appears to be brackish (Chapter V). This suggests that the dispersion processes are quite strong.

Support for the stability of this "inverse estuary" is implied by the repeated observation of the gradient at the Roe Avenue site in Great South Bay, NY (the geochemistry of this site is described in detail in Chapter VI of this dissertation). The inverse estuary feature of this site has been observed for approximately 27 years (Zeitlin, 1980; Capone and Bautista, 1985; Seplow, 1991; Bokuniewicz et al., 2004; personal observation, 2005, and Chapter VI).

The geochemical significance of this mixing zone is arguably greater than that of the deep mixing zone. The geochemical signature of the discharging water will be established during transport of groundwater through the mixing zone at the interface, regardless of the transformations occurring at depth. The existence of preferential

flowpaths is something of a confounding factor, but is unlikely to promote flow of deep water that entirely bypasses the surficial mixing zone. Consequently, this dissertation will focus on the geochemistry of the upper 1-4 m of permeable sediments.

Sampling the subterranean estuary

In any case, SGD chemical flux studies generally collect an extensive set of porewater samples, attribute variability in chemical concentrations to natural heterogeneity, and estimate the SGD-associated flux using a statistical average concentration. Certainly, this is not the best approach, as it blurs fine-scale processes and modifications; several groups have recently developed instruments for sampling high-resolution porewater profiles in coarse-grained, permeable sediments. Most notably, these include multi-level spear samplers used in coral reef sediments (Falter and Sansone, 2000) and carbonate sands (Martin et al., 2003), and shielded-screen drive-point piezometers used in glacial sediments of the US northeast and sands overlying fractured rock aquifers in Brazil (Charette and Allen, 2006; Charette and Sholkovitz, 2006).

With these new sampling techniques, researchers have begun to examine in greater detail the geochemical distribution and cycling of trace elements in the subterranean estuary. Initial work has addressed Fe and Mn (Testa et al., 2002; Windom and Niencheski, 2003; Snyder et al., 2004; Charette and Sholkovitz, 2002, 2006; Spitieri et al., 2006; Windom et al., 2006), U (Duncan and Shaw, 2003; Charette and Sholkovitz, 2006), Mo (Windom and Niencheski, 2003), Sr (Charette and Sholkovitz, 2006), As (Bone et al., 2006), Hg (Bone et al., in press), and rare earth elements (REE, Duncan and Shaw, 2003). Numerous processes have been identified as important factors regulating

trace element distributions, particularly, redox conditions, pH, adsorption and desorption reactions, and precipitation and dissolution of solid phases. There is complex interplay between different chemical components in the sediment porewater, illustrated especially by the redox and sorption behaviors of Fe and Mn. Thus, the numerous and variable geochemistries of different trace metals will result in unique patterns of speciation, mobility, and reactivity. Examination of a suite of trace metals will provide insight into the important cycling mechanisms, and should allow improved predictions about the advective transport and discharge of different metals into the coastal ocean.

Objectives of this dissertation

Therefore, the purpose of this dissertation is three-fold: First, it seeks to examine the absolute magnitude of SGD water flux in two contrasting New York estuaries, Jamaica Bay and Great South Bay. These locations are chosen for the very different settings and surrounding land use characteristics, which should be reflected in trace metal levels and cycling (Montlucon and Sañudo-Wilhelmy, 2001; Romkens and Salomons, 1998). Jamaica Bay is a highly urbanized estuary surrounded by the high density development of New York City; the bay is a unique estuary in that the measurable freshwater dilution is due almost entirely to wastewater discharge. Little or no published information is available on SGD or trace metals in Jamaica Bay. Considering the very substantial anthropogenic modifications and probable pollution issues, Jamaica Bay is an ideal site to study the influence of human activities on metals in permeable sediments and in the estuary water column. Great South Bay is a relatively pristine embayment on the south shore of Long Island. Reports of SGD estimated using hydrologic balance or direct

point measurements are available as early as 1973 (Zektzer et al., 1973; Bokuniewicz, 1980; Bokuniewicz and Zeitlin, 1980; Bokuniewicz and Pavlik, 1990; Seplow, 1991; Bokuniewicz et al., 2004). Information on dissolved trace metals in the water column has been reported recently by Clark et al. (2006). More detailed descriptions of these study areas will be given in Chapters II and III of this dissertation.

Budgets for the four Ra isotopes will be constructed for Jamaica Bay (Ch. II) and Great South Bay (Ch. III), and the flux-by-difference approach will be used to estimate the volume flux associated with SGD (Charette et al., submitted). The mass balance approach should eliminate uncertainty introduced in the commonly used residence time approach (e.g. Kelly and Moran, 2002), and will give insight into the possible input pathways of some trace metals.

The second objective of this dissertation is to examine the importance of SGD to trace metal inputs to coastal estuaries. The distribution of dissolved trace metals in the Jamaica Bay water column will be studied, with special attention to patterns that can be explained by SGD. Here, prior knowledge of Ra cycling and distribution in the bay will provide useful information and serve as a guide for understanding the trace metal patterns. Dissolved metal concentrations in shallow (< 4 m) groundwater will also be examined. While porewater at these shallow depths in Jamaica Bay sediments never is completely fresh, metal distributions will be examined in the limited available portion of the subterranean estuary.

Finally, the last objective is to characterize the distribution and speciation of trace metals in the subterranean estuary. Because fresh water apparently lies so deep in the Jamaica Bay sediments, focus will be turned to Great South Bay. Initial efforts in August

2005 to sample the subterranean estuary in Great South Bay were confounded by the shallowness of the mixing zone; completely fresh water was found by only 1 m depth, and the Retract-a-Tip sampling device (Charette and Allen, 2006) used in Jamaica Bay (described in Ch. IV) was not precise enough to obtain the high resolution desired. Furthermore, we sought to avoid using this device because of the potential contamination due to its metal construction. Consequently, a high-resolution, trace metal clean device (the Multi-Port Piezometer, or MPP) was devised for sampling porewaters of the subterranean estuary in the upper 1 m of Great South Bay sediments. The MPP is described, tested, and its use validated in Chapter V of this dissertation. Then, Chapter VI will discuss trace metal and speciation profiles collected in GSB. These profiles will include Fe, Mn, Cu, Co, Pb, Ni, Mo, and V. Trace metal speciation, as operationally defined using solid-phase extraction onto two resins, will also be determined to further examine the geochemical cycling of metals in the subterranean estuary.

Chapter VII will provide a summary of the results, and will explore some future directions for SGD and trace metal studies. The final objective will be to relate SGD water flux, trace metal transport, and how geochemical cycling in the subterranean estuary may affect SGD-derived trace metal inputs to the coastal ocean.

References

Addy, K., A. Gold, B. Nowicki, J. McKenna, M. Stolt, and P. Groffman, 2005. Denitrification capacity in a subterranean estuary below a Rhode Island fringing salt marsh. Estuaries, 28 (6): 896-908.

Aller, R.C., 1980. Quantifying solute distributions in the bioturbated zone of marine sediments by defining an average microenvironment. Geochim. Cosmochim. Acta, 44: 1955-1965.

Aller, R.C. 2001. Transport and reactions in the bioirrigated zone. In: The Benthic Boundary Layer: Transport processes and biogeochemistry. B. Boudreau and B.B. Jorgensen, eds. Oxford University Press, Oxford. p. 269-301.

Alley, W.M., R.W. Healy, J.W. LaBaugh, and T.E. Reilly, 2002. Flow and storage in groundwater systems. Science, 296: 1985-1990.

Appelo, C.A.J., and A. Willemsen, 1987.Geochemical calculations and observations on salt water intrusions, I. A combined geochemical/ mixing cell model. J. Hydrol., 94: 313-330.

Archer, D., and A. Devol, 1992. Benthic oxygen fluxes on the Washington shelf and slope: a comparison of in situ microelectrode and chamber fluxes. Limnol. Oceanogr.., 37: 614-629.

Basu, A. R., S.B. Jacobsen, R.J. Poreda, C.B. Dowling, and P.K. Aggarwal, 2001. Large groundwater strontium flux to the oceans from the Bengal Basin and the marine strontium isotope record. Science, 293: 1470–1473.

Beck, A.J., Y. Tsukamoto, A. Tovar-Sanchez, M. Huerta-Diaz, H.J. Bokuniewicz, and S.A. Sañudo-Wilhelmy. 2007. Importance of geochemical transformations in determining submarine groundwater discharge-derived trace metal and nutrient fluxes. Applied Geochemistry, 22: 477-490.

Bergamaschi, B.A., E. Tsamakis, R.G. Keil, T.I. Eglinton, D.B. Montlucon, and J.I. Hedges, 1997. The effect of grain size and surface area on organic matter, lignin and carbohydrate concentration, and molecular compositions in Peru Margin sediments. Geochim. Cosmochim. Acta, 61: 1247–1260.

Billerbeck, M., U. Werner, L. Polerecky, E. Walpersdorf, D. de Beer, and M. Huettel, 2006. Surficial and deep pore water circulation governs spatial and temporal scales of nutrient recycling in intertidal sand flat sediment. Mar. Ecol. Prog. Ser., 326: 61-76.

Bokuniewicz, H.J. 1992. Analytical descriptions of subaqueous groundwater seepage. Estuaries 15, 458–464.

Bokuniewicz, H., 1980. Groundwater Seepage into Great South Bay, New York. Estuarine and Coastal Marine Science, 10 (4): 437-444.

Bokuniewicz, H, and B Pavilik. 1990. Groundwater seepage along a barrier island. Biogeochemistry 10: 257-276.

Bokuniewicz, H.J., and Zeitlin, M.J. 1980. Characteristics of groundwater seepage into Great South Bay. MSRC, Special Report 35, SUNY, Stony Brook, NY, 30 p.

Bokuniewicz, H.J., Pollock, M., Blum, J., and Wilson, R., 2004. Submarine groundwater discharge and salt penetration across the sea floor. Ground Water, 42: 983-989.

Bokuniewicz, H., J. Rapaglia, and A. Beck, 2007. Submarine groundwater discharge (SGD) from a volcanic island: A case study in Mauritius Island. International J. of Oceans and Oceanography, submitted.

Bone, S.E., M.E. Gonneea, and M.A. Charette, 2006. Geochemical cycling of arsenic in a coastal aquifer. Environmental Science and Technology. 40: 3273-3278.

Bone, S.E., M.A. Charette, C.H. Lamborg, and M.E. Gonneea, 2007. Has Submarine Groundwater Discharge Been Overlooked as a Source of Mercury to Coastal Waters? Environmental Science and Technology, in press.

Boudreau, B.P., and R.L. Marinelli, 1994. A modeling study of discontinuous biological irrigation. J. Mar. Res., 52: 947–968.

Buddemeier, R.W. 1996. Groundwater flux to the ocean: Definitions, data, applications, uncertainties. In: Groundwater Discharge to the Coastal Zone: Proceedings of an international symposium. R.W. Buddemeier, ed. LOICZ Reports and Studies No. 8, LOICZ, Texel, The Netherlands, pp. 16-21.

Bugna, G.C., J.P. Chanton, J.E. Cable, et al., 1996. The importance of groundwater discharge to the methane budgets of nearshore and continental shelf waters of the northeastern Gulf of Mexico. Geochimica et Cosmochimica Acta, 60 (23):4735-4746.

Burnett, W.C., H.J. Bokuniewicz, M. Huettel, W.S. Moore, and M. Taniguchi, 2003. Groundwater and pore water inputs to the coastal zone. Biogeochemistry, 66: 3-33

Burnett, W.C., P.K. Aggarwal, H. Bokuniewicz, J.E. Cable, M.A. Charette, E. Kontar, S. Krupa, K.M. Kulkarni, A. Loveless, W.S. Moore, J.A. Oberdorfer, J. Oliveira, N. Ozyurt, P. Povinec, A.M.G. Privitera, R. Rajar, R.T. Ramessur, J. Scholten, T. Stieglitz, M. Taniguchi, J.V. Turner. 2006. Quantifying Submarine Groundwater Discharge in the Coastal Zone via Multiple Methods. Science of the Total Environment 367(2-3): 498-543.

Bussmann I, Dando PR, Niven SJ, et al., 1999. Groundwater seepage in the marine environment: role for mass flux and bacterial activity. Mar. Ecol. Prog. Ser., 178: 169-177.
Cable, J.E., W.C. Burnett, J.P. Chanton, and G. Weatherly. 1996. Modeling groundwater flow into the ocean based on 222Rn. Earth Planet. Sci. Lett., 144: 591-604.

Cai, W.J., and Y. Wang, 1998. The chemistry, fluxes, and sources of carbon dioxide in the estuarine waters of the Satilla and Altamaha Rivers, Georgia. Limnol. Oceanogr., 43: 657–668.

Cambareri, T.C., and E.M. Eichner, 1998. Watershed delineation and ground water discharge to a coastal embayment. Ground Water, 36 (4): 626-634.

Capone, D.G. and M.F. Bautista. 1985. A groundwater source of nitrate in nearshore marine sediments. Nature, 313: 214 – 216.

Capone, D.G. and J.M. Slater. 1990. Interannual Patterns of Water Table Height and Groundwater Derived Nitrate in Nearshore Sediments. Biogeochemistry, 10 (3): 277-288.

Charette, M.A., and M.C. Allen, 2006. Precision groundwater sampling in coastal aquifers using a direct push shielded screen well-point system. Groundwater Monitoring & Remediation, 26 (2): 87-93.

Charette M.A., K.O. Buesseler. 2004. Submarine groundwater discharge of nutrients and copper to an urban subestuary of Chesapeake Bay (Elizabeth River). Limnology and Oceanography 49 (2): 376-385.

Charette, M.A., and E.R. Sholkovitz, 2002. Oxidative precipitation of groundwater-derived ferrous iron in the subterranean estuary of a coastal bay. Geophysical Research Letters, 29 (10), DOI: 10.1029/2001GL014512.

Charette, M.A., and E.R. Sholkovitz, 2006. Trace element cycling in a subterranean estuary: Part 2. Geochemistry of the pore water. Geochimica et Cosmochimica Acta, 70 (4): 811-826.

Charette, M.A., K.O. Buesseler, and J.E. Andrews, 2001. Utility of radium isotopes for evaluating the input and transport of groundwater-derived nitrogen to a Cape Cod estuary. Limnology and Oceanography, 46: 465-470.

Charette, M.A., R. Splivallo, C. Herbold, M. Bollinger, and W.S. Moore, 2003. Salt marsh submarine groundwater discharge as traced by radium isotopes. Marine Chemistry, 84: 113-121.

Charette MA, Sholkovitz ER, Hansel CM. 2005. Trace element cycling in a subterranean estuary: Part 1. Geochemistry of the permeable sediments. Geochimica et Cosmochimica Acta, 69 (8): 2095-2109.

Charette, M.A., W.S. Moore, W.C. Burnett, Submitted. Uranium- and thorium-series nuclides as tracers of submarine groundwater discharge. In *Radioactivity in the Environment: U-Th Series Nuclides in Aquatic Systems*.

Church, T.M., 1996. An underground route for the water cycle. Nature, 380 (6575): 579-580.

Clark, L.B., C.J. Gobler, and S.A. Sanudo-Wilhelmy, 2006. Spatial and Temporal Dynamics of Dissolved Trace Metals, Organic Carbon, Mineral Nutrients, and Phytoplankton in a Coastal Lagoon: Great South Bay, New York. Estuaries and Coasts, 29 (5): 841-854.

Crotwell, A.M. and W.S. Moore. 2003. Nutrient and Radium Fluxes from Submarine Groundwater Discharge to Port Royal Sound, South Carolina. Aquatic Geochemistry 9: 191–208.

Crusius J, Koopmans D, Bratton JF, et al., 2005. Submarine groundwater discharge to a small estuary estimated from radon and salinity measurements and a box model. Biogeosciences, 2 (2): 141-157.

D'Andrea, A.F., R.C. Aller, and G.R. Lopez, 2002. Organic matter flux and reactivity on a South Carolina sandflat: the impacts of porewater advection and macrobiological structures. Limnol. Oceanogr., 47: 1056–1070.

D'Andrea, A., G.R. Lopez, and R.C. Aller. 2004. Rapid physical and biological particle mixing on an intertidal sandflat. Journal of Marine Research, 62: 67-92.

D'Elia, C.F., K.L. Webb, J.W. Porter, 1981. Nitrate-rich groundwater inputs to Discovery Bay, Jamaica – A significant source of N to local coral reefs. Bulletin of Marine Science, 31 (4): 903-910.

de Beer, D., F. Wenzhofer, T.G. Ferdelman, S.E. Boehme, Markus Huettel1, J.E.E. van Beusekom, M.E. Bottcher, N. Musat, and N. Dubilier, 2005. Transport and mineralization rates in North Sea sandy intertidal sediments, Sylt-Rømø Basin, Wadden Sea. Limnol. Oceanogr., 50 (1): 113–127.

Devol, A.H., and J.P. Christensen, 1993. Benthic fluxes and nitrogen cycling in sediments of the continental margin of the North Pacific. J. Mar. Res., 51: 345-372.

Duncan, T., and T.J. Shaw, 2003. The Mobility of Rare Earth Elements and Redox Sensitive Elements in the Groundwater/Seawater Mixing Zone of a Shallow Coastal Aquifer. Aquatic Geochemistry, 9: 233–255.

Emerson, S., R. Jahnke, and D. Heggie, 1984. Sediment-water exchange in shallow-water estuarine sediments. J. Mar. Res., 42 (3): 709-730.

Falter, J.L., and F.J. Sansone. 2000. Shallow pore water sampling in reef sediments. Coral Reefs, 19: 93-97.

Freeze, R.A., and J.A. Cherry, 1979. *Groundwater*. Prentice-Hall Inc., Englewood Cliffs, NJ, 604 p.

Froelich, P.N., G.P. Klinkhammer, M.L. Bender, N.A. Luedtke, G.R. Heath, D. Cullen, and P. Dauphin, 1979. Early oxidation of organic matter in pelagic sediments of the eastern equatorial Atlantic: Suboxic diagenesis. Geochim. Cosmochim. Acta, 43: 1075–1090.

Gobler, C.J., and Boneillo, G.E. 2003. Impacts of anthropogenically influenced groundwater seepage on water chemistry and phytoplankton dynamics within a coastal marine system. Mar. Ecol. Prog. Ser., 255: 101-114

Gobler, C.J. and S.A. Sañudo-Wilhelmy, 2001 Temporal variability of groundwater seepage and Brown Tide Blooms in a Long Island Embayment. Marine Ecology Progress Series 217: 299-309

Grant, J., C.W. Emerson, B.T. Hargrave, and J.L. Shortle, 1991. Benthic oxygen consumption on continental shelves off Eastern Canada. Continental Shelf Research, 11: 1083-1097.

Haberstroh, P.R., and F.J. Sansone, 1999. Reef framework diagenesis across wave-flushed oxic-suboxic-anoxic transition zones. Coral Reefs, 18: 229-240.

Huettel, M., and G. Gust, 1992. Impact of bioroughness on interfacial solute exchange in permeable sediments. Mar. Ecol. Prog. Ser., 89: 253–267.

Huettel, M., W. Ziebis, S. Forster, and G.W. Luther II, 1998. Advective transport affecting metal and nutrient distributions and interfacial fluxes in permeable sediments. Geochim. Cosmochim. Acta, 62 (4): 613-631.

Huettel, M., H. Røy, E. Precht, and S. Ehrenhauss, 2003. Hydrodynamical impact on biogeochemical processes in aquatic sediments. Hydrobiologia, 494: 231–236.

Hwang, D.W., Kim, G.B., Lee, Y.W., Yang, H.S., 2005. Estimating submarine inputs of groundwater and nutrients to a coastal bay using radium isotopes. Marine Chemistry, 96 (1-2): 61-71.

Jahnke, R.A., C.R. Alexander, J.E. Kostka, 2003. Advective pore water input of nutrients to the Satilla River Estuary, Georgia, USA. Estuarine, Coastal and Shelf Science, 56: 641–653.

Johannes, R.E., and Hearn, C.J., 1985. The effect of submarine groundwater discharge on nutrient and salinity regimes in a coastal lagoon off Perth, western Australia. Estuarine, Coastal and Shelf Science, 21: 789–800.

Johannes, R.E., 1980. The ecological significance of the submarine discharge of groundwater. Mar. Ecol. Prog. Ser., 3: 365-373.

Kelly, R.P., Moran, S.B., 2002. Seasonal changes in groundwater input to a well-mixed estuary estimated using radium isotopes and implications for coastal nutrient budgets. Limnology and Oceanography, 47 (6): 1796-1807.

Kim, G., and D.W. Hwang, 2002. Tidal pumping of groundwater into the coastal ocean revealed from submarine Rn-222 and CH4 monitoring. Geophys. Res. Lett. 29.

Kim, G., Ryu, J.W., Yang, H.S., Yun, S.T., 2005. Submarine groundwater discharge (SGD) into the Yellow Sea revealed by Ra-228 and Ra-226 isotopes: implications for global silicate fluxes. Earth and Planetary Science Letters 237 (1-2), 156–166.

Krest, J.M., W.S. Moore, L.R. Gardner, AND J.T. Morris, 2000. Marsh nutrient export supplied by groundwater discharge: Evidence from radium measurements. Global Biogeochemical Cycles, 14 (1): 167-176.

LaRoche J., Nuzzi R., Waters R., Wyman K., Falkowski P.G., Wallace D.W.R. (1997) Brown Tide blooms in Long Island's coastal waters linked to interannual variability in groundwater flow. Global Change Biology 3(5): 397-410.

Laurier, F. J. G., Cossa, D., Beucher, C., and Breviere, E., 2006. The impact of groundwater discharges on mercury partitioning, speciation, and bioavailability to mussels in a coastal zone. Mar. Chem., in press.

Lee, DR. 1977. A device for measuring seepage flux in lakes and estuaries. Limnol. Oceanogr., 22 (1):140-147.

Lewis, J.B., 1987. Measurements of groundwater seepage flux onto a coral reef: Spatial and temporal variations. Limnology and Oceanography, 32 (5): 1165-1169.

Li, L., Barry, A., Stagnitti, F., and Parlange, J-Y., 1999. Submarine groundwater discharge and associated chemical input to a coastal sea. Water Resources Research, 35 (11): 3253-3259.

Magaritz, M., and J.E. Luzier, 1985. Water-rock interactions and seawater-freshwater mixing effects in the coastal dunes aquifer, Coos Bay, Oregon. Geochim. COsmochim. Acta, 49: 2515-2525.

Martin, J.B., K.M. Hartl, D.R. Corbett, P.W. Swarzenski, and J.E. Cable. 2003. A Multi-Level Pore-Water Sampler for Permeable Sediments. Journal of Sedimentary Research, 73 (1): 128-132.

Martin, J.B., Cable, J.E., Swarzenski, P., and Lindenberg, M., 2004. Enhanced submarine groundwater discharge from mixing of pore water and estuarine water. Ground Water: Special issue on Oceans and Estuaries, 42: 1000-1010.

Michael, H.A., J.S. Lubetsky, and C.F. Harvey, 2003. Characterizing submarine groundwater discharge: A seepage meter study in Waquoit Bay, Massachusetts. Geophys. Res. Lett., 30 (6): 1297.

Michael, H.A., A.E. Mulligan, C.F. Harvey. (2005) Seasonal oscillations in water exchange between aquifers and the coastal ocean. Nature 436, 1145-1148.

Montlucon, D., and S.A. Sañudo-Wilhelmy. 2001. Influence of net groundwater discharge on the chemical composition of a coastal environment: Flanders Bay, Long Island, New York. Environmental Science and Technology 3, 480-486

Moore W.S. (1996) Large groundwater inputs to coastal waters revealed by Ra-226 enrichments. Nature 380 (6575): 612-614.

Moore, W.S., 1997. High fluxes of radium and barium from the mouth of the Ganges-Brahmaputra River during low river discharge suggest a large groundwater source. Earth and Planetary Science Letters, 150 (1-2): 141-150.

Moore W.S. 1999. The subterranean estuary: a reaction zone of ground water and sea water. Marine Chemistry, 65 (1-2): 111-125.

Nielsen, P., 1990. Tidal dynamics in the water table in a beach. Water Resources Research, 26: 2127–2134.

Oberdorfer, J.A., M.A. Valentino, S.V. Smith. (1990) Groundwater contribution to the nutrient budgets of Tomales Bay, California. Biogeochem., 12: 199-216.

Paerl, H.W., 1997. Coastal eutrophication and harmful algal blooms: importance of atmospheric deposition and groundwater as “new” nitrogen and other nutrient sources. Limnol. Oceanogr., 42: 1154–1165.

Portnoy, J.W., B.L. Nowicki, C.T. Roman, and D.W. Urish, 1998. The discharge of nitrate-contaminated groundwater from developed shoreline to a marsh-fringed estuary. Water Resources Research, 34 (11): 3095-3104.

Riedl, R., N. Huang, and R. Machan, 1972. The subtidal pump: a mechanism of interstitial water exchange by wave action. Mar. Biol., 13: 210–221.

Reimers, C.E., H.A. Stecher III, G.L. Taghon, C.M. Fuller, M. Huettel, A. Rusch, N. Ryckelynck, and C. Wild, 2004. In situ measurements of advective solute transport in permeable shelf sands. Cont. Shelf. Sci., 24: 183–201

Robinson C., B. Gibbes, and L. Li. 2006. Driving mechanisms for groundwater flow and salt transport in a subterranean estuary. Geophysical Research Letters, 33, L03402, doi:10.1029/2005GL025247

Romkens, P.F.A.M., and W. Salomons, 1998. Cd, Cu, and Zn solubility in arable and forest soils: consequences of land use changes for metal mobility and risk assessment. Soil Science, 163 (11): 859-871.

Rowe, G.T., R. Theroux, W. Phoel, H. Quinby, R. Wilke, D. Koschoreck, T.E. Whitledge, P.G. Falkowski, and C. Fray, 1988. Benthic carbon budgets for the continental shelf south of New England. Continental Shelf Research, 8: 511-527.

Rusch, A., M. Huettel, and S. Forster, 2000. Particulate organic matter in permeable marine sands – Dynamics in time and depth. Est. Coast. Shelf Sci., 51: 399-414.

Rusch, A., S. Forster, and M. Huettel, 2001. Bacteria, diatoms and detritus in an intertidal sandflat subject to advective transport across the water–sediment interface. Biogeochemistry, 55: 1–27.

Rusch, A., M. Huettel, C.E. Reimers, G.L. Taghon, and C.M. Fuller, 2003. Activity and distribution of bacterial populations in Middle Atlantic Bight shelf sands. FEMS Microbiol. Ecol., 44: 89–100.

Rutkowski, C.M., W.C. Burnett, R.L. Iverson, and J.P. Chanton, 1999. The effect of groundwater seepage on nutrient delivery and seagrass distribution in the northeastern Gulf of Mexico. Estuaries, 22 (4): 1033-1040.

Seplow, M.S. 1991. The influence of groundwater seepage on pore water salinity in Great South Bay. M.S. thesis, Marine Sciences Research Center, State University of New York, Stony Brook, NY.

Shaw, T.J., J.M. Gieskes, and R.A. Jahnke, 1990. Early diagenesis in differing depositional environments: The response of transition metals in pore water. Geochim. Cosmochim. Acta, 54: 1233–1246.

Shaw, T. J., Moore, W. S., Kloepfer, J. and Sochaski, M. 1998. The flux of barium to the coastal waters of the southeastern United States: The importance of submarine Groundwater Discharge. Geochim. Chosmochim. Acta, 62: 1277–1283.

Shaw, T.J. 2001. Conference provides forum for discussion of subterranean coastal environments. EOS, 82(50): 622-623.

Shum, K.T., and B. Sundby, 1996. Organic matter processing in continental shelf sediments – the subtidal pump revisited. Marine Chemistry, 53: 81-87.

Shum, K.T., 1992. Wave-induced advective transport below a rippled water-sediment interface. J. Geophys. Res., 97: 789-808.

Shum, K.T., 1993. The effects of wave induced pore water circulation on the distribution and flux of pore water constituents in a rippled sediment bed. J. Geophys. Res., 98: 10289-10301.

Slomp, C.P., and P. Van Cappellen, 2004. Nutrient inputs to the coastal ocean through Smith, G.J. and Flegal, A.R., 1993. Silver in San Francisco Bay estuarine waters. Estuaries, 16 (3A): 547-558.

Snyder, M., M. Taillefert and C.D. Ruppel, 2004. Redox zonation at the saline-influenced boundaries of a permeable surficial aquifer: effects of physical forcing on the biogeochemical cycling of iron and manganese. Journal of Hydrology, 296: 164-178.

Spiteri, C., P. Regnier, C.P. Slomp, and M.A. Charette, 2006. pH-Dependent iron oxide precipitation in a subterranean estuary. Journal of Geochemical Exploration, 88: 399–403.

Stieglitz, T., 2005. Submarine groundwater discharge into the near-shore zone of the Great Barrier Reef, Australia. Marine Pollution Bulletin, 51:51–59

Talbot, J.M., K.D. Kroeger, A. Rago, M.C. Allen, M.A. Charette, 2003. Nitrogen flux and speciation through the subterranean estuary of Waquoit Bay, Massachusetts. Biological Bulletin, 205: 244-245.

Testa, J.M., M.A. Charette, E.R. Sholkovitz, M.C. Allen, A. Rago, C.W. Herbold. 2002. Dissolved iron cycling in the subterranean estuary of a coastal bay: Waquoit Bay, Massachusetts. Biological Bulletin, 203: 255-256.

Ullman, W.J., B. Chang, D.C. Miller, and J.A. Madsen, 2003. Groundwater mixing, nutrient diagenesis, and discharges across a sandy beachface, Cape Henlopen, Delaware (USA). Estuarine, Coastal and Shelf Science, 57: 539–552.

Valiela, I., J. Costa, K. Foreman, et al., 1990. Transport of groundwater-borne nutrients from watersheds and their effects on coastal water. Biogeochemistry, 10 (3): 177-197.

Waldbusser, G.G., and R.L. Marinelli, 2006. Macrofaunal modification of porewater advection: role of species function, species interaction, and kinetics. Mar. Ecol. Prog. Ser., 311: 217-231.

Windom, H., and F. Niencheski, 2003. Biogeochemical processes in a freshwater–seawater mixing zone in permeable sediments along the coast of Southern Brazil. Marine Chemistry, 83: 121–130.

Windom, H.L., W.S. Moore, L.F.H. Niencheski, and R.A. Jahnke, 2006. Submarine Groundwater Discharge: a Large, Previously Unrecognized Source of Dissolved Iron to the South Atlantic Ocean. Marine Chemistry, 102: 252–266.

Younger PL. 1996. Submarine groundwater discharge. Nature, 382 (6587): 121-122.

Zeitlin, M.J. 1980. Variability and predictability of submarine ground-water flow into a coastal lagoon, Great South Bay, New York. M.S. thesis, Marine Sciences Research Center, State University of New York, Stony Brook, NY.

Zektzer, I.S., V.A. Ivanov, and A.V. Meskheteli. 1973. The problem of direct groundwater discharge to the seas. Journal of Hydrology, 20: 1-36.

Zimmermann, C.F., J.R. Montgomery, and P.R. Carlson, 1985. Variability of dissolved reactive phosphate flux rates in nearshore estuarine sediments: Effects of groundwater flow. Estuaries, 8 (2B): 228-236.

FIGURES

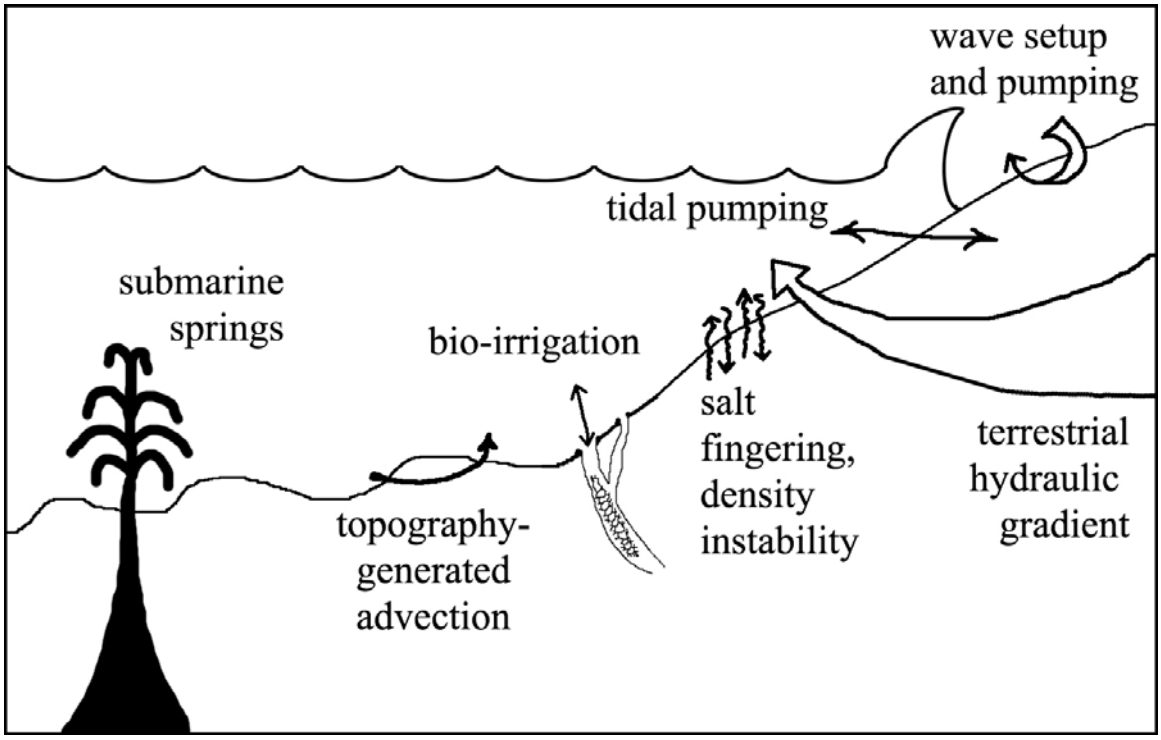

Figure I-1. Cartoon of different mechanisms for advective flow in permeable sediments in the coastal ocean. See text for references and a more detailed description.

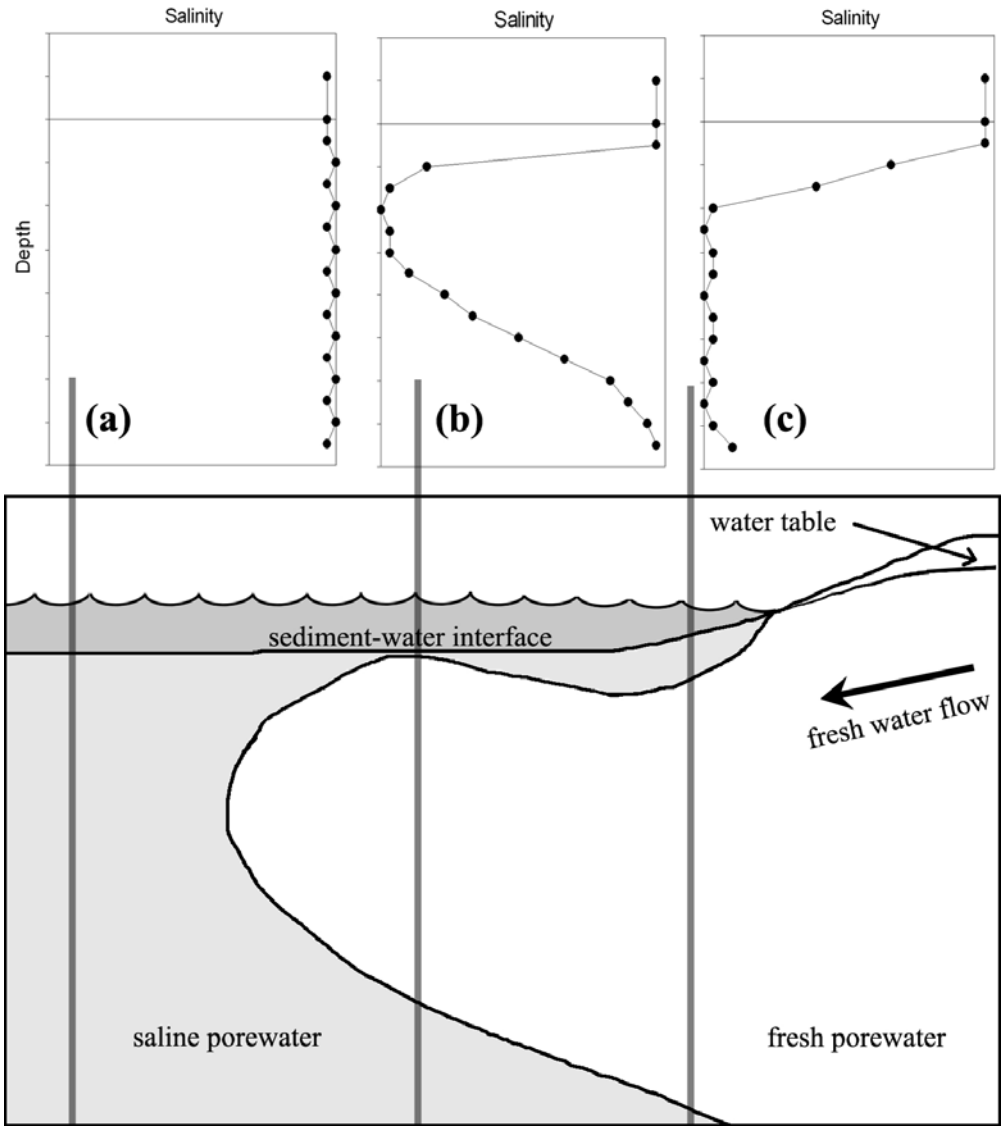

Figure I-2. Schematic of the subterranean estuary. Two mixing zones can be seen here: a deep, stable salt wedge overlain by fresh groundwater, and a shallow, unstable mixing zone near the sediment-water interface. Porewater profiles collected at the locations of the vertical lines would look approximately like the plots above each line. Profiles (a) and (c) will be examined in this dissertation.

CHAPTER II:

Radium mass-balance in Jamaica Bay, NY: Evidence for a substantial flux of submarine groundwater

Beck, A.J., J.P. Rapaglia, J.K. Cochran, and H.J. Bokuniewicz, 2007. Radium mass-balance in Jamaica Bay, NY: Evidence for a substantial flux of submarine groundwater. Marine Chemistry, *in press*.

ABSTRACT

A mass balance for the naturally-occurring radium isotopes (^{224}Ra, ^{223}Ra, ^{228}Ra, and ^{226}Ra) in Jamaica Bay, NY, was conducted by directly estimating the individual Ra contributions of wastewater discharge, diffusion from fine-grained subtidal sediments, water percolation through marshes, desorption from resuspended particles, and water exchange at the inlet. The mass balance revealed a major unknown source term accounting for 19-71% of the total Ra input, which could only be resolved by invoking a source from submarine groundwater. Shallow (<2 m depth) groundwater from permeable sediments in Jamaica Bay was brackish and enriched in Ra relative to surface bay waters by over two orders of magnitude. To balance Ra fluxes, a submarine groundwater input of $0.8\times10^9 - 9.0\times10^9$ liters d^{-1} was required. This flux was similar for all four isotopes, with individual estimates varying by less than a factor of 2. Our calculated groundwater flux was 6 to 70 -fold higher than the fresh groundwater discharge to the bay estimated by hydrological methods, but closely matched direct flow rates measured with seepage meters. This suggests that a substantial portion of the discharge consisted of recirculated seawater. The magnitude of submarine groundwater discharge varied seasonally, in the order: summer > autumn > spring. Chemical analyses suggest that the recirculated seawater component of submarine groundwater delivers as much dissolved nitrogen to the bay as the fresh groundwater flux.

INTRODUCTION

In recent decades, submarine groundwater discharge (SGD) has gained increasing attention as a major component in the global budgets of many elements (e.g. Ba, Ra, U, inorganic C), and as a source of essential nutrients and trace metals to coastal ecosystems (Johannes, 1980; D'Elia et al., 1981; Capone and Bautista, 1985; Capone and Slater, 1990; Gobler and Sañudo-Wilhelmy, 2001). Much of the chemical composition of SGD is the result of reactions occurring in the subterranean estuary, where meteoric groundwater mixes with intruding seawater (Shaw et al., 1998; Moore, 1999; Talbot et al., 2003; Charette and Sholkovitz, 2006). Because of the geochemical processes unique to the subterranean estuary, groundwater composition can be modified substantially before discharging to the coastal ocean. In addition, the fact that the chemically significant portion of SGD is due to seawater intrusion renders useless many conventional hydrologic methods for estimation of groundwater flow (Burnett et al., 2003). To circumvent this problem, and indeed, to exploit it, a variety of geochemical tracers have been developed to assess the magnitude of groundwater discharge to coastal waters (e.g. Moore, 1996; Cable et al., 1996; Burnett and Dulaiova, 2003).

The pioneering work of Moore and coworkers, and the subsequent work of many others, has firmly established naturally occurring Ra isotopes as one of the most oft-utilized and important tracers for measuring SGD (Moore, 1996; Rama and Moore, 1996; Krest et al., 2000; Charette et al., 2001, 2003; Kelly and Moran, 2002; Yang et al., 2002). Ra has four isotopes of widely varying half-lives (^{224}Ra: 3.66 d, ^{223}Ra: 11.3 d, ^{228}Ra: 5.8 y, ^{226}Ra: 1600 y), all of which have been used singly or in concert to elucidate different characteristics of the SGD phenomenon. Ra is produced in the aquifer by decay of Th

parent isotopes contained on or within aquifer solids. In fresh groundwater, Ra tends to be highly particle-reactive, which usually maintains low activities in the dissolved phase; however, intruding saltwater results in ion exchange transformations, and thus, saline groundwater is orders of magnitude enriched with Ra. The advection and discharge of this high activity interstitial water can support an inventory of dissolved Ra in coastal waters in excess of that which can be supplied by other sources.

In addition to SGD, dissolved Ra in the coastal marine environment has several other sources associated with sediment-water interaction. River-borne particles carry adsorbed Ra ions which undergo exchange during mixing with seawater, revealed as non-conservative excess Ra in rivers transporting substantial suspended sediments (Li et al., 1977; Webster et al., 1995). Although there is some Ra initially in the dissolved phase in fresh river water, the greater portion is associated with the particulate fraction. Saline porewaters of fine-grained estuarine muds are enriched in Ra similar to saline groundwater, but diffusion and bio-irrigation tend to dominate in these relatively impermeable sediments. As a result, coastal regions with extensive areas of fine-grained sediments may be subject to significant Ra input through molecular diffusion and/or bioirrigation. Finally, a significant amount of Ra is supplied to estuarine waters by tidal interaction with salt marshes (Elsinger and Moore, 1983; Bollinger and Moore, 1984; Bollinger and Moore, 1993). Tidal oscillation alternately floods and drains marshland, forcing percolation of water through creek banks (Wilson and Gardner, 2006). Although the advection of interstitial water through the marsh is similar to SGD, it is a unique process that can be examined independently.

Thus, dissolved Ra in coastal marine waters is supported by a suite of inputs: river transport, ion exchange from suspended particles, diffusion and bio-irrigation from fine-grained sediments, percolation of interstitial water through marshland, and SGD. The relative importance of these processes varies between isotopes, depending on the time scale regulating the regeneration and loss of each. Generally, SGD studies using Ra as a tracer rely on assumptions to omit one or more source or loss terms, or depend on calculation of a Ra residence time (e.g. Moore, 1996; Charette et al., 2001; Hwang et al., 2005). Our objective in the current study is to quantify each individual flux term in a single estuarine system, and perform a Ra mass balance to understand the true contribution of each source to the total dissolved Ra inventory. Additionally, we compare the results from the mass balance approach to those estimated using other established methods.

METHODS

Site description

Jamaica Bay (Fig. II-1) is a small (~52 km^2), highly urbanized estuary in southern Brooklyn in New York City, New York. Since the 19^{th} century, the bay has been impacted by significant anthropogenic activity, examples of which include fertilizer and fish oil factories, asphalt manufacturing, scrap metal companies, lead smelters, and commercial and recreational fishing (Black, 1981). Physical alteration has been effected through construction of landfills, infilling and bulkhead construction along fringing marshes, and construction of runways for JFK International Airport. Dredging of channels has increased the bay volume by an estimated 70% (Swanson et al., 1992), and

dredge spoils have been used to modify many of the marshlands and islands in the bay. Although Jamaica Bay was established as a wildlife refuge in 1948 and managed by the National Park Service since 1972, it is still subject to heavy anthropogenic pressure through treated sewage effluent, combined sewer overflows (CSOs), landfill leachate, and atmospheric pollutants from New York City (Swanson et al., 1992). Currently, wastewater effluent enters the bay primarily from four major treatment plants – Coney Island, Jamaica, 26th Ward, and Rockaway. These wastewater inputs represent a major source of contaminants such as nutrients to Jamaica Bay. Dissolved nitrogen levels are elevated throughout Jamaica Bay, and may be responsible, in part, for the extensive marsh loss observed throughout the bay (Benotti et al., 2006).

From a geological perspective, Jamaica Bay surface sediments comprise primarily glacial outwash, salt marsh sediments, artificial fill, and beach and dune deposits (Englebright, 1975). These sediments overlie a series of stratigraphic units, and there are in total four aquifers between crystalline bedrock and the surface: the Lloyd, Magothy, Jameco, and Upper Glacial aquifers. Jamaica Bay sits atop the Upper Glacial Aquifer. This is a highly permeable aquifer over 210 m thick composed of till and outwash deposit interbedded with marine clays (Busciolano, 2002). The Upper Glacial Aquifer overlies the Jameco Aquifer which is 170 m thick, composed of fine-to-coarse gravel. The Jameco Aquifer is underlain in turn by the Magothy and Lloyd Aquifers to bedrock at a depth of 550 m (Busciolano, 2002). The aquifers below the Upper Glacial Aquifer are confined by clay units although they may be connected locally (Englebright, 1975). Submarine groundwater discharge is presumed to involve only the Upper Glacial Aquifer.

Water column sampling

Water samples were collected throughout Jamaica Bay during four cruises spanning two years (Fig. II-1), and measured for ^{223}Ra and ^{224}Ra activities following standard methods of extraction and delayed coincidence counting (Rama and Moore, 1996; Charette et al., 2001 and 2003; Hwang et al., 2005). Briefly, Ra isotopes were extracted in the field onto manganese oxide-impregnated acrylic fiber (hereafter, 'Mn-fiber') at flow rates less than 1 L per minute (Moore and Reid, 1973; Moore, 1976; Reid et al., 1979). Quantitative recovery (greater than 95%) was confirmed occasionally using two Mn-fiber columns connected in series (Kelly and Moran, 2002). The Mn-fiber was returned to the laboratory within 24 hours, rinsed with deionized water, partially dried, and analyzed for ^{223}Ra and ^{224}Ra using the RaDeCC delayed coincidence counter described by Moore and Arnold (1996).

Long-lived isotopes were subsequently determined on the same fibers. Mn-fibers were ashed in a muffle furnace at 475^{o}C for 6-12 hours. The ash was then compressed into a small pellet sealed with between five and ten layers of aluminum foil to prevent Rn loss, and counted in a well geometry gamma detector. After allowing three weeks for ingrowth of the ^{222}Rn daughter subsequent to pelletization, ^{226}Ra was determined using the ^{214}Bi photopeak at 352 keV. ^{228}Ra was measured using the ^{228}Ac peak at 911 keV. The detector was calibrated using Mn-fiber and sediment standards prepared in the same geometry as the samples. The low Ra activities observed in Jamaica Bay required long counting times of between one and three days per sample to achieve good statistics. Because of this, we are forced to report fewer analyses for long-lived isotopes than for short-lived isotopes.

In order to assess seasonal variability in bay-wide radium inventories, radium isotopes were collected throughout Jamaica Bay during October 2004 and April 2006. In addition, samples were obtained during September 2004 and 2005, allowing examination of interannual variability. Surface water (50-60 L) was collected during all cruises using 60 L polyethylene drums or multiple 20 L polyethylene cubitainers, and totaled about 60 samples. Similar volumes of deep water were pumped onboard from approximately 1m above the sediment surface during the October 2004 and April 2006 cruises, totaling about 33 samples.

Treated wastewater effluent

Effluent water was sampled on 8 February 2005 directly from holding tanks at the 26th Ward wastewater treatment plant (WWTP) sited on Hendrix Creek on the NNW side of the bay (Fig. II-1). Water was slowly (0.80 L min^{-1}) pumped with a peristaltic pump from the canal between the chlorinating spray and the outfall pipe, and was passed directly through a column containing Mn fiber. Three samples were obtained in this manner over the course of about eight hours, each representing an integrated sample of water pumped for between 0.75 and 1.5 hours.

Sediment cores

Core incubation: flux from bio-irrigation and diffusion

Two whole core incubations were performed using shallow (10-15 cm), large diameter cores (~29 cm) obtained from a subtidal region of the JoCo marsh creek described below (Sec. 2.5, Figs. II-1 and II-2). The first experiment was conducted on

six cores collected in April 2006; water temperature during this experiment was maintained at 17^{o}C, approximately 5^{o}C above *in situ* water temperature at the time of collection. A second experiment was conducted on two cores collected during August 2006 at the same location as previous; the water temperature during this incubation was maintained at the *in situ* temperature of 26^{o}C.

Cores were selected visually to ensure that they were reasonably alike. Core bottoms were sealed as well as possible, and placed in a large bin filled with water to prevent artificially impressed flow through the core. Ra-free bay water (10-15 L, passed through Mn-fiber) was poured gently into the core cylinders to the same level as water in the outer bin. No sediment disturbance was observed during overlying water transfer. The overlying water was aerated well with an air pump to prevent changes in redox characteristics.

In addition, no effort was made to alter the biological community present at time of collection. Two cores were wet-sieved (>0.5mm) to assess the community composition, which comprised primarily small bivalves and gastropods (*Ilyanassa obsoleta*, *Mercenaria mercenaria*, and *Mya arenaria*) and polychaetes (*Pectinaria gouldii*, *Nereis succinea*, and *Glycera* spp.). There were generally one to ten, usually small, specimens of each species per core, except for *I. obsoleta*, for which there were about 25 specimens per core. Therefore, the results reported here as "diffusion" are actually a combination of diffusion and bio-irrigation, and as such, probably represent natural processes more accurately.

Diffusive flux of Ra into the overlying water was determined by incubating cores for progressively longer intervals and sampling the entire volume of water in each core at

the end of the time interval. The overlying water of the cores was replaced with new Ra-free water after each sampling event, allowing multiple time points to be determined using a single core. Thus, each sample did not represent the time of incubation since collection, but only the time of incubation in contact with the sediment surface. Because of this, a 400+ hour time point could have been taken from a core before replacement of the overlying water, incubation, and subsequent collection of a <24 hour time point. This method allowed the collection of a detailed data set, and although it may have introduced some sampling artifacts, the clarity of the trends observed suggests that artifact influence was small compared to the processes we sought to examine.

Sediment porewater

Following the completion of the April diffusion experiment, the overlying water in three cores was decanted and replaced with new Ra-free water. After a 48 h incubation, when diffusive flux should have been closest to the observed average, the overlying water was drained and sediment in the three cores sequentially excavated by ~3 cm intervals. The porewater in this sediment was extracted by centrifugation, filtered, and the Ra measured as described previously. The large size of the cores yielded approximately 500 mL of porewater per 3 cm interval; given the high Ra activities (0.1 – 4 dpm/L) in the porewater, this sample volume was sufficient for the counting technique. One additional core (Core P) was collected in August 2006 and the porewater extracted within 6 hours of collection to verify that the profiles measured in post-incubation cores were representative of natural conditions.

Marsh creek time series

Marsh creek water was sampled during a half-tidal cycle from high tide to low tide in April 2006 to examine the flux of Ra associated with seawater percolation through the marsh. The sampling location was a medium-sized tidal creek on JoCo Marsh in the northeastern corner of Jamaica Bay (Fig. II-1). This particular creek was chosen because it comprised natural channels draining unmodified marshland, and because there was only one point of discharge for water flowing out of the creek on ebb tide (Fig. II-2). The channel dimensions ranged from about 30 m wide by 1.25 m deep at high tide, to about 3 m wide by 0.1 m deep at low tide. The approximate marsh drainage area to this creek is shown in Fig. II-2, and is discussed above.

The tidal pattern in Jamaica Bay is semidiurnal, with small difference in height between successive tides. This suggests that the trends observed during one ebbing tide were representative of both tides on that date. At the sampling site, the difference in height between spring and neap tides is about 20-30%; the sampling date, 17 April, was during the waning gibbous moon phase, exactly halfway between spring and neap tides. Thus, the observed Ra flux described below probably represents a good average of spring and neap tide fluxes.

A hose was secured approximately ten to twenty centimeters above the sediment surface in the deepest portion of the creek channel, and water was pumped into containers on shore and processed as described earlier. Water volume flow out the channel was approximated by measuring the flow speed and channel width and depth at each sampling time point and assuming a triangular channel cross-sectional area.

Desorbable Ra from resuspended sediments

Surface-bound, desorbable Ra was determined by shaking 5-10 g of sediment with ~15 L of filtered (<1 μm), Ra-free seawater (salinity = 27) for 5 minutes. The dilute slurry was then filtered through a column containing raw acrylic fiber to remove the sediment, and the dissolved Ra extracted onto Mn fiber.

Groundwater

There is some argument in the literature regarding the designation of interstitial fluid of estuarine subtidal sediments as "porewater" or "groundwater" (e.g. Charette and Sholkovitz, 2006). Here, we separate the two in a simply qualitative sense, based on sediment physical characteristics and diffusive processes versus advective ones. Because advection tends to dominate in coarse, permeable sediments, we refer to samples collected in sandy environments as "groundwater", and those collected from high porosity, low permeability muds, silts, and clays as "porewater". In reality, the difference is one of semantics, and we use "groundwater" simply to identify samples from sediment types in which advective processes are likely to dominate. Surface groundwater (up to 4 m depth) Ra profiles were sampled at six locations in the bay using the Retract-A-Tip piezometer (AMS, Inc.) described by Charette and Allen (2006).

To prevent reductive dissolution of the Mn-fiber, anoxic groundwater samples (≤ 4 L) were aerated with a portable air pump for a minimum of 60 minutes before extraction onto the Mn-fiber (Epler, 1991; Krest et al., 2000). While it is possible that aeration could cause artifacts by co-precipitating dissolved Ra with Fe- and Mn-oxides, no precipitate was visually evident after aeration. While we have observed substantial

Fe/Mn precipitates formed in aerated groundwater samples from other locations, Ra activities in that precipitate were less than 10% of the dissolved activity. However, when samples of a clearly reducing nature (e.g. highly sulfidic) are passed through Mn-fiber, loss of Mn is visually evident through substantial bleaching of the fiber. Side-by-side extraction of aerated and non-aerated sulfidic samples has indicated that Mn loss from the fibers results in a >50% reduction in extraction efficiency. Thus, artifacts associated with sample aeration were probably less than those that would have been introduced by Ra extraction from non-aerated samples.

Manual seepage meters

Direct point measurements of submarine groundwater discharge were performed using standard benthic chambers (Lee, 1977; Libelo and MacIntyre, 1994) for comparison with values derived from radium measurements. The chambers, which are vented to plastic bags, were inserted 5 to 10 cm in the sediment and allowed to stabilize for at least 30 minutes before measurements were taken. Seepage meter measurements were made at six sites throughout the bay; these coincided with locations where groundwater samples were procured for Ra analysis (Fig. II-1). At each location, 2 to 5 chambers were used to assess local variability in the discharge. Measurements were taken every 30-60 minutes for periods ranging from 3 to 12 hours.

Total dissolved nitrogen (tDIN)

Samples for dissolved nitrogen were collected using trace metal clean sampling techniques (Flegal et al., 1991; Sañudo-Wilhelmy and Gill, 1999). Briefly, water column

samples were pumped onboard through acid-washed Teflon tubing using a peristaltic pump with clean C-Flex tubing in the pump head. Water was filtered through clean polypropylene Calyx capsule filters (0.2 micron pore size) directly into acid-cleaned 0.25 L low-density polyethylene bottles, and were placed on ice until freezing within 8 hours. Groundwater samples were collected in a similar manner using the Retract-a-tip piezometer described above. Nitrogen analyses were performed using standard spectrophotometric techniques (Parsons et al., 1985)

RESULTS

Dissolved Ra in Jamaica Bay

The saline endmember for our Jamaica Bay dataset is considered to be the average of three samples with salinities greater than 30 (shown as a tight cluster of points in Fig. II-3), which were collected as far out of the mouth of the bay as was possible in a small boat. These samples contained low Ra activities, 0.32 ± 0.07 dpm 100 L^{-1} (^{223}Ra), 5.79 ± 0.33 dpm 100 L^{-1} (^{224}Ra), 6.0 ± 1.8 dpm 100 L^{-1} (^{228}Ra), and 7.2 ± 2.6 dpm 100 L^{-1} (^{226}Ra).

Because of the unique bay characteristics described above, the fresh endmember in this system is wastewater effluent, which has lower activities than the ocean endmember. Very low activities were observed in effluent water samples, 0.059 ± 0.02 dpm 100 L^{-1} (^{223}Ra, n=3), 2.21 ± 0.28 dpm 100 L^{-1} (^{224}Ra, n=3), 2.1 ± 0.8 dpm 100 L^{-1} (^{228}Ra, n=2), and 3.9 ± 4.3 dpm 100 L^{-1} (^{226}Ra, n=2). These are the near-zero salinity points shown in Fig. II-3.

All Ra activities show pronounced enrichment in Jamaica Bay relative to conservative mixing between the observed endmembers (Fig. II-3). Excess Ra (Ra_{xs}) was calculated as the difference between the measured activity of each sample and the activity predicted by conservative mixing between fresh and saline endmembers (Kelly and Moran, 2002). Baywide Ra_{xs} averages and ranges are listed in Table II-1.

Ra supplied by bio-irrigation and diffusion from sediments

Core incubations

Whole core incubations were conducted to directly evaluate the bio-irrigation and diffusive flux by observing Ra enrichment in the overlying water with time. This approach represents a refinement of that of Bird et al. (1999); the initial progress toward equilibrium between Ra input and decay was monitored during our experiment, instead of using the final equilibrium Ra concentration. Figure II-4 shows the increase of short-lived Ra in the overlying water as a consequence of bio-irrigation and diffusion from the sediments. (For ^{228}Ra and ^{226}Ra, activities in the overlying water throughout the experiment were at or below the detector background levels of 0.05 and 0.07 cpm, respectively. Thus, diffusion of these nuclides from sediments is low enough to be considered negligible in this study.) As the length of time nears several half-lives of the nuclide, dissolved Ra in the water should approach a steady state between diffusive supply and radioactive decay. For ^{224}Ra, an approximately steady state inventory of 7.5 dpm per core is reached after 200 hours, or 2-3 half-lives. The inventory of ^{223}Ra does not appear to reach a steady state activity during the relatively short incubation time, and the activity in the overlying water continues to increase at 450 hours, or about 1.6 half-

lives. No enrichment of ^{228}Ra or ^{226}Ra was observed over the course of the experiment (Supporting Information, Fig. A).

Repeating the experiment at a temperature increased by ~10^{o}C did not appear to change the flux significantly (Fig. II-4). This suggests that either temperature effects on Ra diffusive flux are minimal, or that bio-irrigation was the dominant process controlling the flux and was not affected by the temperature change examined here.

Ra fluxes from sediments (combined effect of diffusion and bio-irrigation) were estimated assuming that the change in Ra activity in the overlying water is the net effect of input from sediments and removal by decay,

$$dI/dt = (J_{diff} A_{surf}) - \lambda I, \quad [1]$$

where I is the Ra inventory in the overlying water (dpm) in each core, J_{diff} is the diffusive flux (dpm $m^{-2} h^{-1}$), λ = decay constant for each nuclide (h^{-1}), and A_{surf} is the surface area of the core (m^2). This equation can be solved to give the inventory at time *t*,

$$I_t = [(J_{diff} A_{surf})/\lambda] (1 - e^{-\lambda t}). \quad [2]$$

Application of the model with different values for J_{diff} provides the curves illustrated in Fig. II-4, and shows that the data are represented reasonably well by equation [2].

Two artifacts associated with the sampling procedure appear to be evident in the data, and bear mention. First, during the experiment, Ra enrichment of the overlying water occurred to levels 5- to 10-fold higher than observed in natural samples; this decreased the gradient between the porewater and overlying water, significantly diminishing the diffusive flux. Because of this, the data at long incubation times tend to approach the model curve for a lower flux. Second, changing the activity of the overlying water will change the porewater gradient (i.e. will result in higher Ra activities

in surficial porewater), so that when the overlying water is sampled and replaced with new, Ra-free water, the gradient between porewater and overlying water will be maximized. This will tend to force a higher flux at short incubation intervals, and is evident in the data for short time intervals shown in Fig. II-4. However, use of an intermediate flux (0.047 dpm m^{-2} h^{-1} [^{223}Ra] and 1.17 dpm m^{-2} h^{-1} [^{224}Ra]) gives model curves which fit the data reasonably well, and probably provide the best estimate of the natural flux.

Porewater Ra profiles

The diffusive flux of Ra from sediments has often been estimated by measuring porewater Ra profiles and calculating the flux based on observed gradients (Berner, 1980; Rama and Moore, 1996; Charette et al., 2003). In Jamaica Bay, porewater Ra activities average 210 ± 80 dpm 100 L^{-1} (^{223}Ra) and 460 ± 170 dpm 100 L^{-1} (^{224}Ra). We have limited data for the long-lived isotopes, but the available data suggest that the activities are somewhat lower than the short-lived isotopes (~100 dpm 100 L^{-1}). There are insufficient data to discuss profiles of the long-lived isotopes. Porewater profiles for the short-lived isotopes (Fig. II-5) show little or no near-surface concentration gradient, but surface porewater Ra activities are as much as two orders of magnitude higher than those observed in the water column. Thus, a near-interface gradient must exist, although our sampling resolution is not sufficient to distinguish it.

Using the directly measured diffusion fluxes calculated above (see Fig. II-4) and Fick's First Law, one can back-calculate the depth to which diffusive processes will modify the Ra composition of porewaters:

$$dz = -D_s (dC_{Ra})/J_{diff} \quad [3]$$

In this case, we use average diffusion fluxes (J_{diff}) of $4.7 \pm 0.24 \times 10^{-6}$ and $1.17 \pm 0.24 \times 10^{-4}$ dpm cm^{-2} h^{-1} for ^{223}Ra and ^{224}Ra, respectively. The quantity "dC_{Ra}" is calculated with surficial porewater activities ($1.5 \pm 0.29 \times 10^{-4}$ [^{223}Ra] and $4.1 \pm 1.4 \times 10^{-3}$ [^{224}Ra] dpm cm^{-3}, Fig. II-5) and average Ra activities in the water column when the cores were collected ($9.6 \pm 3.1 \times 10^{-6}$ [^{223}Ra] and $1.7 \pm 0.73 \times 10^{-5}$ [^{224}Ra] dpm cm^{-3}). The sediment diffusion coefficient (D_s) for Ra (in seawater, corrected for tortuosity) is approximately 1.71×10^{-2} cm^2 h^{-1} (Cochran and Krishnaswami, 1980).

This approach yields a diffusion length scale (depth below the sediment-water interface) of 0.52 ± 0.11 and 0.58 ± 0.24 cm for ^{223}Ra and ^{224}Ra, respectively. The uncertainty on the length scale for each isotope is 25-50%, and shows that the penetration depths for the two isotopes are indistinguishable from each other. Although one would expect the ^{223}Ra diffusion length to be somewhat longer than that for ^{224}Ra, this calculation provides an upper estimate for both isotopes. Thus, the 3 cm upper section of these sediments was at least 5-fold higher than that required to distinguish the gradient.

Percolation of porewater from marshes

The radium activity in the marsh creek increased from 12 dpm 100 L^{-1} (^{224}Ra) and 0.60 dpm 100 L^{-1} (^{223}Ra) at high tide to 64.3 dpm 100 L^{-1} (^{224}Ra) and 4.07 dpm 100 L^{-1} (^{223}Ra) at low tide (Fig. II-6). There was no significant increase in ^{228}Ra or ^{226}Ra activities in the marsh creek between high and low tides (Fig. II-6). In addition, no consistent change in salinity was observed, suggesting that flow of fresh groundwater out of the marsh was not responsible for the enrichment of the short-lived isotopes.

The difference between high and low tide activities is assumed to be the amount of Ra supplied to the marsh creek during the immediately preceding tidal cycle. The mass flux of water is estimated as the product of water speed, channel width, and water depth. The total Ra flux from the marsh ($F_{Ra\ marsh}$, dpm per tidal cycle) is then calculated by summation of the products of water flux ($F_{marsh\ water}$, L h^{-1}), time elapsed between samples (t_{sample}, h), and excess Ra activity ($C_{Ra\ xs}$, dpm L^{-1}) for each time interval:

$$F_{Ra\ marsh} = (F_{marsh\ water} \times t_{sample} \times C_{Ra\ xs})_t + (F_{marsh\ water} \times t_{sample} \times C_{Ra\ xs})_{t+1} + \ldots(\ )_{t+n} \quad [4]$$

The area drained by the sample creek was estimated visually from aerial photographs. In cases in which it was unclear if a particular section of marshland drained into this creek or another, we assigned it to the creek we sampled (Fig. II-2). As a result, the drainage area is probably slightly overestimated. Dividing the total excess Ra flux by the area of marsh drained on one tidal cycle gives the marsh percolation flux in dpm m^{-2} per tidal cycle. The marsh flux we calculate is 5.82 dpm m^{-2} (^{223}Ra) and 91.8 dpm m^{-2} (^{224}Ra) of marsh surface per tidal cycle.

Desorption of Ra from resuspended particles

There is no natural surface input of fresh water to Jamaica Bay (except precipitation; Rubenstone, 2005; NYS DEP, 2006), and thus, no input of particles carrying surface-adsorbed Ra. However, scour of surficial sediments by tidal currents and waves may resuspend sediment into the water column. Before resuspension, production of desorbable ^{223}Ra and ^{224}Ra from surface-bound ^{228}Th and ^{227}Th can result in a significant inventory of sediment-associated Ra which can be desorbed after the

particles are resuspended. Our desorption experiment suggested that 4.0 ± 2.6 dpm ^{223}Ra and 67 ± 39 dpm ^{224}Ra can be desorbed per kilogram of sediment after resuspension. We have insufficient data to evaluate the input of long-lived Ra isotopes through this mechanism, but because regeneration of desorbable Ra is dependent on the half-life of each nuclide, it is probably negligible for ^{228}Ra and ^{226}Ra. Use of Ra-free water for the desorption experiment probably resulted in more Ra desorption than would occur in the natural setting, as bay water does initially contain a small amount of dissolved Ra. Thus, the results of this experiment represent an upper limit for Ra desorption from resuspended particles. There may also be a suspended particulate source of radiogenic Ra; however, this would be small compared to the desorbable fraction, and as we show the desorbable Ra to be negligible, radiogenic production is insignificant as well.

Ra in Jamaica Bay groundwater

Ra activities measured in 40 samples of shallow groundwater averaged 19 ± 13 dpm 100 L^{-1} (^{223}Ra), 494 ± 202 dpm 100 L^{-1} (^{224}Ra), 196 ± 61 dpm 100 L^{-1} (^{228}Ra, n=16), and 83 ± 39 dpm 100 L^{-1} (^{226}Ra, n=16). These activities were as much as two orders of magnitude higher than those found in the water column, and were comparable to the activities observed in fine-grained, subtidal sediment porewater. However, no consistent trend was observed with location in the bay or sample depth (Fig. II-7). This variability presents a problem when deciding on the appropriate endmember Ra activity for groundwater calculations, and collection of groundwater samples from a variety of sites did not substantially increase the precision of the average (Fig. II-8). In addition, although Ra activities generally increased with groundwater salinity, there was

considerable scatter in the data (Supporting Information, Fig. II-B). Although water samples collected from seepage meters may help identify the true SGD endmember, seepage samples were not collected for Ra analysis.

Seepage meters

Measurement of SGD with seepage meters yielded relatively uniform flow rates across six selected locations (Fig. II-9). Flow rates were generally low, averaging 3.2 ± 3.8 cm d^{-1}, although there is significant variability at every site. This variability appeared to be linked to tidally-driven variation in water height (Supp. Info. Fig. II-C). In most locations both positive and negative discharge (seawater intrusion) were seen. The low flow rates measured throughout Jamaica Bay precluded collection of seepage water for Ra analysis. Given the observed flow rates, little assurance could be had that the device would be completely flushed of ambient water; as well, the low flow rates yielded insufficient sample volumes for Ra analysis.

DISCUSSION

The difference between the total Ra export from the bay via ocean exchange and decay and input from the sources described above can reasonably be ascribed to submarine groundwater discharge. A comprehensive Ra mass balance can be used to assess the magnitude of this input. In order to examine Ra cycling in Jamaica Bay, we assume that the Ra observed in the water column during any season is at approximately steady state. Thus, the mass balance for Ra is

$$J_{out} + J_{decay} = J_{in} + J_{ww} + J_{diff} + J_{marsh} + J_{desorp} + J_{SGD}, \quad [5]$$

where:
J_{out} = Ra export during exchange of bay water with New York Harbor water,
J_{decay} = Ra loss via radioactive decay,
J_{in} = flux of Ra into Jamaica Bay from New York Harbor water,
J_{ww} = flux of Ra from wastewater,
J_{diff} = diffusive flux of Ra from sub- and inter-tidal sediments,
J_{marsh} = flux of Ra associated with percolation of porewater from marshes,
J_{desorp} = Ra desorbed from resuspended particles, and
J_{SGD} = Ra flux from submarine groundwater discharge.

Recirculation of seawater through permeable sediments (i.e. recharge) could potentially represent a sink for Ra in this system. Indeed, we will show such recirculation to be a major process, although we cannot evaluate the Ra export due to this mechanism. Regardless, Ra activities in the porewater were far in excess of those in the water column (e.g. ^{224}Ra: ~500 dpm 100 L^{-1} in groundwater, vs. 10-20 dpm 100 L^{-1} in surface water; Table II-2). Thus, the net result of seawater recirculation will be a source of Ra to the water column, not a sink.

Ra fluxes – Loss from bay

Radioactive decay

In an environment like Jamaica Bay, where water residence time is on the order of one week to one month (National Academy of Science and National Academy of Engineers, 1971; Swanson et al., 1992; Houghton et al., 2005), radioactive decay of short-lived nuclides can be an important removal process. Because of the relatively short residence time of the water, decay is not a significant loss term for the long-lived Ra isotopes.

Absent published volume estimates for Jamaica Bay, we used a value estimated from a high-resolution computer model (Table II-2; C.N. Flagg and R.E. Wilson, MSRC,

personal communication). The bay perimeter is demarcated arbitrarily at the Rockaway Bridge, which spans the western inlet at its narrowest region in Fig. II-1. The average bay volume is the low tide volume plus one-half the tidal prism volume. Here, we assume steady state conditions during each sampling period, and estimate the baywide decay as

$$J_{decay} = V_{bay} \times C_{bay} \times \lambda_{Ra}, \quad [6]$$

where C_{bay} is the average activity of Ra in the bay (dpm L^{-1}), λ_{Ra} is the decay constant of each nuclide (d^{-1}), and V_{bay} is the volume of the bay (L).

Ra loss via water exchange at Rockaway Inlet

The tidal exchange of Ra-enriched bay water with low activity water in New York Harbor (NYH) constitutes the other loss term of Ra from Jamaica Bay (Table II-3). We estimate this loss as

$$J_{out} = V_{out} \times C_{bay} \times 1.91, \quad [7]$$

where V_{out} is the tidal prism volume plus average daily water discharge from the four major WWTP in the bay (Table II-2), and 1.91 is the number of tidal cycles per day.

This calculation implies that wastewater is discharged to the bay, mixed rapidly with bay water, and lost through the bay mouth carrying the average bay Ra activity. It is more likely that the warm, fresh effluent is flushed from the bay more easily than saline water deep in basins such as Grassy Bay (the broad expanse of water bordering JFK Airport along the northwest border of Jamaica Bay). In addition, the largest wastewater input to JB (Coney Island treatment plant) discharges at the mouth of the bay (at the center of the inlet below "PB" in Fig. II-1; NYS DEP, 2006), and much of this wastewater is likely removed from the bay without being mixed with Ra-enriched bay

water. Thus, our estimate of Ra loss through the inlet is probably somewhat overestimated. Lastly, some of the water which leaves the inlet during ebb tide reenters during flood tide; that this occurs is evident in the relatively high ^{224}Ra activities observed in the saline endmember measured outside the inlet (5.79 ± 0.33 dpm 100 L^{-1}) compared to offshore values (e.g. <0.5 dpm 100 L^{-1}; Moore, 1998, 2000). This returning Ra is included as an input flux as described below.

Of the loss terms, radioactive decay accounts for 8% of the total ^{223}Ra loss from the bay, and 21% of the ^{224}Ra loss (Table II-3). However, this is a baywide average, and the local influence of decay is probably highly variable (i.e. much less important near the inlet than in regions of restricted flow at the far reaches of the bay). The remaining 92% and 79% (^{223}Ra and ^{224}Ra, respectively) of total Ra export from the bay is due to water exchange with NY Harbor (Table II-3). For ^{226}Ra and ^{228}Ra, loss via decay is negligible.

Ra fluxes – Input to bay

NY Harbor exchange

Ra input to JB from NYH water exchange is calculated as

$$J_{in} = V_{in} \times C_{ocean} \times 1.91, \quad [8]$$

where V_{in} is the tidal prism volume, C_{ocean} is the average Ra activity in the most saline, seaward samples, and 1.91 is the number of tidal cycles per day.

This gives a Ra input from NYH of 3.8 ± 0.8 ×10^8 dpm d^{-1} (^{223}Ra), 6.81 ± 0.4 ×10^9 dpm d^{-1} (^{224}Ra), 7.1 ± 2.1 ×10^9 dpm d^{-1} (^{228}Ra), and 8.5 ± 3.1 ×10^9 dpm d^{-1} (^{226}Ra). In order to put this and other input fluxes into perspective, we assume that the total Ra export from Jamaica Bay (see Sec. 4.1.) must be balanced by a number of input

pathways. Therefore, the total Ra export is balanced by total input. Hereafter, Ra fluxes into Jamaica Bay will be compared to the total export, but referred to as "percent total input". In this way, it is clear that exchange of water at the bay inlet comprises a significant proportion of the Ra flux into the bay, as ranges between different seasons were 24-57% for ^{223}Ra, 22-51% for ^{224}Ra, 31-62% for ^{228}Ra, and 52-81% for ^{226}Ra (Table II-3).

The assumption of a constant endmember value for the activity of incoming water may not necessarily be valid. Indeed, since much of the Ra in incoming water was discharged from the bay on the previous ebb tide, one would expect the near-shore "ocean" endmember to fluctuate to some degree with the average activities within the bay. This is most likely the reason for the negative values insinuated by the uncertainty in the Ra imbalance during the April cruise (Table II-3). Uncertainties are further discussed in later in this Chapter.

Ra flux from wastewater input

The activities of Ra measured in wastewater effluent from the 26th Ward WWTP were the lowest measured in any water sample from Jamaica Bay. We assume the dissolved Ra activities measured in this facility are representative of the remaining three WWTP. Ra activities of particulate matter in the WWTP were not measured. However, at reasonable particle concentrations in effluent, particulate phase activities should be similar to dissolved levels (on a volume-normalized basis; Parsa et al., 2004). Furthermore, the data points at low salinities in Fig. II-3 do not appear to show significant enrichment in Ra above values that would be expected for conservative

mixing between effluent and bay water. This suggests that desorption of Ra from particles entering Jamaica Bay from wastewater effluent is probably insignificant. Because the proportion of daily wastewater discharge to the tidal prism is approximately 1%, wastewater input of Ra should be negligible compared to inlet exchange. Wastewater input of Ra is given by

$$J_{ww} = F_{ww} \times C_{ww}, \quad [9]$$

where F_{ww} is the average daily water discharge from the four major WWTP in the bay, and C_{ww} is the Ra activities measured in effluent.

As expected, Ra fluxes from wastewater support only $0.006 \pm 0.002 \times 10^8$ dpm d^{-1} (^{223}Ra), $0.02 \pm 0.003 \times 10^9$ dpm d^{-1} (^{224}Ra), $0.02 \pm 0.008 \times 10^9$ dpm d^{-1} (^{228}Ra), and $0.04 \pm 0.04 \times 10^9$ dpm d^{-1} (^{226}Ra), generally less than 1% of the input for any Ra isotope to Jamaica Bay.

Diffusion of Ra from sediments

The diffusion experiments suggest that diffusion (and bioirrigation input) of Ra from fine-grained, subtidal sediments in Jamaica Bay occurs at a rate of 0.47 dpm m^{-2} h^{-1} (^{223}Ra) and 1.17 dpm m^{-2} h^{-1} (^{224}Ra). Thus, the baywide diffusive input is

$$J_{diff} = F_{diff} \times A_{sed}, \quad [10]$$

where F_{diff} is the experimentally determined diffusive flux (per unit area per day), and A_{sed} is the bay area submerged at low tide.

The total Ra flux from diffusion and bioirrigation is then $0.60 \pm 0.31 \times 10^8$ dpm d^{-1} (^{223}Ra) and $1.5 \pm 0.3 \times 10^9$ dpm d^{-1} (^{224}Ra). This represents 4-9% (^{223}Ra) and 5-11% (^{224}Ra) of the Ra input to the bay, with striking similarity between the two isotopes.

Modest variations in the flux estimates do not substantially affect these percentages. As well, our diffusive flux estimate uses a sediment surface area that includes both subtidal and intertidal regions, and in effect, is calculated for a 24 hour high tide. In other words, although diffusion occurs only when sediments are submerged, no correction has been made for the difference in areal coverage between high and low tides. Instead, we use a model-generated estimate of all the land that is covered by deeper than 5 cm water during an average high tide. This should be a significant overestimate, as the intertidal region comprises almost 43% of the area submerged at high tide. Although this is an important distinction for the individual flux, we will show it to be negligible in the general mass balance.

Ra supplied to bay waters by percolation of porewater from marshes

The relative importance of marshes to the Ra budget of the bay was assessed by monitoring the increase in Ra activities in water leaving a marsh creek during ebb tide. The total inventory of Ra leaving the marsh creek can be normalized to the marsh area to give a Ra flux per unit of marshland. Here, the baywide marsh flux is given by

$$J_{marsh} = A_{marsh} \times F_{marsh}, \quad [11]$$

where F_{marsh} is the Ra flux per unit marsh area, and A_{marsh} is the model-estimated bay area covered by five or fewer cm of water at high tide. The contribution of marshes to the Ra inventory of the bay is $0.51\times10^{8} \pm 0.13\times10^{8}$ dpm d^{-1} (^{223}Ra) and $0.80\times10^{9} \pm 0.2\times10^{9}$ dpm d^{-1} (^{224}Ra). This flux is 3-8% of the total ^{223}Ra input and 3-6% of the ^{224}Ra input.

It bears noting that our estimate of Ra flux from marshes was made only by observing the net Ra increase in creek waters during a half tidal cycle, and thus probably

includes some component of diffusion directly from the creek and bank sediment surfaces. The marsh creek flux per unit area is based on an estimate of marsh area drained by the creek used for sampling (3.9×10^4 m^2). If we approximate that the area covered by water increases constantly as the tide rises, the marsh area is under water for 6 hours during each tidal cycle. Applying our diffusive flux estimate, we can account for only 7.7% and 4.8% of the total observed marsh flux of ^{224}Ra and ^{223}Ra, respectively. This is probably an upper estimate, as the initial rising tide fills deep, steep-walled creek channels, and most of the marsh area coverage occurs later, near high tide. There is large uncertainty associated with this assessment, so we have not removed the diffusive component from the marsh flux. As well, we extrapolate our area-normalized marsh flux to all marsh surfaces in the bay, some of which is probably not flooded except in extreme events. Thus, the marsh flux estimate reported here represents an upper limit.

Ra desorption from resuspended particles

Desorption experiments suggest that ^{223}Ra and ^{224}Ra can be released from particle surfaces during resuspension of surface sediments (Table II-2). Combining the average concentration of total suspended solids (TSS; NYS DEP, 2003) with the bay volume gives the maximum amount of sediment which can be resuspended daily. In other words, the total inventory of suspended material in the bay is assumed to be newly resuspended from the bay floor. (No consideration is given to the importation of particles during water exchange with NY Harbor, as that particle-bound Ra should already be in equilibrium with the dissolved phase, and is accounted for in the dissolved flux estimate.) This particle inventory is then assumed to be exported from the bay and replaced by

newly resuspended material each day. Given that most of the Ra desorbs during the initial resuspension event (Webster et al., 1995), this approach should substantially overestimate the possible Ra input from desorption. Using this approach,

$$J_{desorp} = S_{sed} \times V_{bay} \times C_{sed}, \quad [12]$$

where ($S_{sed} \times V_{bay}$) is the maximum amount of sediment (g) resuspended daily (d^{-1}), and C_{sed} is the amount of Ra available for desorption from a quantity of sediment (dpm g^{-1}).

Although we likely use a large overestimation of particles resuspended daily, the desorption flux is only $0.13 \pm 0.09 \times 10^8$ dpm d^{-1} (^{223}Ra) and $0.23 \pm 0.13 \times 10^9$ dpm d^{-1} (^{224}Ra). This suggests that desorption can only provide 1-2% of the total ^{223}Ra or ^{224}Ra input, and as such, suspended sediments in Jamaica Bay provide an almost negligible contribution to the total dissolved ^{224}Ra and ^{223}Ra inventory.

Submarine Groundwater Discharge

There is a very large imbalance in Ra fluxes in Jamaica Bay; more than half of the total Ra entering the bay cannot be accounted for by the inputs detailed above (Table II-3). The significant excess of short-lived Ra observed in Jamaica Bay can reasonably be attributed to submarine groundwater discharge. Using the average Ra measured in shallow groundwater (Table II-2), the observed Ra excess can be converted to baywide groundwater input in unit volume per day.

$$F_{SGD} = J_{SGD} \times C_{GW}^{-1} \quad [13]$$

where J_{SGD} is the Ra flux due to submarine groundwater discharge (excess Ra flux), F_{SGD} is the submarine groundwater volume discharge, and C_{GW} is the activity concentration of dissolved Ra measured in shallow groundwater.

This gives estimates of SGD in Jamaica Bay ranging from 0.8 to 10.9 $\times 10^9$ L d^{-1}, depending on the season and isotope (Table II-4). Note that this groundwater comprises both fresh groundwater and recirculated seawater. On average, our estimates of SGD are about 30-fold higher than the 0.13×10^9 L d^{-1} discharge rate estimated by hydrologic modeling (Misut and Voss, 2004). This is consistent with other work suggesting that submarine groundwater discharge includes >90% recirculated seawater (e.g. Li et al., 1999).

The propagated uncertainty on SGD estimates for individual isotopes is high, from 60 to 250%. This uncertainty derives primarily from the ocean exchange term, as discussed below. However, for a given season, the SGD estimates using different Ra isotopes agree much better than the individual uncertainties would suggest (Table II-4).

Ra-estimated SGD rates also correspond well to direct measurements made with seepage meters. Normalized to the bay floor area, the calculated flow rates are 1.5 – 17 cm d^{-1}, almost exactly the range measured directly (Fig. II-9). In addition, seepage meter measurements suggest seasonal variability, with low rates in winter increasing to summer and declining again in autumn. This corresponds well to the trends observed in Ra distributions (Fig. II-10). In this case, Ra measurements from early September reflect summer discharge conditions, while mid-October Ra inventories are representative of autumn flow rates.

Uncertainty in the Ra mass-balance and SGD calculations

Major variability in Ra activities (concentrations) exists in most estuarine systems in both surface waters and groundwater. This usually causes substantial uncertainty in

the final SGD flux estimate, particularly when applying the 'flux by difference' approach (Charette et al., submitted). In the current instance, propagated uncertainties on the flux imbalance are approximately 30-200% (Table II-3). By examining the individual contributions to the final uncertainty, future work can selectively refine the sampling approach to improve the quality of the final SGD estimate. Table II-5 shows this analysis for the Ra mass balance.

It is clear that for the short-lived isotopes, the uncertainties are relatively uniform across the individual flux terms. For inputs, the least uncertainty originates with the minor wastewater flux, and the remainder increase in the following order: marsh flux < desorption < diffusion < ocean exchange. For the loss terms, decay introduces only a small portion of the final uncertainty, compared to water exchange. For the long-lived isotopes, most of the individual fluxes are negligible, and the only source of uncertainty is the ocean exchange term. Thus, for all isotopes, it is the exchange of bay and ocean water that introduces the most uncertainty in the flux difference.

Furthermore, despite the variability observed in Ra activities in the groundwater samples (Fig. II-8), the uncertainty on the average is only 14-71%. This is different for each isotope, with ^{223}Ra exhibiting the highest variability, and ^{228}Ra the least. Thus, the variability in the groundwater endmember is less than the uncertainty associated with ocean exchange. Future studies may benefit from this analysis by concentrating on accurately representing the exchange of Ra through an inlet (e.g. Charette et al., 2003), rather than focusing on determining the groundwater endmember with high precision (Crucius et al., 2006). Certainly, as we begin to understand the processes regulating the

groundwater concentrations of Ra isotopes (Gonneea et al., 2006), we will be able to further reduce the influence of variability in this endmember.

Application of Ra isotopes to Jamaica Bay residence time

Jamaica Bay residence time

A "retention time of about 35 days" was calculated for Jamaica Bay using unspecified, conservative tracers on the assumption that the pollution and freshwater sources were "near the head of the estuary" (National Academy of Sciences, 1971). On the basis of two dye studies done in Grassy Bay (the open water area between "HB" and "JoCo" in Fig. II-1), a "Grassy Bay bulk flushing time of approximately one week" was calculated (Houghton et al., 2005). Mathematical, hydrodynamic models have also been used to estimate residence time. One calculated the "age . . . of surface water mixing" to range up to 40 days, with locations in Grassy Bay appearing as between 25 and 35 days, while open water in the east side of the bay had calculated surface water ages of between 5 and 20 days (R. Isleib, HydroQual Inc., 2002 written communication as cited in Benotti et al., 2006). Modeled calculation of tidal prism and salinity lead to estimates of the residence time of 5.6 days and 11.8 days, respectively (R. Wilson, Marine Sciences Research Center, Stony Brook University, 2006, personal communication). The values in Table II-2 and an average salinity of 26.49 (measured in April 2006 - it was 25.61 in October 2004), yield a residence time of 1.4 days applying the tidal prism, and 33 days using the average salinity in April 2006 (38 days if we use the average, measured salinity in October 2004). A residence time of 1.4 days is essentially the same as our estimate

based solely on the Ra flux/inventory, both of which assume that no Ra that leaves the bay on the ebb tide, returns on the flood.

Residence time calculated with Ra isotopes

The age of individual water parcels can be estimated by observing the change in ratio between Ra isotopes of different half lives. If the primary source of dissolved Ra to the bay is SGD, and if the ratios of Ra isotopes in the groundwater endmember are relatively constant, then the apparent age of the water in each sample can be calculated following the approach of Moore et al. (2006):

$$T_w = [R_{SGD} - R_{surface}]/[R_{surface} \times \lambda_{Ra}] \quad [14]$$

Where T_w is the water age, R_{SGD} is the ratio of ^{224}Ra and ^{228}Ra in the SGD endmember, $R_{surface}$ is the same isotope ratio in the water column, and λ_{Ra} is the decay constant of ^{224}Ra.

Calculated ages for the different water samples from Jamaica Bay range from 1.2 to 21 d (Fig. II-11), consistent with the estimates described previously. Low ages occur at all salinity ranges, while long ages are present only in mid-salinity samples (Fig. II-11). Three water sources in Jamaica Bay have high ^{224}Ra:^{228}Ra ratios and young apparent ages: those affected by wastewater, ocean water, and SGD. All of these high ratio samples correspond to relative dissolved Ra concentrations of low, low, and high magnitudes, respectively.

It is interesting, though perhaps coincidental, that the samples which appear oldest (T_w > 10 d) are from areas of the bay that presumably have longer residence times (R. Isleib, HydroQual Inc., 2002, written communication as cited in Benotti et al., 2006).

These sub-regions are Grassy Bay (the large, open area at the north-east side of Jamaica Bay; Fig. II-1), and Thurston Basin (the large, semi-enclosed basin to the farthest east; Fig. II-1). A long residence time has been shown previously for Grassy Bay (Houghton et al., 2006), and it is reasonable also to imagine that the thick deposits of fine-grained sediments that underlay Grassy Bay would prevent any appreciable input from SGD. However, Thurston Basin actually had some of the highest Ra activities observed for the entire bay (Cochran et al., 2006). This suggests that the SGD endmember for this particular basin may actually have a lower ^{224}Ra:^{228}Ra ratio than elsewhere in the system. Consequently, using the isotope ratio approach fails to account for the otherwise self-evident input of SGD to this sub-region of the bay.

SGD calculation using Ra-estimated residence time

An average water residence time of 7.5 ± 5.1 days is calculated with the Ra isotope ratios. This can be combined with the observed excess ^{226}Ra inventory for each season to estimate the flux of ^{226}Ra due to SGD (after Charette et al., 2001; subscript notation as in Table II-2):

$$J_{SGD}^{226} = [(^{226}Ra_{Bay} - {}^{226}Ra_{ocean}) \times V_{Bay} \times T_w^{-1}] - {}^{226}Ra_{ww} \times F_{ww} \quad [15]$$

J_{SGD}^{226} in equation [15] can be expressed as:

$$J_{SGD}^{226} = F_{SGD} \times C_{GW} \quad [16]$$

Because the ^{226}Ra mass balance calculation also includes the excess inventories, the T_w-estimated SGD (Eq. 16) follows the same seasonal trend (Fig. II-12). However, the T_w-estimated flux is a factor of 2-10 lower, suggesting that either T_w is too large, or that the mass balance is incorrect. As discussed earlier, many of the largest T_w values are clearly

not correct ("Thurston Basin", Fig. II-11), as the isotope ratios do not reflect the SGD input necessary to account for the high observed activities. Consequently, it is more reasonable to doubt the T_w estimate, not the mass balance.

To approximately match the mass balance-estimated SGD flux, a residence time of ~1.5 days is required (Fig. II-12). Given that the tidal prism residence time is implicit in the mass balance calculation, this result is unsurprising. If 1.5 days is unrealistically low, then the mass balance-derived SGD is probably an overestimate. However, examination of Fig. II-12 also reveals that the slopes of the trends are below unity, suggesting that T_w is not constant for all four seasons. By back-calculating equation [15] with the mass balance-estimated values for J_{SGD}^{226}, T_w can be estimated for each season. To achieve a 1:1 relationship, residence times of 1.3, 1.9, 1.7, and 2.7 d are required for Sept. 2004, Oct. 2004, Sept. 2005, and Apr. 2006, respectively. Reasonable return flow factors (Moore et al., 2006) of 0, 0.50, and 0.75 would result in water residence times in Jamaica Bay of 1.4, 2.9, and 5.7 days, respectively (R. Wilson, 2006, pers. comm.). The magnitudes of back-calculated T_w are similar to reasonable estimates of return flow, suggesting that the mass balance estimate is relatively accurate.

Clearly, the mass balance approach provides a good method for circumventing the T_w requirement for calculating SGD. However, it is dependent on accurately quantifying the water exchange at the inlet. In other words, constraining the return flow factor (Moore et al., 2006) is critical for knowing the inlet exchange and determining an accurate residence time. Efforts to better quantify the inlet exchange have the doubly beneficial result of reducing the uncertainty on the mass balance estimate. Considering the issues associated with using the Ra isotopes to calculate T_w (and subsequently, SGD),

the best approach for using Ra as a tracer of SGD may be assessing the mass balance with careful attention to accurately characterizing the water exchange at the inlet.

Geochemical importance of SGD in Jamaica Bay

The groundwater discharge rates we calculate here are as much as 10-fold greater than the total wastewater effluent input. Because surface water inputs are negligible compared to wastewater, there are four pathways by which contaminants may enter Jamaica Bay: (1) wastewater (and other anthropogenic inputs such as combined sewer overflow events (CSOs), subway dewatering practices, and landfill leachate; Benotti et al., 2006), (2) direct atmospheric deposition, (3) ocean exchange and (4) submarine groundwater discharge. For a nutrient-type contaminant such as total dissolved inorganic nitrogen (tDIN = NO_x + NH_4), wastewater is the obvious major source. Here we assume that net ocean input is zero or negative. Known nitrogen inputs to Jamaica Bay are compiled in Table II-6 (Benotti et al., 2006).

Surficial groundwater profiles of total dissolved nitrogen (tDIN) in Jamaica Bay show significant variation with depth, and the elevated levels observed suggest that N is being regenerated during the remineralization of organic matter (Fig. II-13). Levels of tDIN in the near-surface (<20 cm) porewater are elevated relative to the overlying water, and have an average tDIN concentration of 43.9 ± 22 μM. Surface waters in the bay away from obvious wastewater influence average approximately 33 μM. Assuming that our estimates of SGD represent primarily recirculated seawater, then the flux of N associated with its discharge will be due to the ~10 μM enrichment in porewater relative

to surface water. Taking the average rate of groundwater discharge to be 4.4×10^{9} L d^{-1} (Table II-4), we estimate an SGD flux of dissolved N of 44,000 moles N per day.

Thus, in Jamaica Bay, the contribution of SGD to the nitrogen budget of the system is minor, representing only about 4% of the total input (Table II-6). This is similar to that estimated for the fresh groundwater input, and thus, subsurface fluid advection accounts for about 8% of the N input to the bay. The major input of DIN associated with wastewater discharge clearly, though not unexpectedly, dominates in this system.

Similar porewater analyses show dissolved Fe levels in our groundwater profiles as high as 0.15 mM (data not shown), indicating active redox cycling in the sediments. This may have a substantial effect on trace metal cycling within the bay through sequestration or release of dissolved metals (Huettel et al., 1998; Testa et al., 2002; Duncan and Shaw, 2003; Windom and Niencheski, 2003; Charette and Buessler, 2004; Snyder et al., 2004; Dalai et al., 2005; Charette and Sholkovitz, 2006; Bone et al., 2006a, 2006b). Future groundwater research in Jamaica Bay should be directed towards resolving the importance of SGD on trace metal budgets in the bay.

SUMMARY and CONCLUSIONS

A comprehensive mass balance has been constructed for short-lived Ra isotopes (^{223}Ra and ^{224}Ra), as well as the long-lived isotopes (^{226}Ra and ^{228}Ra), in Jamaica Bay, and individual budget components have been evaluated separately. The mass balance accounts for Ra export via radioactive decay and ocean exchange, and Ra input from marshes, diffusion from sediments, desorption from resuspended particles, and

wastewater discharge. A significant imbalance between input and export was observed for all isotopes: ^{223}Ra (22-67%), ^{224}Ra (31-71%), ^{226}Ra (19-47%), and ^{228}Ra (38-69%). This imbalance can be resolved by invoking a source from submarine groundwater discharge, which is saline and has elevated Ra activities.

The magnitude of individual short-lived Ra sources to the total bay budget indicates that the importance of each flux is similar between isotopes, and increases in significance in this order: wastewater discharge (<0.07%), desorption (<0.3%), percolation from marshes (3-10%), diffusion from submerged sediments (5-12%), ocean exchange (22-60%), and SGD (22-71%). For long-lived isotopes, the only significant terms are SGD and ocean exchange. Uncertainty associated with the estimation of this Ra input and loss at the Jamaica Bay inlet accounts for the major portion of the final uncertainty.

The magnitude of SGD in Jamaica Bay implied by dissolved excess Ra is about 0.8×10^{9} - 9×10^{9} L d^{-1}. Mass balance estimates of groundwater flow agree very well across isotopes (generally differing by less than a factor of 2). In addition, submarine groundwater discharge rates measured with seepage meters match closely to the rates estimated with Ra isotopes. This discharge rate is about 30 times greater than the estimated fresh groundwater input to the bay, and comprises primarily recirculated seawater.

Because of the magnitude of SGD in Jamaica Bay, its associated chemical transport may be important in regulating the health and productivity of the ecosystem. However, we show that for nitrogen, SGD supplies only a minor portion (~4%) of the total input. This small percentage is certainly due to the major wastewater input that

dominates the nitrogen budget in the bay. Despite the minor relative contribution of inorganic nitrogen to the bay, the fact that SGD substantially enriches bay waters with Ra suggests it may play the same role for similar chemical constituents such as Ba, Sr, and trace metals. Considering the declining health of many marshes in Jamaica Bay, future work should assess the importance of SGD-associated chemical transport to ecosystem processes in the bay.

ACKNOWLEDGEMENTS

This research was supported by New York Sea Grant (project R/CTP-40) and A. Beck was supported by a Sea Grant Scholarship. We thank W. Moore and two anonymous reviewers for their comments. Sampling assistance, logistical support, and miscellaneous equipment was provided by M. Benotti, D. Hirschberg, R. Flood, and G. Davis. We are also indebted to Dr. A. DiLernia for his gracious loan of dock space at Kingsborough Community College.

REFERENCES

Benotti M.J., P.E. Misut, M. Abbene, and S.A. Terracciano, 2006. Historic Nitrogen Loading in Jamaica Bay, Long Island, New York: predevelopment to 2005. USGS Open File Report SIR 2007-5051.

Berner, R. A., 1980. *Early diagenesis: A theoretical approach*. Princeton.

Bird, F.L., P.W. Ford, G.J. Hancock, 1999. Effect of burrowing macrobenthos on the flux of dissolved substances across the water-sediment interface. Mar. Freshwater Res., 50: 523-532

Black, F.R., 1981. *Jamaica Bay – A History*. Washington, D.C.: Cultural Resource Study 3, Division of Cultural Resources, North Atlantic Regional Office, National Parks Service of the U.S. Department of the Interior. 113 pp.

Bollinger, M. S., and W. S. Moore. 1984. Radium fluxes from a salt marsh. Nature, 309: 444-446.

Bollinger, M.S. and W.S. Moore, 1993, Evaluation of salt marsh hydrology using radium as a tracer. Geochimica et Cosmochimica Acta, 57: 2203-2212.

Bone, S.E., M.E. Gonneea, M.A. Charette, 2006a. Geochemical cycling of arsenic in a coastal aquifer. Environ. Sci. Technol., 40: 3273-3278.

Bone, S., Lamborg, C., Gonneea, M.E., Charette, M, 2006b. Biogeochemical Cycling of As and Hg in a Subterranean Estuary. Eos Trans. AGU, 87(36), Ocean Sci. Meet. Suppl., Abstract OS26B-20

Burnett, W.C. and H. Dulaiova, 2003. Estimating the dynamics of groundwater input into the coastal zone via continuous radon-222 measurements. Journal Environmental Radioactivity, 69: 21-35.

Burnett, WC, HJ Bokuniewicz, M Huettel, WS Moore, and M Taniguchi. 2003. Groundwater and pore water inputs to the coastal zone. Biogeochemistry, 66: 3-33.

Busciolano, R., 2002. Water Table and the Potentiometric-Surface Altitudes of the Upper Glacial, Magothy and Lloyd Aquifers on Long Island, New York, in March-April 2000, with a Summary of Hydrogeologic Conditions. Water-Resources Investigations Report 01-4165, United States Geological Survey.

Cable, J.E., W.C. Burnett, J.P. Chanton, and G.L. Weatherly, 1996. Estimating groundwater discharge into the northeastern Gulf of Mexico using radon-222. Earth and Planetary Science Letters, 144 (3-4): 591-604.

Capone, D.G. and M.F. Bautista, 1985. A groundwater source of nitrate in nearshore marine sediments. Nature, 313: 214 – 216.

Capone, D.G. and J.M. Slater, 1990. Interannual Patterns of Water Table Height and Groundwater Derived Nitrate in Nearshore Sediments. Biogeochemistry, 10 (3): 277-288.

Charette, M.A., K.O. Buesseler, and J.E. Andrews, 2001. Utility of radium isotopes for evaluating the input and transport of groundwater-derived nitrogen to a Cape Cod estuary. Limnology and Oceanography, 46: 465-470.

Charette, M.A., R. Splivallo, C. Herbold, M. Bollinger, and W.S. Moore, 2003. Salt marsh submarine groundwater discharge as traced by radium isotopes. Marine Chemistry, 84: 113-121.

Charette M.A., K.O. Buesseler, 2004. Submarine groundwater discharge of nutrients and copper to an urban subestuary of Chesapeake Bay (Elizabeth River). Limnology and Oceanography, 49 (2): 376-385.

Charette, M.A., M.C. Allen, 2006. Precision groundwater sampling in coastal aquifers using a direct push shielded screen well-point system. Groundwater Monitoring & Remediation, 26 (2): 87-93.

Charette, M.A., E.R. Sholkovitz, 2006. Trace element cycling in a subterranean estuary: Part 2. Geochemistry of the pore water. Geochimica et Cosmochimica Acta, 70 (4): 811-826.

Charette, M.A., W.S. Moore, W.C. Burnett, Submitted. Uranium- and thorium-series nuclides as tracers of submarine groundwater discharge. In *Radioactivity in the Environment: U-Th Series Nuclides in Aquatic Systems*.

Cochran, J.K. and S. Krishnaswami, 1980. Radium, thorium, uranium, and Pb-210 in deep-sea sediments and sediment pore waters from the North Equatorial Pacific. American Journal of Science, 280 (9): 849-889.

Cochran, J.K., H. Feng, D. Amiel, A. Beck, 2006. Natural radionuclides as tracers of coastal biogeochemical processes. J. Geochem. Exploration, 88: 376-379.

Crusius, J., Trescott, A., Bratton, J., Giblin, A., Koopmans, D., 2006. Strengths and limitations of groundwater discharge estimates based on radon and radium isotopes: An example from a small Massachusetts estuary. Eos Trans. AGU, 87(36), Ocean Sci. Meet. Suppl., Abstract OS15B-04

D'Elia, C.F., K.L. Webb, J.W. Porter, 1981. Nitrate-rich groundwater inputs to Discovery Bay, Jamaica – A significant source of N to local coral reefs. Bulletin of Marine Science, 31 (4): 903-910.

Dalai, T.K., K. Nishimura, and Y. Nozaki, 2005. Geochemistry of molybdenum in the Chao Phraya River estuary, Thailand: Role of suboxic diagenesis and porewater transport. Chemical Geology, 218: 189-202.

Duncan, T. and T.J. Shaw, 2003. The mobility of REE and RSE in the groundwater/seawater mixing zone of a shallow coastal aquifer. Aquat. Geochem., 9: 233-255.

Elsinger, R. J., and W. S. Moore, 1983. 224Ra, 228Ra, and 226Ra in Winyah Bay and Delaware Bay. Earth Planet. Sci. Lett., 64: 430-436.

Englebright, S., 1975. Jamaica Bay: A case study of geo-environmental stress. NYS Geological Association Guidebook, 47th Annual Meeting. pp. 279-291.

Epler, N., 1991. A multiple tracer study of ground water from a shallow, unconfined aquifer. Ph.D. Thesis, Marine Sciences Research Center, Stony Brook University, Stony Brook, NY, unpublished.

Ferguson, P.L., C.R. Iden, and B.J. Brownawell, 2001. Distribution and fate of alkylphenol ethoxylate metabolites in a sewage-impacted urban estuary. Environ. Sci. Technol., 35: 2428-2435.

Flegal, A.R., Smith, G.J., Gill, G.A., Sañudo-Wilhelmy, S.A., Anderson, L.C.D., 1991. Dissolved trace element cycles in the San Francisco estuary. Mar. Chem., 36: 329–363.

Gobler, C.J. and S.A. Sañudo-Wilhelmy, 2001 Temporal variability of groundwater seepage and Brown Tide Blooms in a Long Island Embayment. Marine Ecology Progress Series 217: 299-309

Gonneea, M.E., Charette, M., Mulligan, A., 2006. Seasonal Trends in Radium Activities Within the Mixing Zone of a Subterranean Estuary, Waquoit Bay, MA. Eos Trans. AGU, 87(36), Ocean Sci. Meet. Suppl., Abstract OS15B-01.

Houghton, R., A. Gordon, and B. Huber., (2005) Dye tracer experiments in Jamaica Bay. In: Integrated Reconnaissance of the Physical and Biogeochemical Characteristics of Jamaica Bay: Initial Activity Phase. A Coordinated Program of the Gateway National Recreational Area and the Columbia Earth Institute. pp. 51-53.

Huettel, M., W. Ziebis, S. Forster, and G.W. Luther III, 1998. Advective transport affecting metal and nutrient distributions and interfacial fluxes in permeable sediments. Geochimica et Cosmochimica Acta, 62 (4): 613–631.

Hwang, D.W., Kim, G.B., Lee, Y.W., Yang, H.S., 2005. Estimating submarine inputs of groundwater and nutrients to a coastal bay using radium isotopes. Marine Chemistry, 96 (1-2): 61-71.

Johannes, R.E., 1980. The ecological significance of the submarine discharge of groundwater. Mar. Ecol. Prog. Ser., 3: 365-373.

Kelly, R.P., Moran, S.B., 2002. Seasonal changes in groundwater input to a well-mixed estuary estimated using radium isotopes and implications for coastal nutrient budgets. Limnology and Oceanography, 47 (6): 1796-1807.

Krest, J.M., W.S. Moore, L.R. Gardner, AND J.T. Morris, 2000. Marsh nutrient export supplied by groundwater discharge: Evidence from radium measurements. Global Biogeochemical Cycles, 14 (1): 167-176.

Lee, DR., 1977. A device for measuring seepage flux in lakes and estuaries. Limnol. Oceanogr., 22 (1): 140-147.

Li, Y.-H., G. Mathieu, P. Biscaye and H.J. Simpson, 1977. The flux of 226Ra from estuarine and continental shelf sediments. Earth and Planetary Science Letters, 37 (2): 237-241.

Li, L., Barry, A., Stagnitti, F., and Parlange, J-Y., 1999. Submarine groundwater discharge and associated chemical input to a coastal sea. Water Resources Research, 35 (11): 3253-3259.

Libelo, E. L., and W. G. MacIntyre, 1994. Effects of surfacewater movement on seepage-meter measurements of flow through the sediment-water interface. Appl. Hydrogeol., 2: 49-54.

Misut, P.E., and Voss, C.I., 2004. Simulation of subsea discharge to Jamaica Bay in New York City with a three-dimensional, variable density, finite-element model. In: Finite Element Models, MODFLOW, and More: Solving Groundwater Problems, Koval-Hrkal-Bruthans (eds.) pp. 391-394.

Moore, W.S. and D.F. Reid, 1973. Extraction of radium from natural waters using manganese-impregnated acrylic fibers. Journal of Geophysical Research 78 (36): 8880-8886

Moore, W.S., 1976. Sampling Ra-228 in the deep ocean. Deep-Sea Res., 23 (7): 647-651.

Moore, W.S., 1996. Large groundwater inputs to coastal waters revealed by Ra-226 enrichments. Nature, 380 (6575): 612-614.

Moore, W.S., Arnold, R., 1996. Measurement of Ra-223 and Ra-224 in coastal waters using a delayed coincidence counter. J Geophys. Res. - Oceans, 101 (C1): 1321-1329.

Moore, W.S., 1998. Application of Ra-226, Ra-228, Ra-223, and Ra-224 in coastal waters to assessing coastal mixing rates and groundwater discharge to oceans. P. Indian As-Earth, 107 (4): 343-349.

Moore, W.S., 1999. The subterranean estuary: a reaction zone of ground water and sea water. Marine Chemistry, 65 (1-2): 111-125.

Moore, W.S., 2000. Determining coastal mixing rates using radium isotopes. Cont. Shelf Res., 20 (15): 1993-2007.

Moore, W.S., J.O. Blanton, S.B. Joye, 2006. Estimates of flushing times, submarine groundwater discharge, and nutrient fluxes to Okatee Estuary, South Carolina. J. Geophys. Res., 111, C09006, doi:10.1029/2005JC003041.

NYS DEP, 2003. New York State Department of Environmental Protection: New York Harbor Water Quality Report. 60 pp.

NYS DEP, 2006. New York State Department of Environmental Protection: Jamaica Bay Watershed Protection Plan – Interim Report (September 1, 2006) 57 pp.

National Academy of Science and National Academy of Engineers, 1971. Jamaica Bay and Kennedy Airport. Report of the Jamaica Bay Environmental Study Group, Vol. II. Port Authority of New York and New Jersey. 149 pp.

Parsa, B., R.N. Obed, W.K. Nemeth, G. Suozzo, 2004. Concurrent determination of 224Ra, 226Ra, 228Ra, and unsupported 212Pb in a single analysis for drinking water and wastewater: dissolved and suspended fractions. Health Physics, 86 (2):145-149.

Parsons, T.R., Maita, Y., Lalli, C.M., 1984. *A Manual of Chemical and Biological Methods for Seawater Analysis*. Pergamon Press.

Rama, Moore, W.S., 1996. Using the radium quartet for evaluating groundwater input and water exchange in salt marshes. Geochim. Cosmochim. Acta, 60 (23): 4645-4652.

Reid, D.F., R.M. Key, D.R Schink, 1979. Radium, thorium, and actinium extraction from seawater using an improved manganese-oxide-coated fiber. Earth Planet. Sci. Lett., 43 (2): 223-226.

Rubenstone, J., 2002. Stable Isotope Evidence for Water Mass Mixing in Jamaica Bay. Chapter 1 in: Jamaica Bay Ecosystem Research and Restoration Team (JABERRT) Final Report, Vol. 1.

Sañudo-Wilhelmy, S.A., and G.A. Gill, 1999. Impact of the Clean Water Act on the Levels of Toxic Metals in Urban Estuaries: The Hudson River Estuary Revisited. Environ. Sci. Technol., 30 (20): 3477-3481.

Shaw, T. J., Moore, W. S., Kloepfer, J. and Sochaski, M., 1998. The flux of barium to the coastal waters of the southeastern United States: The importance of Submarine Groundwater Discharge. Geochim. Chosmochim. Acta, 62, 1277–1283.

Snyder, M., M. Taillefert and C.D. Ruppel, 2004. Redox zonation at the saline-influenced boundaries of a permeable surficial aquifer: effects of physical forcing on the biogeochemical cycling of iron and manganese. Journal of Hydrology, 296: 164-178.

Swanson, R.L., West-Valle, A.S., and Decker, C.J., 1992. Recreation vs. Waste Disposal: The Use and Management of Jamaica Bay: Long Island History Journal, 5 (1): 21-24.

Talbot, J.M., K.D. Kroeger, A. Rago, M.C. Allen, M.A. Charette, 2003. Nitrogen flux and speciation through the subterranean estuary of Waquoit Bay, Massachusetts. Biological Bulletin, 205: 244-245.

Testa, J.M., M.A. Charette, E.R. Sholkovitz, M.C. Allen, A. Rago, C.W. Herbold, 2002. Dissolved iron cycling in the subterranean estuary of a coastal bay: Waquoit Bay, Massachusetts. Biological Bulletin, 203: 255-256.

Webster, I.T., G.J. Hancock, and A.S. Murray, 1995. Modeling the effect of salinity on radium desorption from sediments. Geochim. Cosmochim. Acta, 59 (12): 2469-2476.

Wilson, A.M. and L.R. Gardner, 2006. Tidally driven groundwater flow and solute exchange in a marsh: Numerical simulations. Water Resource Research, 42, W01405, doi:10.1029/2005WR004302.

Windom, H., and F. Niencheski, 2003. Biogeochemical processes in a freshwater–seawater mixing zone in permeable sediments along the coast of Southern Brazil. Marine Chemistry, 83: 121–130.

Yang, H.-S., D.-W. Hwang, and G. Kim, 2002. Factors controlling excess radium in the Nakdong River estuary, Korea: submarine groundwater discharge versus desorption from riverine particles. Marine Chemistry, 78: 1–8.

TABLES and FIGURES

Cruise	$^{224}Ra_{xs}$	$^{223}Ra_{xs}$	$^{228}Ra_{xs}$	$^{226}Ra_{xs}$	$^{224}Ra_{xs}/^{228}Ra_{xs}$	$^{223}Ra_{xs}/^{228}Ra_{xs}$	$^{228}Ra_{xs}/^{226}Ra_{xs}$
Sep-04	15.1 ± 7.9	0.97 ± 0.46	14.9 ± 4.5	9.9 ± 2.8	1.01 ± 0.84	0.065 ± 0.051	1.51 ± 0.88
Oct-04	7.9 ± 3.9	0.50 ± 0.20	10.8 ± 5.1	7.8 ± 0.5	0.73 ± 0.71	0.046 ± 0.040	1.38 ± 0.74
Sep-05	12.7 ± 6.3	0.76 ± 0.32	12.2 ± 3.3	7.5 ± 2.1	1.04 ± 0.8	0.062 ± 0.043	1.63 ± 0.90
Apr-06	3.4 ± 5.7	0.27 ± 0.22	5.3 ± 2.9	4.1 ± 2.0	0.64 ± 1.4	0.051 ± 0.069	1.29 ± 1.34

Table II-1. Average excess Ra activities in the JB water column (dpm 100 L^{-1}) and isotopic ratios.

	General bay parameters		Units
F_{ww}	Wastewater discharge	7.46×10^8	L d^{-1}
A_{sed}	Subtidal surface area	5.36×10^7	m^2
A_{marsh}	Marsh area	4.49×10^6	m^2
S_{sed}	Suspended solids	0.02	g L^{-1}
V_{in}	Tidal prism	6.06×10^{10}	L
V_{bay}	Bay volume	1.68×10^{11}	L
F_{SGD}	SGD	**?**	L d^{-1}

	Ra terms*	^{224}Ra	^{223}Ra	^{228}Ra	^{226}Ra	
C_{ww}	Wastewater effluent	2.21 ± 0.28 (3)[a]	0.06 ± 0.02 (3)	2.1 ± 0.8 (2)	3.9 ± 4.3 (2)	dpm 100 L^{-1}
F_{diff}	Diffusive flux	28.1 ± 5.8	1.12 ± 0.58	[b]	[b]	dpm m^{-2} d^{-1}
F_{marsh}	Percolation from marsh	91.8 ± 23.0	5.8 ± 1.5	[b]	[b]	dpm m^{-2} $tide^{-1}$
C_{desorp}	Desorbable Ra	67 ± 39 (4)	4.0 ± 2.6 (4)	[b]	[b]	dpm kg^{-1}
C_{ocean}	Ocean endmember	5.79 ± 0.33 (4)	0.32 ± 0.07 (4)	7.9 ± 3.5 (3)	7.7 ± 2.0 (3)	dpm 100 L^{-1}
C_{gw}	Groundwater	494 ± 202 (40)	19 ± 13 (40)	196 ± 61 (16)	83.2 ± 38.7 (16)	dpm 100 L^{-1}
C_{Bay}	Water column averages					
	Sept 2004	20.7 ± 7.9 (15)	1.22 ± 0.45 (15)	19.4 ± 4.4 (5)	14.8 ± 2.6 (5)	dpm 100 L^{-1}
	Oct 2004	13.1 ± 3.8 (23)	0.74 ± 0.2 (23)	15.1 ± 5.1 (3)	12.1 ± 0.5 (3)	dpm 100 L^{-1}
	Sept 2005	17.8 ± 6.1 (11)	0.99 ± 0.31 (11)	16.6 ± 3.2 (6)	12.0 ± 1.9 (6)	dpm 100 L^{-1}
	Apr 2006	8.9 ± 5.6 (31)	0.51 ± 0.21 (31)	9.8 ± 3.1 (16)	8.9 ± 2.3 (16)	dpm 100 L^{-1}

[a] Values in parentheses indicate the number of samples on which the average is based.
[b] None detected for long-lived isotopes.

Table II-2. Values used to calculate Ra fluxes into Jamaica Bay.

		Fluxes into JB (10^9 dpm d^{-1})					
	Cruise	Wastewater	Diffusion	Marsh flux	Desorption	Ocean exchange	Sum input
^{224}Ra	Sept 2004	0.02 ± 0.003	1.50 ± 0.30	0.80 ± 0.13	0.23 ± 0.13	6.81 ± 0.4	**9.36 ± 0.5**
	Oct 2004	"	"	"	"	"	"
	Sept 2005	"	"	"	"	"	"
	Apr 2006	"	"	"	"	"	"
^{223}Ra	Sept 2004	0.0006 ± 0.0004	0.06 ± 0.03	0.05 ± 0.02	0.013 ± 0.009	0.38 ± 0.8	**0.50 ± 0.09**
	Oct 2004	"	"	"	"	"	"
	Sept 2005	"	"	"	"	"	"
	Apr 2006	"	"	"	"	"	"
^{228}Ra	Sept 2004	0.02 ± 0.008	[c]	[c]	[c]	7.1 ± 2.1	**7.1 ± 2.1**
	Oct 2004	"	[c]	[c]	[c]	"	"
	Sept 2005	"	[c]	[c]	[c]	"	"
	Apr 2006	"	[c]	[c]	[c]	"	"
^{226}Ra	Sept 2004	0.04 ± 0.04	[c]	[c]	[c]	8.5 ± 3.1	**8.5 ± 3.1**
	Oct 2004	"	[c]	[c]	[c]	"	"
	Sept 2005	"	[c]	[c]	[c]	"	"
	Apr 2006	"	[c]	[c]	[c]	"	"

[c] Flux negligible or not able to be determined for long-lived isotopes.

Table II-3. Individual Ra fluxes in Jamaica Bay. The difference between the known sources and sinks is listed at the right-had side of the continued table on the following page; this excess Ra flux is presumably due to submarine groundwater discharge.

		Fluxes out of JB (10^9 dpm d^{-1})			
	Cruise	**Ocean exchange**	**Decay**	**Sum removal**	**Flux imbalance (10^9 dpm d^{-1})**
^{224}Ra	Sept 2004	24.5 ± 9.3	6.62 ± 2.5	**31.1 ± 9.7**	**21.8 ± 9.7**
	Oct 2004	15.5 ± 4.5	4.19 ± 1.2	**19.7 ± 4.7**	**10.4 ± 4.7**
	Sept 2005	21.1 ± 7.3	5.70 ± 2.0	**26.8 ± 7.5**	**17.5 ± 7.6**
	Apr 2006	10.5 ± 6.7	2.83 ± 1.8	**13.3 ± 6.9**	**4.0 ± 6.9**
^{223}Ra	Sept 2004	1.44 ± 0.54	0.12 ± 0.05	**1.57 ± 0.54**	**1.07 ± 0.54**
	Oct 2004	0.88 ± 0.23	0.076 ± 0.02	**0.95 ± 0.23**	**0.45 ± 0.25**
	Sept 2005	1.17 ± 0.37	0.101 ± 0.032	**1.27 ± 0.37**	**0.77 ± 0.38**
	Apr 2006	0.61 ± 0.25	0.052 ± 0.022	**0.66 ± 0.26**	**0.16 ± 0.27**
^{228}Ra	Sept 2004	23.0 ± 5.2	[c]	**23.0 ± 5.2**	**15.7 ± 5.6**
	Oct 2004	17.9 ± 6.1	[c]	**17.9 ± 6.1**	**10.8 ± 6.4**
	Sept 2005	19.7 ± 3.8	[c]	**19.7 ± 3.8**	**13.3 ± 5.9**
	Apr 2006	11.6 ± 3.7	[c]	**11.6 ± 3.7**	**4.3 ± 4.3**
^{226}Ra	Sept 2004	17.5 ± 3.1	[c]	**17.5 ± 3.1**	**7.6 ± 3.3**
	Oct 2004	14.3 ± 0.6	[c]	**14.3 ± 0.6**	**5.8 ± 3.1**
	Sept 2005	14.7 ± 2.3	[c]	**14.7 ± 2.3**	**5.1 ± 4.3**
	Apr 2006	10.5 ± 2.7	[c]	**10.5 ± 2.7**	**2.1 ± 4.2**

[c] Flux negligible or not able to be determined for long-lived isotopes.

Table II-3, continued.

	Sep-04	*Oct-04*	*Sep-05*	*Apr-06*
^{224}Ra	4.4 ± 3.8	2.1 ± 1.8	3.5 ± 3.0	0.8 ± 1.7
^{223}Ra	5.7 ± 7.0	2.4 ± 3.1	4.1 ± 5.0	0.8 ± 2.0
^{228}Ra	8.1 ± 5.4	5.5 ± 5.0	6.4 ± 4.2	2.3 ± 2.9
^{226}Ra	10.9 ± 10.3	7.0 ± 7.0	6.9 ± 7.8	2.5 ± 6.1
Average	7.3 (2.9)	4.3 (2.4)	5.3 (1.8)	1.6 (0.9)

Table II-4. Groundwater flow rates ($\times 10^9$ L d^{-1}) calculated using the different Ra isotopes. "Average" denotes the average SGD calculated across all isotopes for a single season; the number in parenthesis is simply the standard deviation of that average.

	^{224}Ra	^{223}Ra	^{228}Ra	^{226}Ra
Wastewater	0	0	0	1
Diffusion	32	21	0	0
Marsh flux	13	16	0	0
Desorption	14	6	0	0
Ocean exchange in	41	57	100	99
Total	*100*	*100*	*100*	*100*
Ocean exchange out	79	92	100	100
Decay	21	8	0	0
Total	*100*	*100*	*100*	*100*

Table II-5. Proportion of final uncertainty (on the Ra flux imbalance) originating with individual fluxes.

Source[1]	Load	Flux %
Wastewater discharge	100.0 ± 8.7	85.3
CSO events/storm-water discharge	1.7	1.5
Subway dewatering	1.6 ± 0.1	1.4
Landfill leachate	1.9	1.6
Fresh groundwater discharge	4.9 ± 0.4	4.2
Atmospheric deposition	2.6	2.2
Submarine Groundwater Discharge	4.4	3.8

[1] All N fluxes except SGD are from Benotti et al., 2006

Table II-6. Dissolved inorganic nitrogen fluxes to Jamaica Bay (10^4 mol d^{-1}).

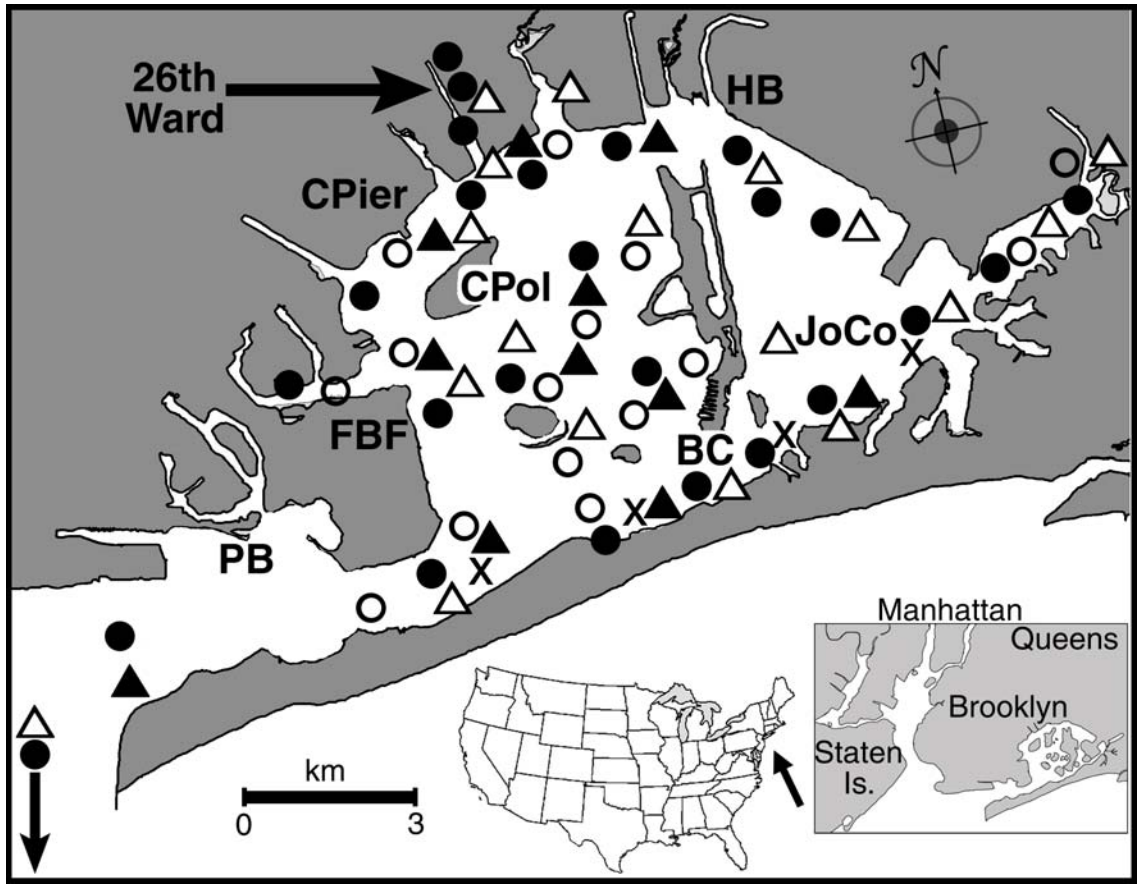

Figure II-1. Map of Jamaica Bay. Inset shows Bay location relative to United States and New York City. Water column sample sites for all cruises are indicated; symbols indicate Aug 2004 (crosses), Sept 2004 (hollow circles), Oct 2004 (filled circles), Sept 2005 (filled triangles), and Apr 2006 (hollow triangles). Shallow groundwater sample sites are noted in large, boldface font; the site codes are (PB) Plumb Beach, (FBF) Floyd Bennett Field, (CPol) Canarsie Pol, (CPier) Canarsie Pier, (HB) Howard Beach, (BC) Broad Channel. The large, boldface font label "JoCo" indicates the approximate location on JoCo Marsh of marsh creek sampling and sediment coring. The large font label and arrow identify the location and effluent outfall of the 26th Ward wastewater treatment plant.

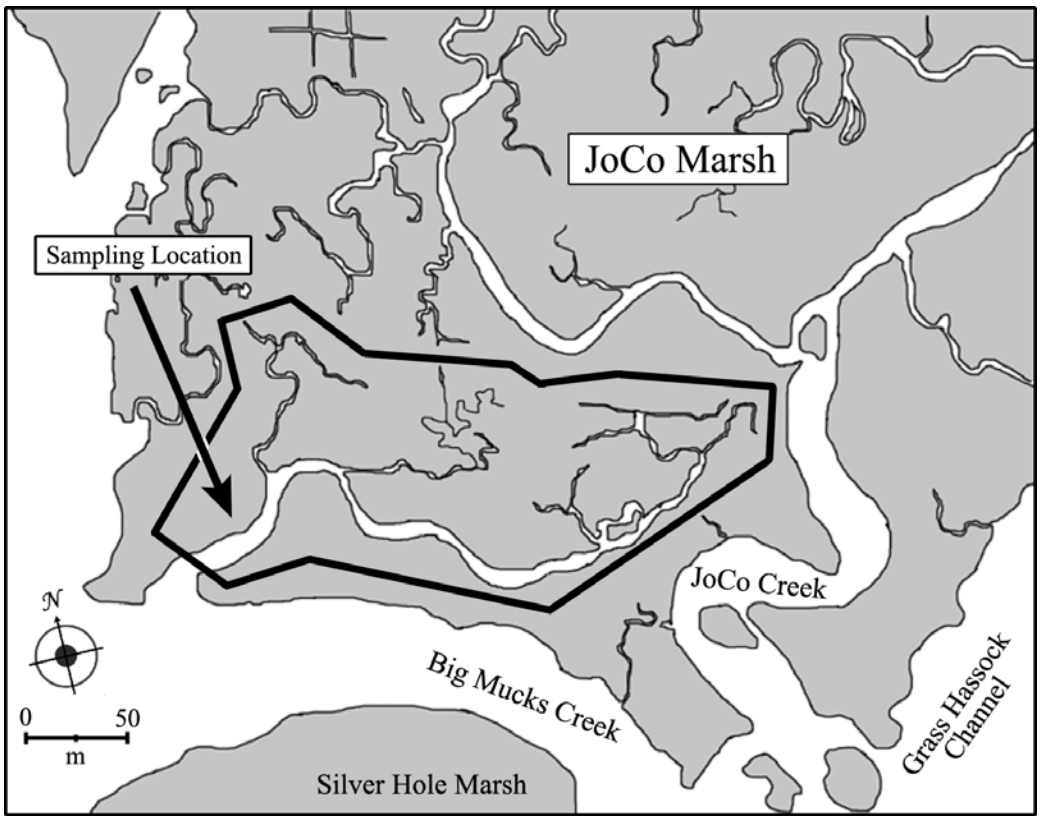

Figure II-2. Location of creek sampling on JoCo Marsh. Drainage area was estimated to be approximately the region encircled by the heavy black outline.

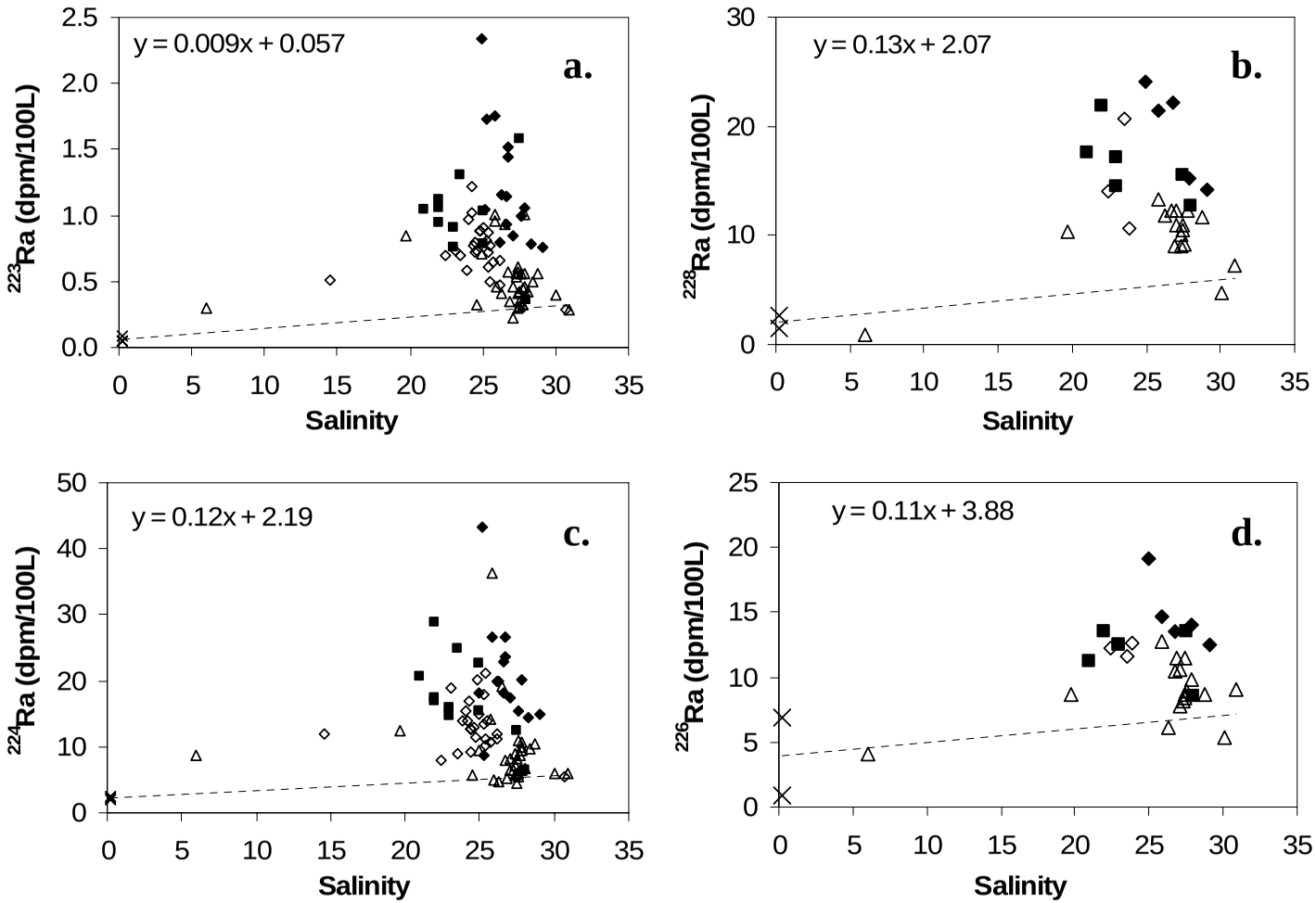

Figure II-3. Ra activities in water column samples from Jamaica Bay, (a) ^{223}Ra, (b) ^{228}Ra, (c) ^{224}Ra, (d) ^{226}Ra. Symbols are as follows: solid diamonds indicate Sept. 2004 cruise, hollow circles indicate Oct. 2004, solid squares indicate Sept. 2005, hollow triangles indicate April 2006, and crosses indicate wastewater effluent. The dashed line and equation represent conservative mixing between wastewater and ocean endmembers. (See text for discussion.)

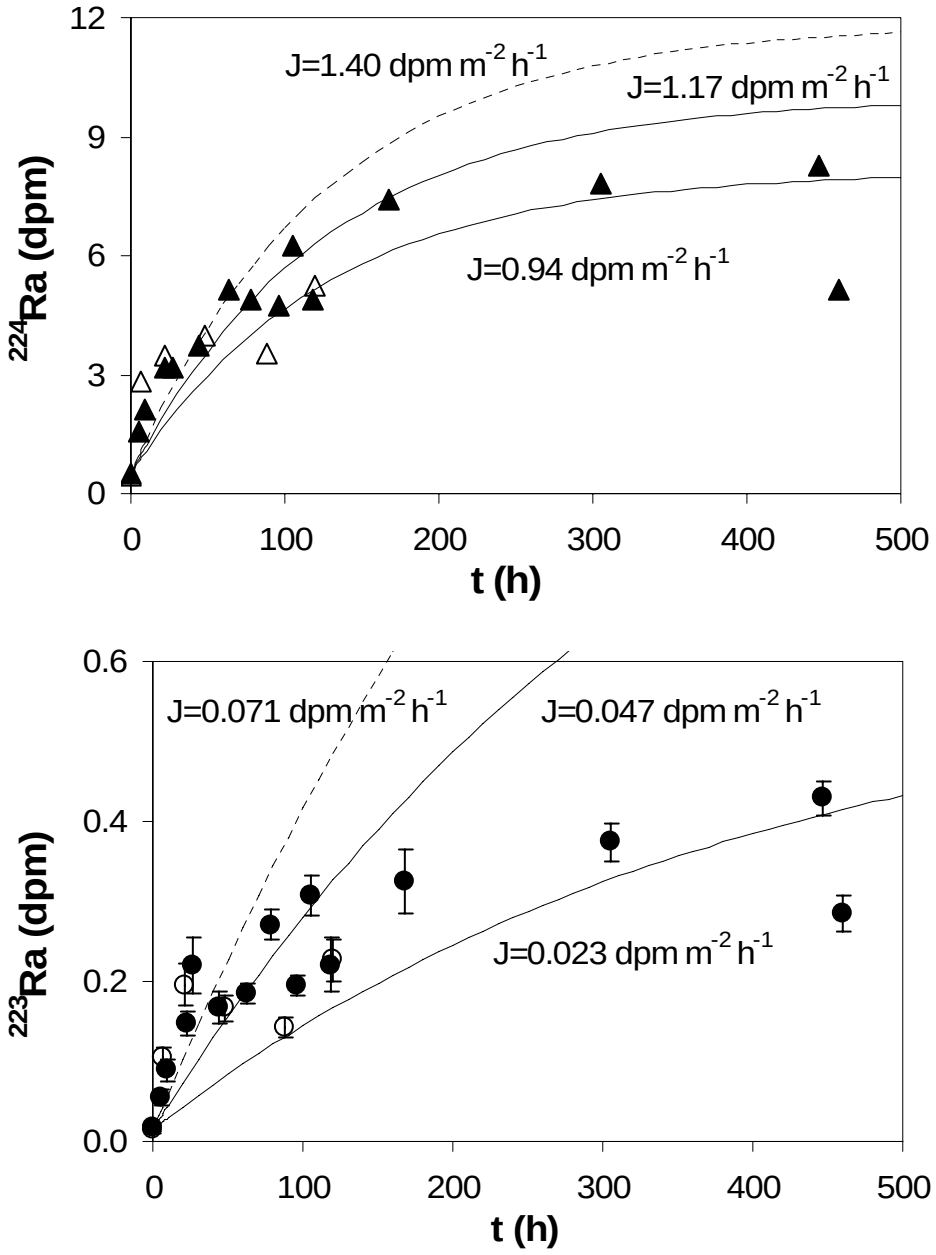

Figure II-4. Total short-lived Ra inventories in overlying water of whole core incubations. Closed symbols are from April 2006 (n = 15, incubated at 17^{o}C), and open symbols are from August 2006 (n = 6, incubated at 26^{o}C). Curves describe modeled flux rates indicated by the labels. Error bars are 1σ counting error. Note that the error bars for ^{224}Ra are smaller than the size of the symbols.

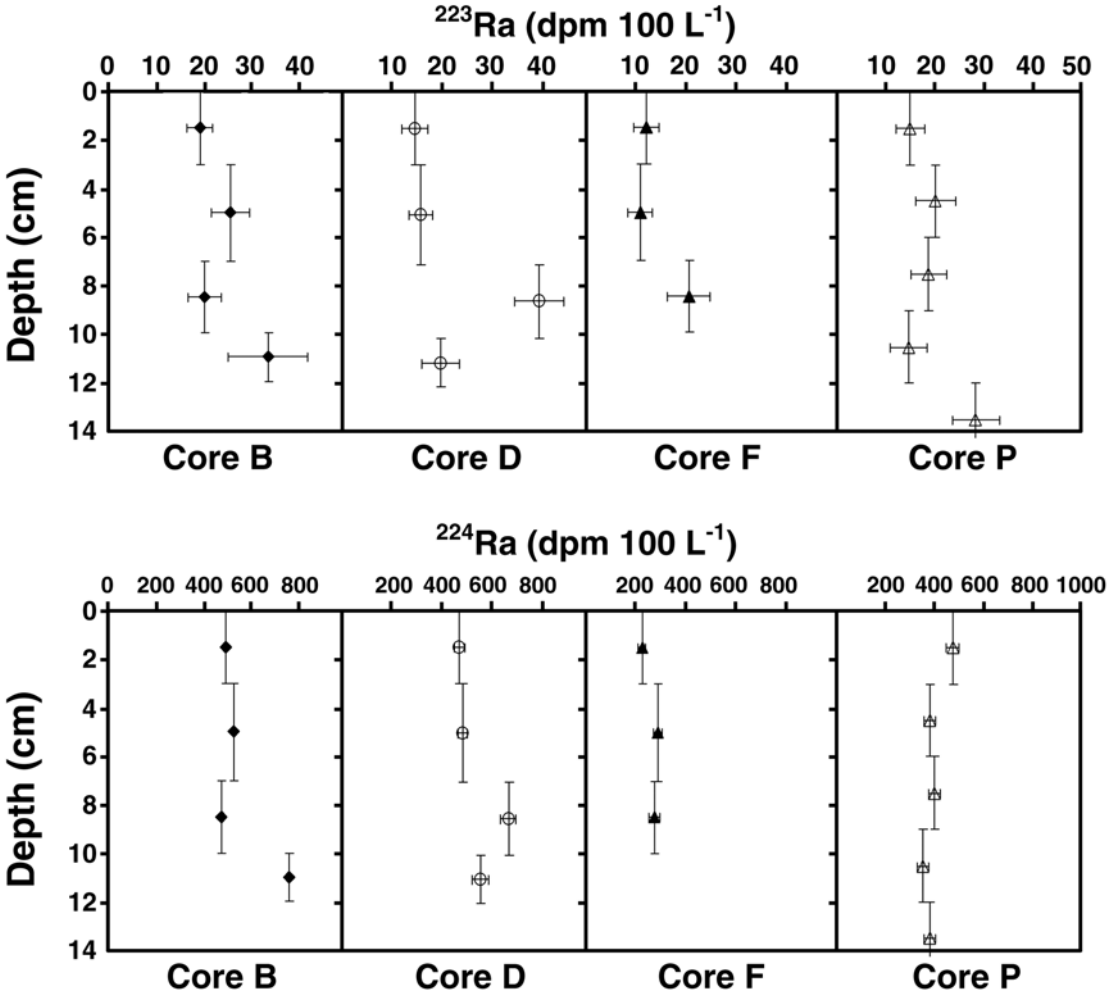

Figure II-5. Porewater ^{223}Ra and ^{224}Ra profiles in subtidal sediment cores. Cores B, D, and F were collected in April 2006, and were measured following the completion of the diffusion experiment (see text). Core P was collected in August 2006, and was measured within 6 hours of collection. Vertical error bars indicate each integrated depth interval (2-4 cm), and horizontal error bars are 1σ counting error.

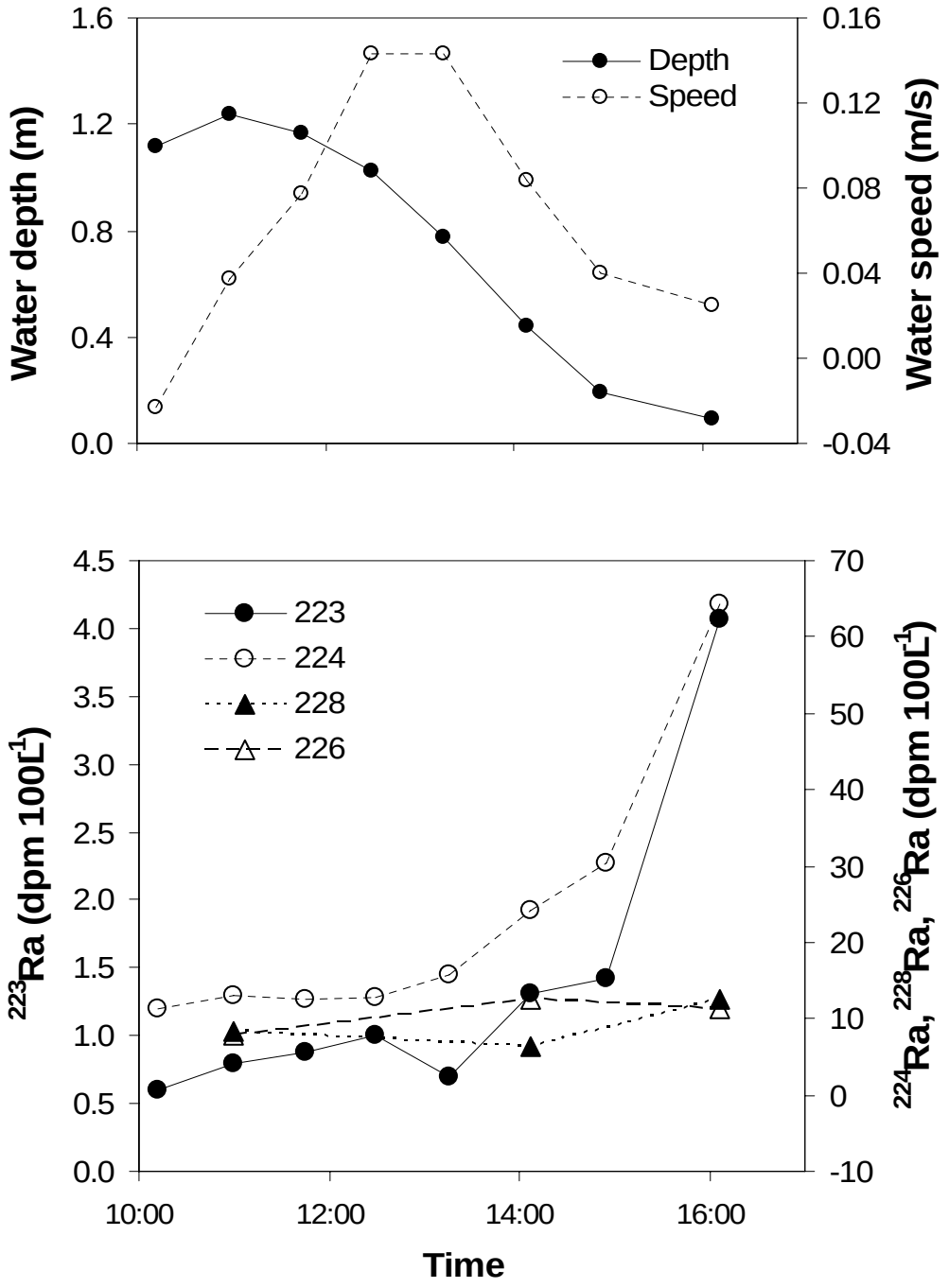

Figure II-6. (a) Water depth and speed in the marsh creek channel during the sampling period. (b) Ra enrichment in water leaving the tidal creek. The series ranges from high tide at approximately 10:00 to low tide at 16:00. Error bars are not shown, as they are smaller than the symbols. Note that the ^{224}Ra axis is offset to prevent overlap between data points between the different isotopes.

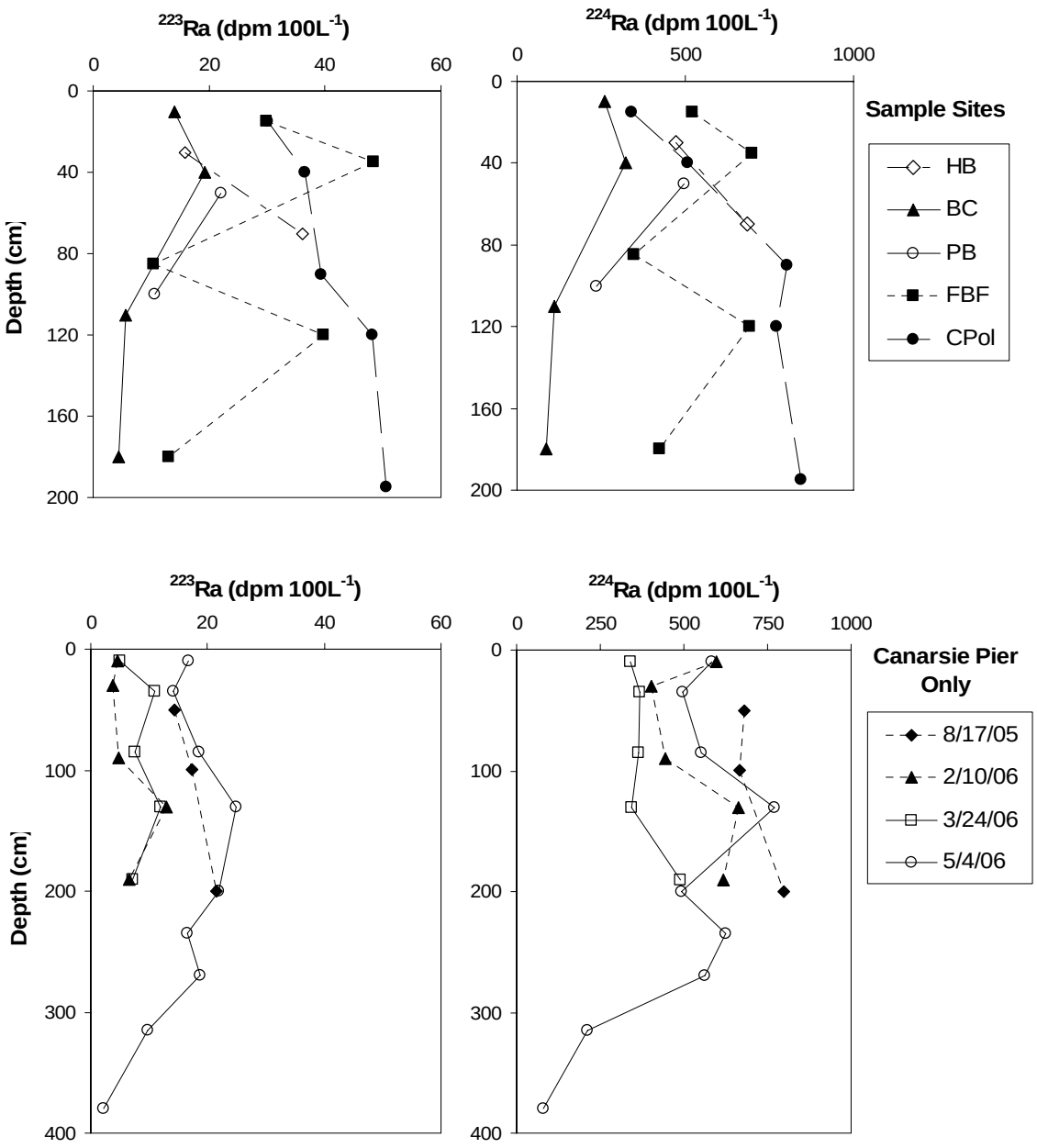

Figure II-7. Shallow groundwater Ra profiles. Upper figures compare five different sites, not including Canarsie Pier. Lower figures show four profiles obtained at a single location near Canarsie Pier during different months. Note the different depth ranges between upper and lower figures. The site ID notation is the same as in Figure II-1.

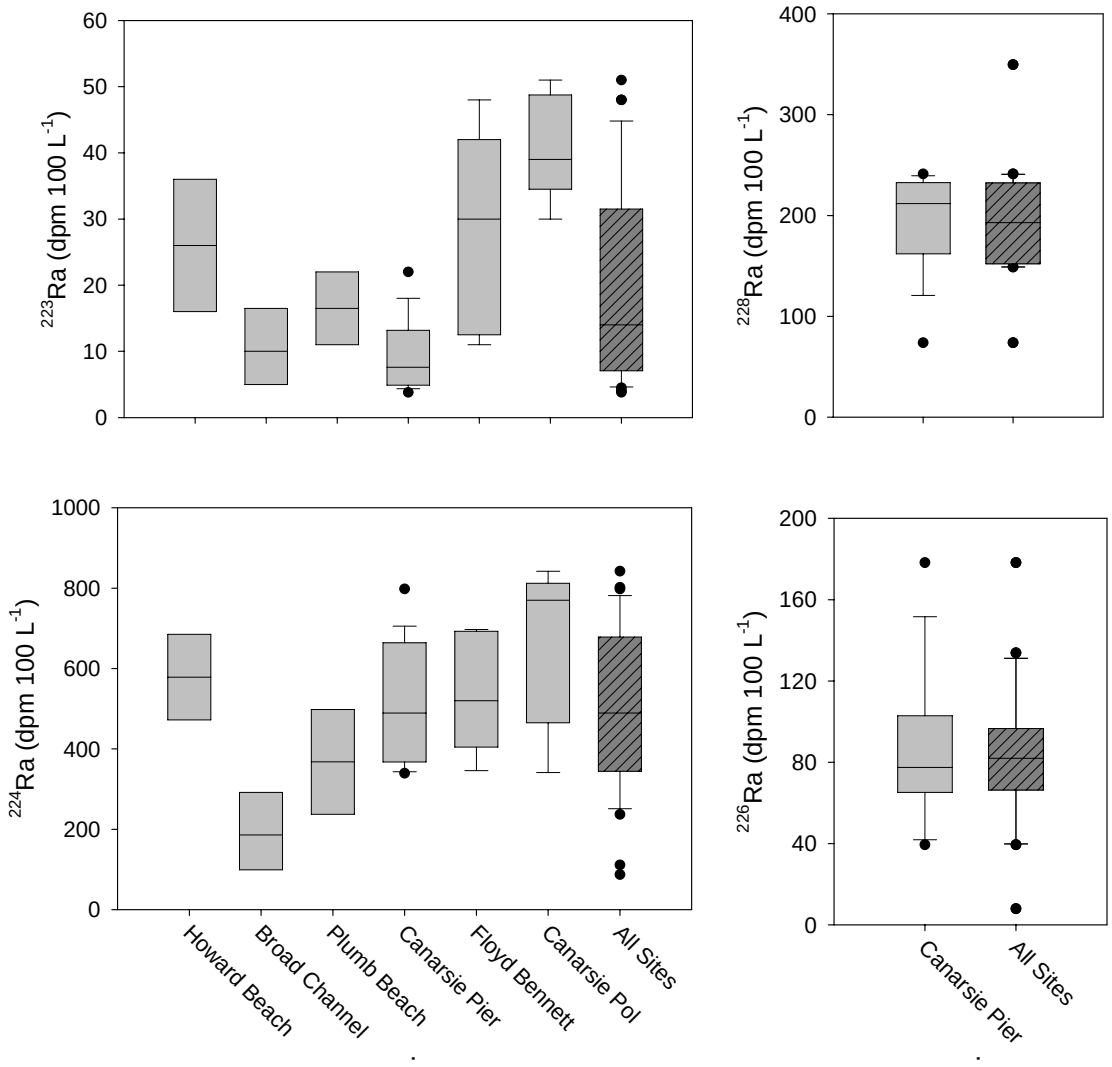

Figure II-8. Box-and-whisker plot of groundwater Ra activities in Jamaica Bay. The dark, shaded box at the right of each graph is a composite of all sites. For the long-lived isotopes, only the Canarsie Pier location is singled out from the "All Sites" box. This location has 11 of the 16 total groundwater long-lived Ra activity measurements. There is one measurement each for the Plumb Beach, Canarsie Pol, and Floyd Bennett locations, and two measurements for Broad Channel. The horizontal line within each box is the median, and the boundaries of the boxes indicate the 25th and 75th percentiles. Error bars above and below the boxes indicate the 10th and 90th percentiles. Filled circles identify outlying points.

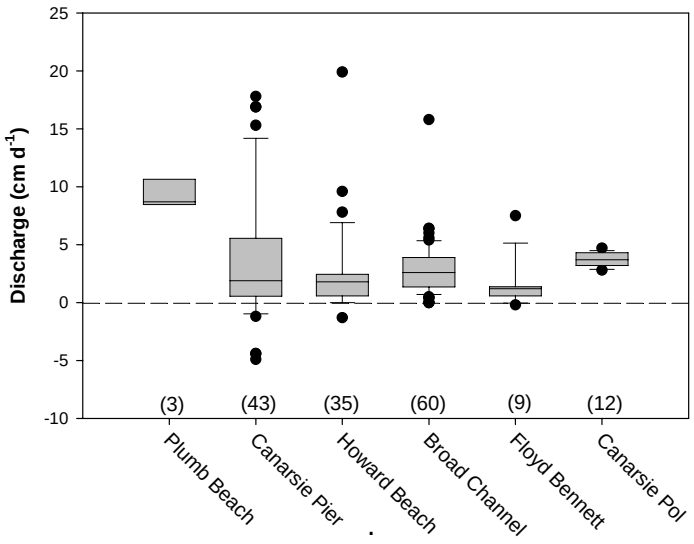

Figure II-9. Discharge at different sites in Jamaica Bay measured by seepage meters. Symbols as in Fig. II-8.

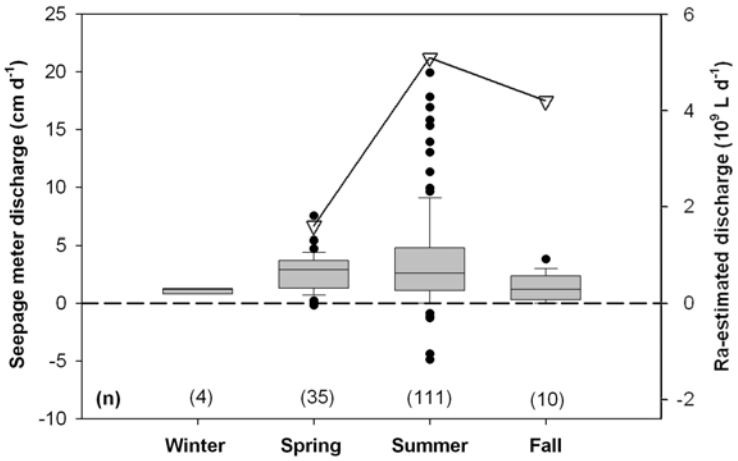

Figure II-10. Seasonal variability in submarine groundwater discharge measured by seepage meters and as estimated by Ra mass balance. Box and whisker plot represents direct measurement of SGD (symbols as in Fig. II-8), while the line shows the seasonal trend in average Ra-derived SGD (see Table II-4). The numbers in parentheses indicate the number of direct measurements that are included in the individual boxes for each season. Seasons have been defined as: "Winter" – mid-Dec through mid-Mar, "Spring" – mid-Mar through mid-June, "Summer" – mid-June through mid-Sept, and "Fall" – mid-Sept through mid-Dec.

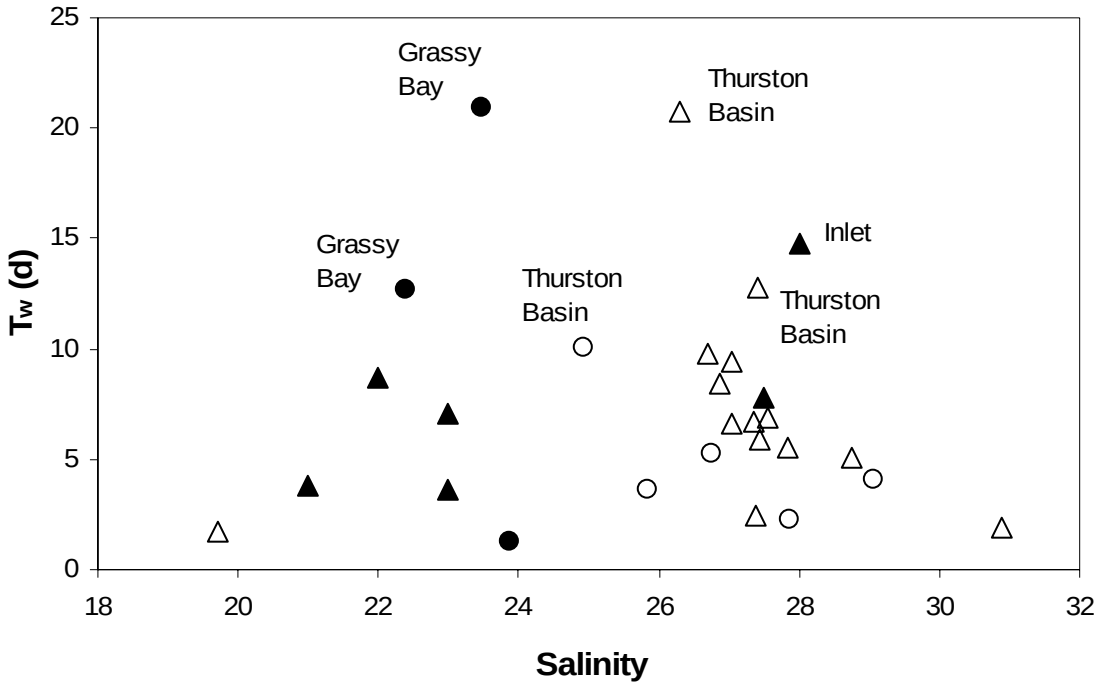

Figure II-11. Variation in Ra-estimated T_w (using ^{224}Ra:^{228}Ra ratios, see text) with salinity. Labels indicate locations of samples with T_w values higher than 10 d. Symbols as in Fig. II-1.

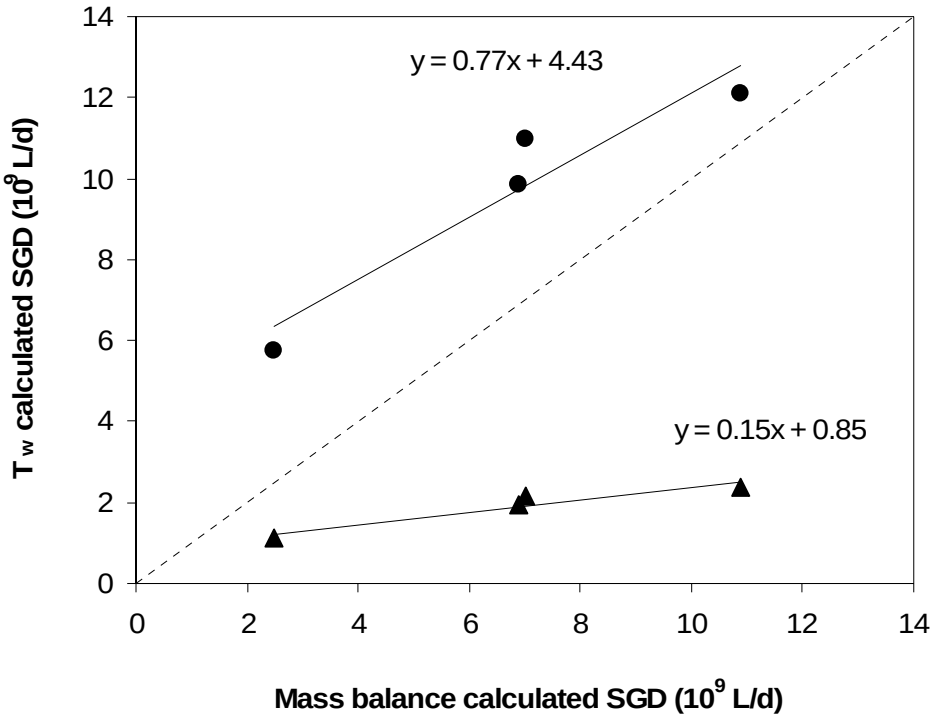

Figure II-12. Comparison of different techniques for estimating SGD using Ra isotopes. Filled triangles represent SGD calculated with an average T_w of 7.5 d (Equation 14). Circles represent SGD estimates using a T_w of 1.5 d. (see text). The solid lines and equations represent linear regressions of the data, and the dashed line represents the 1:1 relationship between SGD estimates.

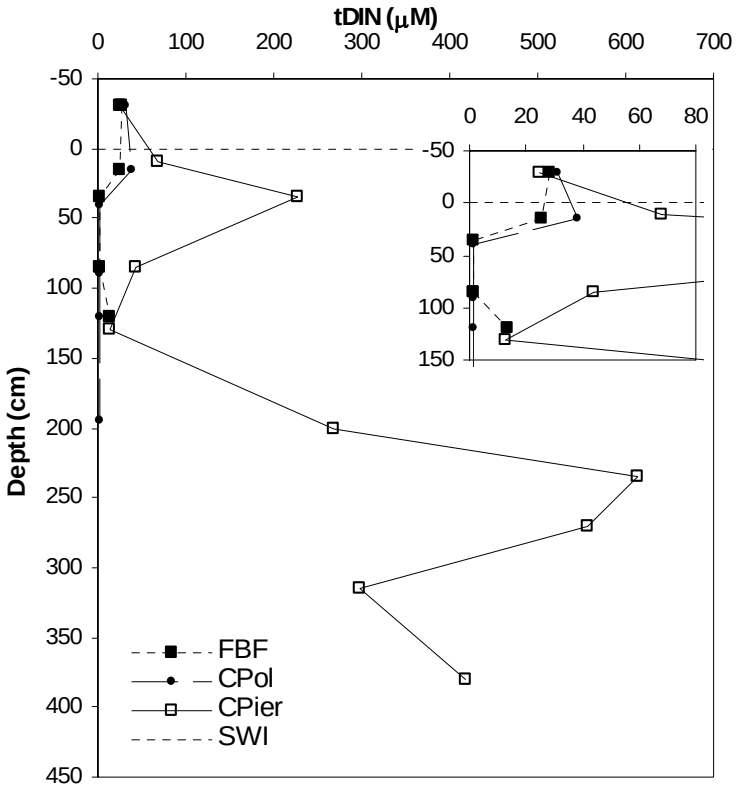

Figure II-13. Total dissolved nitrogen (tDIN) in shallow groundwater profiles in Jamaica Bay. Inset provides an expanded view of concentrations <80 μM at depths <150 cm. The horizontal dashed line represents the sediment-water interface (SWI).

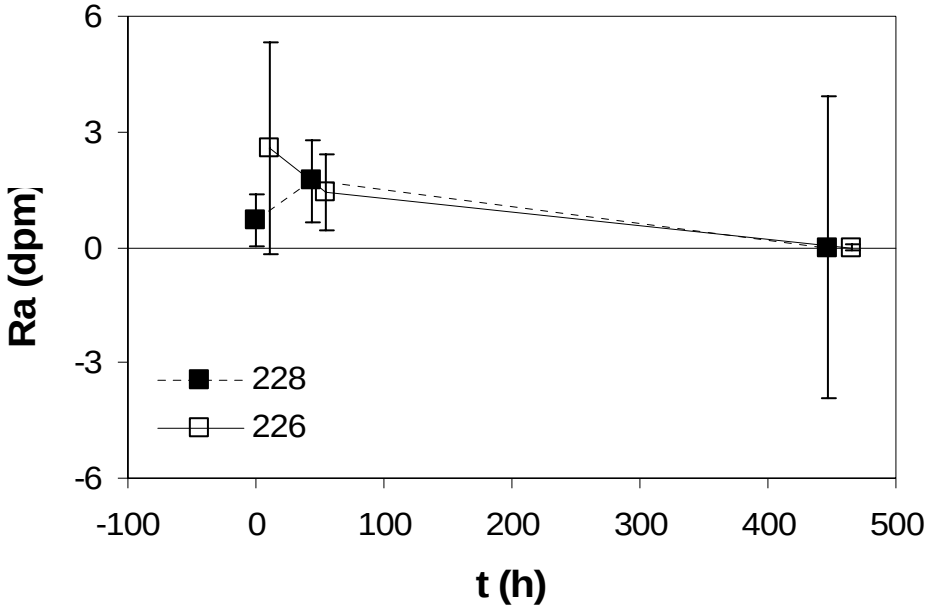

Figure II-A. Diffusion experiment data for long-lived Ra isotopes. Note that the data points have been offset by a few hours to improve the clarity of the graph.

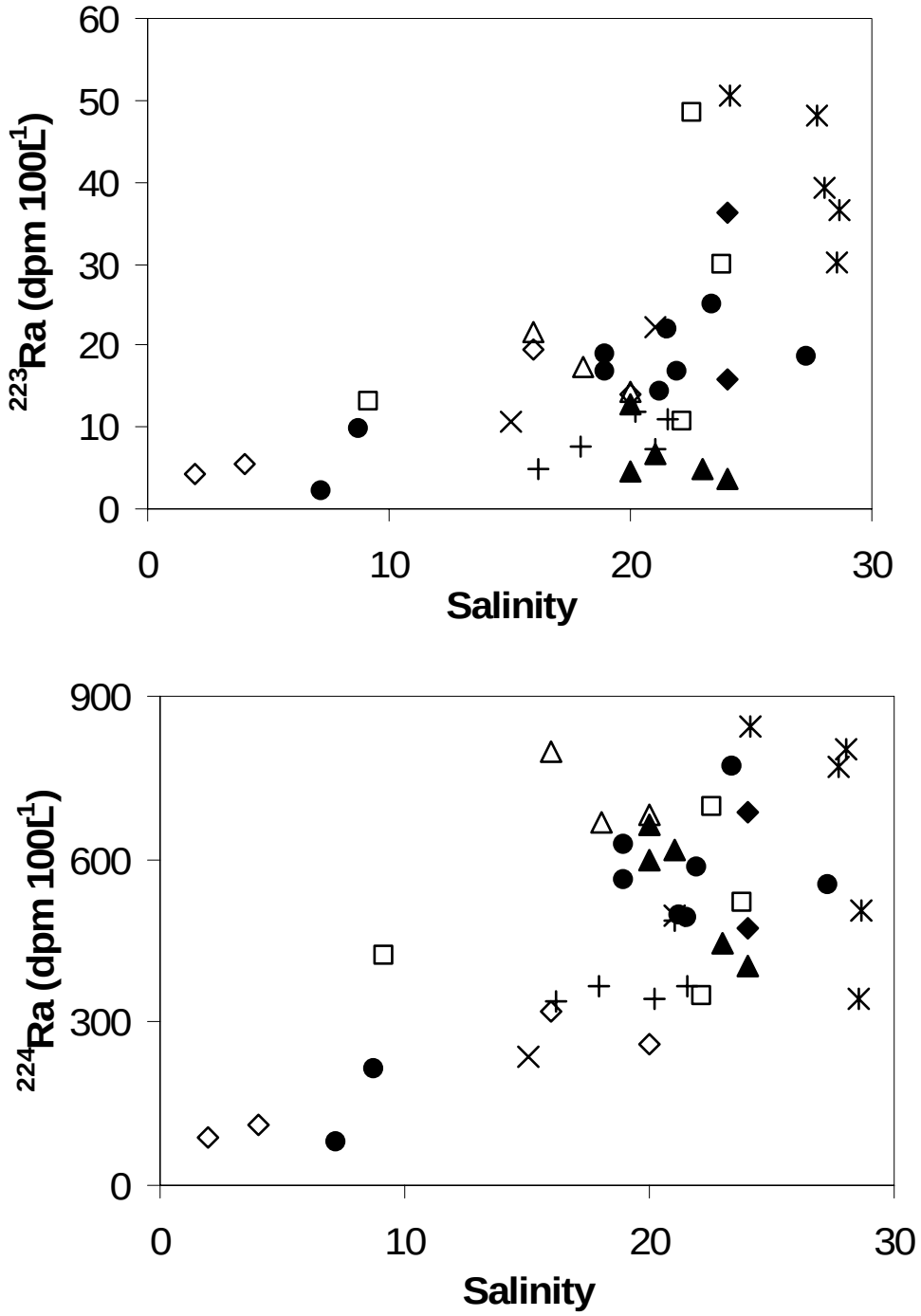

Figure II-B. Relationship between groundwater Ra concentrations and salinity. Symbols are: HB (solid diamonds), BC (hollow diamonds), PB (crosses), CPier 1 (hollow triangles), CPier 2 (plusses), CPier 3 (filled triangles), CPier 4 (filled circles), CPol (asterisks), FBF (hollow squares). Samples "CPier 1-4" represent different sampling dates at the Canarsie Pier location. Site ID notation as in Figure II-1.

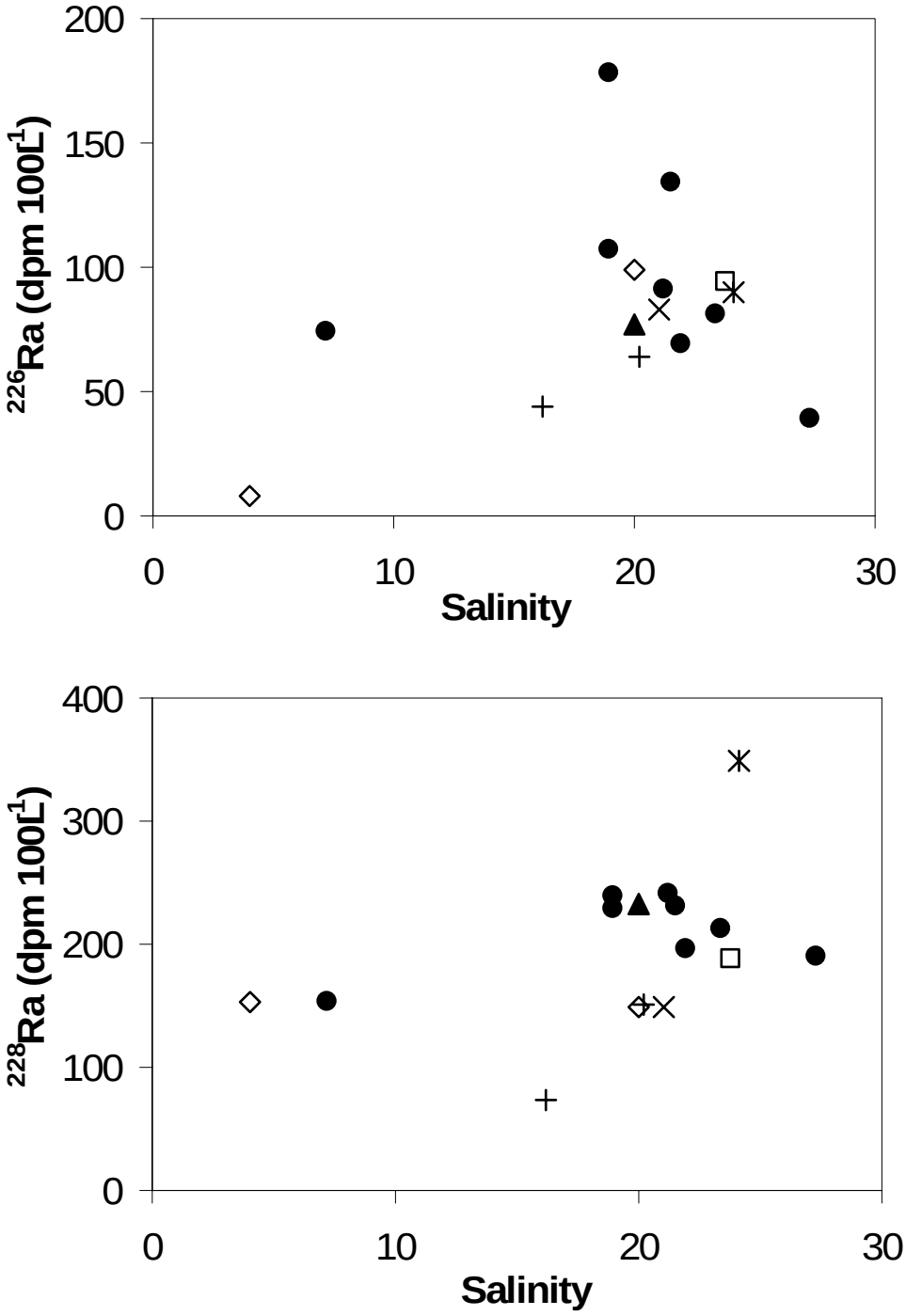

Figure II-B, continued.

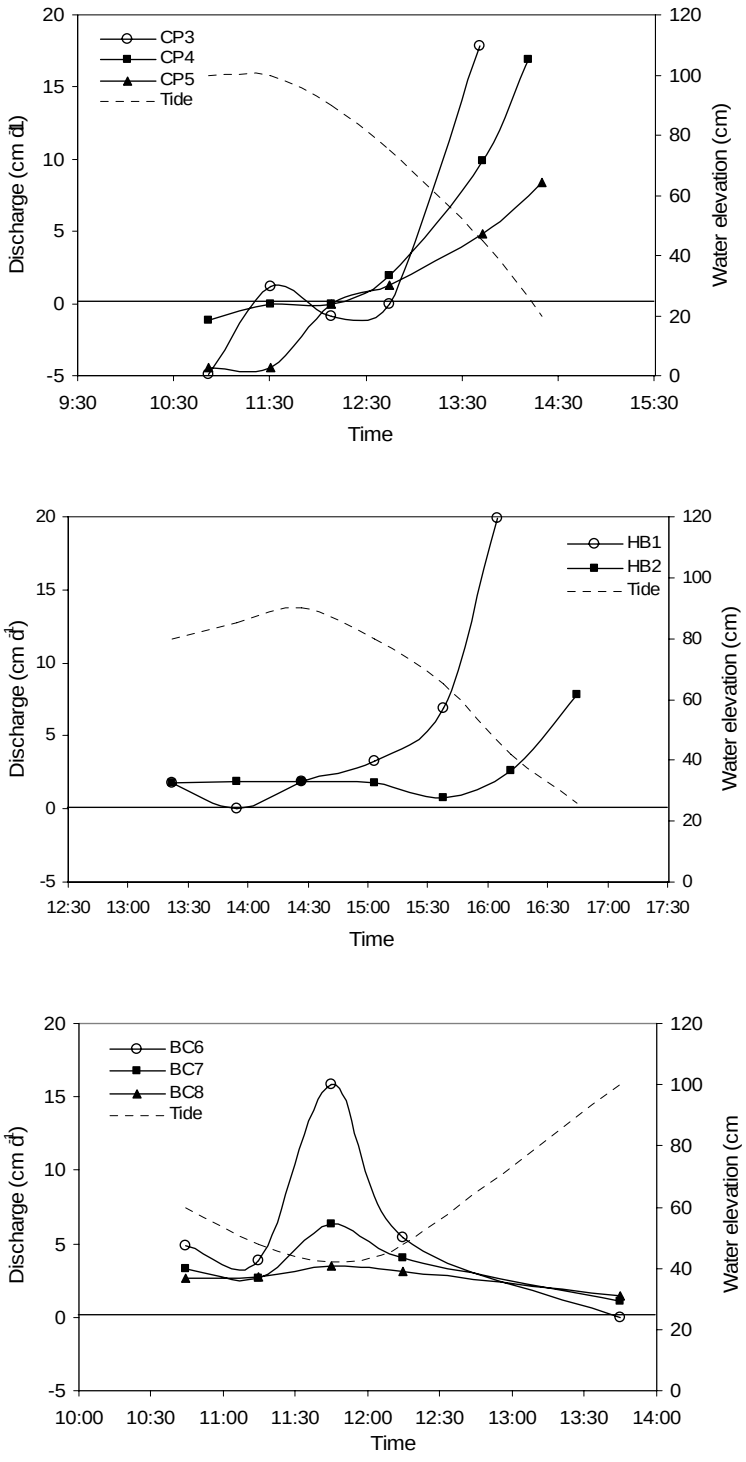

Figure II-C. Variation in SGD and water elevation with time at three sites. (a) Canarsie Pier; there is a significant increase in discharge as the tide falls below 60 cm above mean sea level (msl). Note the seawater intrusion observed at high tide. (b) Howard Beach; a similar peak in discharge occurs once the tide falls below 60 cm above msl. (c) Broad Channel, three chambers show a sharp peak at low tide.

CHAPTER III:

Submarine groundwater discharge to Great South Bay, NY, estimated using Ra isotopes

Beck, A.J., J.P. Rapaglia, J.K. Cochran, H.J. Bokuniewicz, S. Yang, 2007. Submarine groundwater discharge to Great South Bay, NY, estimated using Ra isotopes. Marine Chemistry, submitted.

ABSTRACT

There is increasing evidence that submarine groundwater discharge (SGD) represents a major source of dissolved chemical constituents to the coastal ocean. In Great South Bay, NY, previous studies have shown that the discharge of nutrients with SGD may cause harmful algal blooms. This study estimates SGD to Great South Bay during August 2006 by performing a mass balance for each of the dissolved Ra isotopes (^{224}Ra, ^{223}Ra, ^{228}Ra, ^{226}Ra). The budget indicates a major source (between 30 and 60 percent of the steady-state flux) of Ra to the bay. This imbalance can be resolved by the input of Ra-enriched groundwater on the order of $3.1 – 8.1 \times 10^{9}$ L d^{-1}, depending on the Ra isotope. As much as 40% of this discharge is apparently due to flow along preferential flowpaths which are not included in models previously developed for SGD in Great South Bay. Compared to previous reports for fresh groundwater discharge to the bay, the Ra-estimated discharge must comprise approximately 90% recirculated seawater. The substantial source of Ra to the bay suggests that SGD may be a major pathway for input of other dissolved constituents such as trace metals, although the existence of channelized or preferential flow may make quantifying these chemical fluxes difficult.

INTRODUCTION

The importance of submarine groundwater discharge (SGD) in chemical fluxes to the coastal ocean is well established (Johannes, 1980; Capone and Bautista, 1985; Oberdorfer et al., 1990; Krest et al., 2000; Crotwell and Moore, 2003; Charette and Buessler, 2004; Kim et al., 2005; Hwang et al., 2005), although it remains uncertain how best to measure its magnitude (Zektzer et al., 1973; Buddemeier, 1996; Burnett et al., 2001; Shaw, 2001; Beck et al., 2007). In addition, with increasing ability to identify this discharge, the impact of SGD-associated chemical fluxes on ecological processes in coastal ecosystems is also beginning to be understood (Johannes, 1980; LaRoche et al., 1997; Rutkowski et al., 1999; Gobler and Sanudo-Wilhelmy, 2001; Gobler and Boneillo, 2003; Boudreau et al., 2001). The ecological significance of SGD has been particularly well documented in Long Island, NY, with chemical discharge associated with SGD implicated in the initiation and proliferation of harmful algal blooms over the past few decades (Taylor et al., 2006; Gobler and Boneillo, 2003; Gobler and Sanudo-Wilhelmy, 200; LaRoche et al., 1997).

An important consideration is that SGD comprises both fresh (meteoric) groundwater and recirculated seawater (Burnett et al., 2006), yet most of the previous studies in Great South Bay have considered only the former portion. Each of these components has unique geochemical characteristics, and both tend to be variable on differing temporal and spatial scales (Michael et al, 2005; Robinson et al., 2006). There is significant spatial variability of SGD in Great South Bay; discharge rates are typically highest near shore, and decline bayward (Bokuniewicz and Zeitlin, 1980; Zeitlin, 1980; Seplow, 1990; Bokuniewicz et al, 2004). However, discharge does not always follow this

pattern, and sites of increased discharge have been occasionally but consistently observed (Bokuniewicz and Zeitlin, 1980; Bokuniewicz et al, 2004). The design of conventional seepage meters makes them somewhat unable to account for spatial variability. This shortcoming can be reduced by increasing the number of observations, but this is time-consuming and inefficient. Therefore, a number of natural geochemical tracers, such as Rn and Ra, have been developed for indirect quantification of SGD (e.g. Burnett and Dulaiova, 2003; Moore, 1996), and provide an assessment of SGD that integrates over the area of the entire system. Ra is perhaps the tracer examined most thoroughly, and has been utilized extensively over the past decade in numerous coastal settings (e.g. Charette et al., *submitted*, and references therein). In the present study, we construct a mass balance for Ra in Great South Bay. Using the flux-by-difference approach, we estimate the average rate of SGD into the entire bay.

Site Description

Great South Bay is the largest of several shallow embayments along the southern Long Island coast. Great South Bay is approximately 35 - 40 km in length, and ~9 km across at its widest point (Bokuniewicz and Zeitlin, 1980; Wong, 1993). The bay covers a surface area of about 235 km^2 (Wong, 1993), and has an average depth of 1.2 m, although it may reach depths of up to 4 m (Wilson et al., 1991). The tidal range in the bay is generally less than about 0.25 m (Bokuniewicz and Zeitlin, 1980). The bay exchanges water with the Atlantic Ocean primarily through Fire Island Inlet, but a small amount of water passes through South Oyster Bay to the west and Moriches Bay to the

east (Wong, 1993). Salinity in Great South Bay ranges between 20 and 30, depending on the fresh water input and exchange with Atlantic water (Moskowitz, 1976).

There are two primary surface sources of fresh water to Great South Bay, the Carmans River at the far eastern end, and the Connetquot River at the center the bay (Fig. III-1). In addition, as much as 20 – 30% of the freshwater input to the bay may be attributable to submarine groundwater discharge (Bokuniewicz and Zeitlin, 1980). Groundwater flow into the bay is facilitated by permeable, sandy sediments that characterize the surficial Upper Glacial Aquifer (Perlmutter and Crandell, 1959, as cited by Bokuniewicz and Zeitlin, 1980). Comprehensive discussions of previous groundwater studies in Great South Bay can be found in Bokuniewicz and Zeitlin (1980) and Bokuniewicz et al. (2004). Briefly, direct measurement of SGD in the bay has yielded relatively low flow rates ranging between 1 and 7 cm d^{-1} (cm^3 cm^{-2} d^{-1}) (Bokuniewicz and Zeitlin, 1980; Zeitlin, 1980; Seplow, 1991; Bokuniewicz et al, 2004). Fresh porewater can be found at depths in the sediment of less than 1 m (Seplow, 1991), and salt fingering has been proposed as one mechanism driving groundwater advection (Seplow, 1991; Bokuniewicz, 1992).

METHODS

Large volume (~50 L) surface water samples were collected for dissolved Ra analysis throughout Great South Bay during 14-16 August 2006 (Fig. III-1). Water samples were passed slowly (< 1 L min^{-1}) through Mn-oxide impregnated acrylic fiber (Mn-fiber) to quantitatively extract dissolved Ra (Moore and Reid, 1973; Moore, 1976; Reid et al., 1979). The fibers were returned to the laboratory, rinsed, and partially dried

before analysis of short-lived isotopes (^{223}Ra and ^{224}Ra) by delayed coincidence scintillation counting (Moore and Arnold, 1996). The fibers were then ashed in a muffle furnace at 475^{o}C for 8-12 hours, and compressed into pellets sealed with Al foil. After allowing a minimum of three weeks for ingrowth of ^{222}Rn, long-lived isotopes (^{228}Ra and ^{226}Ra) were counted in a well-geometry gamma detector.

A series of samples was also collected from high to low tide at one location at the mouth of the Connetquot River to determine the Ra input from fringing marshes. The location was chosen because the shores of this river have the greatest density of marshland in Great South Bay. Surface samples were collected approximately once per hour over a six-hour period, and processed as described above.

To estimate diffusive flux of Ra from fine-grained sediments, six shallow (~ 20 cm deep), large-diameter (~ 29 cm) subtidal sediment cores were collected near the Roe Avenue site (Fig. III-1) and incubated in the lab following the procedure of Beck et al. (submitted). Briefly, the overlying water in each core was replaced with Ra-free bay water, and cores were placed in a large, water-filled bin. Diffusive Ra flux was determined by incubating the cores for various time intervals, after which the overlying water was drained and analyzed for dissolved Ra. The overlying water was then replaced with new Ra-free water, and incubation begun anew. Thus, as many as three time points were determined using a single core.

Shallow groundwater samples (~4 L) were collected using a shielded screen drive-point piezometer (Charette and Allen, 2006). Before being passed through the Mn-fiber, samples were immediately aerated with a small air pump for at least 60 minutes in order to prevent reductive dissolution of the Mn-oxides (Epler, 1991; Krest et al., 2000).

RESULTS

Dissolved Ra isotopes in bay and river surface waters

The near-zero salinity (S = 0.86) Connetquot River endmember contained measurable dissolved activities of all Ra isotopes (Fig. III-2): ^{223}Ra (1.1 dpm 100 L^{-1}), ^{224}Ra (6.4 dpm 100 L^{-1}), ^{226}Ra (7.0 dpm 100 L^{-1}), ^{228}Ra (3.0 dpm 100 L^{-1}). The "ocean" endmember was collected as far out the mouth of Fire Island Inlet as possible in a small craft (Fig. III-1). However, the salinity of that sample (S = 31.00) was lower than expected for ocean water, so it was clearly not free of the influence of water from inside Great South Bay. This was also observed in the Ra composition of the sample, such that both ^{223}Ra (0.61 dpm 100 L^{-1}) and ^{224}Ra (14.4 dpm 100 L^{-1}) were elevated relative to offshore values (e.g. <0.3 dpm ^{223}Ra 100 L^{-1}, <0.5 dpm ^{224}Ra 100 L^{-1}; Moore, 2000). Both short- and long-lived Ra isotopes in surface waters of the bay show pronounced enrichment relative to conservative mixing between the observed river and ocean endmembers (Fig. III-2).

A consistent linear increase in short-lived Ra activities with salinity was evident along a transect from the head of the Connetquot River to the bay; a similar pattern was not observed for the Carmans River, where Ra activities at the high salinity mouth of the river were lower than those measured at mid-salinity.

Ra input from marshes – Tidal series

The tidal series appeared to show a peak in Ra at low tide (Fig. III-3a), although the linear relationship of Ra with salinity showed that the enrichment was simply due to a

greater fraction of high-Ra river water (Fig. III-3b). Thus, there was no observable contribution of fringing marshes to the Ra inventory in the receiving water, as has been observed elsewhere (Elsinger and Moore, 1983; Bollinger and Moore 1984, 1993; Beck et al., submitted).

Ra in core incubations

Core incubation experiments showed significant diffusion of short-lived Ra isotopes across the sediment-water interface (Fig. III-4). ^{223}Ra and ^{224}Ra activities in the overlying water in these cores increased to a maximum inventory of about 0.45 dpm and 11 dpm, respectively. Long-lived Ra isotopes did not reach measurable levels in the overlying water during the time period examined. The trends observed for the short-lived isotopes follow clear a clear pattern of steady increase until about 100 hours, after which there is considerable scatter in the data. We believe that the data points at times greater than 100 h are not representative of the true diffusive flux; for that portion of the experiment, the overlying water volume was not maintained at a constant level, and substantial evaporative loss occurred. As described in Beck et al. (submitted), Ra accumulation in the overlying water reduced the porewater-overlying water Ra gradient, thus decreasing the diffusive flux. As well, variability in the amount of evaporation resulted in the inconsistent pattern observed in the data during the later part of the experiment.

However, the initial portion of the experiment yielded a pattern of enrichment that could be predicted well for both short-lived isotopes (Fig. III-4). The inventory of Ra in the core overlying water increases at a rate determined by input from diffusion/bio-

irrigation, and loss due to radioactive decay. Thus, the net Ra enrichment in the overlying water can be described by equation [1] (after Beck et al., submitted):

$$I_t = [(J_{diff} A_{surf})/\lambda] (1 - e^{-\lambda t}) \quad [1]$$

where I_t is the Ra inventory (dpm per core) of the overlying water at time t (h), J_{diff} is the Ra flux from the sediment (dpm m^{-2} h^{-1}), A_{surf} is the sediment surface area (m^2), and λ is the decay constant for each Ra isotope (0.0608 and 0.189 d^{-1} for ^{223}Ra and ^{224}Ra, respectively).

For ^{223}Ra, the initial data were consistent with an input flux of 0.052 dpm m^{-2} h^{-1}; for ^{224}Ra, the data best fit a flux of 2.2 dpm m^{-2} h^{-1} (Fig. III-4). These fluxes are higher than reported for elsewhere on Long Island (Jamaica Bay; Beck et al., submitted). The difference was smaller for ^{223}Ra (by only 0.005 dpm m^{-2} h^{-1}, or about 10%) than for ^{224}Ra (higher in Great South Bay by 1.3 dpm m^{-2} h^{-1}, a twofold increase), probably reflecting differences in sediment mineralogy between the two systems.

Ra in shallow groundwater

Short-lived Ra activities showed considerable variability in shallow (<2m) groundwater samples, ranging from 0.3 to 58 dpm 100 L^{-1} (^{223}Ra), 72 to 1797 dpm 100 L^{-1} (^{224}Ra), 372 to 302 dpm 100 L^{-1} (^{226}Ra), and 28 to 750 dpm 100 L^{-1} (^{228}Ra) (Fig. III-5). No consistent trend was observed with depth across all profiles, although the high Ra activities measured at the Roe Avenue site in August 2006 showed evidence of depletion at the near surface and increased to nearly constant activities by approximately 25 cm depth. Interestingly, the lowest activity profile was measured in February 2006 at the Roe Avenue site, the same site where the highest activities were observed during summer

of the previous year. Fresh porewater has consistently been observed below a very shallow, saline, surface layer at this site (Seplow, 1991; Bokuniewicz et al., 2004), and it is likely that the low activities observed during the February 2006 sampling simply reflect the high distribution coefficient of Ra in fresh water (Li and Chan, 1979).

DISCUSSION

Ra mass balance in Great South Bay

Using each of the parameters assessed above, a mass balance can be constructed for Ra in Great South Bay. Assuming that the system is approximately at steady state, the mass balance is:

$$J_{out} + J_{decay} = J_{in} + J_{Conn} + J_{Car} + J_{diff} + J_{marsh} + J_{desorp} + J_{SGD}, \quad [1]$$

where the left-hand terms describe Ra loss from the bay via water exchange at the inlet (J_{out}) and radioactive decay (J_{decay}). The other terms represent the various input pathways: water exchange at the Fire Island Inlet (J_{in}), fluvial input by the Connetquot and Carmans Rivers (J_{Conn} and J_{Car}, respectively), Ra enrichment by percolation of water through fringing marshes (J_{marsh}), Ra desorption from river-borne and resuspended sediments (J_{desorp}), and submarine groundwater discharge (J_{SGD}). Each of these fluxes will be quantified using the parameters listed in Table III-1.

The Ra export flux at the inlet is estimated as the product of the water flux out of the bay and the average Ra activity in the bay. The volume of water leaving the bay comprises approximately the tidal prism and river input (primarily the Connetquot and Carmans Rivers). The diurnal tidal prism is 5.2×10^{10} L, assuming a maximum tidal range of 0.25 m and a bay area of 2.1×10^{8} m^2. This gives a Ra export through the inlet

of 1.5×10^9 dpm d^{-1} (^{223}Ra), 2.9×10^{10} dpm d^{-1} (^{224}Ra), 1.4×10^{10} dpm d^{-1} (^{226}Ra), and 2.2×10^{10} dpm d^{-1} (^{228}Ra).

Radioactive decay at steady-state is estimated using the baywide Ra inventory (calculated with average Ra activity and bay volume) and decay coefficients for each isotope. During the sampling period, decay represented a Ra loss from the bay of 2.3×10^8 dpm d^{-1} (^{223}Ra), 1.4×10^{10} dpm d^{-1} (^{224}Ra), 4×10^4 dpm d^{-1} (^{226}Ra), and 1.8×10^7 dpm d^{-1} (^{228}Ra).

The only input fluxes we consider to be significant here are those due to inlet exchange, river transport, diffusion from fine-grained sediments, and SGD. The following evidence provides support for excluding other terms from this Ra mass balance: No marsh input of Ra was observed during the tidal series (see Section 3.2 and Fig. III-3). The linearity of the Connetquot River transect (Fig. III-2) indicates that Ra is mixing conservatively between the fresh river endmember and bay water, and provides evidence that there is minimal input of Ra due to desorption from river-borne particles (Li et al., 1977; Li and Chan, 1979). In another Long Island estuary, even gross overestimates (i.e. assuming all of the suspended material in the water column is fresh sediment resuspended daily) showed that Ra desorption from resuspended sediments could only supply less than 2% of the Ra input (Beck et al., submitted). We therefore exclude the desorption term from the mass balance as well.

Input of Ra from water entering the bay through Fire Island Inlet is estimated as the product of the tidal prism volume and the Ra activity measured outside the inlet at high tide (Table III-1). This gives an input of 6×10^8 dpm d^{-1} (^{223}Ra), 1.5×10^{10} dpm d^{-1} (^{224}Ra), 9×10^9 dpm d^{-1} (^{226}Ra), and 1.3×10^{10} dpm d^{-1} (^{228}Ra). The activities measured

at the inlet are substantially higher than expected for a true ocean water endmember. Here, ^{224}Ra activity measured outside the inlet is 14.4 dpm 100 L^{-1}, substantially higher than that measured in New York Harbor (5.8 dpm 100 L^{-1}; Beck et al., submitted) and offshore (<0.5 dpm 100 L^{-1}; Moore, 1998, 2000). Thus, this input flux accounts for the return of Ra exported from the bay on the previous tidal cycle.

To estimate fluvial Ra input, the freshwater endmember is approximated using the activity concentration measured at the mouth of the river. Ra activities in the Connetquot River increase in a linear fashion with salinity (Fig. III-2). As noted above, we assume that desorption of Ra from particles would occur at low salinities (Li and Chan, 1979); thus, the linearity of the Connetquot River transect suggests that an input due to desorption is negligible in this system. In both the Carmans and Connetquot Rivers, Ra activities increase substantially downstream (e.g. ^{224}Ra increases from 6.4 to 65.9 dpm 100 L^{-1} in the Connetquot R.), suggesting that groundwater discharge is occurring throughout the river flowpath. Thus, the fluvial Ra flux to the bay is best estimated using the highest value measured at each river mouth. Although this is an upper estimate for river Ra input, we show below that the mass balance is insensitive to changes in the river endmember Ra activities.

The river discharge for the sampling period was calculated by averaging over the sampling period and the week prior to sampling (Connetquot: 5.9×10^4 m^3 d^{-1}, Carmans: 8.7×10^4 m^3 d^{-1}; http://waterdata.usgs.gov/). During this period, the Connetquot and Carmans River discharges were approximately 30% below and above mean flow, respectively, for the period 1998-2004. Ra fluxes from Carmans River calculated for the sampling period were 2.19×10^6 dpm d^{-1} (^{223}Ra), 2.15×10^7 dpm d^{-1} (^{224}Ra), 5.93×10^6

dpm d^{-1} (^{226}Ra), and 5.86×10^6 dpm d^{-1} (^{228}Ra). Ra input from the Connetquot River was calculated to be 4.23×10^6 dpm d^{-1} (^{223}Ra), 5.28×10^7 dpm d^{-1} (^{224}Ra), 1.46×10^7 dpm d^{-1} (^{226}Ra), and 1.75×10^7 dpm d^{-1} (^{228}Ra). Despite its lower flow rate, the higher endmember Ra activity of the Connetquot River makes it the larger fluvial source of Ra to Great South Bay.

The Ra input via diffusion (and bioirrigation) from fine-grained sediments is estimated from the core incubation experiment described in Section 3.3. A model describing balance between diffusive input and radioactive decay provides estimates of the Ra flux from sediments (Fig. III-4). The best flux estimate is 0.052 dpm m^{-2} h^{-1} and 2.2 dpm m^{-2} h^{-1} for ^{223}Ra and ^{224}Ra, respectively. The surface area of fine-grained sediments in Great South Bay is about 30% of the total surface area (Seplow, 1991), or approximately 0.7×10^8 m^2. This gives a Ra input from non-advective benthic processes of 7.82×10^7 dpm d^{-1} (^{223}Ra) and 3.31×10^9 dpm d^{-1} (^{224}Ra).

Radium fluxes to Great South Bay for August 2006 are compiled in Table III-2. Although the magnitude of each flux for short-lived Ra was different between isotopes (higher for ^{224}Ra by about a factor of 20), the relative importance of the different fluxes to the total budget was similar for both ^{223}Ra and ^{224}Ra. Long-lived isotope fluxes were relatively similar to each other in both magnitude and proportion. Loss of Ra from the bay was greatest due to water exchange at the inlet, representing 86, 67, 100, and 100 percent of the total export flux for ^{223}Ra, ^{224}Ra, ^{226}Ra, and ^{228}Ra, respectively (Table III-3). Due to its shorter half-life, radioactive decay was more important for ^{224}Ra (33%) than for ^{223}Ra (14%). Decay was negligible for the long-lived isotopes.

Similar to Ra export, input fluxes were dominated by the inlet exchange term, which represented 38, 35, 67, and 58 percent of the total for ^{223}Ra, ^{224}Ra, ^{226}Ra, and ^{228}Ra, respectively (Table III-3). Diffusion from fine-grained sediments accounted for 5 and 8 percent (^{223}Ra and ^{224}Ra, respectively) of the Ra input. As mentioned above, fluvial Ra inputs were very low, with the Connetquot River supporting only 0.3, 0.12, 0.11, and 0.08 percent of the ^{223}Ra, ^{224}Ra, ^{226}Ra, and ^{228}Ra input, respectively (Table III-3). Similarly, the Carmans River could only provide 0.13, 0.05, 0.04, and 0.03 percent of the input for ^{223}Ra, ^{224}Ra, ^{226}Ra, and ^{228}Ra, respectively (Table III-3).

Submarine Groundwater Discharge

Ultimately, the major portion of Ra export from Great South Bay could not be balanced by the known inputs. The flux imbalance for the different isotopes was 9.68×10^8, 2.45×10^{10}, 4.45×10^9, 9.14×10^9 dpm d^{-1} (^{223}Ra, ^{224}Ra, ^{226}Ra, and ^{228}Ra, respectively; Table III-2), representing 57, 57, 32, and 42 percent of the total flux for ^{223}Ra, ^{224}Ra, ^{226}Ra, and ^{228}Ra, respectively (Table III-3). As shown for numerous other estuaries (Rama and Moore, 1996; Krest et al., 2000; Kelly and Moran, 2002; Hussain et al., 1999; Hancock et al., 2000; Charette et al., 2001), this large Ra imbalance can be resolved by an input from submarine groundwater discharge. Average Ra activities measured in shallow (< 2 m) groundwater are nearly an order of magnitude higher than the highest activities observed in the surface water (e.g. 66 vs. 467 dpm 100 L^{-1} for ^{224}Ra; Fig. III-5, Table III-1).

If all of this unbalanced Ra input is due to SGD, it requires an SGD flux of about 7.0×10^9 L d^{-1} (^{223}Ra), 5.3×10^9 L d^{-1} (^{224}Ra), 4.2×10^9 L d^{-1} (^{226}Ra), 3.8×10^9 L d^{-1}

(^{228}Ra). These water fluxes are approximately 10% of the tidal prism volume and 1% of the total bay volume (Table III-1). Normalized to the total area of the bay floor, these volume fluxes represent a linear flow rate of about 2 cm d^{-1}, and are consistent with measurements made using Lee-type seepage meters (Bokuniewicz and Zeitlin, 1981; Bokuniewicz and Pavlik, 1990; Bokuniewicz et al., 2004). As discussed below, it may not be reasonable to extrapolate a single flow rate to the entire surface area, and variability in discharge throughout the bay is undoubtedly high.

The distribution of dissolved Ra in bay surface water showed the highest activities in the rivers (Fig. III-2). In fact, there appeared to be a clear trend of mixing between three endmembers: low Ra water at the head of each river, and Ra-depleted seawater represent two of the endmembers. The third endmember, with high Ra, is evident during mixing of bay water with river water; for the Carmans River, this occurs at a salinity of approximately 10-15, while for the Connetquot River, it is at a salinity of 15-20. Bokuniewicz and Zeitlin (1980) suggested that the greater portion of SGD in Great South Bay occurs along the rivers. The Ra distribution supports this hypothesis, with the saline, high Ra river water being diluted after entering the bay. However, the high salinity samples also show Ra enrichment independent of the mixing lines described by the ocean and rivers, indicating that the rivers do not represent the only significant sites of SGD in the bay.

Spatial variability in SGD

In addition to the apparent increase in discharge near rivers, there is a high degree of spatial variability in SGD associated with heterogeneous flowpaths; indeed a regular

pattern of preferential discharge along the shoreline has been previously reported (Bokuniewicz et al., 2004). However, at one location in the bay (Roe Avenue) Bokuniewicz et al. (2004) and Bokuniewicz and Zeitlin (1980) observed a region of consistently higher discharge at 70 m from shore (note that this feature persisted for nearly a quarter century). Bokuniewicz et al. (2004) suggested that this was due to shallow, discontinuous confining layers which forced the groundwater to discharge farther from shore. Because the offshore discharge feature was probably not unique to this one location, SGD point measurements using seepage meters would tend to underestimate the total discharge to the bay. This issue can be circumvented by the use of geochemical tracers (i.e. Ra) which integrate over the entire system. Thus, using the total bay SGD flux calculated above with the Ra mass balance, and the discharge estimated by a model assuming exponential decrease away from shore (Bokuniewicz and Zeitlin, 1980; Bokuniewicz, 1992; Bokuniewicz et al., 2004), one can estimate the relative importance of irregular SGD flow patterns to the total input to the bay.

First, the empirically-determined (using point measurement data collected with seepage meters) exponential model of Bokuniewicz et al. (2004) estimates an SGD flux of 3,300 L day^{-1} per meter of shoreline. The Bokuniewicz and Zeitlin (1980) estimate is higher at 7,800 – 16,000 L day^{-1} m^{-1}. Given a bay length of 34 km and an average width of about 6.2 km, there is a total discharge length of roughly 80.4 km. Thus, there is a total shoreline discharge of 0.27×10^9 L d^{-1} (using the 2004 estimate) to 1.29×10^9 L d^{-1} (using the high-end 1980 estimate).

The shoreline discharge occurs along a narrow 260 m seepage face (Bokuniewicz et al., 2004). This leaves approximately 191 km^2 of surface area in the center of the bay

unaccounted for. Given that the model describes exponential decrease away from shore, the rate of SGD beyond the shoreline seepage face is approximately asymptotic. Thus, an upper limit can be approximated as the 1.8 cm d^{-1} seepage observed at 100 m offshore (Bokuniewicz et al., 2004). Extrapolated across the surface area of the center of the bay, this gives a non-shoreline SGD flux of 3.44×10^9 L d^{-1}. Although the highest rates of discharge are observed along the shore, the small area over which it occurs makes it less than about 30% of the total discharge to the bay.

Combined, these give a total modeled SGD flux for the bay of $3.6 – 4.7 \times 10^9$ L d^{-1}. The SGD estimated from the Ra mass balance is $3.8 – 7.0 \times 10^9$ L d^{-1}. This suggests that as much as 30% of the SGD in Great South Bay occurs in a somewhat random fashion that may not be consistently observed by seepage meters. Furthermore, this also implies that a major portion of the submarine groundwater flux to Great South Bay does not occur in a predictable manner.

Preferential flowpaths have been observed elsewhere (Rapaglia, 2005; Robinson et al., 2006; Beck et al., in prep), and are probably important mechanisms governing submarine groundwater transport and discharge. Such behavior confounds current approaches for estimating SGD-associated chemical fluxes (Hwang et al., 2005; Kim et al., 2005; Oberdorfer et al., 1990); combined with geochemical transformations occurring in the subterranean estuary (Charette and Sholkovitz, 2006; Testa et al., 2002; Talbot et al., 2003; Beck et al., 2007), flow channelization may make accurate chemical flux estimates nearly impossible. Certainly, more work is necessary to fully understand the mechanisms regulating SGD chemical fluxes.

SUMMARY and CONCLUSIONS

This study has used a mass balance for the 4 naturally-occurring Ra isotopes to estimate SGD to Great South Bay, NY. The budget indicated that diffusive input represented 8% of the total for ^{224}Ra, 5% for ^{223}Ra, and was negligible for ^{226}Ra and ^{228}Ra. No desorption of Ra from river-borne particles was evident. River input of dissolved Ra was very low – less than 1% for all isotopes - but river water was enriched in Ra relative to the Bay, due to direct submarine groundwater discharge to the river. Exchange of bay water with ocean water at Fire Island Inlet was the largest flux term, representing 35 – 67% of the total Ra input, and 67 – 100% of the export. Radioactive decay was only a significant removal term for ^{224}Ra and ^{223}Ra, at 33% and 14%, respectively.

The Ra budget for Great South Bay revealed a major imbalance, with an unaccounted-for source representing 32 – 57% of the total input. This unknown input was assumed to be discharge of brackish groundwater with high Ra activities. Applying the Ra activities measured in shallow groundwater in the bay, we estimate an SGD flux of $3.1 – 8.1 \times 10^9$ L d^{-1}. This input is as much as 40% higher than that estimated by a model developed from direct seepage measurements (Bokuniewicz et al., 2004), suggesting that much of the SGD in Great South Bay is due to spatially heterogeneous flow, presumably along preferential flowpaths.

The ecological importance of SGD to Great South Bay has been shown previously (Capone and Bautista, 1985; Taylor et al., 2006), with particular attention to nutrient input. It is probable that SGD is also a source of other dissolved constituents such as trace metals to the bay (Clark et al., 2006). We are currently working to elucidate

processes governing trace metal cycling in the subterranean estuary in Great South Bay, and the possibility for trace metal transport to the water column. Qualitatively, we may already observe such input in this data: Clark et al. (2006) showed very high (2 – 5 nM) levels of dissolved Pb in the Connetquot and Carmans Rivers. As discussed above, the rivers appear to be major sites of SGD. We have measured high levels of dissolved Pb (1.3 – 4.2 nM) in fresh groundwater at the Roe Avenue site (unpublished data). Thus, elevated Pb levels in the rivers may reflect input due to SGD. We have estimated that ~90% of the SGD in Great South Bay is recirculated seawater. Many previous reports of ecologically important groundwater chemical input to Long Island coastal waters have focused on fresh discharge alone. More work is necessary to determine the effect of seawater recirculation and processes occurring in the subterranean estuary on the SGD-derived flux of dissolved chemical constituents to Great South Bay.

Acknowledgements

This research was supported by New York Sea Grant (Project RCTP-40) and the Long Island Groundwater Research Institute (LIGRI).

REFERENCES

Beck, A.J., Y. Tsukamoto, A. Tovar-Sanchez, M. Huerta-Diaz, H.J. Bokuniewicz, and S.A. Sanudo-Wilhelmy. 2007. Importance of geochemical transformations in determining submarine groundwater discharge-derived trace metal and nutrient fluxes. Applied Geochemistry, 22: 477-490.

Beck, A.J., J.P. Rapaglia, J.K. Cochran, and H.J. Bokuniewicz. Radium mass-balance in Jamaica Bay, NY: Evidence for a substantial flux of submarine groundwater. Marine Chemistry, submitted.

Bokuniewicz, H.J., and Zeitlin, M.J. 1980. Characteristics of groundwater seepage into Great South Bay. MSRC, Special Report 35, SUNY, Stony Brook, NY, 30 p.

Bokuniewicz, H, and B Pavilik. 1990. Groundwater seepage along a barrier island. Biogeochemistry 10: 257-276

Bokuniewicz, H.J. 1992. Analytical descriptions of subaqueous groundwater seepage. Estuaries 15, 458–464.

Bokuniewicz, H.J., Pollock, M., Blum, J., and Wilson, R., 2004. Submarine groundwater discharge and salt penetration across the sea floor. Ground Water, 42: 983-989.

Bollinger, M.S. and W.S. Moore, 1993, Evaluation of salt marsh hydrology using radium as a tracer. Geochimica et Cosmochimica Acta, 57:2203-2212.

Bollinger, M. S., and W. S. Moore. 1984. Radium fluxes from a salt marsh. Nature 309: 444-446.

Boudreau, B.P., M. Huettel, S. Forster, R.A. Jahnke, A. McLachlan, J.J. Middleburg, P. Nielsen, F. Sansone, G. Taghon, W.V. Raaphorst, I. Webster, J.M. Weslawski, P. Wiberg, and B. Sundby. 2001. Permeable marine sediments: Overturning an old paradigm. EOS, 82(11): 133-136

Buddemeier, R.W. 1996. Groundwater flux to the ocean: Definitions, data, applications, uncertainties. In: Groundwater Discharge to the Coastal Zone: Proceedings of an international symposium. R.W. Buddemeier, ed. LOICZ Reports and Studies No. 8, LOICZ, Texel, The Netherlands, pp. 16-21.

Burnett, W.C., M. Taniguchi, J. Oberdorfer. 2001. Measurement and significance of the direct discharge of groundwater into the coastal zone. Journal of Sea Research, 46: 109-116.

Burnett, W.C. and H. Dulaiova, 2003. Estimating the dynamics of groundwater input into the coastal zone via continuous radon-222 measurements. Journal Environmental Radioactivity, 69, 21-35.

Burnett, W.C., P.K. Aggarwal, H. Bokuniewicz, J.E. Cable, M.A. Charette, E. Kontar, S. Krupa, K.M. Kulkarni, A. Loveless, W.S. Moore, J.A. Oberdorfer, J. Oliveira, N. Ozyurt, P. Povinec, A.M.G. Privitera, R. Rajar, R.T. Ramessur, J. Scholten, T. Stieglitz, M. Taniguchi, J.V. Turner. 2006. Quantifying Submarine Groundwater Discharge in the Coastal Zone via Multiple Methods. Science of the Total Environment 367(2-3): 498-543.

Capone, D.G. and M.F. Bautista. 1985. A groundwater source of nitrate in nearshore marine sediments. Nature 313, 214 – 216.

Charette, M.A., K.O. Buesseler, and J.E. Andrews. 2001. Utility of radium isotopes for evaluating the input and transport of groundwater-derived nitrogen to a Cape Cod estuary. Limnology and Oceanography, 46, 465-470

Charette, M.A., M.C. Allen. 2006. Precision groundwater sampling in coastal aquifers using a direct push shielded screen well-point system. Groundwater Monitoring & Remediation. 26 (2) 87-93.

Charette, M.A., E.R. Sholkovitz. 2006. Trace element cycling in a subterranean estuary: Part 2. Geochemistry of the pore water. Geochimica et Cosmochimica Acta, 70 (4): 811-826.

Charette M.A., K.O. Buesseler. 2004. Submarine groundwater discharge of nutrients and copper to an urban subestuary of Chesapeake Bay (Elizabeth River). Limnology and Oceanography 49 (2): 376-385.

Charette, M.A., W.S. Moore, W.C. Burnett. Submitted. Uranium- and thorium-series nuclides as tracers of submarine groundwater discharge. In *Radioactivity in the Environment: U-Th Series Nuclides in Aquatic Systems*.

Clark, L.B., C.J. Gobler, and S.A. Sanudo-Wilhelmy. 2006. Spatial and Temporal Dynamics of Dissolved Trace Metals, Organic Carbon, Mineral Nutrients, and Phytoplankton in a Coastal Lagoon: Great South Bay, New York. Estuaries and Coasts, 29(5): 841-854.

Crotwell, A.M. and W.S. Moore. 2003. Nutrient and Radium Fluxes from Submarine Groundwater Discharge to Port Royal Sound, South Carolina. Aquatic Geochemistry 9: 191–208.

Elsinger, R. J., and W. S. Moore. 1983. ^{224}Ra, ^{228}Ra, and ^{226}Ra in Winyah Bay and Delaware Bay. Earth Planet. Sci. Lett. 64: 430-436.

Epler, N. 1991. A multiple tracer study of ground water from a shallow, unconfined aquifer. PhD Thesis, MSRC-SUNYSB, Stony Brook, NY.

Gobler, C.J. and S.A. Sañudo-Wilhelmy. 2001 Temporal variability of groundwater seepage and Brown Tide Blooms in a Long Island Embayment. Marine Ecology Progress Series 217, 299-309

Gobler, C.J., and Boneillo, G.E. 2003. Impacts of anthropogenically influenced groundwater seepage on water chemistry and phytoplankton dynamics within a coastal marine system. Mar. Ecol. Prog. Ser., 255: 101-114

Hancock G.J., Webster I.T., Ford P.W., et al. 2000. Using Ra isotopes to examine transport processes controlling benthic fluxes into a shallow estuarine lagoon. Geochimica et Cosmochimica Acta, 64 (21): 3685-3699

Hussain, N., T.M. Church, and G. Kim, 1999. Use of 222Rn and 226Ra to trace groundwater discharge into the Chesapeake Bay. Mar. Chem., 65: 127-134.

Hwang, D.-W., G. Kim, Y.-W. Lee, H.-S. Yang. (2005) Estimating submarine inputs of groundwater and nutrients to a coastal bay using radium isotopes. Mar. Chem., 96: 61-71.

Johannes, R.E. 1980. The ecological significance of the submarine discharge of groundwater. Mar. Ecol. Prog. Ser., 3: 365-373.

Kelly, R.P., Moran, S.B. (2002) Seasonal changes in groundwater input to a well-mixed estuary estimated using radium isotopes and implications for coastal nutrient budgets. Limnology and Oceanography 47 (6): 1796-1807

Kim, G. J.-W. Ryu, H.-S. Yang, S.-T. Yun. (2005) Submarine groundwater discharge (SGD) into the Yellow Sea revealed by 228Ra and 226 Ra isotopes: Implications for global silicate fluxes. Earth and Planetary Science Letters, 237: 156-166

Krest, J.M., W.S. Moore, L.R. Gardner, and J.T. Morris. (2000) Marsh nutrient export supplied by groundwater discharge: Evidence from radium measurements. Global Biogeochemical Cycles 14 (1): 167-176.

LaRoche J., Nuzzi R., Waters R., Wyman K., Falkowski P.G., Wallace D.W.R. (1997) Brown Tide blooms in Long Island's coastal waters linked to interannual variability in groundwater flow. Global Change Biology 3(5): 397-410.

Li, Y.H., G. Mathieu, P. Biscaye and H.J. Simpson. (1977) The flux of 226Ra from estuarine and continental shelf sediments. Earth and Planetary Science Letters 37 (2) 237-241.

Li, Y.H. and L.H. Chan. (1979) Desorption of Ba and 226Ra from river-borne sediments in the Hudson estuary. Earth and Planetary Science Letters 37, 237-241.

Michael, H.A., A.E. Mulligan, C.F. Harvey. (2005) Seasonal oscillations in water exchange between aquifers and the coastal ocean. Nature 436, 1145-1148.

Moore, W.S. (1976) Sampling Ra-228 in the deep ocean. Deep-Sea Research 23 (7): 647-651.

Moore W.S. (1996) Large groundwater inputs to coastal waters revealed by Ra-226 enrichments. Nature 380 (6575): 612-614.

Moore W.S. (2000) Determining coastal mixing rates using radium isotopes. Continental Shelf Research 20 (15): 1993-2007.

Moore, W.S. and D.F. Reid. (1973) Extraction of radium from natural waters using manganese-impregnated acrylic fibers. Journal of Geophysical Research 78 (36): 8880-8886

Moore WS. (1998) Application of Ra-226, Ra-228, Ra-223, and Ra-224 in coastal waters to assessing coastal mixing rates and groundwater discharge to oceans. P. Indian As-Earth 107 (4): 343-349

Moore WS, Arnold R. (1996) Measurement of Ra-223 and Ra-224 in coastal waters using a delayed coincidence counter. J Geophys Res-Oceans 101 (C1): 1321-1329

Moskowitz, P.D. 1976. An analysis of salinity variations within Great South Bay, NY. Limnology and Oceanography 21(5): 740-742.

Oberdorfer, J.A., M.A. Valentino, S.V. Smith. (1990) Groundwater contribution to the nutrient budgets of Tomales Bay, California. Biogeochem., 12: 199-216.

Perlmutter, N.M., and H.C. Crandell. 1959. Geology and ground-water supplies of the south shore beaches of Long Island, NY. New York Acad. Sci. Annals, 50: 1060-1076.

Rama, Moore WS. 1996. Using the radium quartet for evaluating groundwater input and water exchange in salt marshes. Geochim. Cosmochim. Ac. 60 (23): 4645-4652

Rapaglia J. 2005. Submarine Groundwater Discharge into the Venice Lagoon, Italy. Estuaries 28(5): 705-713.

Reid, D.F., R.M. Key, and D.R. Schink. 1979. Radium, thorium, and actinium extraction from seawater using an improved manganese-oxide-coated fiber. Earth. Planet. Sci. Lett., 43(2): 223-226.

Robinson C., B. Gibbes, and L. Li. 2006. Driving mechanisms for groundwater flow and salt transport in a subterranean estuary. Geophysical Research Letters, 33, L03402, doi:10.1029/2005GL025247

Rutkowski, C.M., W.C. Burnett, R.L. Iverson, and J.P. Chanton. 1999. The effect of groundwater seepage on nutrient delivery and seagrass distribution in the northeastern Gulf of Mexico. Estuaries, 22(4): 1033-1040.

Seplow, M.S. 1991. The influence of groundwater seepage on pore water salinity in Great South Bay. M.S. thesis, Marine Sciences Research Center, State University of New York, Stony Brook, NY.

Shaw, T.J. 2001. Conference provides forum for discussion of subterranean coastal environments. EOS, 82(50): 622-623.

Taylor, G.T., C.J. Gobler, and S.A. Sanuso-Wilhelmy. 2006. Speciation and concentrations of dissolved nitrogen as determinants of brown tide *Aureococcus anophagefferens* bloom initiation. Mar. Ecol. Prog. Ser., 312: 67-83.

Talbot, J.M., K.D. Kroeger, A. Rago, M.C. Allen, M.A. Charette. (2003) Nitrogen flux and speciation through the subterranean estuary of Waquoit Bay, Massachusetts. Biological Bulletin, 205: 244-245.

Testa, J.M., M.A. Charette, E.R. Sholkovitz, M.C. Allen, A. Rago, C.W. Herbold. (2002) Dissolved iron cycling in the subterranean estuary of a coastal bay: Waquoit Bay, Massachusetts. Biological Bulletin, 203: 255-256.

Wilson, R.E., K.-C. Wong, and H.H. Carter. 1991. Aspects of circulation and exchange in Great South Bay, p. 9–22. In J. R. Schubel, T. M. Bell, and H. H. Carter (eds.), The Great South Bay. State University of New York Press, Albany, New York.

Wong, K.-C. 1993. Numerical simulation of the exchange process within a shallow bar-built estuary. Estuaries 16:335–345.

Zeitlin, M.J. 1980. Variability and predictability of submarine ground-water flow into a coastal lagoon, Great South Bay, New York. M.S. thesis, Marine Sciences Research Center, State University of New York, Stony Brook, NY.

Zektzer, I.S., V.A. Ivanov, and A.V. Meskheteli. 1973. The problem of direct groundwater discharge to the seas. Journal of Hydrology, 20: 1-36.

TABLES and FIGURES

Description	Symbol	^{223}Ra	^{224}Ra	^{226}Ra	^{228}Ra	Units
Carman's River	C_{Car}	3.72	36.4	10.05	9.93	dpm 100 L^{-1}
Connetquot River	C_{Conn}	4.92	61.39	17.00	20.30	dpm 100 L^{-1}
Ocean	C_{ocean}	0.61	14.4	8.85	11.99	dpm 100 L^{-1}
Average bay value	C_{Bay}	1.40	27.40	13.13	20.75	dpm 100 L^{-1}
Diffusive flux	J_{diff}	0.052	2.2	0	0	dpm m^{-2} h^{-1}
Groundwater (n=16)	C_{gw}	14	467	106	240	dpm 100 L^{-1}
Decay constant	λ	0.0608	0.193	0.000001	0.00033	d^{-1}
Carman's R discharge	F_{Car}		5.90×10^4			m^3 d^{-1}
Connetquot discharge	F_{Conn}		8.60×10^4			m^3 d^{-1}
Bay surface area	A_{Bay}		2.09×10^4			m^2
Fine-grain sed fraction	$\%_{fines}$		0.3			
Bay depth	z_{Bay}		1.3			m
Tidal range	dz		0.25			m per cycle

Table III-1. Parameters used to calculate Ra fluxes in Great South Bay.

	Fluxes into Great South Bay (10^9 dpm d^{-1})					Fluxes out of the Bay (10^9 dpm d^{-1})			
	Carmans River	Connetquot River	Diffusion	Ocean exchange	**Sum input**	Ocean exchange	Decay	**Sum removal**	**Flux imbalance (10^9 dpm d^{-1})**
^{224}Ra	0.021	0.053	3.3	15.1	18.4	28.6	14.33	43.0	24.5
^{223}Ra	0.002	0.004	0.078	0.64	0.72	1.46	0.23	1.69	0.97
^{228}Ra	0.006	0.017		12.5	12.6	21.7	0.02	21.7	9.1
^{226}Ra	0.006	0.015		9.2	9.3	13.7	0.00	13.7	4.5

Table III-2. Ra fluxes in Great South Bay for August 2006.

		^{224}Ra	^{223}Ra	^{228}Ra	^{226}Ra
Fluxes out	Ocean exchange	67	86	100	100
	Decay	33	14	0.1	0
Fluxes in	Carmans River	0.05	0.13	0.03	0.04
	Connetquot River	0.12	0.25	0.08	0.11
	Diffusion	8	5	0	0
	Ocean exchange	35	38	58	67
	SGD	57	57	42	32

Table III-3. Percent contribution of different sources and sinks to the total Ra budget of Great South Bay.

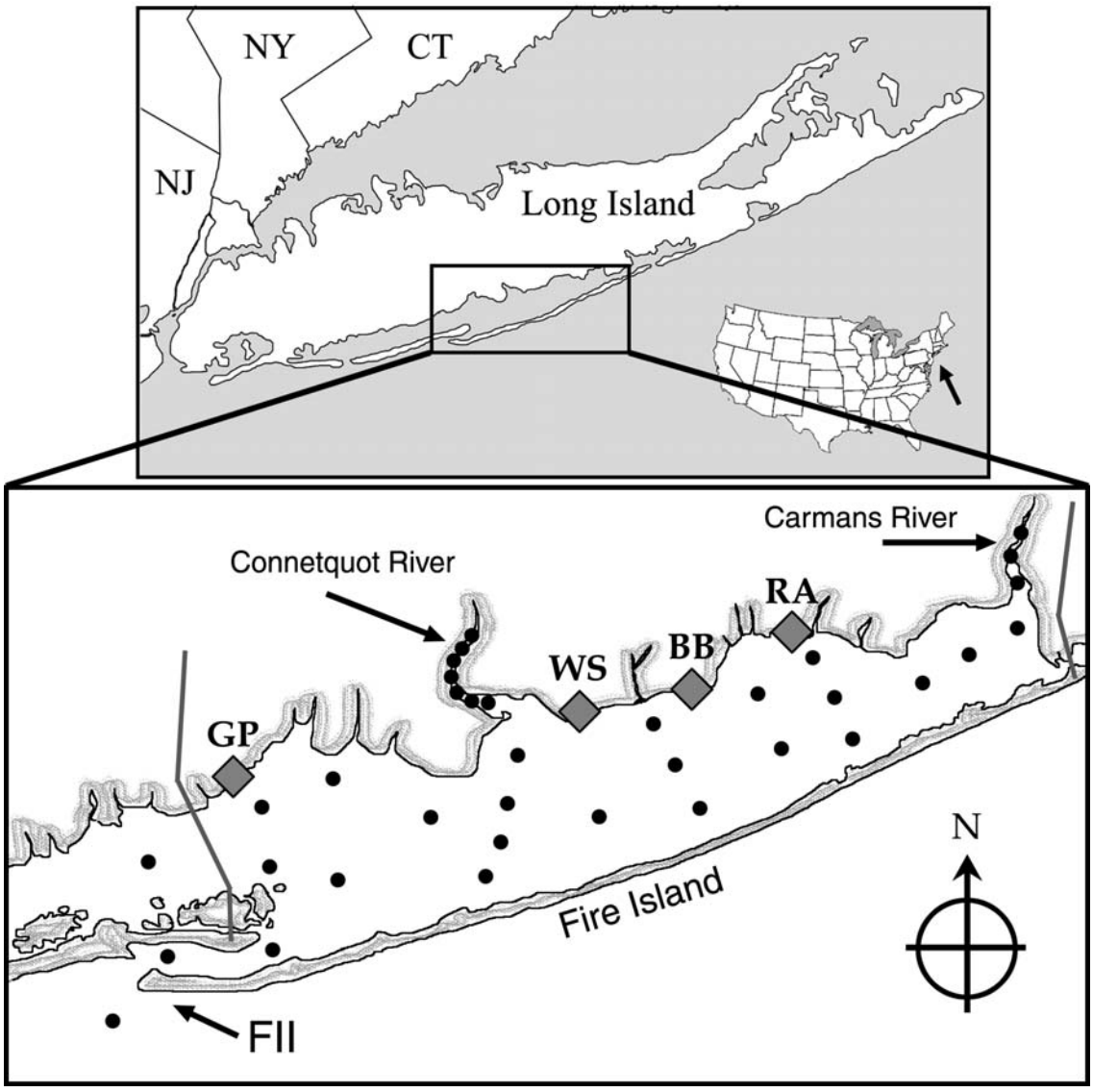

Figure III-1. Great South Bay, NY. Sampling stations are indicated by solid circle symbols. Fire Island Inlet (FII) is indicated, as are the Connetquot and Carmans River locations. Groundwater sampling sites are marked with gray diamonds; site IDs are: GP – Gardiners Park, WS – West Sayville, BB – Bayport Beach, RA – Roe Avenue. The sharp gray lines at the east and west borders of the Bay show locations of the Smith Point and Jones Beach causeways, respectively.

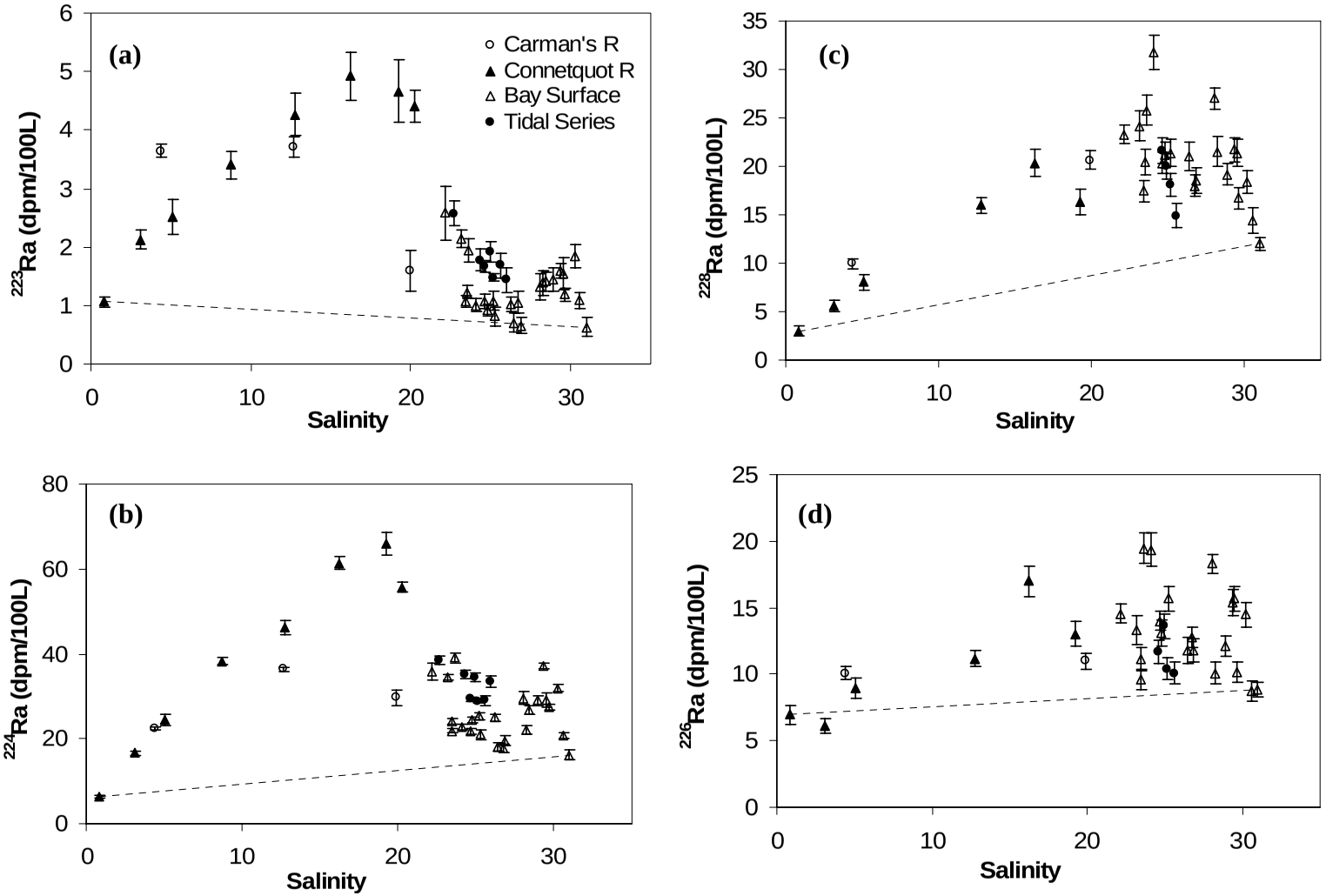

Figure III-2. Dissolved Ra in surface waters of Great South Bay, Carmans River, and Connetquot River. (a) ^{223}Ra, (b) ^{224}Ra, (c) ^{228}Ra, (d) ^{226}Ra. Error bars represent 1σ counting error.

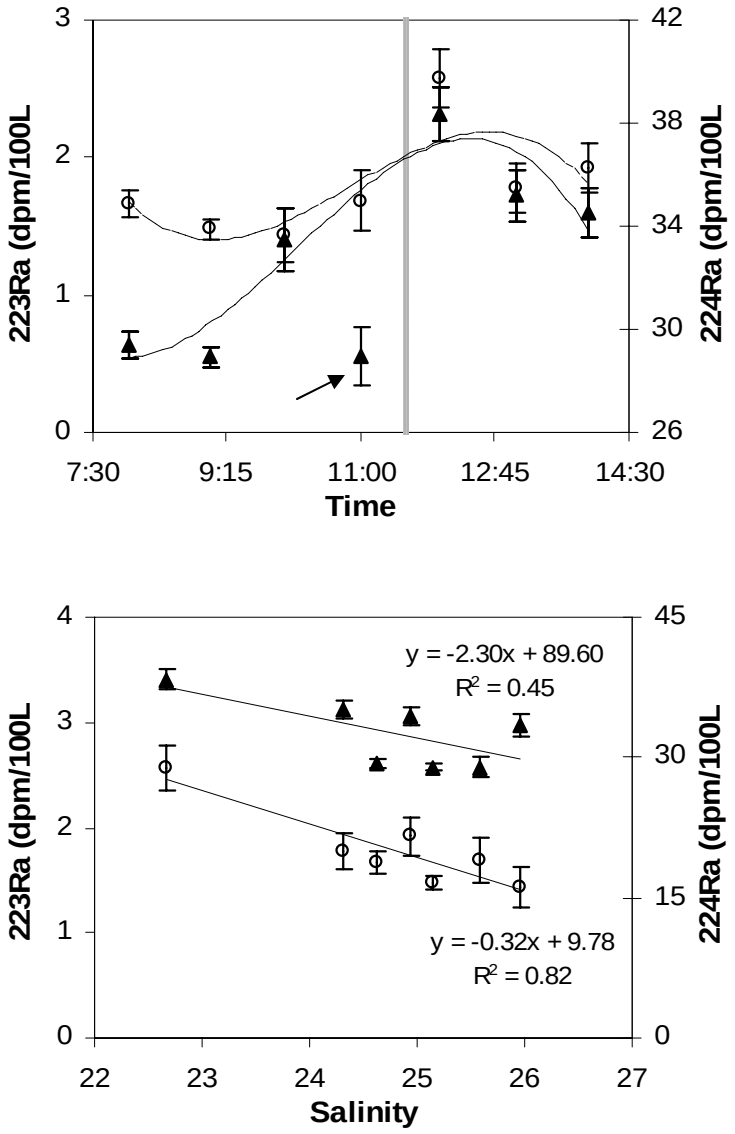

Figure III-3. Tidal series at the Connetquot River mouth. Hollow and filled symbols denote ^{223}Ra and ^{224}Ra, respectively. Error bars are 1σ counting uncertainty. **(a)** Activity trends with time. The vertical dotted line identifies low tide. The curved dotted and solid lines show approximate best fit trends for ^{223}Ra and ^{224}Ra, respectively. The solid line is drawn excluding the low value measured at 11:00 (identified by the arrow). **(b)** Relationship between Ra activity and salinity. Solid lines represent a linear regression of the data for each isotope; best fit equations and correlation coefficients are also shown.

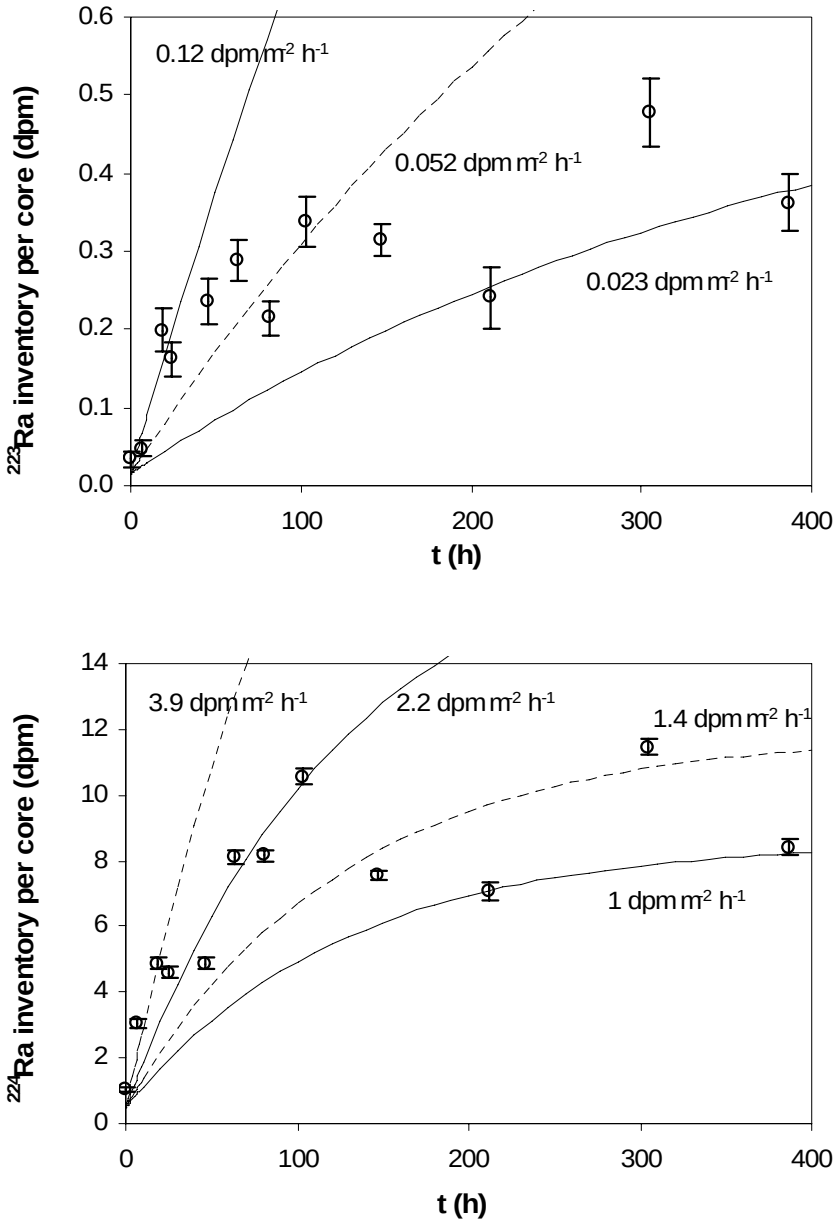

Figure III-4. Increase of Ra inventory in sediment core overlying water. Solid and dashed lines represent modeled curves (after Beck et al., submitted) for the different flux rates indicated next to each curve. Error bars represent 1σ counting error.

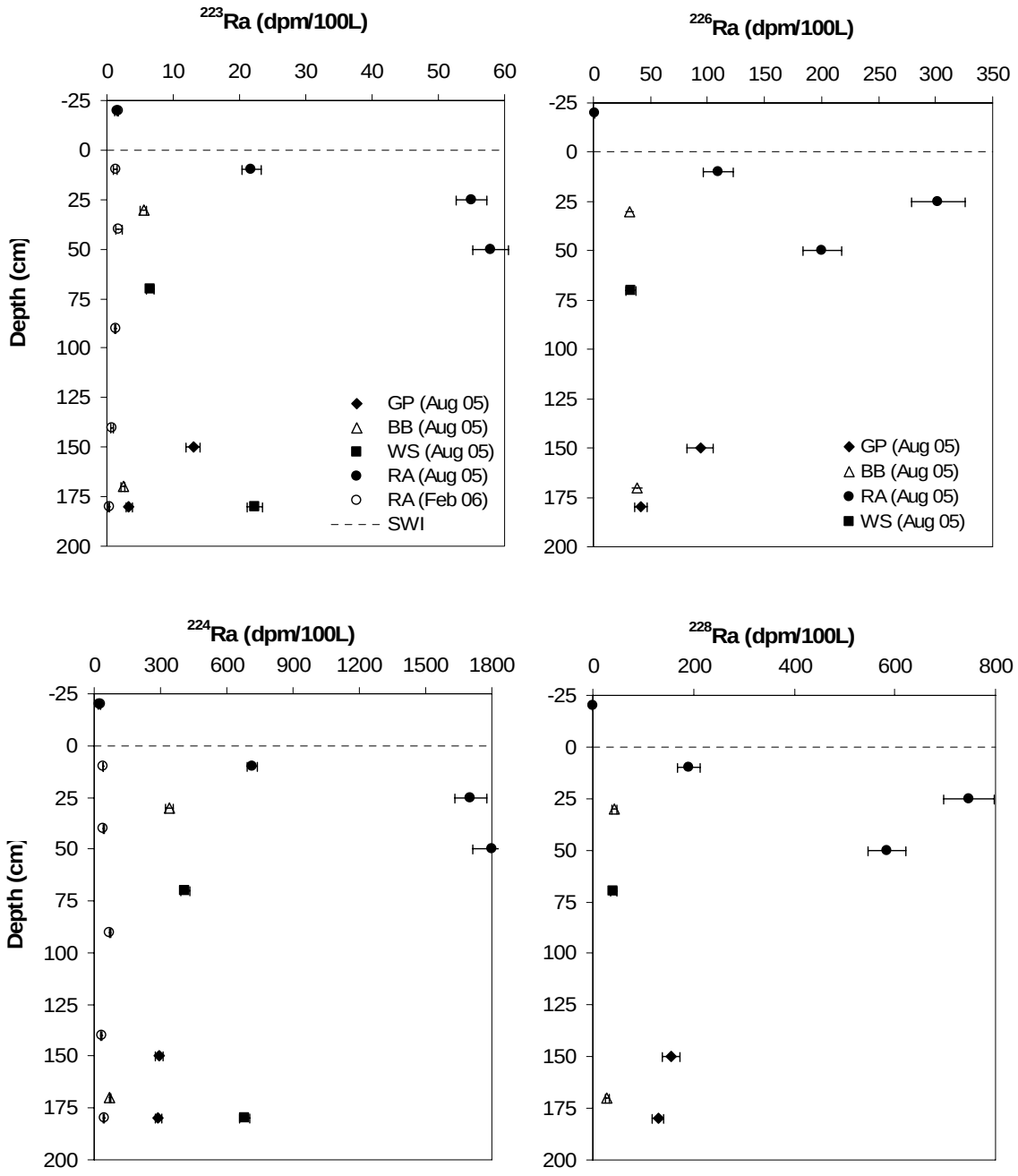

Figure III-5. Profiles of dissolved Ra in shallow groundwater. Site IDs are: GP – Gardiners Park (solid diamonds), BB – Bayport Beach (hollow triangles), WS – West Sayville (solid squares), RA – Roe Avenue (circles). Error bars represent 1σ counting error.

CHAPTER IV:

Temporal trends of dissolved trace metals in Jamaica Bay, NY: Importance of wastewater input and submarine groundwater discharge

ABSTRACT

Jamaica Bay, NY, is a highly urbanized estuary within the boroughs of New York City conspicuously lacking published information on dissolved trace metal levels. The current study examines the distribution and cycling of trace metals in Jamaica Bay based on data gathered during three cruises over the period 2004-2006. Most of the metal distributions are explained by the input of substantial volumes of treated wastewater effluent. The wastewater source was particularly significant for Ag, Zn, Pb, and Cu. Metal behavior in the "sewage estuary," where effluent mixed with bay water, indicated conservative behavior of Fe and Mo, moderate (≤ 30 %) non-conservative removal of Co, Ni, Pb, and Cu, and substantial (~ 50 %) removal of Ag and Zn in the mixing zone. The removal apparently occurred primarily in the region where salinity was less than 5. Correlation with ^{223}Ra in bottom water during periods of vertical thermohaline stratification indicated that submarine groundwater discharge (SGD) was an additional source of dissolved Co, Zn, Fe, and Ni to the water column during the summer season. Conversely, the distribution of dissolved Mo throughout the water column during all seasons could only be interpreted as non-conservative removal, and differences in the magnitude of depletion between seasons indicated that SGD (i.e. recirculation of bay water through reducing permeable sediments) was the removal mechanism. This was confirmed by the nearly quantitative removal of Mo with respect to salinity in permeable sediment porewaters. This study provides the first measurements of dissolved trace metals in Jamaica Bay, NY. It also reports new data on some dissolved contaminant trace metals in the subterranean estuary, and provides evidence for trace metal input due to SGD.

INTRODUCTION

With the promulgation of the Clean Water Act in 1972, lawmakers sought to reduce the input of contaminants into U.S. coastal waters. Although the legislation was successful in reducing point-source discharges of contaminants (US EPA, 1995), it may not have resulted in significant reduction of trace metal levels in some estuaries (Sañudo-Wilhelmy et al., 2004). Some recent work has shown that a large portion of dissolved contaminant metal pools is currently attributable to non-point sources such as benthic remobilization (Sañudo-Wilhelmy and Gill, 1999; Buck et al., 2005). In a similar manner, Gobeil et al. (2005) found that wastewater effluent contributed only a small portion of the total load for numerous trace metals in the St. Lawrence River estuary, although they could not definitively determine the identity of the dominant fluxes. However, Sañudo-Wilhelmy et al. (2004) note that some of our current inability to observe declines in contamination may simply be a lack of high-quality trace metal data necessary for observing statistically-significant trends. Additional data are necessary to assess the level of trace metal pollution in U.S. coastal waters and potential non-point source inputs.

Benthic trace metal release by diffusion from fine-grained sediments is well-established (Aller and Benninger, 1981; Hunt, 1983; Aller, 1994; Rivera-Duarte and Flegal, 1997; Berelson et al., 2003). However, during the last decade, a large body of evidence has been gathered showing that advection of porewater through permeable sediments may also represent a major direct source of trace elements to coastal waters (Shaw et al., 1998; Basu et al., 2001; Windom and Niencheski, 2003; Charette and Buessler, 2004; Charette and Sholkovitz, 2006, Bone et al., 2006, in press; Windom et al.,

2006; Beck et al., 2007). Considering the increasing volume of research confirming the large magnitude and global ubiquity of this submarine groundwater discharge (SGD), it is not unreasonable to expect that permeable sediments represent a significant trace metal source in both local and global budgets (Moore, 1997; Shaw et al., 1998; Basu et al., 2001; Charette and Sholkovitz, 2006). The importance of chemical transport by SGD is certainly not a geologically-recent process (indeed, some researchers have inferred it from geologic records [e.g. Ingram and Sloan, 1992; Cochran et al., 2003]), but as anthropogenic activities modify the trace element composition of coastal marine sediments (Luoma and Phillips, 1988; Wolfe et al., 1996; Mecray and Buchholtz ten Brink, 2000), so also will they affect the composition of porewaters in contact with those sediments (Froelich et al., 1979; Shaw et al., 1990). Consequently, anthropogenic contamination of the sediments will affect the trace metal load transported in SGD, and as more data are collected, SGD will likely be implicated as a significant source of trace metals to coastal waters.

Therefore, the purpose of the present study is twofold: first, it establishes the first measurements of dissolved trace metals in a heavily impacted urban estuary, Jamaica Bay, NY, and examines the cycling of metals in that system. Second, because trace metal samples were collected coincident with SGD tracers (i.e. naturally-occurring radium isotopes), this study is also uniquely able to assess how SGD affects the dissolved trace metal composition of the water column.

Study Site

Jamaica Bay, NY, is a small (~52 km^2) estuary located within the confines of Brooklyn, one of the boroughs of New York City (Fig. IV-1). Jamaica Bay is a unique estuary in that the freshwater source is almost entirely anthropogenic, mainly treated wastewater effluent; there is no non-sewage surface input of fresh water (Houghton et al., 2005), and groundwater discharge supplies less than 10% of the fresh water flux (Misut and Voss, 2004). Brackish SGD in Jamaica Bay is ~10-fold higher than the fresh groundwater input, representing between 1.6 and 7.3 billions of liters per day, depending on the season (Chapter II).

Four major and two minor wastewater treatment plants (WWTP) discharge effluent directly into Jamaica Bay (Benotti et al., 2006). The major WWTPs, Coney Island, Jamaica, 26th Ward, and Rockaway, discharge a combined average volume of about 8×10^8 L d^{-1} of secondary-treated effluent. The locations of the outfalls of these WWTPs are shown in Fig. IV-1.

The bay is relatively shallow (< 5 m depth), although some channels may be deeper. The deepest channels run along the western and southeastern borders of the bay. The residence time of water in Jamaica Bay has been estimated at 7-35 days (Houghton et al., 2005; Swanson et al., 1992), and is shortest in these deep, well-flushed channels (R. Islieb, written communication, as cited in Benotti et al., 2006). Grassy Bay is the large, deep basin to the north (Fig. IV-1), and restricted water flow results in a long residence time and seasonal hypoxia (Swanson et al., 1992). To the northeast, limited flushing of the wide, shallow Thurston Basin also results in long residence time of the water (R. Islieb, written communication, as cited in Benotti et al., 2006).

Grassy Bay is bordered to the north by JFK International Airport, a major runway of which covers a substantial portion of former marshland (Bopp et al., 1993) and restricts water circulation through that portion of the bay (Swanson et al., 1992). The center of the bay is bisected by Rulers Bar Hassock, an island which supports a small residential population. There is extensive marshland in the center of the bay on either side of this central island, and the water depth is shallowest in this region of the bay. Extensive marsh loss has been documented for many marshes in Jamaica Bay during the past half-century (Hartig et al., 2002), although the exact reasons for this loss are unclear.

Trace metal data are lacking in Jamaica Bay. To our knowledge, the only peer-reviewed data on trace metals in Jamaica Bay were reported by Bopp et al. (1993). Their sediment data suggest that trace metal inputs to Jamaica Bay have declined since the late 1960s or early 1970s. Bopp et al. (1993) also argue that storm events and combined sewage overflow events can deliver large pulses of metal contaminants to the bay that are visible in the sedimentary record. Finally, evidence from eggs indicates that herring gulls in Jamaica Bay are exposed to levels of some trace metals that are similar in magnitude to other locations in urban New York and New Jersey, but Jamaica Bay gull eggs show particularly elevated levels of cadmium (Gochfield, 1997).

METHODS

Water column samples

Detailed information regarding the different cruises is available elsewhere (Chapter II). Water sampling for trace metals analysis was conducted during three cruises in Sept. 2004, Oct. 2005, and April 2006. Water column conditions (e.g. temperature, dissolved oxygen, etc.) during the Sept. and Oct. cruises were characteristic of late summer, while the April cruise represented early spring conditions. Bay water samples for trace metal analysis were collected throughout the bay (Fig. IV-1) using clean techniques described in detail elsewhere (Flegal et al., 1991). Briefly, water samples were pumped onboard through acid-cleaned Teflon tubing using a peristaltic pump with clean C-Flex tubing in the pumphead. During Oct. 2005 and April 2006, samples were collected from both surface (~ 1 m depth) and bottom (~ 1 m above sediment) depths. Water was filtered through an acid-washed 0.22 μm calyx capsule filter directly into acid-washed 1 L low density polyethylene (LDPE) bottles. Water samples were double-bagged in polyethylene bags and returned to the clean lab for processing. DOC samples were filtered in the same way, collected in pre-combusted glass bottles, and kept on ice until they could be frozen.

Samples for measurement of total dissolved trace metals were acidified to pH <2 with Optima-grade HNO_3, and stored for at least one month before extraction. Metals were then preconcentrated following the APDC/DDDC organic extraction of Bruland et al. (1985), and analyzed by ICP-MS (ThermoFinnigan Element2) using Indium as an internal standard. Trace elements, including P, in groundwater samples were directly analyzed by ICPMS after 20- or 40-fold dilution with ultrapure 1N HNO_3. The

uncertainty of trace metal measurements made on replicate field samples was generally less than 5%, except for Ag (9%) and Fe and Pb (7%). Blank levels were less than 5% of the lowest sample for all metals except Ag, for which blanks were approximately 20% of the sample concentrations.

Stable Pb isotope ratios were also measured by ICPMS in preconcentrated samples. Mass bias was corrected using the NIST 981 standard reference material (SRM) analyzed after every third unknown sample. Analysis of this SRM (n=37) gave ratios of 2.1691 ± 0.0065 ($^{208}Pb/^{206}Pb$) and 0.9136 ± 0.0018 ($^{207}Pb/^{206}Pb$), compared to the certified values of 2.1681 ± 0.0008 ($^{208}Pb/^{206}Pb$) and 0.91464 ± 0.00033 ($^{207}Pb/^{206}Pb$).

DOC was determined by high-temperature catalytic oxidation (Sugimura and Suzuki, 1988; Benner and Strom, 1993). Salinity was measured with a YSI-880 handheld probe. Chloride was analyzed by titration with Ag on a Radiometer Copenhagen CMT10 automatic chloride titrator.

Groundwater

Four shallow groundwater (< 4 m depth) profiles were collected at three locations in the bay (Canarsie Pol, Canarsie Pier, Broad Channel; Fig. IV-1). Sample sites were chosen because they represent some of the most expansive sandy beaches in the bay. Groundwater advection through permeable sediments has been shown to be a major process in Jamaica Bay (Chapter II), and groundwater profiles were collected at the presumed sites of discharge. Canarsie Pier is located on the northwestern mainland side of the bay, while Broad Channel is located on the southern end of the large, developed island in the center of the bay. Canarsie Pol is a large, undeveloped island in the north-

west corner of the bay; this island is surrounded mostly by sandy shores, stands well above sea level, and is covered by dense thickets of large trees.

We have observed groundwater seepage occurring on the beachface at both the Canarsie Pier and Canarsie Pol locations. In fact, at the seepage site on Canarsie Pol, an orange-red precipitate was visible on the sediment surface (Fig. IV-2a). Shallow excavation revealed that the orange color was only at the surface, and sub-surface sands were a gray color (Fig. IV-2b). The same pattern was observed for relict bivalve shells within the seep (Fig. IV-2c), where exposed portions were colored orange and submerged portions had the same grayish color as the subsurface sands. We conclude that the groundwater seep was transporting reduced Fe species which then precipitated out of solution upon entering an oxic environment, similar to the "Iron Curtain" described by Charette and Sholkovitz (2002). This provides anecdotal evidence for the significance of SGD to trace metal inputs and cycling in Jamaica Bay, as discussed below.

Shallow groundwater profiles were sampled using a stainless steel Retract-a-Tip (AMS, Inc.) drive-point piezometer with acid-washed Teflon tubing (Charette and Sholkovitz, 2006; Charette and Allen, 2006). Before collecting a sample at each depth, enough water was purged to flush the volume of the sampling system three times. Small volume samples (60-250 mL) were either pump-filtered through 0.22 μm polypropylene Calyx capsule filters or syringe-filtered using 0.45 μm nylon filters. Sufficient sample was flushed through the filter before each collection to prevent artifacts associated with changing the redox characteristics of the sample (Bray et al., 1973; Lyons et al., 1979).

Wastewater effluent

Filtered water samples were collected inside the 26th Ward WWTP on 08 February 2005 (Fig. IV-1). The samples were pumped from the holding tank immediately preceding the outfall canal. Three 1 L samples were collected across a 4.25 h time span at 11:45, 14:20, and 16:00 h, and were processed as described for bay surface water.

Sewage estuary

In order to understand the effect of sewage discharge on dissolved trace metal levels in the bay, it is necessary to examine the behavior of these constituents across the salinity gradient of a mixing zone near a wastewater treatment plant (WWTP) outfall. We have chosen the outfall from the 26th Ward WWTP, located at the north-northwest border of the bay (Fig. IV-1). The treatment plant discharges its effluent (annual average discharge: ~85 millions of gallons per day, or approximately 320 millions of liters per day) near the head of Hendrix Creek. Along the creek, well-defined pseudo-estuarine circulation is evident, with fresh effluent water exiting the creek in a shallow layer that overlays saltier water with approximately the same salinity as most of the bay. We refer to the mixing zone in this creek as the "sewage estuary". At the time of sampling in April 2006, the less saline (less than 10 psu) surface layer was about 50 cm thick.

A 5-point depth profile was sampled through this surface layer at approximately 10 cm intervals in an attempt to obtain samples with a range of salinities. As shown in Fig. IV-3, the salinity gradient actually sampled was rather coarse, with four samples in the salinity range between 8 and 11, and one sample with a salinity of 21. With these, we

include three surface water samples collected immediately before in the same vicinity; two of these samples were collected at the mouth of the creek, and had salinities of 26-28. A sample with a salinity of 6 was collected near the WWTP outfall. The wastewater endmember sample collection is described above.

RESULTS and DISCUSSION

Comparison of trace metal levels in Jamaica Bay with other regions

Ranges of dissolved trace metal concentrations are shown in Table IV-1 for Jamaica Bay and other estuaries in the New York area and United States.

During September and October, Ag levels in the bay (4 – 91 pM) were the same or lower than those reported for other estuaries. Compared to other estuaries in the NY region, Ag levels during these months in Jamaica Bay were as low as the relatively pristine Great South Bay (12 – 73 pM; Clark et al., 2006). During April, measured Ag concentrations were still at the lower end of the range reported for many other urban estuaries. The very large wastewater source in Jamaica Bay would lead one to expect higher Ag levels than were actually observed (Sañudo-Wilhelmy and Flegal, 1992).

Two possible explanations for the low observed concentrations include: removal from the dissolved phase, and/or a decline in the sewage source. First, Jamaica Bay has substantial suspended particle concentrations, averaging approximately 20 mg/L (NYS DEP, 2003). Given the high particle-reactivity of Ag (Sañudo-Wilhelmy and Flegal, 1992), low dissolved concentrations may simply reflect partitioning into the particulate phase. This is consistent with the non-conservative removal observed in the sewage estuary (discussed below, Fig. IV-3h). A second possible explanation is simply that the

Ag source from sewage to coastal waters is declining. The high levels of Ag observed in wastewater effluent derive from development of photographic film. As photography becomes increasingly digital, the Ag input to coastal waters may also be diminishing.

Furthermore, these mechanisms are not mutually exclusive, and both may be affecting the distribution. Thus, one may speculate that dissolved Ag is being scavenged onto particles and removed from the water column. As the wastewater source decreases, much of the observed Ag in the water column may have a source from benthic remobilization. This is consistent with estimates of benthic Ag flux reported for San Francisco Bay nearly a decade ago (Rivera-Duarte and Flegal, 1997). In other words, the benthic source of Ag to the water column may become increasingly important as declining point-source anthropogenic input (inferred from this Jamaica Bay data) increases the gradient between overlying water and porewater (Flegal and Sañudo-Wilhelmy, 1993; Smith and Flegal, 1993).

Dissolved Co levels in Jamaica Bay (0.2 – 2.8 nM) were similar to those measured in other highly impacted estuaries such as Galveston Bay, TX (0.37 – 9.6 nM; Wen et al., 1999), and San Francisco Bay, CA (0.2 – 5.3 nM; Tovar-Sanchez et al., 2004). The upper end of the observed Co range is consistent with measurements reported for the nearby, sewage-impacted Hudson River Estuary (0.11 – 2.5 nM; Tovar-Sanchez et al., 2004).

Dissolved Cu concentrations (3 – 48 nM) were also within the range reported for other estuaries. The values measured in April (up to 48 nM) were some of the highest reported for the NY region; however, the highest value measured in September (8 nM) was actually lower than the lowest values reported in the region (average: 13.6 nM). This

major difference highlights the temporal variability observed for dissolved Cu in Jamaica Bay during this study.

Dissolved Pb in Jamaica Bay was elevated (39 – 1,550 pM), but still within the range reported for the region and nation (5 – 6,760 pM). In general, NY regional estuaries have some of the highest levels (up to 3,400 pM) reported for the nation, with the notable exceptions of Texas (San Antonio Bay – 1,207 pM, and Corpus Christi Bay – 960 pM) and Washington (Puget Sound – 6,760 pM), and Jamaica Bay ranks with the most contaminated. As for dissolved Cu, there was extreme seasonal variability, with order-of-magnitude differences between maximum concentrations in September (164 pM) and April (1,550 pM).

Dissolved Ni concentrations (3 – 23 nM) were similar to other estuaries impacted by anthropogenic activities. Because of the temperature dependence of diagenetic remobilization (Aller, 1994), the higher levels of Ni observed during high-flow, cold-water, spring conditions (April: 6 – 23 nM) as compared to low-flow, warm, summer conditions (October: 4 – 12 nM) suggest that wastewater discharge was the primary source of Ni to Jamaica Bay, not diagenetic remobilization (Topping and Kuwabara, 2003). However, levels tended to be lower than elsewhere in the NY region, and were a factor of 3 or 4 lower than the highest measurements reported for elsewhere in the United States (Narragansett Bay, RI – 91 nM, and San Francisco Bay, CA – 71 nM).

The concentrations of dissolved Zn in Jamaica Bay (2 – 191 nM) were some of the highest reported for the United States. In fact, the highest levels observed in April (191 nM) were only exceeded by values reported for Puget Sound, WA (413 nM; Paulson and Feely, 1985). Zn concentrations in the Hudson River Estuary (Sañudo-Wilhelmy and

Gill, 1999) were also very elevated (8 – 124 nM), and similar to the levels observed in Jamaica Bay. This suggests a similarity in the wastewater source, as both of these systems receive wastewater originating in New York City, and have elevated Zn levels relative to the rest of the NY region.

Behavior of dissolved trace metals in the sewage estuary

The samples collected in the "sewage estuary" will be used to examine the behavior of dissolved trace metals during the mixing of sewage effluent and bay water. In this case, we assume that the WWTP samples collected in February 2005 are representative of that endmember during April 2006, and that the 26th Ward WWTP is the primary source of fresh water to this local region of the bay.

The data show relatively coherent trends for the different trace metals (Fig. IV-3). Mo and Fe appear to be mixed conservatively with respect to salinity (although the trends are inverse), while Co, Pb, and Zn show pronounced removal. For Ag, Ni, and Cu, the trend is less clear due to variability in the fresh (sewage) endmember. For each of these elements, two of the WWTP samples are similar to within about ten percent, while the third differs from the other two by 25 to 50 percent. Because of this, the trends can be interpreted either as nearly conservative, or as non-conservative removal. We cannot definitively identify the source of this variability, although it may simply suggest that dissolved metals concentrations in the wastewater plant are not at steady state, the water in the holding tank is not well mixed, and/or that there is diel variability in the chemical composition of municipal influent (Ternes and Hirsch, 2000; Benotti; 2006).

For Ag, the dominant process is probably removal, owing to its particle-reactive nature and usual similarity in distribution to Pb (Sañudo-Wilhelmy and Flegal, 1992). Indeed, the general constancy of the Pb/Ag ratio at a value of about 7 across the mixing zone suggests similarity in the cycling of these two elements (Fig. IV-4). In fact, the molar ratios throughout the bay tend to be relatively high, averaging 6.2 ± 4.6 Pb/Ag throughout all three cruises.

Ni and Cu (Figs. IV-3d and IV-3e) exhibit relatively similar trends, although there is one high Ni measurement observed in the wastewater endmember. As noted previously, it is possible that there is significant variability in the dissolved chemical composition of the wastewater endmember (Ternes and Hirsch, 2000; Gobeil et al., 2005; Benotti, 2006), but the samples collected in this study provide only a snapshot of the wastewater metal concentrations. The one elevated Ni sample would suggest significant removal of Ni in the sewage estuary. However, if the other data are more representative of the true endmember, then both Cu and Ni exhibit only slight removal (less than 30%) relative to conservative mixing between the endmembers.

Non-conservative removal appears to be most substantial in the region where salinity is less than about 5, as metal concentrations are approximately linear at higher salinities. The degree of removal can be estimated as the difference between the concentration measured in the effluent and the concentration calculated for S = 0 by extrapolation of a regression line drawn through the approximately linear portion of the data. Following this approach, the degree of removal ranges from ~23% for Ni to 58% for Ag (Table IV-2).

The fact that all of these metals show removal below 5 psu and relatively linear trends at salinities between 5 and 27 suggests that a portion of the metal pool in the wastewater is relatively labile or particle-reactive, and that this fraction is removed rapidly upon mixing with bay water. This is consistent with previous studies of sewage-impacted estuaries, with much of the wastewater metal load removed from the dissolved pool within the estuary, and not exported to the coastal ocean (Gobeil et al., 2005). The remaining dissolved metal pool is more stable or refractory, and tends to behave conservatively during mixing. The low degree of removal calculated for Cu and Ni is consistent with previous work showing that these metals tend to be strongly complexed with anthropogenic organic ligands in wastewater (Sedlak et al., 1997). On the other hand, the conservative mixing behavior of Fe in the sewage estuary contrasts starkly with the nearly quantitative removal commonly observed in river estuaries (e.g. Boyle et al., 1974; Sholkovitz et al., 1978). This is probably due to different flocculating agents in wastewater and river water; in riverine systems, coagulation of humic organic material is responsible for the Fe removal. It is probable that the wastewater effluent sampled here contains a limited amount of these humic substances.

Distribution of dissolved trace metals in the JB water column

The trace metal distribution with salinity in the JB water column is shown in Fig. IV-5. Samples with salinities below 20 have been excluded from these graphs because during five cruises in Jamaica Bay (trace metal data exist for only three of these cruises), we have only observed substantially decreased salinities within the creek that receives

effluent from the 26th Ward WWTP. As we have discussed those data above, we exclude them to improve the clarity of the high salinity graphs.

For nearly all elements, the salinity distributions show differences between cruises, with highest concentrations observed in April 2006, intermediate levels in October 2004, and lowest levels measured in September 2005. However, little difference was observed between the Sept. and Oct. cruises for Pb and Fe (Figs. IV-5g and IV-5a). The greatest difference between April and Sept. cruises was observed for Mo, Zn, and Fe, which were higher in April by factors of approximately 1.5, 5, and 5, respectively. Taking the measured effluent concentrations as the correct fresh endmember, nearly all metals showed removal relative to conservative mixing, except during the April cruise, when non-conservative input of Co, Cu, and Fe was evident, and Ni appeared to be approximately conservative.

This apparent non-conservative input of Cu and Co (Figs. IV-5e and IV-5c) is somewhat problematic in that mixing within the sewage estuary indicated that these elements were removed during mixing with bay water (Figs. IV-4e and IV-4c). Maximum water temperatures in April were approximately 10^{o}C, whereas temperatures during the summer cruises were typically greater than 22^{o}C; because of the temperature-dependence and seasonal patterns of diffusive (Aller, 1994; Aller and Benninger, 1981) and SGD (Chapter II) fluxes, it is unlikely that the non-conservative excess of these metals during April is due to diagenetic remobilization and benthic input. Thus, the apparent input observed during the April cruise probably results from variability in the WW endmember.

For the sewage estuary discussed above, close spatial proximity of the samples indicates probable influence only from the observed WW and bay water endmembers. However, the remainder of the bay is subject to effluent from three other major WWTPs. Because of this, apparent non-conservative input likely reflects variable endmember concentrations and the fact that Jamaica Bay is not a simple two-endmember system. In reality, each WWTP may discharge water with a unique trace metal signature. An accurate mass balance for trace metals in Jamaica Bay would probably require monitoring of individual WW inputs.

Co-variation of Cu, Ni, and Zn with DOC

Dissolved organic carbon (DOC) data only exist for the September 2005 cruise, when the lowest dissolved metals levels were observed (Fig. IV-5). During that cruise, Cu, Ni, and Zn showed strong co-variation with DOC (Fig. IV-6). The good correlation between the metals and organic carbon suggests that organic complexation was a significant process regulating the solubility of Cu, Ni, and Zn in Jamaica Bay, perhaps resulting from the input of strong organic ligands from wastewater (Sedlak et al., 1997).

Although all three of these metals exhibited a positive correlation with DOC, the intercepts of the trends differ. Ni and Cu both showed positive y-intercepts, suggesting that DOC was not the only factor keeping these metals in solution. Conversely, the negative intercept observed for Zn implies that DOC may be the most important variable for maintaining the elevated concentrations observed in the Jamaica Bay water column (Table IV-1).

Dissolved trace metals in the Jamaica Bay subterranean estuary

As described in the Methods section, four depth profiles of shallow (< 400 cm depth) groundwater were collected from three different locations throughout Jamaica Bay (Fig. IV-1). Although several of the profiles did show a decline in salinity with depth, the minimum salinity observed was still higher than 6 (Fig. IV-7). This supports the argument in Chapter II, which suggested that most of the SGD in this bay was brackish, not fresh.

Concentrations of dissolved trace metals in Jamaica Bay groundwater were highly variable, and had vertical structure indicative of diagenetic processes and redox zonation (Fig. IV-8). The different locations generally are similar settings, and we cannot definitively identify the source of differing trace metal behavior between sites. The Canarsie Pol location may potentially represent a less-contaminated environment, as it is isolated from direct contact with human activities such as run-off from roads. However, it is directly across a wide channel (~50 m) from the Canarsie Pier location, so the influence of contaminants transported by bay waters should be identical. Differences in the vertical distribution of trace metals in groundwaters of these two sites probably reflect differences in the magnitudes and patterns of groundwater advection through the sediments.

Redox-sensitive elements: Fe, Mn, Mo, V

Dissolved Mn and Fe followed generally similar patterns with depth in the subterranean estuary (Fig. IV-8a and IV-8b), although Mn concentrations peaked at a higher salinity than did Fe (Fig. IV-9).

At the Canarsie Pier location in March (CPier – 05/04/06), dissolved Mo showed a pattern of depletion at the surface, remobilization and increase at 100 cm, decrease to nearly zero between 200 and 300 cm, and a small increase at 400 cm (Fig. IV-8c). Although the magnitudes are different, this pattern generally follows the trends of dissolved Mn (Fig. IV-8b), indicating that Mo is scavenged by Mn-oxides, and is returned to solution when the oxides are dissolved (Shimmield and Price, 1986; Shaw et al., 1990; Emerson and Huested, 1991; Morford et al., 2005). The same argument appears to hold for the other Canarsie Pier (CPier – 03/24/06) and Broad Channel (BC – 09/14/06) profiles, although it is less clear in the Canarsie Pol (CPol – 05/04/06) data (Fig. IV-8).

It is not clear what mechanism is regulating the concentration of dissolved V in these profiles. It is interesting to note that Mo and V display opposite trends, especially in the profile "CPier – 05/04/06" (Fig. IV-8c and IV-8d). DOC complexation may explain the 2-3 fold enrichment of V over water column values (Brumsack and Gieskes, 1983; Emerson and Huested, 1991; Shaw et al., 1990), but without actual DOC measurements, this is simply conjecture.

Ag, Co, Cu, Ni, P, Pb, and Zn

The Ni profiles generally show similar behavior to Mo (as with Mn and Mo, there is not a direct correlation, but trends in concentration with depth match fairly well for these elements), consistent with previously reported variation between Mn and Ni in the subterranean estuary (Beck et al., 2007). However, in that same study (West Neck Bay, NY), Co also co-varied with Mn. In Jamaica Bay groundwaters, Co appears to be

decoupled from Mn cycling (Fig. IV-8g). To some degree, the Co profiles (particularly "CPier – 05/04/06") match the trends observed for P, V, and Pb (Figs. IV-8e, 8d, and 8k). In West Neck Bay (Beck et al., 2007), Co was also observed to co-vary with dissolved organic carbon (DOC). Thus, it may be reasonable to again invoke DOC (Shafer et al., 1997) to also explain the Co, P, and Pb profiles.

Furthermore, complexation of Fe with DOC (Luther et al., 1996) may provide a satisfactory explanation for the observed decoupling of P and Fe (Figs. IV-8a and 8e). The lack of correlation of Fe and P in Jamaica Bay porewaters contrasts with the positive covariation observed by Charette and Sholkovitz (2002 and 2006). Dissolved Fe concentrations in groundwater were much higher than in the water column; it is likely, therefore, that SGD may represent a source of Fe to the bay waters, as discussed below.

Zn was undetected in two of the profiles (CPol and CPier – 03/24/06), but where it was measurable, the trends suggested that it may be cycled in a similar manner to V and Co (Fig. IV-8i). In general, the measurable levels of Zn were the same or slightly higher than in the water column. Thus, similar to Fe, advection of these porewaters out of the sediment could represent a source of Zn to the bay.

Except for one profile ("CPier – 03/24/06"), dissolved Cu in the subterranean estuary was much lower than observed in the water column (Fig. IV-8j). This suggests that recirculation of seawater through the sediments may represent a sink for Cu in Jamaica Bay. This contrasts the results of Charette and Buessler (2004), who showed that SGD was a source of Cu to the Elizabeth River (VA). However, the mechanism of Cu sequestration in permeable sediments should be clarified before comparing different settings.

Dissolved Ag and Pb profiles were quite variable, depending on the location and time of sampling (Fig. IV-8f and 8k). In some instances, the concentrations were higher than the water column, while in other cases, the levels were lower in the porewater. This suggests that SGD may represent either a source or a sink for these metals, depending on the location of recirculation and discharge.

The effect of Submarine Groundwater Discharge on dissolved metals in Jamaica Bay

It has been previously shown that SGD supplies most of the substantial excess Ra observed in the Jamaica Bay water column (Chapter II). The input of Ra suggests that SGD may represent a similar source for other dissolved groundwater constituents as well (Moore, 1999).

Molybdenum (Mo)

The effect of SGD is evident in the dissolved Mo distribution in the Jamaica Bay water column (Fig. IV-8c), although in this case, it represents a sink, not a source as has been observed in another estuary (Dalai et al., 2006). Given that Mo behaves conservatively in oxic seawater and has a relatively constant concentration of approximately 110 nM (Collier, 1985), the observed Mo distribution in Jamaica Bay waters cannot be explained by other than a removal mechanism. In other words, if the oceanic concentration is fixed, the observed concentrations in surface waters of the bay cannot be explained by variations in the wastewater endmember, as might be argued for the other metals. Furthermore, the conservative behavior of Mo in the sewage estuary

(Fig. IV-3b) and at high salinities (Fig. IV-5b) suggests that Mo is mixing conservatively, and an independent process is responsible for its removal within the bay.

The pattern of Mo depletion observed for the three cruises matches that of the Ra-estimated SGD flux (Sept.>Oct.>April; Chapter II). This SGD comprises primarily recirculated seawater, and Mo depletion in the water column apparently is the result of Mo precipitation as oxic seawater is recirculated through suboxic, reducing permeable sediments. Indeed, Mo concentrations measured in shallow groundwater profiles in JB show nearly quantitative removal at salinities greater than 20 (Fig. IV-9). Thus, substantial recirculation of seawater through the bay floor extracts Mo while leaving salinity largely unchanged.

In fact, the salinity distribution for the three cruises does show a slight decrease in the bay from highest average levels in April 2006 to lowest levels in Sept 2005 (Fig. IV-5). Although factors such as station locations, depth, and tidal stage at sampling varied on the different dates, the fact that the salinity decrease was not accompanied by a concomitant increase in Ag levels (Fig. IV-5h) suggests that the freshening was not due to wastewater effluent (Sañudo-Wilhelmy and Flegal, 1992). This suggests that during periods of high SGD, increased seawater recirculation may be accompanied by an increase in fresh submarine groundwater discharge as well.

Zinc (Zn), Cobalt (Co), Iron (Fe), and Nickel (Ni)

Dissolved Zn, Co, Fe, and Ni were all enriched in surficial groundwater relative to surface water concentrations (Figs. IV-5 and IV-8), suggesting that SGD may be a source of these metals to the water column. Indeed, co-variation of Co, Zn, Ni, and Fe with

^{223}Ra indicated an input from benthic sources (Fig. IV-10). This co-variation was only observed in bottom water samples during the October 2004 cruise, likely resulting from the strong vertical stratification associated with summer conditions that effectively isolated bottom waters from the sewage-impacted surface waters. Such stratification was not evident during the spring cruise. Because diffusion of Ra during summer could only support 4-9% of the observed inventory (Beck et al., submitted; Chapter II), most of this benthic trace metal input is probably due to advective input of porewater .

Element:element plots to identify sources

To further support the input of metals due to SGD, metal:metal plots can be used to identify different sources (e.g. Paulsen, 2005). Because co-variation with Ra suggests that Co and Zn have an SGD source, these two metals may be the best tracers. In addition, their distribution in the sewage estuary showed strong removal of both Zn and Co from wastewater during mixing with bay waters. Thus, the wastewater signature will be slightly diminished, allowing the SGD input to be better distinguished.

Figure IV-11 shows a plot of dissolved Zn vs. Co in the Jamaica Bay water column. The wastewater samples are clearly distinguishable with high Co and Zn levels, and samples in the sewage estuary fall on a mixing line between bay samples and this wastewater endmember. The bulk of the bay water samples fall on a mixing line between the inlet (near the origin in Fig. IV-11) and the most saline samples at the mouth of the sewage estuary. The different slopes between the samples from the sewage estuary and those in the bay water column suggest that the removal of Zn and Co occurs primarily within the sewage estuary. Thus, after the water is mixed to a salinity greater than about

20 psu, the Co:Zn ratio is relatively constant. This results in an apparent intermediate endmember, such that ocean water and effluent water both mix with a secondary bay water endmember.

A third endmember is evident with high dissolved Co concentrations relative to Zn (Fig. IV-11). The samples farthest from the sewage estuary mixing line are from Thurston Basin, the large semi-enclosed basin at the northeast corner of the bay (Fig. IV-1). This is the location where some of the highest dissolved Ra activities in Jamaica Bay have been observed (Cochran et al., 2006), suggesting that it is a region of significant SGD input. Indeed, groundwater modeling efforts have indicated that much of the groundwater discharge to Jamaica Bay occurs in the region near Thurston Basin (Misut and Voss, 2004). Furthermore, that this basin is far from any of the major WWTP point-source inputs suggests that the possibility of a second unique wastewater signature cannot account for this deviation from the other bay samples.

Pb isotope ratios

Pb isotope ratios have been widely utilized to identify sources of Pb input (Stukas and Wong, 1980; Veron et al., 1998; Frank, 2002; Sañudo-Wilhelmy and Flegal, 2003; Soto-Jimenez et al., 2006). In the Jamaica Bay water column, there is a consistent trend between $^{207}Pb/^{206}Pb$ and $^{208}Pb/^{206}Pb$ (Fig. IV-12a). Pb isotope ratios in wastewater effluent tend to have relatively low ^{208}Pb and ^{207}Pb relative to ^{206}Pb, as do samples from the sewage estuary. Samples collected outside the Jamaica Bay inlet have $^{207}Pb/^{206}Pb$ ratios of approximately 0.845, and $^{208}Pb/^{206}Pb$ ratios of 2.06-2.07. Most of the bay water samples have Pb ratios that plot between these two endmembers.

However, many of the water column samples, particularly those collected during the Oct 2004 cruise, plot outside of the inlet and wastewater endmember range. The sample with the highest $^{207}Pb/^{206}Pb$ ratio also had high Ra activities, suggesting that it reflected groundwater input. In fact, samples farthest from the effluent-inlet mixing line and with the most radiogenic signature (Fig. IV-12a) were collected in the western region of the bay, where the spatial distribution of Ra suggests high SGD input (Cochran et al., 2006). Furthermore, there was a positive relationship between $^{207}Pb/^{206}Pb$ and ^{223}Ra, indicating an SGD input of Pb with a more radiogenic signature (Fig. IV-13).

Comparing the Pb ratios measured in the Jamaica Bay water column with reported values for the NY and Hudson River region gives some indication as to the Pb sources in the bay. Figure IV-12b is a plot that includes Pb ratios from possible sources. The relatively low ratios measured in wastewater and the sewage estuary correspond fairly well with anthropogenic, atmospheric Pb ratios (Marcantonio et al., 2002). As well, these ratios tend towards the low values found in sandstones and shales in the upper Hudson River watershed (Bock et al., 1998). Therefore, the Pb in the wastewater may reflect contamination from runoff (collected by storm drains) or water piped to NYC from upstate aquifers (Houghton et al., 2005).

The high endmember ratios measured in the water column appear to reflect Pb contamination originating from a mine in upstate NY. Chillrud et al. (2003) measured Pb ratios in sediment cores from the upper Hudson River, and found a wide range of ratios that corresponded to different Pb sources during changing decades. A particularly anomalous sediment layer was found that had the high ratios shown in Fig. IV-12b; to explain these ratios, Chillrud et al. (2003) argued that the ratios represented Pb

contamination from a local pigment factory, one that probably would have used local Pb from a mine in Balmat, NY. This is relevant here because a Pb smelter was operated for several decades at the turn of the 20th century in Jamaica Bay (Black, 1981). Black (1981; p. 41) reports that, "In [1890, Mill Basin] passed into the hands of Robert L. Crooke, who erected on part of the island a large lead smelting plant. Subsequently, Crooke Smelting Company was bought out by National Lead Company. In 1906, Mill Island reportedly received annually 4,000 tons of ore and produced 3,800 tons of solder, tin, and lead, worth $1,250,000." Mill Island, now obscured under artificial fill (Englebright, 1975), was formerly located near the present-day Canarsie Pier (Fig. IV-1). This is the very location where Ra distributions indicated a particularly large source of SGD (Cochran et al., 2006). Black's references are somewhat obscure (historical town records), so we cannot be certain of the source of the Pb, but it would probably have been from a source not too distant. Therefore, it can be argued that the high Pb ratios, of a presumable SGD source, are reasonably attributable to Balmat, NY, given the contamination history of Jamaica Bay.

Because there was no correlation between total dissolved Pb and Ra (Fig. IV-14) as was observed for Co, Zn, Ni, and Fe, SGD probably does not represent a significant source of total Pb to Jamaica Bay. However, the Pb isotope data suggest that SGD is supplying a small, but significant, amount of isotopically-distinct Pb. These data suggest that Pb isotopes may provide a useful tracer of SGD in locations where subsurface Pb contamination is present, and warrant further investigation.

Quantitative estimates of dissolved metal flux due to SGD

Using the dissolved metal concentrations observed in the subterranean estuary (e.g. Fig. IV-9), one can theoretically calculate SGD-associated metal fluxes. However, the variability in metal concentrations observed with depth in the permeable sediments makes it difficult to identify what value best represents the SGD endmember. For some metals (e.g. Fe, V, and Pb; Fig. IV-9), the linear distribution with chloride in the most saline porewater samples suggests that a reasonable "effective zero-salinity endmember" can be estimated (e.g. Charette and Sholkovitz, 2006; Beck et al., 2007; Bone et al., in press). However, for most of the metals, scatter in the data makes it less clear how to calculate a good SGD endmember. In this case, use of an average concentration presumably serves best (Shaw et al., 1998; Montlucon and Sañudo-Wilhelmy, 2001; Charette and Buessler, 2004).

The mass flux of trace metals in SGD is then calculated as the product of average metal concentration (mol L^{-1}) and Ra-estimated SGD flux (L d^{-1}). Average metal concentrations are shown in Table IV-3. Using the SGD water fluxes calculated in Chapter II, metal fluxes can then be calculated for the different cruises; these are also shown in Table IV-3. Fluxes into Jamaica Bay range from 0.06 mol d^{-1} for Ag to 1.6×10^5 mol d^{-1} for Fe. To put these fluxes into perspective, we can compare them to the wastewater metal flux. Using C* (Table IV-2) for dissolved metal concentrations in wastewater, and the wastewater flux reported in Chapter II (7.46×10^8 L d^{-1}), the flux can be calculated. These estimates are shown in Table IV-3. Although the metal concentrations are much higher in wastewater than in the groundwater, the much smaller amount of WW discharge compared to SGD results in comparable magnitudes between

the two fluxes. In fact, using this method for estimating SGD metal fluxes leads to the conclusion that SGD accounts for a dissolved metal flux that exceeds wastewater metal input in Jamaica Bay for a number of metals: Ag, Co, and Ni. Fluxes of Pb, Cu, and Zn are comparable between SGD and wastewater, and the Fe flux is about half or lower in SGD than wastewater.

Although it seems profound that SGD can deliver as substantial a trace metal load to Jamaica Bay as treated wastewater, it is intuitively untenable. Many of the elements shown in Figs. IV-8 and IV-9 show lowest concentrations in the saline porewater near the sediment-water interface. Assuming homogeneous vertical flow, this suggests that metals are being removed from the porewater as it flows toward the surface. However, total removal would disallow the trends between metals and Ra observed in Fig. IV-10. Therefore, there must be a mechanism by which trace metals in the groundwater can escape the sediment surface--perhaps through channelized, preferential flowpaths that are not captured by the porewater sampling technique used here. Future research should examine this problem more closely; more accurate estimates of the dissolved metal endmember concentration in SGD are required if metal fluxes are to be better constrained.

SUMMARY

1. This study provides some of the first measurements of dissolved trace metals in Jamaica Bay, NY. Metals levels in the Jamaica Bay water column are highly elevated relative to offshore waters, and clearly reflect contamination due primarily to wastewater input. The elevated metals levels observed in Jamaica Bay are comparable to other urban estuaries in the United States.

2. The trends observed for dissolved trace metals within the mixing zone between wastewater and bay surface water indicate that Ag, Pb, Co, and Zn are highly removed from the dissolved phase relative to conservative mixing; Ni and Cu show removal to a lesser degree, and Mo and Fe exhibit approximately conservative behavior. Most metals show further removal within the bay water column. Association with dissolved organic carbon was only observed for Cu, Zn, and Ni.

3. The influence of SGD on trace metal distributions within the bay was observed for several metals. The pattern of Mo depletion in the water column matched the variation in SGD previously reported for Jamaica Bay. The non-conservative removal of Mo observed in shallow groundwater suggests that seawater recirculation through permeable, anoxic sediments acted as a sink for dissolved Mo. In contrast, other metals (Cu, Ni, Zn, and Fe) showed positive co-variation with dissolved Ra in bottom waters when the water column was stratified, suggesting an SGD source.

4. The trends observed for stable Pb isotope ratios in the water column could largely be explained by mixing between wastewater and coastal ocean waters, but samples that were more radiogenic required a third endmember. Although the lack of relationship between total dissolved Pb and Ra suggested that SGD did not supply a significant amount of total

Pb, co-variation between Pb isotope ratios and dissolved ^{223}Ra did indicate that SGD was the source of the radiogenic Pb.

5. Although wastewater input was the dominant source of trace metal contamination to Jamaica Bay, the effect of SGD on dissolved trace metal distributions was also observed. This suggests that SGD may play an even more significant role in trace metal cycling in coastal regions that are less obviously impacted by anthropogenic activities.

6. SGD-derived trace metal fluxes were calculated crudely as the product of average groundwater metal concentration and Ra-estimated SGD water flux. Using this approach, SGD appeared to represent a dissolved trace metal flux of equal proportion to wastewater inputs. The clear evidence of chemical reactions occurring in the subterranean estuary strongly indicated that this method of estimating fluxes does not accurately represent the real SGD metal flux. Methods for directly collecting and measuring the groundwater as it crosses the sediment-water interface are needed to better constrain the true dissolved metal flux associated with SGD.

REFERENCES

Aller, R.C., 1994. The sedimentary Mn cycle in Long Island Sound – Its role as intermediate oxidant and the influence of bioturbation, O2, and C(org) flux on diagenetic reaction balances. J. Mar. Res., 52: 259-295.

Aller, R.C., and L.K. Benninger, 1981. Spatial and temporal patterns of dissolved ammonium, manganese, and silica fluxes from bottom sediments of Long Island Sound, USA. J. Mar. Res., 39: 295-314.

Basu, A. R., S.B. Jacobsen, R.J. Poreda, C.B. Dowling, and P.K. Aggarwal, 2001. Large groundwater strontium flux to the oceans from the Bengal Basin and the marine strontium isotope record. Science, 293: 1470–1473.

Beck, A.J., Y. Tsukamoto, A. Tovar-Sanchez, M. Huerta-Diaz, H.J. Bokuniewicz, and S.A. Sanudo-Wilhelmy. 2007. Importance of geochemical transformations in determining submarine groundwater discharge-derived trace metal and nutrient fluxes. Applied Geochemistry, 22: 477-490.

Benner, R., and M. Strom, 1993. A critical evaluation of the analytical blank associated with DOC measurements by high temperature catalytic oxidation. Mar. Chem., 41: 153-160.

Benoit, G., S.D. Oktay-Marshall, A. Cantu, II, E.M. Hood, C.H. Coleman, M.O. Corapcioglu, P.H. Santschi, 1994. Partitioning of Cu, Pb, Ag, Zn, Fe, Al, and Mn between filter-retained particles, colloids, and solution in six Texas estuaries. Marine Chemistry, 45: 307-336.

Benotti, M., 2006. Occurrence and fate of pharmaceuticals in wastewater-impacted environments using HPLC-TOF-MS. PhD dissertation, unpublished. Stony Brook University. 324 p.

Benotti M.J., P.E. Misut, M. Abbene, and S.A. Terracciano. 2006. Historic Nitrogen Loading in Jamaica Bay, Long Island, New York: predevelopment to 2005. USGS Open File Report SIR 2007-5051.

Berelson, W., J. McManus, K. Coale, K. et al., 2003. A time series of benthic flux measurements from Monterey Bay, CA. Continental Shelf Research, 23: 457–481.

Black, F.R., 1981. *Jamaica Bay – A History.* Washington D.C.: Cultural Resource Study 3, Division of Cultural Resources, North Atlantic Regional Office, National Parks Service of the US Dept. of the Interior.

Bock, B., S.M. McLennan, and G.N. Hanson, 1998. Geochemistry and provenance of the Middle Ordovician Austin Glen Member (Normanskill Formation) and the Taconian Orogeny in New England. Sedimentology, 45: 635-655.

Bone, S.E., M.E. Gonneea, and M.A. Charette, 2006. Geochemical cycling of arsenic in a coastal aquifer. Environmental Science and Technology. 40: 3273-3278.

Bone, S.E., M.A. Charette, C.H. Lamborg, and M.E. Gonneea, 2007. Has Submarine Groundwater Discharge Been Overlooked as a Source of Mercury to Coastal Waters? Environmental Science and Technology, *In press*.

Bopp, R.F., H.J. Simpson, S.N. Chillrud, and D.W. Robinson, 1993. Sediment-derived chronologies of persistent contaminants in Jamaica Bay, New York. Estuaries, 16 (3B): 608-616.

Boyle, E., R. Collier, A.T. Dengler, J.M. Edmond, A.C. Ng, and R.F. Stall, 1974. On the chemical mass-balance in estuaries. Geochimica et Cosmochimica Acta, 38:1719-1728.

Bray, J.T., O.P. Bricker, B.N. Troup, 1973. Phosphate in Interstitial Waters of Anoxic Sediments: Oxidation Effects during Sampling Procedure. Science, 180 (4093): 1362-1364.

Breslin, V.T., and S.A. Sañudo-Wilhelmy, 1999. High Spatial Resolution Sampling of Metals in the Sediment and Water Column in Port Jefferson Harbor, New York. Estuaries, 22 (3A): 669-680.

Breuer, E., S.A. Sañudo-Wilhelmy, and R.C. Aller, 1999. Trace Metals and Dissolved Organic Carbon in an Estuary With Restricted River Flow and a Brown Tide Bloom. Estuaries, 22 (3A): 603-615.

Brumsack H. J. and Gieskes J. M., 1983. Interstitial water trace-metal chemistry of laminated sediments from the Gulf of California, Mexico. Mar. Chem., 14, 89–106.

Buck, N.J.; Gobler, C.J., Sañudo-Wilhelmy, S.A., 2005. Dissolved trace element concentrations in the east River-long Island Sound System: Relative importance of autochthonous versus allochthonous sources. Environ. Sci. Technol., 39: 3528-3537.

Caccia, V.G., and F.J. Millero, 2003. The Distribution and Seasonal Variation of Dissolved Trace Metals in Florida Bay and Adjacent Waters. Aquatic Geochemistry, 9: 111-144.

Charette M.A., and K.O. Buesseler, 2004. Submarine groundwater discharge of nutrients and copper to an urban subestuary of Chesapeake bay (Elizabeth River). Limnology and Oceanography 49 (2): 376-385

Charette, M.A., and E.R. Sholkovitz, 2006. Trace element cycling in a subterranean estuary: Part 2. Geochemistry of the pore water. Geochimica et Cosmochimica Acta, 70 (4): 811-826.

Charette, M.A., and M.C. Allen, 2006. Precision groundwater sampling in coastal aquifers using a direct push shielded screen well-point system. Groundwater Monitoring & Remediation, 26 (2): 87-93.

Charette, M.A., and E.R. Sholkovitz, 2002. Oxidative precipitation of groundwater-derived ferrous iron in the subterranean estuary of a coastal bay. Geophysical Research Letters, 29 (10), DOI: 10.1029/2001GL014512.

Chillrud, S.N., S. Hemming, E.L. Shuster, H.J. Simpson, R.F. Bopp, J.M. Ross, D.C. Pederson, D.A. Chaky, L.-R. Tolley, and F. Estabrooks, 2003. Stable lead isotopes, contaminant metals, and radionuclides in upper Hudson River sediment cores: implications for improved time stratigraphy and transport processes. Chemical Geology, 199: 53-70.

Clark, L.B., C.J. Gobler, and S.A. Sanudo-Wilhelmy, 2006. Spatial and Temporal Dynamics of Dissolved Trace Metals, Organic Carbon, Mineral Nutrients, and Phytoplankton in a Coastal Lagoon: Great South Bay, New York. Estuaries and Coasts, 29 (5): 841-854.

Cochran, J.K., N.H. Landman, K.K. Turekian, A. Michard, and D.P. Schrag, 2003. Paleoceanography of the Late Cretaceous (Maastrichtian) Western Interior Seaway of North America: evidence from Sr and O isotopes. Palaeogeography, Palaeoclimatology, Palaeoecology, 191: 45-64.

Cochran, J.K., H. Feng, D. Amiel, and A. Beck, 2006. Natural radionuclides as tracers of coastal biogeochemical processes. J. Geochem. Exploration, 88: 376-379.

Collier, R.W., 1985. Molybdenum in the Northeast Pacific Ocean. Limnol. Oceanogr., 30: 1351–1353.

Dalai, T.K., K. Nishimura, and Y. Nozaki, 2005. Geochemistry of molybdenum in the Chao Phraya River estuary, Thailand: Role of suboxic diagenesis and porewater transport. Chemical Geology, 218: 189-202.

Emerson, S.R., and S.S. Huested, 1991. Ocean anoxia and the concentration of molybdenum and vanadium in seawater. Mar. Chem., 34: 177–196.

Engelbright, S., 1975. Jamaica Bay: A case study of geo-environmental stress. NY State Geological Assn. Handbook, 47th Annual Meeting, Hofstra University.

Ferguson, P.L., C.R. Iden, and B.J. Brownawell, 2001. Distribution and fate of alkylphenol ethoxylate metabolites in a sewage-impacted urban estuary. Environ. Sci. Technol., 35: 2428-2435.

Flegal, A.R., and S.A. Sañudo-Wilhelmy, 1993. Comparable Levels of Trace Metal Contamination in Two Semi-Enclosed Embayments: San Diego Bay and South San Francisco Bay. Environ. Sci. Technol., 27: 1934-1936.

Flegal, A.R., G.J., Smith, G.A. Gill, S.A. Sañudo-Wilhelmy, and L.C.D. Anderson, 1991. Dissolved trace element cycles in the San Francisco Bay estuary. Mar. Chem., 36: 329-363.

Frank, M., 2002. Radiogenic isotopes: Tracers of past ocean circulation and erosional input. Reviews of Geophysics, 40 (1): Art. # 1001.

Froelich, P.N., G.P. Klinkhammer, M.L. Bender, N.A. Luedtke, G.R. Heath, D. Cullen, and P. Dauphin, 1979. Early oxidation of organic matter in pelagic sediments of the eastern equatorial Atlantic: Suboxic diagenesis. Geochim. Cosmochim. Acta, 43: 1075–1090.

Gobeil, C., B. Rondeau, and L. Beaudin, 2005. Contribution of municipal effluents to metal fluxes in the St. Lawrence River. Environ. Sci. Technol., 39: 456-464.

Gochfeld, M., 1997. Spatial Patterns in a Bioindicator: Heavy Metal and Selenium Concentration in Eggs of Herring Gulls (Larus argentatus) in the New York Bight. Arch. Environ. Contam. Toxicol., 33: 63–70.

Hartig, E.K., V. Gornitz, A. Kolker, F. Mushacke, and D. Fallon, 2002. Anthropogenic and climate-change impacts on salt marshes of Jamaica Bay, New York City. Wetlands, 22 (1): 71-89.

Houghton, R., A. Gordon, and B. Huber, 2005. Dye tracer experiments in Jamaica Bay. In: Integrated Reconnaissance of the Physical and Biogeochemical Characteristics of Jamaica Bay: Initial Activity Phase. A Coordinated Program of the Gateway National Recreational Area and the Columbia Earth Institute. p51-53.

Hunt, C.D., 1983. Variability in the benthic Mn flux in coastal marine ecosystems resulting from temperature and primary productivity. Limnol. Oceanogr. 28: 913-923.

Ingram, B.L., and D. Sloan, 1992. Strontium isotopic composition of estuarine sediments as paleosalinity-paleoclimate indicator. Science, 255 (5040): 68-72.

Kozelka, P.B. and K.W. Bruland, 1998. Chemical speciation of dissolved Cu, Zn, Cd, Pb in Narragansett Bay, Rhode Island. Marine Chemistry, 60: 267–282.

Luoma, S.N., and D.J.H. Phillips, 1988. Distribution, variability and impacts of trace elements in San Francisco Bay. Mar. Poll. Bull., 19 (9): 413-425.

Luther II, G.W., P.A. SHellenbarger, and P.J. Brendel, 1996. Dissolved organic Fe(III) and Fe(II) complexes in salt marsh porewaters. Geochim. Cosmochim. Acta, 60 (6):951-960.

Lyons, W.B., H.E. Gaudette, and G.M. Smith, 1979. Porewater sampling in anoxic carbonate sediments: oxidation artefacts. Nature, 277: 48-49.

Marcantonio, F., A. Zimmerman, Y. Xu, and E. Canuel, 2002. A Pb isotope record of mid-Atlantic US atmospheric Pb emissions in Chesapeake Bay sediments. Marine Chemistry, 77: 123-132.

Mecray, E.L., and M.R. Buchholtz ten Brink, 2000. Contaminant distribution and accumulation in surface sediments of Long Island Sound. Journal of Coastal Research, 16 (3): 575-590.

Misut, P.E., and Voss, C.I., 2004. Simulation of subsea discharge to Jamaica Bay in New York City with a three-dimensional, variable density, finite-element model. In Finite Element Models, MODFLOW, and More: Solving Groundwater Problems, Koval-Hrkal-Bruthans (eds.) p. 391-394.

Montlucon, D., and S.A. Sañudo-Wilhelmy. 2001. Influence of net groundwater discharge on the chemical composition of a coastal environment: Flanders Bay, Long Island, New York. Environmental Science and Technology 3, 480-486

Moore, W.S., 1997. High fluxes of radium and barium from the mouth of the Ganges-Brahmaputra River during low river discharge suggest a large groundwater source. Earth and Planetary Science Letters, 150 (1-2): 141-150.

Moore, W.S., 1999. The subterranean estuary: a reaction zone of ground water and sea water. Marine Chemistry, 65 (1-2): 111-125.

Morford, J.L., S.R. Emerson, E.J., Breckel, S.H., Kim, 2005. Diagenesis of oxyanions (V, U, Re and Mo) in pore waters and sediments from a continental margin. Geochim. Cosmochim. Acta, 69 (21): 5021–5032.

Paulsen, A.J., 2005. Tracing water and suspended matter in Raritan and Lower New York Bays using dissolved and particulate elemental concentrations. Marine Chemistry, 97: 60– 77.

Paulson, A.J. and R.A. Feely. 1985. Dissolved Trace Metals in the Surface Waters of Puget Sound. Marine Pollution Bulletin, 16 (7): 285-291.

Powell, R.T., W.M. Landing, J.E. Bauer, 1996. Colloidal trace metals, organic carbon and nitrogen in a southeastern U.S. estuary. Marine Chemistry, 55: 165-176.

Rivera-Duarte, I., and A.R. Flegal, 1997. Pore-water silver concentration gradients and benthic fluxes from contaminated sediments of San Francisco Bay, California, U.S.A. Marine Chemistry, 56:15-26.

Sañudo-Wilhelmy, S.A., and A.R. Flegal, 1992. Anthropogenic Silver In the Southern California Bight: A New Tracer of Sewage in Coastal Waters. Environ. Sci. Technol., 26: 2147-2151.

Sañudo-Wilhelmy, S.A. and G. A. Gill, 1999. Policy Analysis. The impact of the Clean Water Act on the levels of toxic metals in urban estuaries: The Hudson River estuary revisited. Environmental Science and Technology 33, 3477-3481

Sañudo-Wilhelmy, S.A., I. Rivera-Duarte, and A.R. Flegal, 1996. Distribution of colloidal trace metals in the San Francisco Bay estuary. Geochimica et Cosmochimica Acta, 60 (24): 4933-4944.
Sañudo-Wilhelmy SA, Flegal AR., 2003. Potential influence of Saharan dust on the chemical composition of the Southern Ocean. Geochem. Geophys. Geosys. 4: Art. # 1063

Sañudo-Wilhelmy, S.A., A. Tovar-Sanchez, N. Fisher, and A.R. Flegal, 2004. Examining dissolved toxic metals in U.S. estuaries. Environmental Science and Technology, pp. 34A-38A.

Sedlak, D.L., J.T. Phinney, and W.W. Bedsworth, 1997. Strongly complexed Cu and Ni in wastewater effluents and surface runoff. Environmental Science and Technology, 31 (10): 3010-3016.

Shafer M.M., Hoffmann S.R., Overdier J.T., et al. 2004. Physical and Kinetic Speciation of Copper and Zinc in Three Geochemically Contrasting Marine Estuaries. Environmental Science and Technology, 38: 3810-3819.

Shaw, T.J., J.M. Gieskes, and R.A. Jahnke, 1990. Early diagenesis in differing depositional environments: The response of transition metals in pore water. Geochim. Cosmochim. Acta, 54: 1233–1246.

Shaw, T.J., W.S. Moore, J. Kloepfer, et al. 1998. The flux of barium to the coastal waters of the southeastern USA: The importance of submarine groundwater discharge. Geochimica et Cosmochimica Acta, 62 (18): 3047-3054.

Shimmield, G.B. and N.B. Price. 1986. The behavior of molybdenum and manganese during early sediment diagenesis – offshore Baja California, Mexico. Marine Chemistry 19: 261-280.

Sholkovitz, E.R., E.A. Boyle, and N.B. Price, 1978. The removal of dissolved humic acids and iron during estuarine mixing. Earth and Planetary Science Letters, 40: 130-136.

Smith, G.J. and Flegal, A.R., 1993. Silver in San Francisco Bay estuarine waters. Estuaries, 16 (3A): 547-558.

Soto-Jimenez, M.F., S.A. Hibdon, C.W. Rankin, J. Aggarawl, A.C. Ruiz-Fernandez, F. Paez-Osuna, and A.R. Flegal, 2006. Chronicling a century of lead pollution in Mexico:

Stable lead isotopic composition analyses of dated sediment cores. Environ. Sci. Technol., 40 (3): 764-770.

Stukas, V.J., and C.S. Wong, 1980. Stable lead isotopes as a tracer in coastal waters. Science, 194: 179-183.

Sugimura, Y., Suzuki, Y., 1988. A high temperature catalytic oxidation method for the determination of nonvolatile dissolved organic carbon in seawater by direct injection of a liquid sample. Mar. Chem., 24: 105-131.

Swanson, R.L., West-Valle, A.S., and Decker, C.J., 1992: Recreation vs. Waste Disposal: The Use and Management of Jamaica Bay: Long Island History Journal, 5 (1): 21-24.

Sweeny, A., and Sañudo-Wilhelmy, S.A., 2004. Dissolved metal contamination in the East River-Long Island Sound system: potential biological effects. Mar. Poll. Bull., 48: 663-670.

Ternes, T.A., and R. Hirsch, 2000. Occurrence and behavior of X-ray contrast media in sewage facilities and the aquatic environment. Environ. Sci. Technol., 34: 2741-2748.

Tovar-Sanchez, A., S.A. Sañudo-Wilhelmy, A.R. Flegal, 2004. Temporal and spatial variations in the biogeochemical cycling of cobalt in two urban estuaries: Hudson River Estuary and San Francisco Bay. Estuarine, Coastal and Shelf Science, 60: 717-728.

US EPA, 1995. National Water Quality Inventory; 1994 Report to Congress; EPA/841/R-95/005. U.S. Environmental Protection Agency. Washington, D.C.

Veron, A.J., T.M. Church, and A.R. Flegal, 1998. Lead isotopes in the Western North Atlantic Ocean: transient tracers of pollutant lead inputs. Environmental Research, 78: 104-111.

Wells, M.L., G.J. Smith, and K.W. Bruland, 2000. The distribution of colloidal and particulate bioactive metals in Narragansett Bay, RI. Mar. Chem., 71 (1–2): 143–163.

Wen, L.-S., P. Santschi, G. Gill, and C. Paternostro, 1999. Estuarine trace metal distributions in Galveston Bay: importance of colloidal forms in the speciation of the dissolved phase. Marine Chemistry, 63: 185–212.

Windom, H., and F. Niencheski. 2003. Biogeochemical processes in a freshwater–seawater mixing zone in permeable sediments along the coast of Southern Brazil. Marine Chemistry 83: 121– 130

Windom, H.L., W.S. Moore, L.F.H. Niencheski, and R.A. Jahnke, 2006. Submarine Groundwater Discharge: a Large, Previously Unrecognized Source of Dissolved Iron to the South Atlantic Ocean. Marine Chemistry, 102: 252–266.

Wolfe, D.A., E.R. Long, and G.B. Thursby, 1996. Sediment toxicity in the Hudson-Raritan Estuary: Distribution and correlations with chemical contamination. Estuaries, 19 (4): 901-912.

Location	Date	Ag (pM)	Co (nM)	Cu (nM)	Pb (pM)	Ni (nM)	Zn (nM)	*Ref.**
This work								
Jamaica Bay, NY								
October 2004	2004	4 - 91	0.2 - 2.5	5 - 24	39 - 588	4 - 12	4 - 88	*1*
September 2005	2005	5 - 11	0.2 - 0.5	3 - 8	52 - 164	3 - 6	2 - 11	*1*
April 2006	2006	18 - 191	0.5 - 2.8	8 - 48	128 - 1550	6 - 23	13 - 191	*1*
Other Estuaries - NY Region								
Long Island Sound	2000-2001	3.5 - 223		8 - 34	5 - 264	10 - 51	4 - 52	*2*
Raritan and Lower NY Bays	1999			16 - 30	70 - 770	6 - 28		*3*
East River, NY	1999	30 - 353		17 - 36	5 - 954	22 - 55	31 - 51	*2, 4*
Great South Bay, NY	1998-1999	12 - 73		5 - 38	17 - 1510			*5*
Port Jefferson Harbor, NY	1997	16 - 163		21 - 28	50 - 180	12 - 16	22 - 87	*6*
Hudson River, NY	1995-1997	5 - 261	0.11 - 2.5	12 - 40	70 - 3400	8 - 26	8 - 124	*7, 8*
Peconic Bays, NY	1995	9.9 - 165	0.8 - 2.6	16 - 51	22 - 619	1 - 13	6 - 57	*9*
Other Estuaries - United States								
Florida Bay, FL	2000-2002		0.2 - 1.2	0.3 - 3.3	<30 - 1360	0.7 - 11		*10*
Galveston Bay, TX	1993-1995		0.37 - 9.6	3.5 - 27	39 - 765	3 - 32	2 - 33	*11*
Narragansett Bay, RI	1994			13 - 28	130 - 320		16 - 72	*12*
Narragansett Bay, RI	1994			12 - 27		17 - 91	16 - 72	*13*
San Francisco Bay, CA	1994	10 - 75	0.2 - 3.4	4.4 - 36		7 - 41	3 - 29	*8, 14*
Ochlockonee Estuary, FL	1994			2 - 5.4		3 - 6		*15*
San Diego Bay, CA	1989	66 - 307	0.5 - 2.4	14 - 44	120 - 184	6 - 16		*16*
S. San Francisco Bay, CA	1989	24 - 244	0.4 - 5.3	22 - 73	52 - 308	21 - 71		*16*
Texas Bays	1989	26 - 281		13 - 50	174 - 1207		11 - 72	*17*
Puget Sound, WA	1980-1981			1.4 - 104	97 - 6760	4 - 24	3 - 413	*18*

Table IV-1. Comparison of dissolved trace metals in Jamaica Bay with other estuarine studies throughout the New York area and United States.
**References*: 1. This work; 2. Buck et al., 2005; 3. Paulson, 2005; 4. Sweeny and Sanudo-Wilhelmy, 2004; 5. Clark et al., 2006; 6. Breslin and Sanudo-Wilhelmy, 1999; 7. Sanudo-Wilhelmy and Gill, 1999 (except Co); 8. Tovar-Sanchez et al., 2004 (Co only); 9. Breuer et al., 1999; 10. Caccia and Millero, 2003; 11. Wen et al., 1999; 12. Kozelka and Bruland, 1998; 13. Wells et al., 2000; 14. Sanudo-Wilhelmy et al., 1996; 15. Powell et al., 1996; 16. Flegal and Sanudo-Wilhelmy, 1993; 17. Benoit et al., 1994; 18. Paulson and Feely, 1985

	C_{ww}	C*	% removal
Ag	0.475	0.2	58
Co	3.9	2.8	28
Cu	73	51	30
Fe	735	735	0
Mo	28	28	0
Ni	35	27	23
Pb	2.75	2	27
Zn	450	235	48

Table IV-2. Percent removal of trace metals in the sewage estuary due to non-conservative mixing trends with salinity. "C_{ww}" indicates actual wastewater endmember (nM), "C*" indicates the apparent freshwater concentration (nM) based on extrapolation of a straight line drawn through the linear portion of the most saline data points (see text). These values are estimated from Fig. IV-3.

	Average dissolved concentration in groundwater						
	Ag (pM)	Pb (pM)	Co (nM)	Cu (nM)	Fe (uM)	Ni (nM)	Zn (nM)
	40	135	1.6	3.4	22	11	18

	SGD dissolved metal flux (mol d^{-1})						
Cruise	Ag	Pb	Co	Cu	Fe	Ni	Zn
Sept 04	0.31	1.0	12	26	1.7×10^5	86	141
Oct 04	0.17	0.6	7	15	0.94×10^5	48	79
Sept 05	0.21	0.7	8	18	1.2×10^5	59	97
Apr 06	0.06	0.2	3	5	0.35×10^5	18	29

	Wastewater dissolved metal flux (mol d^{-1})						
	Ag	Pb	Co	Cu	Fe	Ni	Zn
	0.15	1.5	2.1	38	5.5×10^5	20	175

Table IV-3. Average groundwater concentrations for selected dissolved metals in Jamaica Bay. Rough estimates of metal flux associated with SGD are calculated using these metal concentrations and Ra-estimated SGD flux. The wastewater metal flux is calculated using C* from Table IV-2 and the average daily wastewater discharge.

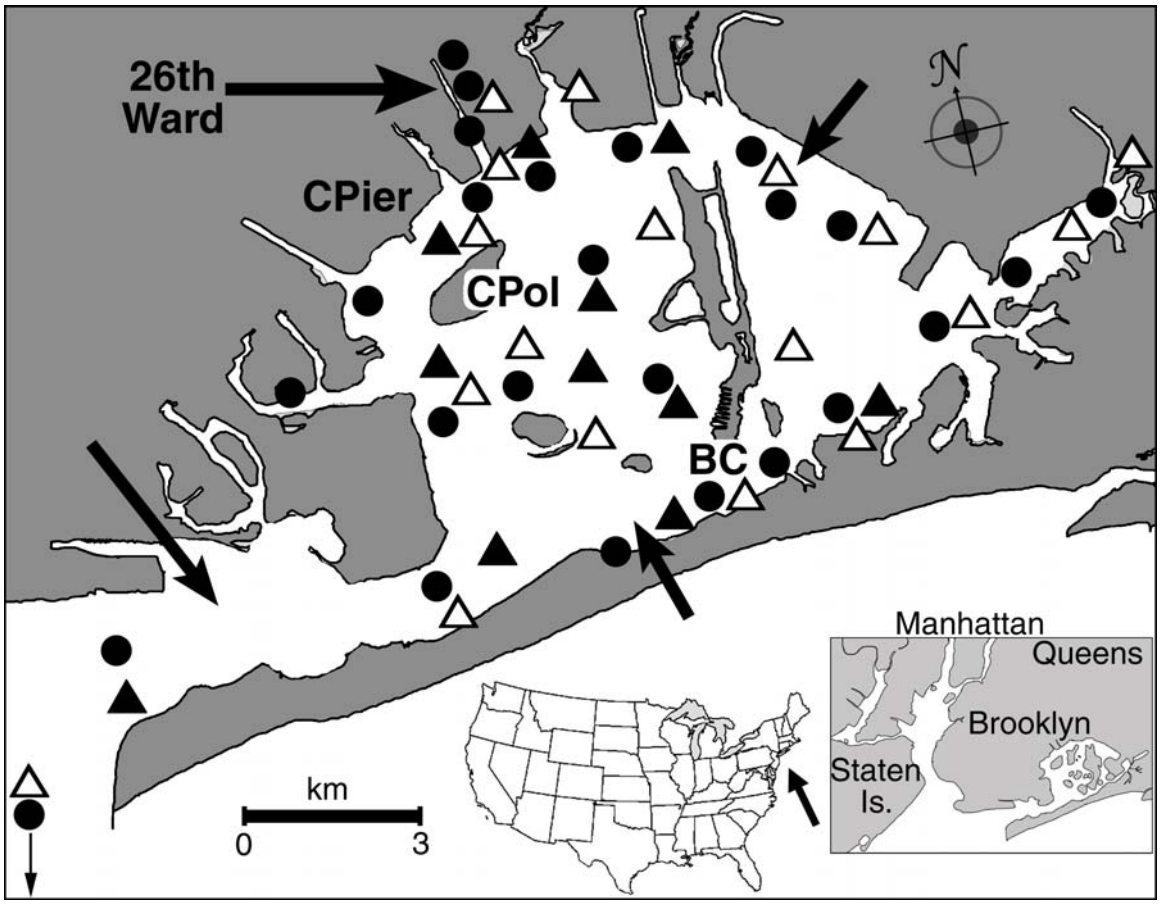

Figure IV-1. Map of Jamaica Bay. Inset shows Bay location relative to United States and New York City. Water column sample sites for all cruises are indicated; symbols indicate Oct 2004 (filled circles), Sept 2005 (filled triangles), and Apr 2006 (hollow triangles). Shallow groundwater sample sites are noted in large, boldface font; the site codes are (CPol) Canarsie Pol, (CPier) Canarsie Pier, and (BC) Broad Channel. The large, boldface font label and arrow identify the location and effluent outfall of the 26th Ward wastewater treatment plant. The approximate outfall locations of three other major wastewater treatment plants are indicated with large black arrows (Ferguson et al., 2001). JFK International Airport is located at approximately the same point on the map as the direction compass. Note that extensive marshland exists in the bay, but has been removed from this map for clarity. (After Beck et al., submitted; Chapter II)

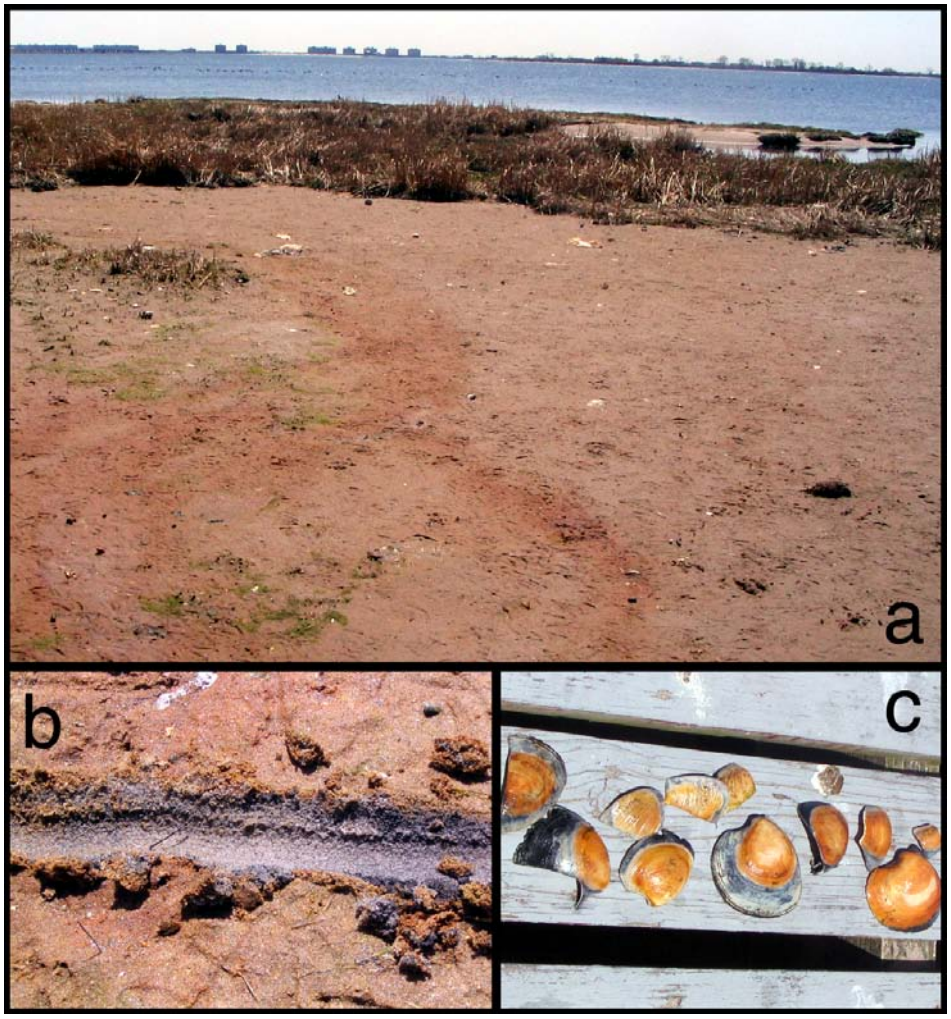

Figure IV-2. (a) Groundwater seep on the beachface of Canarsie Pol outlined by an orange-red precipitate, presumably an Fe-oxide. (b) Shallow excavation reveals gray sand underlying the red precipitate at the surface. (c) Bivalve shells located within the seepage zone. Gray portions of the shells were submerged in the sand at the time of collection.

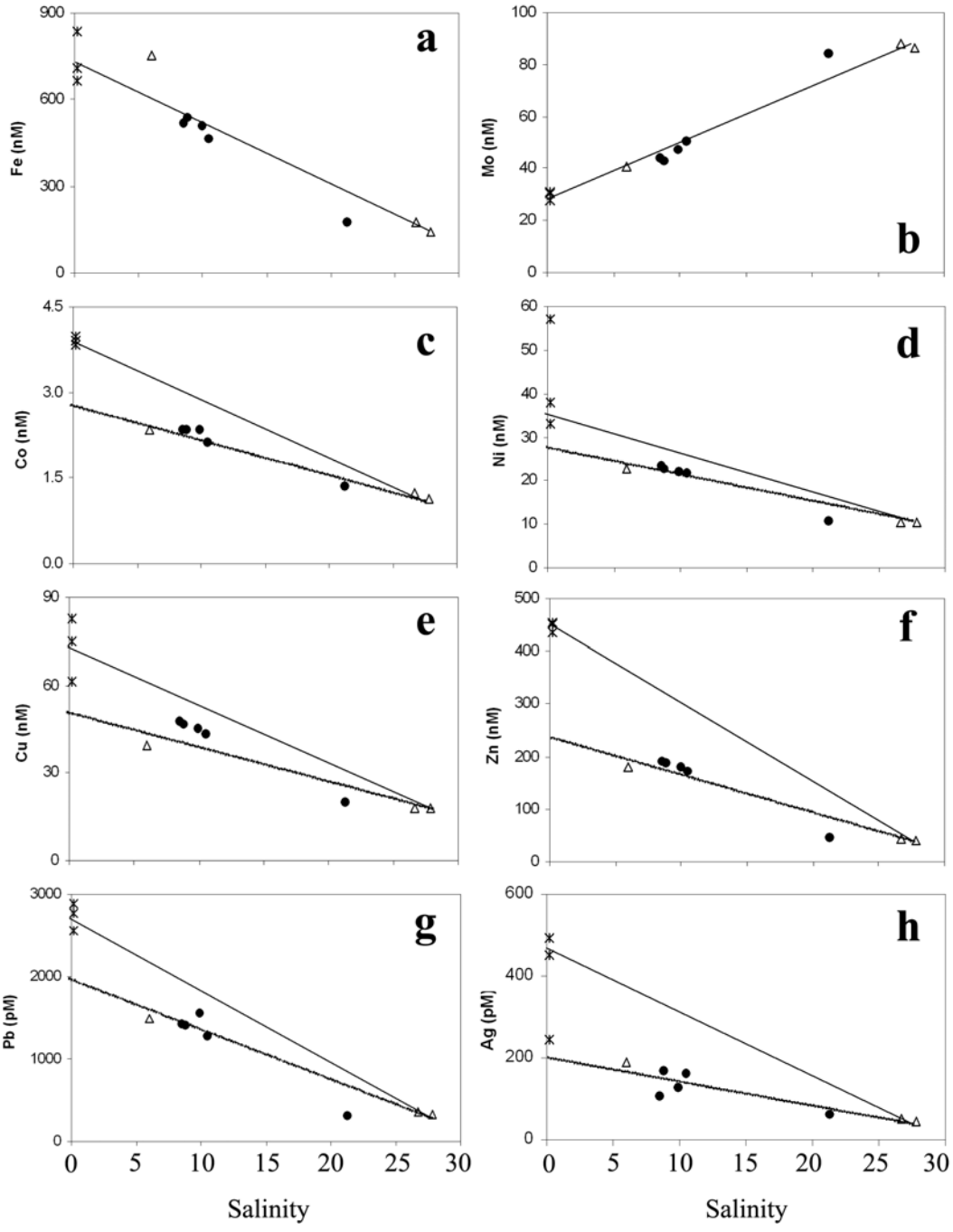

Figure IV-3. Distribution of dissolved trace metals in the mixing zone, or "sewage estuary", near the 26th Ward WWTP outfall. Symbol shapes are as follows: crosses indicate 26th Ward wastewater samples (collected Feb 2005), hollow triangles indicate surface water samples in the vicinity of the outfall creek (collected Apr 2006), and solid circles indicate samples collected in a shallow surface profile (collected Apr 2006; see text for explanation). The solid line represents conservative mixing between endmembers of wastewater at the head and bay water at the mouth of the creek. The dotted line indicates an approximate best fit through the bay water and sewage estuary samples, excluding the wastewater endmember.

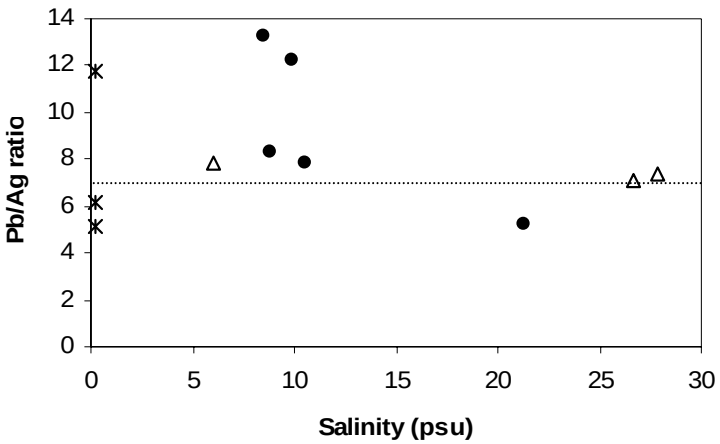

Figure IV-4. Pb/Ag ratio across the mixing zone of the sewage estuary. Symbols as in Fig. IV-3. The dotted line indicates a ratio of 7 (see text).

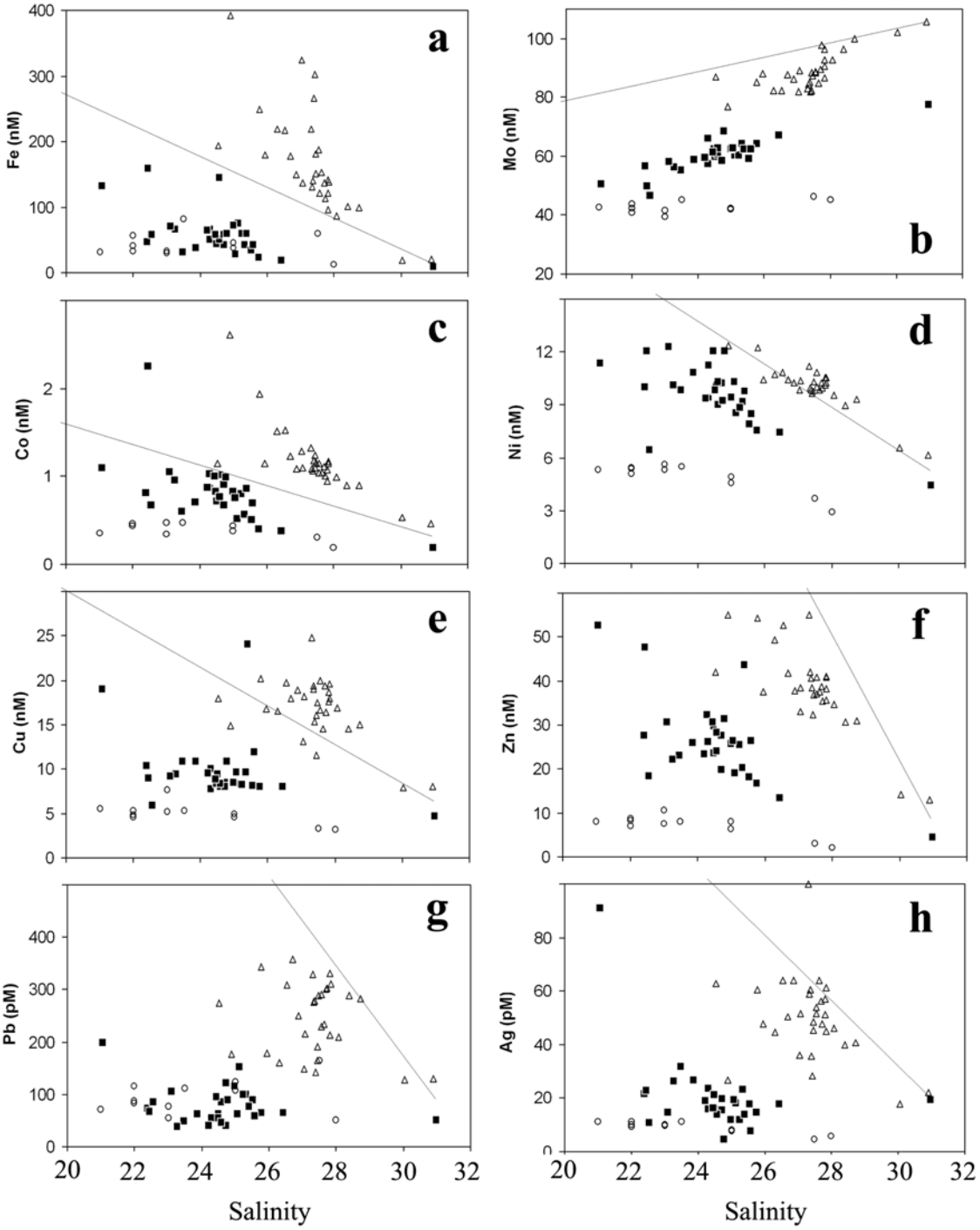

Figure IV-5. Trace metal vs. salinity plots. Because the bulk of the water column samples have high salinity, the x-axis has been cropped to exclude values less than 20 psu (see Fig. IV-3). Solid square symbols indicate Sept 2004 cruise, hollow circles indicate Oct 2005 cruise, and hollow triangles indicate April 2006 cruise. Solid lines represent theoretical conservative mixing between wastewater (S ~ 0) and coastal ocean endmembers (S = 31).

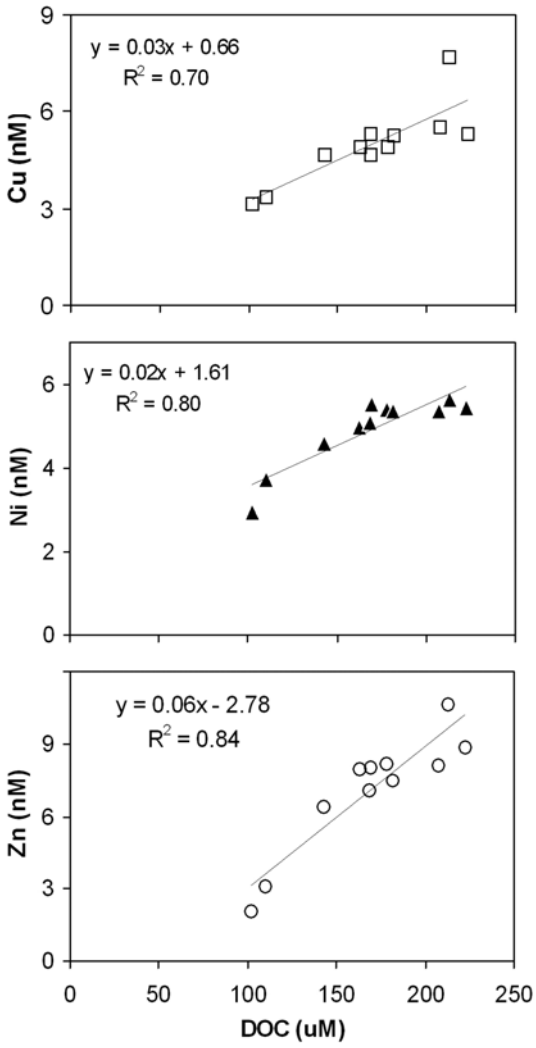

Figure IV-6. Co-variation of DOC and (a) Cu, (b) Zn, and (c) Ni.

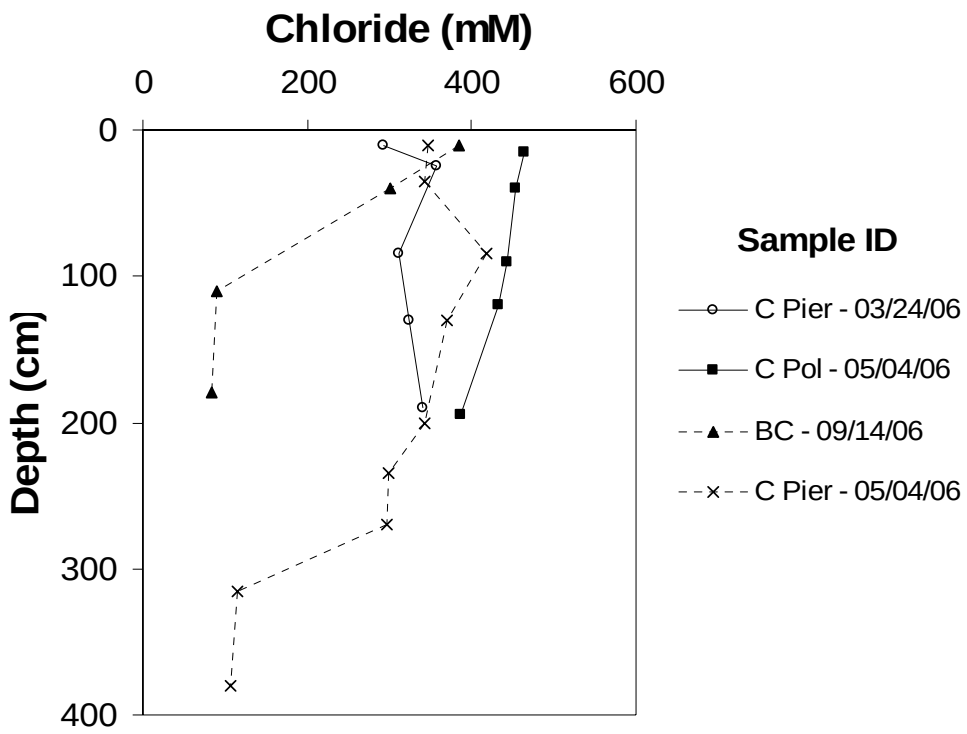

Figure IV-7. Chloride profiles in shallow groundwater in Jamaica Bay. Site IDs are the same as in Fig. IV-1.

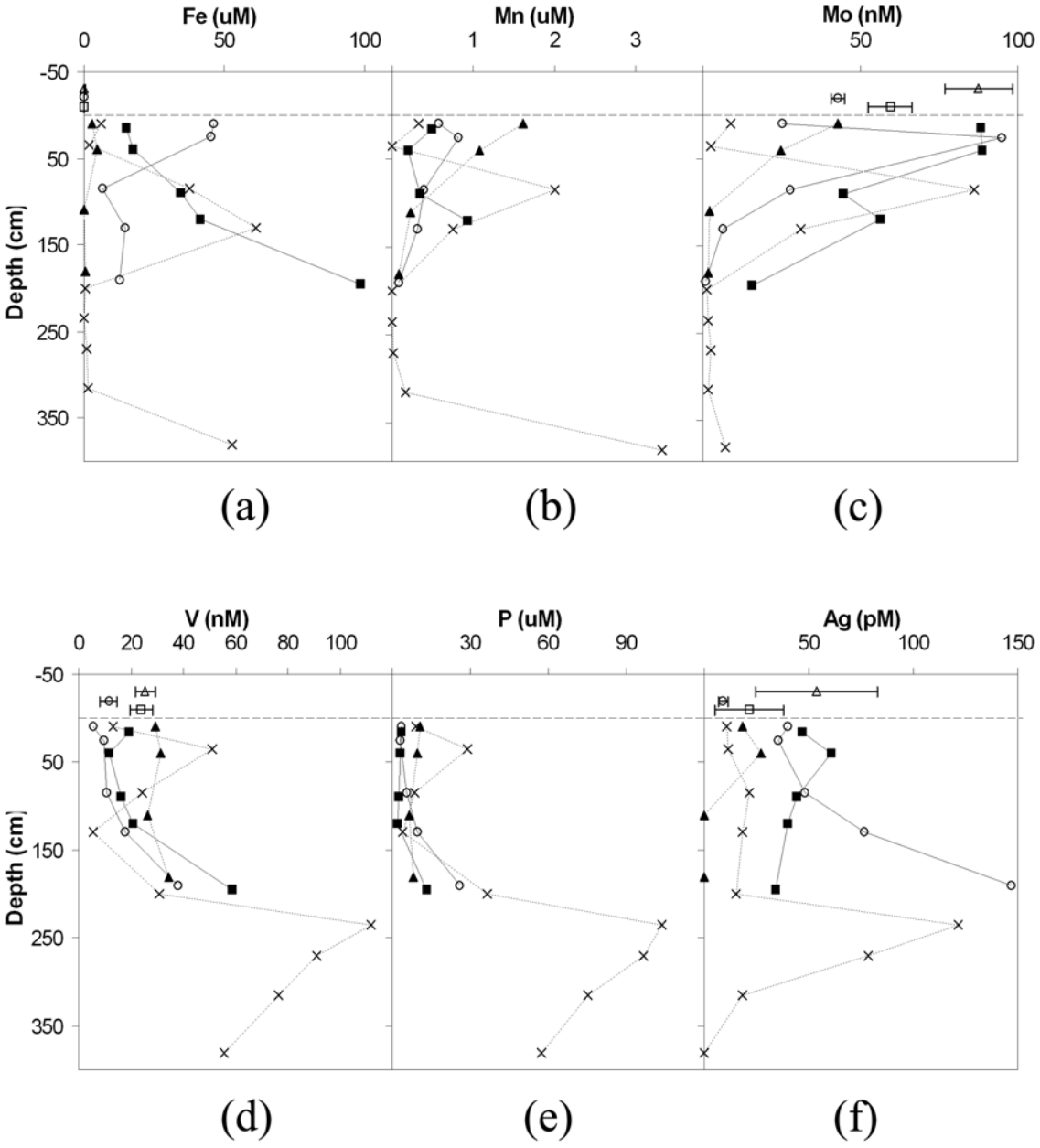

Figure IV-8. Profiles of dissolved trace metals in groundwater in Jamaica Bay. Symbols are the same as those shown in Fig. IV-7.

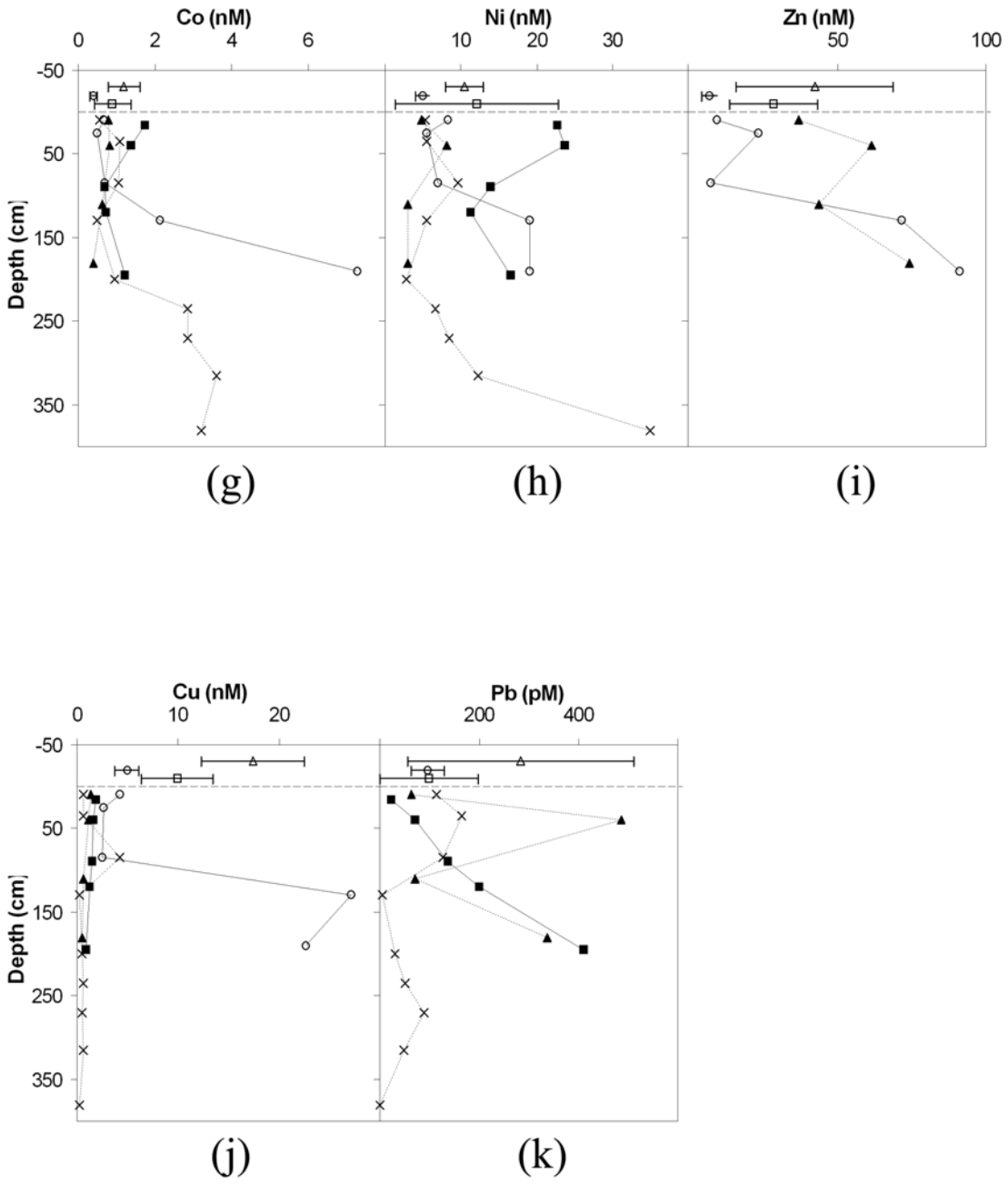

Figure IV-8, continued.

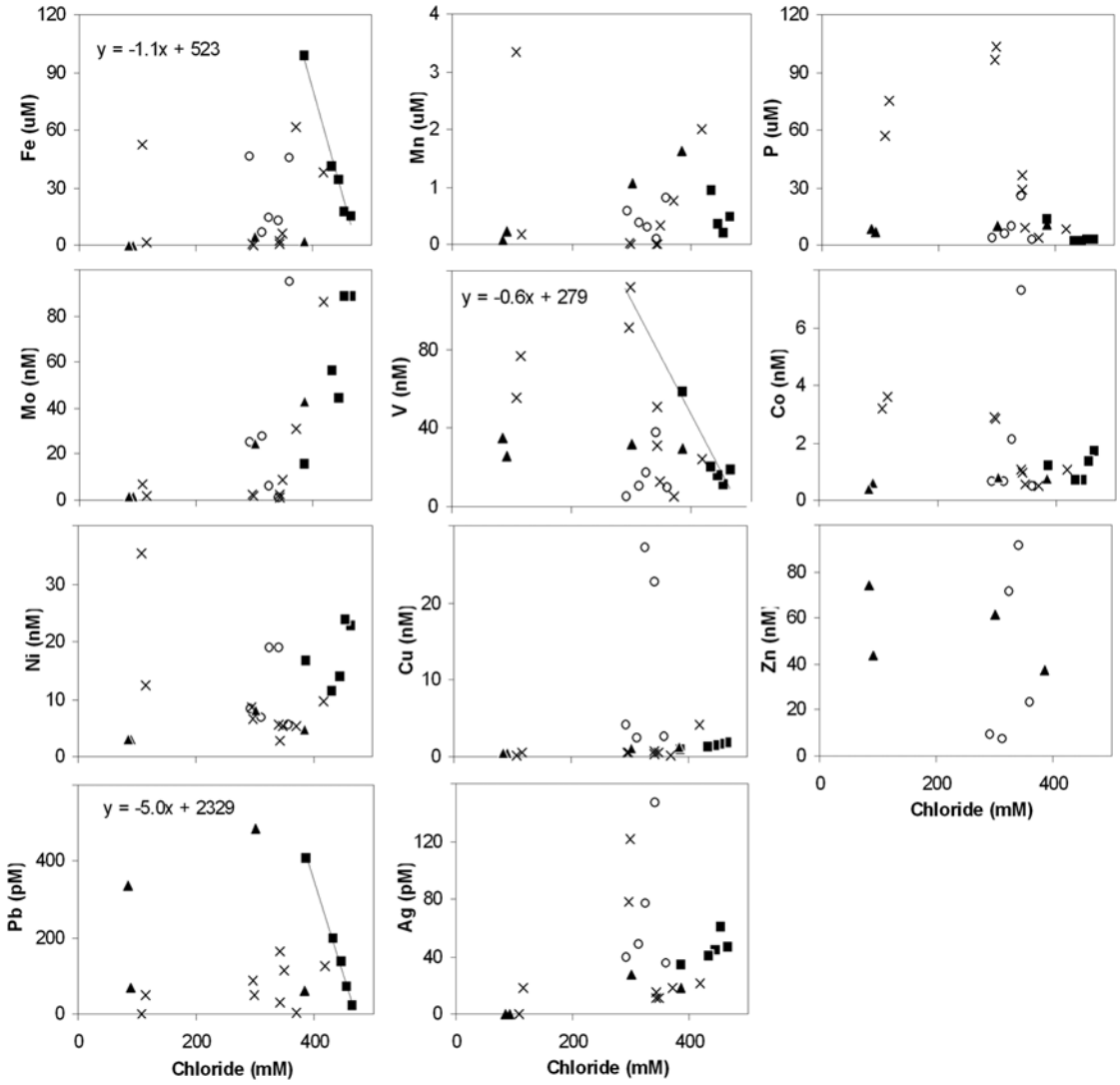

Figure IV-9. Dissolved elements in shallow (<4 m depth) groundwater. Different symbols correspond to different sampling locations, and are the same as those in Fig. IV-7. The lines and equations shown in the Fe, V, and Pb plots represent linear regression of the most saline samples; such regression lines can be used to estimate effective zero-salinity endmember concentrations (see text), but only work well for these three elements.

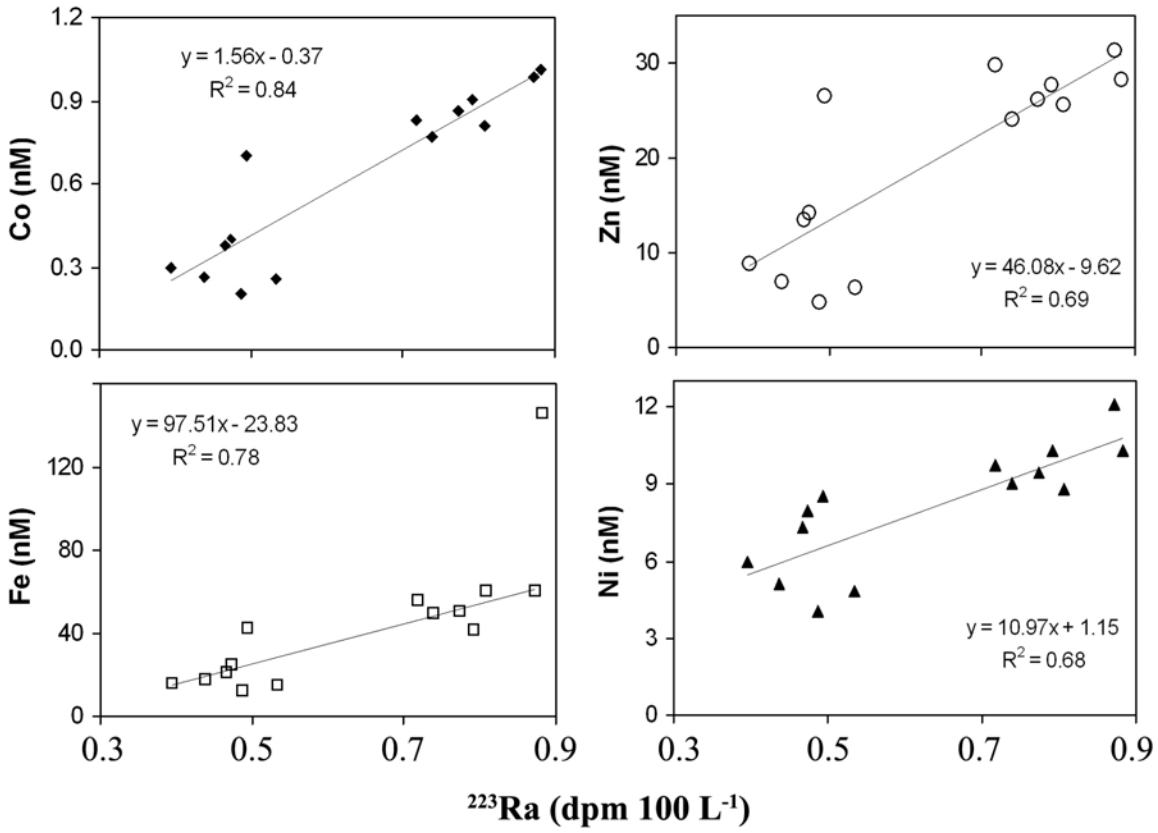

Figure IV-10. Co-variation of dissolved metals and ^{223}Ra. Only bottom water samples from the October 2004 cruise are shown. The solid line represents a linear regression of the data. The regression line of the Fe data does not include the 145 nM point. Ra data from Chapter II.

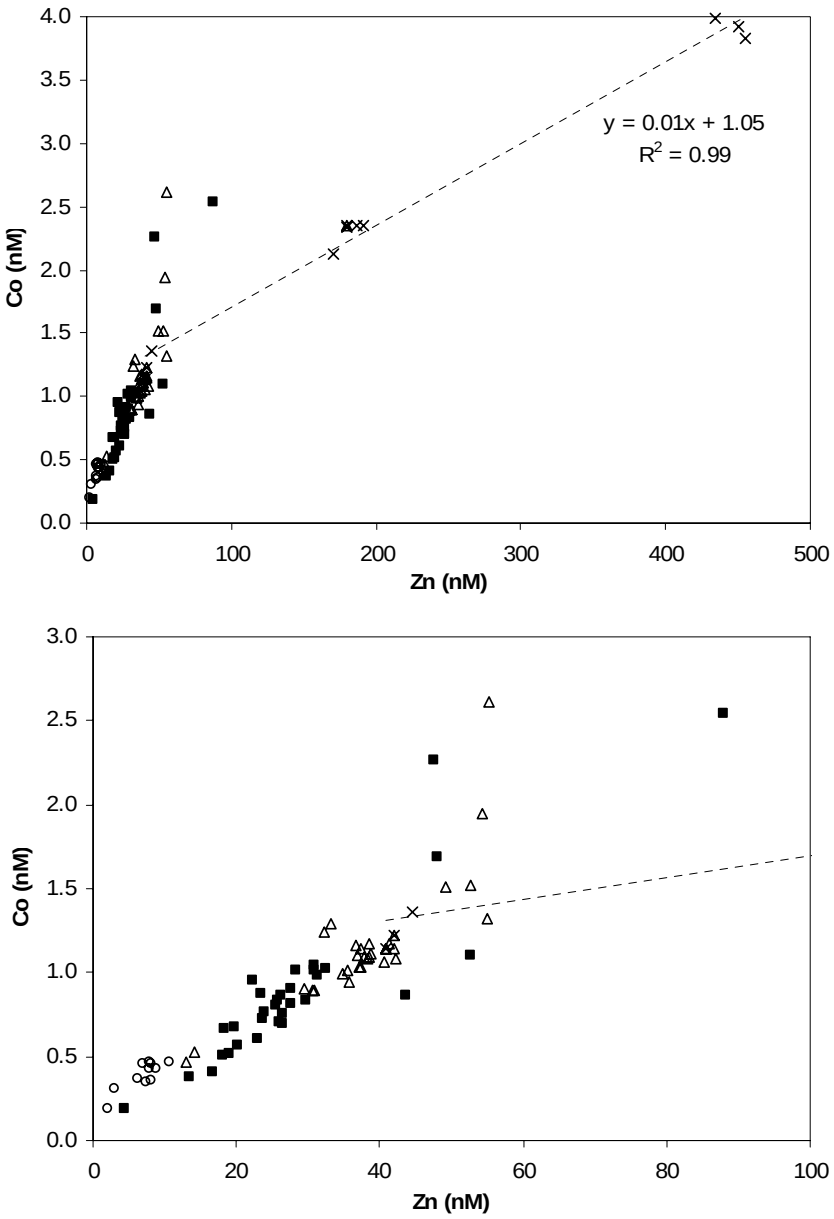

Figure IV-11. Water column dissolved Zn vs. Co. The lower graph provides an expanded view near the origin for clarity. Symbols are the same as in Fig. IV-5, except the x-shaped symbols indicate effluent *and* sewage estuary samples here. The dashed line and equation in the upper plot represent a regression of the sewage estuary data points.

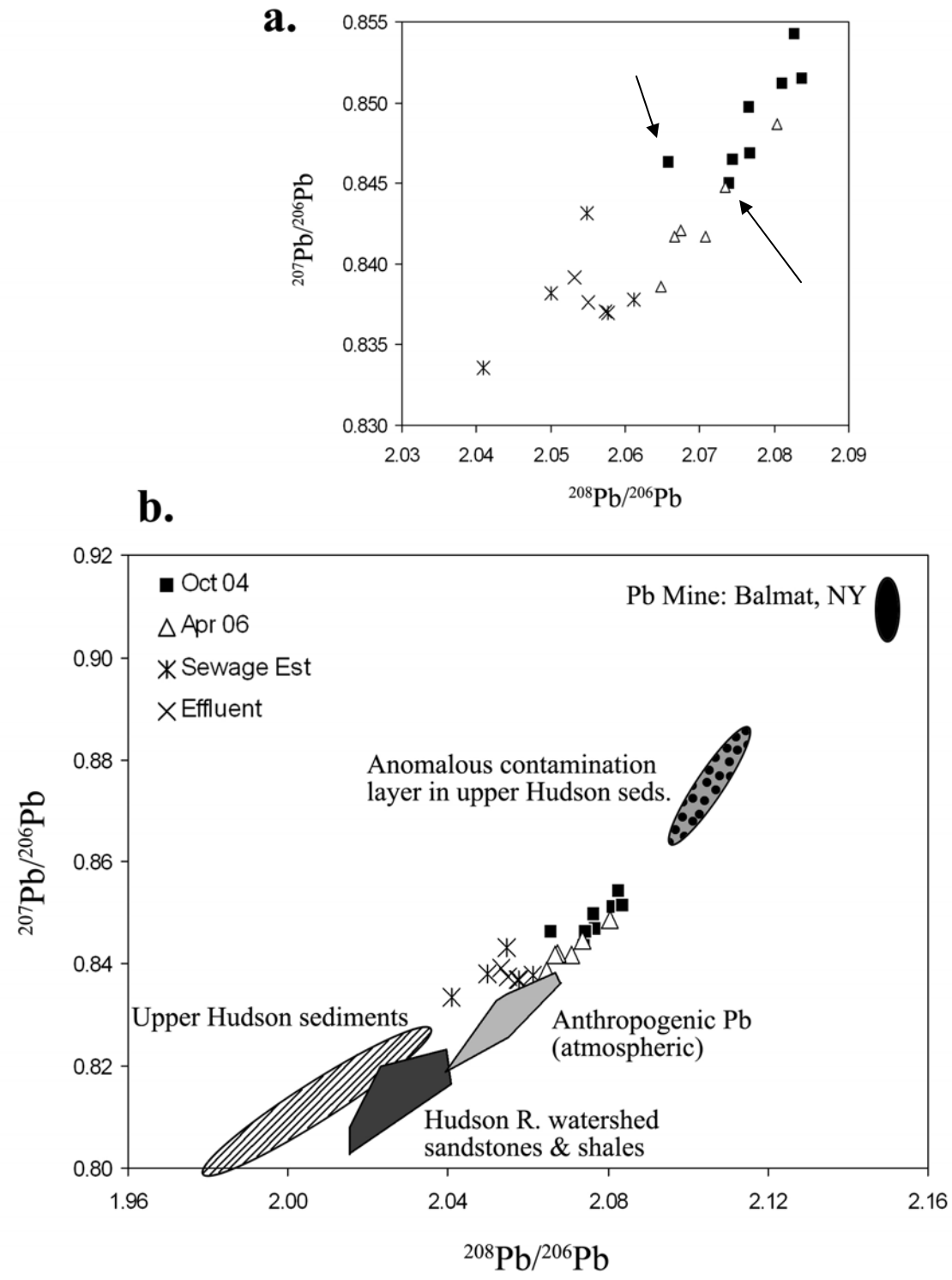

Figure IV-12. (a) Pb isotope ratio plot for JB water column samples. Solid square symbols indicate Oct 2004 cruise, hollow triangles indicate Apr 2006 cruise, crosses indicate wastewater samples, asterisks indicate sewage estuary samples. The arrows indicate high salinity samples collected during both cruises at the JB inlet (see also Fig. IV-5). (b) JB water column Pb isotopes plotted with potential sources from the local watershed and region. References for Pb sources include: Hudson sediments and Balmat Pb mine (Chillrud et al., 2003), atmospheric (Marcantonio et al., 2002), and sandstones/shales (Bock et al., 1998).

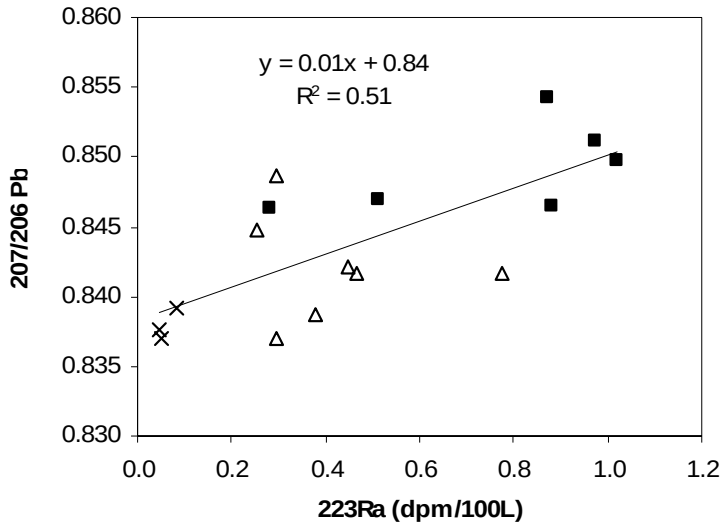

Figure IV-13. 207/206Pb ratio vs. ^{223}Ra in water column and effluent samples. Symbols as in Fig. IV-5. Note that two samples from the Oct 2004 cruise that are shown in Fig. IV-12 are not included because Ra data do not exist for those samples. The solid line represents a linear regression of all the data shown. Ra data from Chapter II.

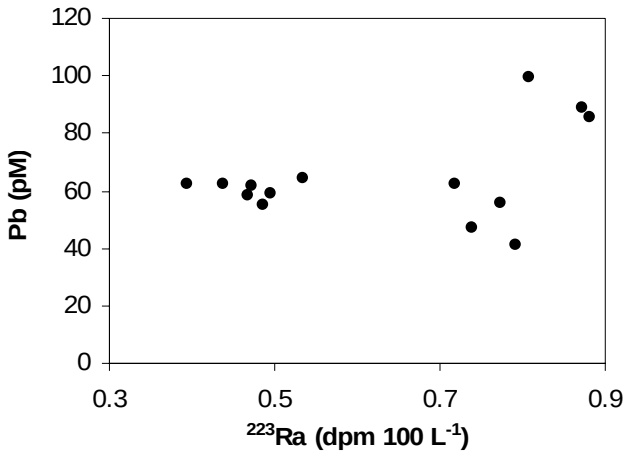

Figure IV-14. Co-variation of total dissolved Pb and ^{223}Ra. Only bottom water samples from the October 2004 cruise are shown (see Fig. IV-10). Ra data from Chapter II.

CHAPTER V:

Simultaneous use of a new high-resolution Multi-Port Piezometer and seepage meters to characterize the physical and geochemical discharge of submarine groundwater

Beck, A.J., J.P. Rapaglia, R. Coffey, J.K. Cochran, H.J. Bokuniewicz, and S.A. Sañudo-Wilhelmy, 2007. Simultaneous use of a new high-resolution Multi-Port Piezometer and seepage meters to characterize the physical and geochemical discharge of submarine groundwater. Limnology and Oceanography: Methods, submitted.

ABSTRACT

There is an increasing body of evidence suggesting that submarine groundwater discharge (SGD) is an important component of chemical budgets in coastal marine waters. However, quantifying this input is often made difficult by spatial and temporal variability in discharge rates, and by chemical transformations occurring in the subterranean estuary. The objective of the current study was to develop a trace-metal clean, high resolution multi-port piezometer, and to use it in conjunction with conventional seepage meters to better quantify SGD-derived trace element fluxes. A total of sixteen shallow (<30 cm depth) profiles were sampled through the mixing zone of the subterranean estuary on three occasions in May 2006. The salinity profiles showed clear evolution with time, with salinity at a given depth increasing or freshening in apparent response to tidal forcing. Seepage meters also showed tidally-variable seepage, with measured discharge rates ranging from -4 to 245 cm d^{-1}. A mass balance for salt in the seepage meters was used to calculate the SGD endmember; comparison of the calculated endmember with the salinity profiles suggested an SGD endmember originating from the water lens at 7-15 cm depth, probably flowing through a preferential vertical flowpath. This was further supported by trace element trends, as trace metal concentrations in one seepage meter could only result from the non-conservative behavior observed at 12 cm depth in the piezometer. Finally, trace metal fluxes calculated with the endmember concentration measured at 12 cm were the closest to the metal flux measured by the seepage meter. This study describes a simple tool for rapid collection of clean porewater profiles, and provides a method for identification of the correct endmember for trace element flux calculations.

INTRODUCTION

The geochemical significance of submarine groundwater discharge (SGD) has gained much attention in recent years, in part because of improvement in techniques and equipment for determining the magnitude and composition of the discharging water. From the development of devices for determining local rates of seepage (Lee, 1977; Taniguchi and Fukuo, 1993; Krupa et al., 1998; Paulsen et al., 2001, 2004; Sholkovitz et al., 2003) to geochemical tracers which integrate SGD over entire systems (Moore, 1996; Cable et al., 1996; Burnett and Dulaiova, 2003), the magnitude and ubiquity of SGD is beginning to be understood.

Estimates of SGD have been used in conjunction with chemical analyses in groundwater to approximate fluxes of dissolved chemical constituents. The impact of SGD in terms of its dissolved load has been shown to be significant, and is often a major component of chemical mass balances in the coastal ocean (Johannes, 1980; D'Elia et al., 1981; Capone and Bautista, 1985; Capone and Slater, 1990; Gobler and Sanudo-Wilhelmy, 2001; Charette and Buessler, 2004; Beck et al., 2007). Despite this recognition of the chemical importance of SGD in coastal ecosystems, limited work has been conducted to identify the true composition of the fluid which actually comprises "submarine groundwater". Most of the chemical flux estimates cited above simply use large collections of groundwater (porewater) measurements to obtain a good statistical average, which can then be applied to the total volume discharge. However, recent work in permeable intertidal sediments has shown that the chemical composition of submarine porewaters is highly variable, and fundamentally dependent on the reactions occurring in the subterranean estuary (Testa et al., 2002; Talbot et al., 2003; Charette and Sholkovitz,

2006). Furthermore, taking these chemical transformations into consideration can change flux estimates dramatically, by as much as an order-of-magnitude (Beck et al., 2007).

Thus, in order to estimate chemical fluxes associated with the discharge of submarine groundwater, it is necessary to assess the subsurface processes which modify the groundwater, and to identify the water actually being advected across the sediment-water interface. Here, we report the use of a trace metal clean multi-port piezometer to obtain high resolution porewater profiles in coarse subtidal sediments. We show that by installing this piezometer along with seepage meters in a location with high rates of SGD, we are able to examine how porewater profiles change with temporally-variable SGD. We use salinity and trace elements to identify the depth of the SGD source, thus furthering our understanding of the physical and chemical characteristics of submarine groundwater transport and discharge.

MATERIALS and PROCEDURES

Field Site

The site location used in this study is a small beach located in Mattituck, NY, on the southern edge of the North Fork of Long Island (Fig. V-1). The beach sediment comprises relatively uniform medium to coarse sands ($\varphi < 0.5$) lightly interspersed with shell fragments and other refractory marine detritus.

The North Fork of Long Island is underlain by an unconfined upper glacial aquifer (UGA) whose water table is highly impacted by local precipitation. The UGA is a highly permeable aquifer up to 210 m thick, and is composed of glacial till and outwash deposits interbedded with marine clays (Busciolano, 2002). Submarine groundwater

discharge has been observed previously at this site; seepage is strongly tidally-modulated, with rates of seawater intrusion at high tide of up to 60 cm d^{-1}, and discharge rates at low tide reaching 210 cm d^{-1} (J.P. Rapaglia, unpublished data). The high flow rates measured at this site are similar to other locations in the Peconic Estuary system; Gobler and Boneillo (2003) report maximum flow rates of approximately 330 cm d^{-1} during spring 2000 and 2001 in the North Sea Harbor, and Dulaiova et al. (2006) measured rates as high as 37 cm d^{-1} during spring 2002 at West Neck Bay.

Multi-port piezometer design and construction

Our multi-port piezometer (MPP) combines characteristics of several previous porewater samplers (Huettel, 1990; Falter and Sansone, 2000a; Berg and McGlathery, 2001; Seeberg-Elverfeldt et al., 2005; Charette and Allen, 2006), and is well-suited for our particular environment and purpose. It is closely related to the design of Martin and coworkers (2003); we have modified the materials and construction for three reasons: (1) to decrease trace metal blanks and allow acid-washing, (2) to allow rapid collection of small-volume samples, and (3) to obtain shallow profiles with high depth resolution. A schematic of our design is shown in Fig. V-2.

The MPP is constructed from a section of 1" (2.54 cm) outer diameter white PVC pipe. The pipe is cut in half lengthwise to provide access to the inside walls. Ports are cut into the outside wall of the pipe to accommodate the porous sampling tips, with a thin bar of PVC left spanning the port to provide support at the back of the sampling tip. The tips we have employed are actually air diffuser tips designed for under-gravel aquarium filters (Aqua-Tech, Inc). These tips are both porous and flexible, and can be bent into a

semi-circle that protrudes from the pipe face. In this way, the ends of the air diffuser are concealed within the pipe body, while most of the body is exposed (see "Side View," Fig. V-2). The length of the exposed portion can vary to match the desired resolution, although lengths shorter than 0.5 cm are probably not practical. There is also the important consideration of balancing attempted resolution with desired sample size; if large volumes of water are drawn from closely spaced ports, adjacent ports will draw water from overlapping spheroids. We discuss this in detail in the following section. We have chosen to use a port length of 2 cm, with ports separated from each other by 2 cm. Each port is attached to an individual sampling tube. This allows sampling of all the ports almost simultaneously, and prevents cross-contamination between depths. The air diffuser tips also provide a pre-filter, which reduces particle loading during sample filtration, and helps reduce the possibility of contamination of dissolved samples.

The air diffuser is connected to the sampling tubing with a short section of C-Flex (Cole Parmer) pump tubing. The flexible nature of this tubing allows it to fit over the much larger diameter air diffuser, providing a tight grip and preventing detachment from the sampling tubing. For our initial experiments with this system, we used vinyl tubing, but have since switched to narrow-diameter (1/8" (0.318 cm) O.D., 1/16" (0.159 cm) I.D.) Teflon tubing to minimize contamination and dead volume. For the latter tubing, a 30-cm section has a volume of only 5 mL.

The bottom point on the MPP is cast from epoxy-like fiberglass resin, with a male-female, 3/4" to 1" PVC reducing fitting embedded at the top during casting. This tip can be attached neatly to the end of the piezometer, and is removable for cleaning.

All the piezometer materials are readily available from hardware and pet supply stores, and the total cost of the unit is less than US$50.

Ultimately, the entire MPP is constructed of non-metal components, and sample water comes in contact only with the tubing, air diffuser, and probably a small region of the PVC pipe. This makes it suitable for the collection of trace-metal clean samples. All portions of the system can be acid-washed, although it may be advisable to remove the cast resin drive point prior to doing so to prevent weakening. Here, we present some chemical analyses of samples collected with a system that had undergone only precursory cleaning, and we have subsequently found that the contamination we observed (discussed below) can be avoided with more stringent acid-washing protocols.

Overlap of samples collected from adjacent ports

When collecting high resolution profiles with a device such as the MPP, it is important to consider how sample volume affects the collection depth and whether adjacent samples include water from overlapping regions (Berg and McGlathery, 2001). Initially, we can approximate that each port pulls water equally from the entire surrounding region, excepting only the volume blocked by the cylinder of the multi-port sampler (i.e. $V_{sample} = V_{sphere} - V_{cylinder}$). Thus, the sampling region is a spheroid of radius a minus a cylinder with radius x and a height equivalent to $2a$:

$$V_{sample} = [4/3 \times \pi \times a^3] - 2a \times \pi \times x^2 \qquad [1]$$

We ignore the slight error resulting from use of a “flat-ended” cylinder which extends partially beyond the surface of the sphere, and from the likelihood that water is probably not drawn as easily from the region on the side of the cylinder opposite the

sampling port. At a sample volume of 60 mL, a sediment porosity of 0.5, and a cylinder radius of 2.5 cm, this approximation gives a sampling radius *a* of 4.1 cm. The sampler we constructed, and describe below, had a port spacing of 4 cm. Thus, one might suspect that each sample represents a sphere that overlaps its neighboring sample spheres by nearly a half volume. However, the detailed profiles shown in Fig. V-4 (discussed below) suggest that this is not the case, and that the sample is not pulled evenly to the port from all directions.

Marine sediments are deposited in layers which allow advective flow to occur more rapidly in a horizontal direction than a vertical one, a phenomenon termed anisotropy (Charbeneau, 2000). The anisotropy, or horizontal/vertical hydraulic conductivity ratio (*S*), of the UGA is between 10:1 and 2.5:1 (Bokuniewicz and Zeitlin, 1980). This allows equation [1] to be rewritten, replacing the spheroid sampling volume with an ellipsoid:

$$V_{sample} = [4/3 \times \pi \times a \times b \times c] - 2a \times \pi \times x^2, \qquad [2]$$

where *a* is the vertical sampling radius, and *b* and *c* are the horizontal radii of the ellipsoid. The equation can be further simplified by setting b and c equal to each other, and related to *a* by the anisotropy ratio, *S*. Thus, equation [2] becomes

$$V_{sample} = [4/3 \times \pi \times a^3 \times S^2] - 2a \times \pi \times x^2. \qquad [3].$$

Because of the nonlinear nature of the relationship between *a* and *S*, a slight increase in *S* results in significant reduction in *a*, particularly at low degrees of anisotropy (Fig. V-3).

The low end of the range for *S* in the UGA is 2, which for our particular case, gives a vertical sampling radius of 2.3 cm. This is an overlap of sampling volumes between ports of only 0.3 cm. Increasing the anisotropy factor to 3 further reduces the

vertical radius to 1.7 cm. This is well within the range reported for *S* in the UGA, and suggests that overlap of samples acquired from adjacent ports may be very low or zero.

Sample collection and analysis

A ~1 m MPP was constructed with 8 ports spanning the lower ~30 cm. In this way, a profile could be obtained to 30 cm below the sediment surface, while allowing the top of the MPP with the free tubing ends to be above the ambient water surface. (Because the sample ports are completely sealed except for the sampling face, the entire piezometer can be submerged if necessary.) The sampler was deployed below the low tide line, with ambient water height of 20-50 cm depending on the tidal level. The MPP was driven manually into the sediment using a slide hammer (AMS, Inc.), with a piece of wood as a buffer between the hammer and top of the sampler.

Samples were drawn from individual tubes using dedicated plastic 60 mL syringes after purging each tube of ~30 mL of sample with a syringe. By cocking the plunger in the vacuum position with sections of ½" rigid Teflon tubing, all syringes could be set to fill nearly simultaneously (flow rates less than 100 mL min^{-1}). For inorganic chemical analyses, small-volume (~15 mL) samples were syringe-filtered through 0.45 μm nylon filters directly into clean centrifuge tubes pre-charged with 100 μL of Optima-grade concentrated HCl (Fisher Scientific). Metal analyses were conducted by dilution and direct injection into a Finnigan Element2 ICPMS. The remaining ~45 mL of sample collected was retained for salinity measurement using a handheld YSI 556 multi-probe field meter.

Reagent, filter, and field sample container blanks were determined with Milli-Q water added to acid-charged vials transported to and from the field site. These blanks are subtracted from sample concentrations, and represented less than 1% of the lowest sample concentration for the analytes shown here.

Seepage meters

Vented benthic chambers (2-3 on each date), first described by Lee (1977), were installed near the MPP to directly measure the SGD rate coincident with collection of subsurface salinity profiles. Briefly, these chambers consist of circular drums vented to ~5 L plastic bags. The open face of the drum is inserted into the sediment surface, leaving a head space of about 5-10 cm between the sediment and the closed face of the drum. As groundwater discharge enters the drum, the water in the headspace is flushed into the bag, and the volume discharge is converted to linear flow rate using the surface area of the drum. Sampling frequency is primarily dependent on flow rate; higher flow rates require more frequent sampling, lest the bags fill to capacity. At very low flow rates, the bags are pre-filled with a small volume (0.5 – 1 L) of water to reduce artifact influence (Shaw et al., 1990; Libelo and McIntyre, 1994). In addition, although it precludes obtaining salinity measurements, this allows groundwater recharge (i.e. removal of water from the bag) to be observed. We report such recharge as a negative flow rate (e.g. see "M3", Fig. V-5). Seepage meter samples collected for chemical analysis were not pre-filled, and had been flushed by previous samples totaling approximately 20 L.

ASSESSMENT

We found the MPP sampler simple to install, and very easy to use. In particular, the design was such that a single individual could sample the entire 8-depth profile in less than one minute. In our test setting, where submarine groundwater discharge exhibits clear and rapid tidal forcing, it was important that a nearly instantaneous profile could be acquired at regular 30-45 minute intervals. The robustness of the construction, and the short length of this particular sampler, allowed for easy removal and later redeployment.

On 09 May and 24 May 2006, we sampled five profiles at 30-90 min intervals for salinity measurement only. On 31 May 2006, six profiles were sampled at the same time interval for salinity measurement. Additionally on the latter date, the samples from the second (9:50) and final (12:00) profiles were reserved for trace element analyses. This initially allowed the sampler to equilibrate for approximately one hour, and ensured that each port was well-flushed before samples for chemical analysis were taken.

Salinity profiles

Depth profiles of salinity showed somewhat similar patterns on all sampling dates: decrease from 20-25 near the surface to 5 or less at 25 cm (Figs. V-4a through V-4c). On 09 May, the measured salinity profile did not vary consistently with time over the depths sampled, probably because the sampling period spanned the change from flood to ebb tide (Fig. V-4a). Initially, the 09 May profile had a broad, deep salinity maximum from 15-21 cm; this maximum had decreased by the next time point (80 min elapsed), and was not evident in any of the subsequent profiles. Again, this was probably a result of tidal forcing: at the 12 cm depth, the salinity was low (~12) on the initially rising tide.

As the tide continued to rise, the salinity at 12 cm increased by 6. At full high tide, the salinity at 12 cm peaked at 20.1. This was clear evidence of tidally-forced groundwater recharge, as the rising tide reversed the hydraulic gradient and forced seawater into the sediment. The salinity decreased again as the tide began to ebb and fresher water at depth began to flow upward again. The salinity continued to decrease when monitoring ceased at nearly low tide.

The salinity profiles on 24 May and 31 May were more similar to each other than to the 9 May profile. The 24 May salinity profile declined to <1 at 24 cm, while the 31 May profile only reached ~7 at the same depth. On both of these sampling dates, a deep salinity maximum was observed, although it was more shallow and broader on 31 May than on 24 May. On the latter sampling date, the salinity at each depth tended to decrease with time, similar to the 9 May profile on ebb tide. The profile was generally constant over the sampling period, likely because the tidal phase did not reverse (Fig. V-4b). The opposite was true for the 31 May sampling date. The profiles were sampled beginning shortly before low tide, and continued through the start of flood tide. The large salinity changes observed (nearly 7 for 15 cm depth) were likely the result of sampling across the changing tide, as on 9 May. Thus, variability in the porewater salinity profiles was consistent on all dates with tidal forcing.

Seepage meters

On the dates of piezometer deployment, seepage meters recorded very high, though variable, rates of SGD (Fig. V-5). Flow ranged from -4 to 244 cm d^{-1}. Clear inverse tidal modulation was observed, with highest discharge at low tide, and seawater

intrusion at high tide (see tidal curves in Fig. V-4). Flow rates were sufficiently high that the headspace in the drums was flushed rapidly, and the salinity of the discharging water decreased with time (Fig. V-6). All seepage meters collected water with declining salinity, although the rate of decrease differed between the sampling dates and between different seepage meters deployed on individual days. The rate of salinity decrease is determined by both flow rate (i.e. flushing time) and endmember salinity. On 9 May, meters M2 and M3 showed nearly identical discharge rates (Fig. V-5), although the salinity in meter M2 decreased substantially more rapidly (Fig. V-6). In a similar manner, the flow rates of M1 and M3 were very different, but the salinity change was similar. This strongly suggests that each meter was being affected by groundwater endmembers with slightly different salinities.

Trace element composition of the porewater

In order to keep this discussion relatively succinct, we restrict our examination to a suite of elements which are representative of different geochemical behaviors, with particular focus on redox chemistry and particle affinity. We focus on Sr (an alkaline earth element that is generally conservative with respect to salinity in seawater), V (a redox-sensitive transition metal that is usually conservative in oxic seawater, but can show nutrient-type depletion in surface waters and scavenging under anoxic conditions), Co (a transition metal that can be particle-reactive and can act as a micronutrient), and Pb (a particle-reactive, toxic transition metal with an often anthropogenic source).

Profiles of these four elements are shown in Fig. V-7. Sr and V (Fig. V-7b and V-7c, respectively) show similar trends to each other, with concentrations highest in surface

waters, a decrease to 10 cm depth, a broad peak from ~12-17 cm, and decrease again to 27 cm. These trends mimic those observed in salinity (Fig. V-7a), and element-salinity plots are highly linear, suggesting conservative behavior of these elements (Fig. V-8a and V-8b). The conservative behavior for V is not surprising, as low Mn concentrations (<1.5 μM) suggest oxic conditions throughout the profiles (data not shown).

The profiles of Pb and Co are generally similar, with high concentrations measured in water immediately above the sediment-water interface (Fig. V-7d and V-7e). The samples immediately below this interface are lower by a factor of 2 or 3, and concentrations show a broad peak between depths of 12 and 17 cm. Element-salinity plots (Fig. V-8c and V-8d) of these metals show non-conservative input of both relative to mixing between the observed endmembers. The non-conservative behavior is greatest in the 10-15 salinity range, although the trend is clearer for Co than Pb.

Potential contamination

We assume that profiles exhibiting clear trends with depth are probably not subject to contamination or sediment disturbance. Since all sample ports are identical in construction, it would be difficult to believe that contaminated profiles would still show coherent trends. For an element such as Zn, contamination was obvious, as concentrations ranged from 0.6 to 3.47 μM, and showed no clear variation with depth (Fig. V-9). These levels are unreasonably high, as levels measured in groundwater elsewhere on Long Island are less than 140 nM (Sanudo-Wilhelmy et al., 2002).

For Pb, concentrations were also unusually elevated at some depths (up to 1.7 nM, compared to ~0.1 nM or less in other groundwaters; Rossi, 2000), but very low levels

were measured consistently in surface waters (0.04 nM) and at other depths (0.2 nM). Furthermore, depth trends showed smooth peaks and repeatable profiles (Fig. V-7d). Thus, we believe the high Pb levels measured at this site probably result from geochemical processes occurring in the subterranean estuary, and are not an artifact of the sampling technique.

DISCUSSION

The purpose of this study is twofold: first, to examine how subsurface salinity profiles vary with tidally-forced SGD flow and to determine if this could offer information on the discharge mechanism, and second, to verify that the MPP could collect uncontaminated samples for trace elements that could then be used as tracers to verify trends observed in the salinity profiles.

Using seepage meters and salinity profiles to identify the SGD endmember

A non-saline SGD endmember is required to explain the decrease in salinity observed in the seepage meters. However, the salinity trend observed in seepage meter "M6" approaches a salinity asymptote well before reaching completely fresh levels (Fig. V-10), suggesting that the endmember is brackish, not fresh. Brackish discharge is consistent with the modeled results of Robinson et al. (2006), who identified that fresh SGD occurs slightly offshore via a freshwater "tube". This tube is bounded by regions of saline intrusion, and the tube borders are delineated by brackish regions as much as two meters thick. Where the tube intersects the sediment-water interface, both fresh and brackish discharge may be observed depending on the exact sampling location.

In order to follow the evolution of this brackish endmember over time, a mass balance can be constructed for salt within the drum. The salinity of the water exiting the drum, S_{out}, can be represented by:

$$S_{out} = [S_{in}V_{in} + S_{drum}V_{drum}] \times [V_{in} + V_{drum}]^{-1} \quad [4]$$

where S_{in} is the salinity of the water entering the drum, S_{out} is the salinity measured in the bag, S_{drum} is that measured in the drum headspace, $V_{in,out}$ are the volumes of the water entering and leaving the drum, and V_{drum} is the volume of the drum headspace (estimated using the height of drum above the sediment surface). In the case of the seepage meter, V_{in} equals V_{out} and is the volume measured in the sample bag, and V_{drum} is constant. In addition, S_{out} is the salinity measured in the sample bag. The salinity inside the drum (S_{drum}) can be approximated as the salinity measured in the sample bag for the previous interval. Thus, the only unknown is the salinity of the water entering the drum (i.e. the salinity of the SGD endmember), for which equation [4] can be rearranged:

$$S_{in} = [S_{out}(V_{in} + V_{drum}) - S_{drum}V_{drum}] \times V_{in}^{-1} \quad [5]$$

Applying equation [5] to the data we collected from the seepage meters indicates that the salinity of the SGD endmember varies with time (Fig. V-11). The highest endmember salinities (~20-25) correspond to the period immediately following high tide. Thus, the seawater intrusion observed in meter “M3” around 10:00 (Fig. V-5) resulted in high porewater salinity which is subsequently discharged with the ebbing tide. The most consistent endmember salinities are calculated with the high flow samples collected on 05/31/06 (“M6” in particular). In seepage meter M6, the endmember salinity ranges from 12.3 to 5.8. That the end member salinity changed somewhat erratically suggests to us

that the system achieved steady state rapidly; small variations in the endmember were distinguishable even with high frequency sample collection.

By comparing the salinity variation of the calculated SGD end member with the salinity variation measured at different depths in the MPP, we can determine the depth from which the SGD endmember is obtained. To present only the most relevant data here, we assume that the calculated endmember salinity must correlate well with the salinity measured at the depth of interest, and that the slope of a linear regression line drawn through the data must be relatively close to the 1:1 relationship.

The calculation of S_{in} requires that the first seepage meter sample be used for determining S_{drum} (i.e. the first drum sample represents the salinity of the water inside the drum), so one data point need necessarily be omitted. Also, only seepage meter samples which have companion porewater profiles can be used. This results in relatively few data points, and reduces the statistical significance of the observed correlations. However, the correlation coefficient between the calculated endmember salinity and the salinity at a given depth (as shown in Fig. V-12) was always much higher for one depth than any others, and the slope of this particular regression line always matched the 1:1 line most closely. To illustrate this point, Table V-1 shows the slopes and r^2 values given by all the data on 05/31/06 (i.e. replicating Fig. V-12c for each individual depth). Furthermore, the depth with the best correlation on all three sampling dates was consistently between 7 and 16 cm. This is the very depth at which, as discussed previously, the greatest variation in salinity was observed during each time series (Fig. V-4). These two indicators give us further confidence that this was in fact the depth from which the water in the seepage meter was derived.

An apparent end-member between 7 and 16 cm seems to be an indication of the existence of small-scale vertical preferential flow paths along which pore water from a depth of between 7 and 16 cm may rapidly reach the sediment-water interface to be discharged. These may be caused, for example, by the physical interfingering of downward-flowing columns of saltier water interspersed between upward-flowing fingers of fresher water by density-induced instabilities, or by bioirrigation (Martin et al., 2004). Salt-fingering has not been observed in the field, but theoretical calculations give the finger widths on the order of centimeters (Bokuniewicz et al., 2004). The piezometer could probably not resolve individual advection cells or burrows, but would sample an average salinity across cells. Thus, preferential flow pathways at depths of between 7 and 16 cm could be formed by either mechanism, or perhaps some others, on a horizontal scale too small to be resolved by the piezometer.

As well, the salinity change at each depth in the MPP profiles was not monotonic. This suggests to us that the movement of pore water within the subsurface mixing zone does not simply flow in a vertical, homogeneous direction. The observations of these local maxima and minima in the porewater salinity profiles give indication that transport processes near the sediment-water interface may not be adequately represented by a one-dimensional advection-dispersion model. However, the subsurface maxima in the salinity profiles (Fig. V-4) may be an indication of lateral flow at preferred levels. Alternatively, the vertical profiles could reflect a pattern of non-local transport due to biogenic advection and complex burrow structures (e.g. Fig. 11.9 in Aller, 2001, p.281). Biogenic transport processes have been shown to produce deviations from 1D model behavior particularly at depths of 7-15 cm (Martin and Banta, 1992; Marinelli, 1992), and

a similar argument was invoked by Falter and Sansone (2000b) to explain subsurface (~50 cm depth) O_2 maxima in permeable coral reef sediments.

Biogenic advection is on the order of ~0.2 - 4 cm d^{-1} (Aller, 2001), as much as one and a half orders of magnitude lower than the measured SGD rates. Even if there is not active irrigation, however, relict burrows could result in a system of conduits of higher permeability sands (Aller, 1984; D'Andrea et al., 2004). On the three sampling dates, MPP placement was not in exactly the same location on the beachface; the repeated observation of salinity maxima at similar depths of 12-20 cm on all dates suggests that at this site, there is an abundant population of biota influencing sediment permeability and water advection. Indeed, several deeply burrowing benthic organisms, such as *Chaetopteridae*, are found in the area (R. Cerrato, Stony Brook University, 2007, personal communication). In any event, biogenic, nonlocal transport processes may play a major role in regulating flow patterns. Not only may this lead to commonplace spatial heterogeneity in SGD (Burnett et al., 2006), but it directly affects how chemical profiles are interpreted and SGD chemical fluxes are estimated.

Dissolved trace elements as indicators of SGD source

Considering that the salinity in the drum is necessarily a mix of fresh and saline waters, it can be argued that the composition inside the drum may not necessarily reflect a particular source, but only mixing between arbitrary, though proper, endmembers. To strengthen our argument for the presumed SGD source, we more closely examine the trace element data. The conservative behavior of Sr and V are unhelpful, as the chemical composition in the seepage meter sample would fall on the mixing line whether the

sample was from a single depth or a mixture of different depths (Fig. V-8a and V-8c). However, the non-conservative behavior of Pb and Co (Fig. V-8c and V-8d) must be reflected in the seepage meter sample, if the assumption of a 12 cm deep endmember is indeed appropriate.

The water inside the drum headspace initially has the same chemical composition as the ambient water. As this water is flushed from the drum, the composition should approach that of the endmember, as discussed previously. Thus, the trace metal composition must either be similar to the endmember, or must be the result of mixing between surface water and any one or combination of the observed depths. For both Co and Pb, the composition in the M6 drum sample (taken at the end of the sampling period) cannot be formed by mixing between the seawater concentration and that measured at any depth (Fig. V-8c and V-8d). However, both neatly match the concentrations in samples from the MPP with salinity of ~10 (Figs. V-8c and V-8d), the endmember calculated in earlier. This provides an independent estimate of the SGD endmember source, and is convincing support for the earlier discussion.

Influence of endmember choice on flux calculation

In order to accurately calculate the SGD-derived flux of dissolved constituents to the coastal ocean, it is necessary to identify the water actually crossing the sediment-water interface. This is unnecessary for constituents exhibiting conservative mixing (such as previously discussed for Sr and V), but is highly important for non-conservative constituents (Beck et al., 2007). For example, we have shown that Co is non-conservative in the subterranean estuary we sampled (Fig. V-8d). An instantaneous flux

(F_{Co}) can be calculated as the product of the SGD endmember Co concentration (C_{Co}) and the flow rate measured in the seepage meter sample at the time when the profile was sampled (F_{SGD} = 165 cm d^{-1} for meter M6 at 12:00):

$$F_{Co} = C_{Co} \times F_{SGD} \quad [6]$$

Assuming that SGD can be best represented by the water sampled immediately below the sediment-water interface gives an endmember Co concentration of 0.66 nM. Applying this endmember to equation [6] gives a SGD flux of 1.09 μmol Co m^{-2} d^{-1}. However, the Co concentration in the endmember discussed earlier is 1.8 nM. Calculation of the flux using this endmember concentration gives 3.02 μmol Co m^{-2} d^{-1}. This flux is nearly 3-fold higher than that calculated for the immediately subsurface endmember. Ultimately, the "true" flux is determined by the Co concentration measured in the water sample from the seepage meter (2.1 nM); this gives a flux of 3.47 μmol Co m^{-2} d^{-1}. Thus, use of the proposed endmember gives a better flux estimate (87% of the "true" flux) than the near-interface endmember (31%). We have proposed elsewhere (Beck et al., 2007) that geochemical transformations occurring in the subterranean estuary must be taken into account before trace metal fluxes to the coastal ocean can be accurately determined. The results of the current study reinforce that conclusion, and suggest that determining the appropriate endmember may provide better chemical flux estimates.

SUMMARY

The multi-port piezometer we have described here has proved to be easy to construct and deploy, can be sampled rapidly, and has sufficiently high resolution to be useful for sampling through the near-surface subterranean estuary. We have used the

MPP to collect multiple profiles for salinity and trace metal analysis, and its ease of use has allowed us to examine the evolution of the subterranean estuary over the duration of several hours. This was particularly important at our sample site because of significant and rapid tidal forcing of submarine groundwater discharge.

Seepage meters revealed high rates of SGD, and a salt mass balance for water inside the meters indicated that the endmember for the discharging water was brackish and variable over the tidal cycle. At a maximum discharge of greater than 200 cm d^{-1}, the endmember salinity was approximately 8. Using seepage meters in conjunction with the MPP revealed that the water entering the seepage meters had a chemical composition resembling that of porewater found at depths of 7-15 cm.

By combining trace metal and salinity analyses in both the MPP and seepage meters, it was possible to determine the composition of the true SGD endmember, and thus, estimate chemical fluxes from SGD more accurately. Future studies of the geochemical and ecological significance of SGD may benefit from application of the methods we have outlined here. In particular, seepage meters and the MPP can be used together to observe trends in salinity and identify the SGD endmember. Subsequently, fluxes can be calculated using chemical measurements made on that endmember collected with the MPP. This ensures clean, reliably uncontaminated chemical data, as is particularly important for trace metals. Furthermore, this procedure avoids artifacts associated with the emplacement of seepage meters, notably, isolation of surficial porewaters from oxygenated surface water. Ignoring contamination resulting from the meter itself, alteration of the redox conditions within the meter may cause substantial artifacts in the trace metal flux. This can even be extended to Ra (a groundwater

constituent commonly used to trace SGD), as emplacement of seepage meters may cause reduction of surficial Mn-oxide layers, thus increasing the Ra concentration in SGD collected by the meter. When estimating chemical fluxes due to SGD, it is vital to be able to characterize heterogeneous flow patterns while maintaining natural conditions as much as possible. The approach outlined in this study provides a method for doing so.

REFERENCES

Aller, R.C. 1984. The importance of relict burrow structures and burrow irrigation in controlling sedimentary solute distributions. Geochimica et Cosmochimica Acta, 48: 1929-1934.

Aller, R.C. 2001. Transport and reactions in the bioirrigated zone. In: The Benthic Boundary Layer: Transport processes and biogeochemistry. B. Boudreau and B.B. Jorgensen, eds. Oxford University Press, Oxford. p 269-301.

Beck, A.J., Y. Tsukamoto, A. Tovar-Sanchez, M. Huerta-Diaz, H.J. Bokuniewicz, and S.A. Sanudo-Wilhelmy. 2007. Importance of geochemical transformations in determining submarine groundwater discharge-derived trace metal and nutrient fluxes. Applied Geochemistry, 22: 477-490.

Berg, P. and K.J. McGlathery. 2001. A high resolution pore water sampler for sandy sediments. Limnol. Oceanogr., 46 (1): 203-210.

Bokuniewicz, H.J., Pollock, M., Blum, J., and Wilson, R., 2004. Submarine groundwater discharge and salt penetration across the sea floor. Ground Water, 42: 983-989.

Burnett, W.C. and H. Dulaiova, 2003. Estimating the dynamics of groundwater input into the coastal zone via continuous radon-222 measurements. Journal Environmental Radioactivity, 69: 21-35.

Burnett, W.C., P.K. Aggarwal, H. Bokuniewicz, J.E. Cable, M.A. Charette, E. Kontar, S. Krupa, K.M. Kulkarni, A. Loveless, W.S. Moore, J.A. Oberdorfer, J. Oliveira, N. Ozyurt, P. Povinec, A.M.G. Privitera, R. Rajar, R.T. Ramessur, J. Scholten, T. Stieglitz, M. Taniguchi, J.V. Turner. 2006. Quantifying Submarine Groundwater Discharge in the Coastal Zone via Multiple Methods. Science of the Total Environment 367(2-3): 498-543.

Busciolano, R., 2002. Water Table and the Potentiometric-Surface Altitudes of the Upper Glacial, Magothy and Lloyd Aquifers on Long Island, New York, in March-April 2000, with a Summary of Hydrogeologic Conditions. Water-Resources Investigations Report 01-4165, United States Geological Survey.

Cable, J.E., W.C. Burnett, J.P. Chanton, and G. Weatherly. 1996. Modeling groundwater flow into the ocean based on 222Rn. Earth Planet. Sci. Lett., 144: 591-604.

Capone, D.G. and M.F. Bautista. 1985. A groundwater source of nitrate in nearshore marine sediments. Nature, 313: 214 – 216.

Capone, D.G. and J.M. Slater. 1990. Interannual Patterns of Water Table Height and Groundwater Derived Nitrate in Nearshore Sediments. Biogeochemistry, 10 (3): 277-288.

Charette, M.A., M.C. Allen. 2006. Precision groundwater sampling in coastal aquifers using a direct push shielded screen well-point system. Groundwater Monitoring & Remediation, 26 (2): 87-93.

Charette, M.A., E.R. Sholkovitz. 2006. Trace element cycling in a subterranean estuary: Part 2. Geochemistry of the pore water. Geochimica et Cosmochimica Acta, 70 (4): 811-826.

Charette, M.A., Buesseler, K.O. 2004. Submarine groundwater discharge of nutrients and copper to an urban subestuary of Chesapeake Bay (Elizabeth River). Limnology and Oceanography, 49 (2): 376-385.

Charbeneau, R.J. 2000. *Groundwater Hydraulics and Pollutant Transport.* Prentice-Hall, Inc. New Jersey, USA. 593 pp.

D'Andrea, A., G.R. Lopez, and R.C. Aller. 2004. Rapid physical and biological particle mixing on an intertidal sandflat. Journal of Marine Research, 62: 67-92.

D'Elia, C.F., K.L. Webb, J.W. Porter. 1981. Nitrate-rich groundwater inputs to Discovery Bay, Jamaica – A significant source of N to local coral reefs. Bulletin of Marine Science, 31(4): 903-910.

Dulaiova, H., W.C. Burnett, J.P. Chanton, W.S. Moore, H.J. Bokuniewicz, M.A. Charette, E. Sholkovitz. 2006. Assessment of groundwater discharges into West Neck Bay, New York, via natural tracers. Continental Shelf Research, 26: 1971–1983.

Falter, J.L., and F.J. Sansone. 2000a. Shallow pore water sampling in reef sediments. Coral Reefs, 19: 93-97.

Falter, J.L., and F.J. Sansone. 2000b. Hydraulic control of pore water geochemistry within the oxic-suboxic zone of a permeable sediment. Limnology and Oceanography, 45(3): 550-557.

Gobler, C.J., Sañudo-Wilhelmy, S.A. 2001. Temporal variability of groundwater seepage and brown tide blooms in a Long Island embayment. Mar. Ecol. Prog. Ser., 217: 299-309.

Gobler, C.J., G.E. Boneillo. 2003. Impacts of anthropogenically influenced groundwater seepage on water chemistry and phytoplankton dynamics within a coastal marine system. Mar. Ecol. Prog. Ser., 255: 101-114.

Huettel, M., 1990. Influence of the lugworm Arenicola marina on pore water nutrient profiles of sand flat sediments. Marine Ecology Progress Series, 62: 241-248.

Johannes, R.E. 1980. The ecological significance of the submarine discharge of groundwater. Mar. Ecol. Prog. Ser., 3: 365-373.

Krupa S., T. Belanger, H. Heck, J. Brock, and B. Jones, 1998. Krupaseep: the next-generation seepage meter. Journal of Coastal Research, 25: 210–13.

Lee, DR. 1977. A device for measuring seepage flux in lakes and estuaries. Limnol. Oceanogr., 22 (1):140-147.

Libelo, E. L., and Macintyre, W. G. 1994. Effects of Surface-Water Movement on Seepage-Meter Measurements of Flow Through the Sediment Water Interface. Applied Hydrology, 4 (94): 49-54.

Marinelli, R.L. 1992. Effects of polychaetes on silicate dynamics and fluxes in sediments: Importance of species, animal activity, and polychaete effects on benthic diatoms. Journal of Marine Research, 50: 745-779.

Martin, W.R., and G.T. Banta. 1992. The measurement of sediment irrigation rates: a comparison of the Br- tracer and 222Rn/226Ra disequilibrium techniques. Journal of Marine Research, 50: 125-154.

Martin, J.B., K.M. Hartl, D.R. Corbett, P.W. Swarzenski, and J.E. Cable. 2003. A Multi-Level Pore-Water Sampler for Permeable Sediments. Journal of Sedimentary Research, 73 (1): 128-132.

Martin, J.B., Cable, J.E., Swarzenski, P., and Lindenberg, M., 2004. Enhanced submarine groundwater discharge from mixing of pore water and estuarine water. Ground Water: Special issue on Oceans and Estuaries, 42: 1000-1010.

Moore W.S. 1996. Large groundwater inputs to coastal waters revealed by Ra-226 enrichments. Nature, 380 (6575): 612-614.

Moore W.S. 1999. The subterranean estuary: a reaction zone of ground water and sea water. Marine Chemistry, 65 (1-2): 111-125.

Paulsen R.J., Smith C.F., O'Rourke D., and Wong T.F., 2001. Development and Evaluation of an Ultrasonic Ground Water Seepage Meter, Ground Water, 39 (6): 904-911.

Robinson C., B. Gibbes, and L. Li. 2006. Driving mechanisms for groundwater flow and salt transport in a subterranean estuary. Geophysical Research Letters, 33, L03402, doi:10.1029/2005GL025247

Rossi, FK. 2000. Size-fractionated trace metals, organic carbon, and inorganic nutrients in groundwater: Importance of colloidal forms. Unpublished MS Thesis. Stony Brook University.

Sañudo-Wilhelmy, S.A., F.K. Rossi, H. Bokuniewicz, R.J. Paulsen. (2002) Trace metal levels in uncontaminated groundwater of a coastal watershed: Importance of colloidal forms. Environmental Science and Technology, 36 (7): 1435-1441.

Seeberg-Elverfeldt, J., M. Schlüter, T. Feseker, and M. Kölling. 2005. Rhizon sampling of porewaters near the sediment-water interface of aquatic systems. Limnol. Oceanogr.: Methods, 3: 361–371.

Shaw, T. J., Moore, W. S., Kloepfer, J. and Sochaski, M. 1998. The flux of barium to the coastal waters of the southeastern United States: The importance of submarine Groundwater Discharge. Geochim. Chosmochim. Acta, 62: 1277–1283.

Shaw, R. D., Shaw, J. F. H., Fricker, H., and Prepas, E. E., 1990. An Integrated Approach to Quantify Groundwater Transport of Phosphorous to Narrow Lake, Alberta. Limnology and Oceanography, 35 (4): 870-886.

Talbot, J.M., K.D. Kroeger, A. Rago, M.C. Allen, M.A. Charette. 2003. Nitrogen flux and speciation through the subterranean estuary of Waquoit Bay, Massachusetts. Biological Bulletin, 205: 244-245.

Taniguchi M. and Fukuo Y. 1993. Continuous Measurements of groundwater seepage using an automatic seepage meter. Ground Water, 31: 675-679.

Testa, J.M., M.A. Charette, E.R. Sholkovitz, M.C. Allen, A. Rago, C.W. Herbold. 2002. Dissolved iron cycling in the subterranean estuary of a coastal bay: Waquoit Bay, Massachusetts. Biological Bulletin, 203: 255-256.

TABLES and FIGURES

Depth (cm)	Slope	r^2
0.5	0.19	0.16
3.5	0.36	0.19
7.5	0.18	0.08
11.5	1.04	0.93
15.5	0.11	0.05
19.5	0.11	0.01
23.5	0.85	0.53
27.5	0.36	0.01

Table V-1. Slopes and correlation coefficients of regression lines through calculated endmember salinities at different times (S_{in}) and the salinity at a given piezometer depth for each corresponding time.

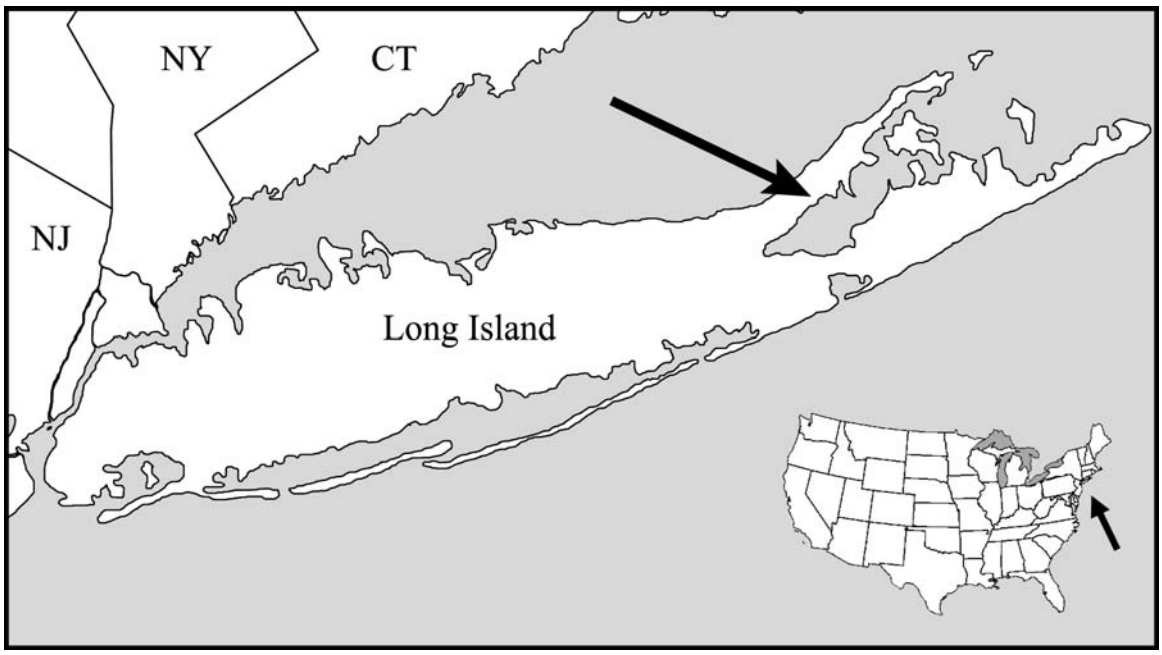

Figure V-1. Sampling Site – Mattituck, NY.

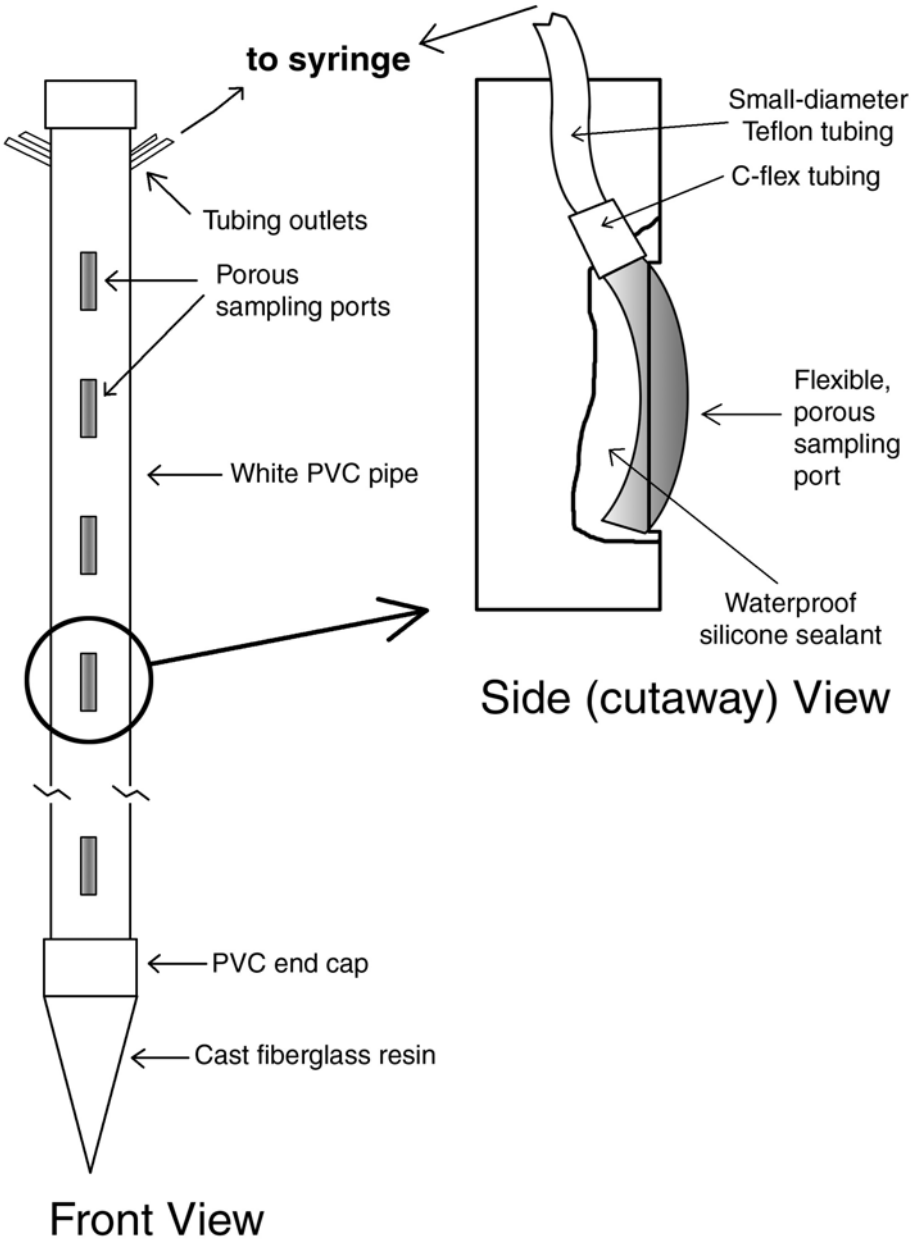

Figure V-2. Diagram of the multi-port porewater sampler (MPP).

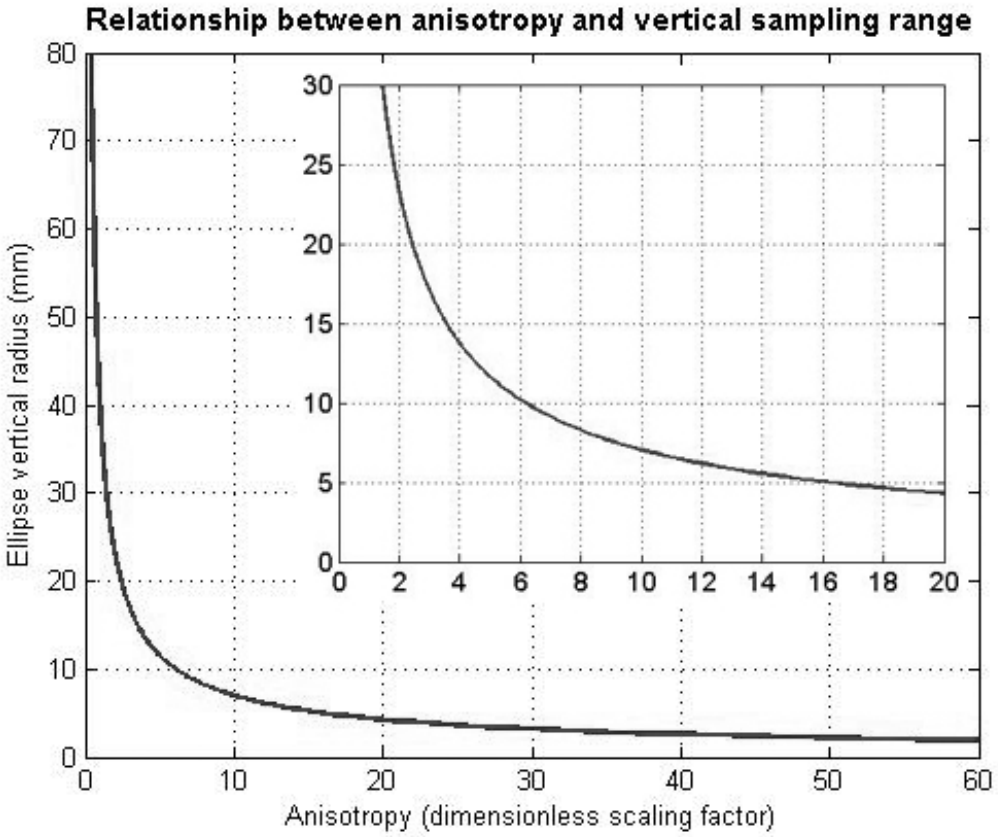

Figure V-3. Relationship between anisotropy (*S*) and vertical radius of sample ellipsoid (*a*), as described in equation 3 (for a sample volume of 120 mL). Inset shows expanded view near origin. Note that the units for the vertical scale are millimeters.

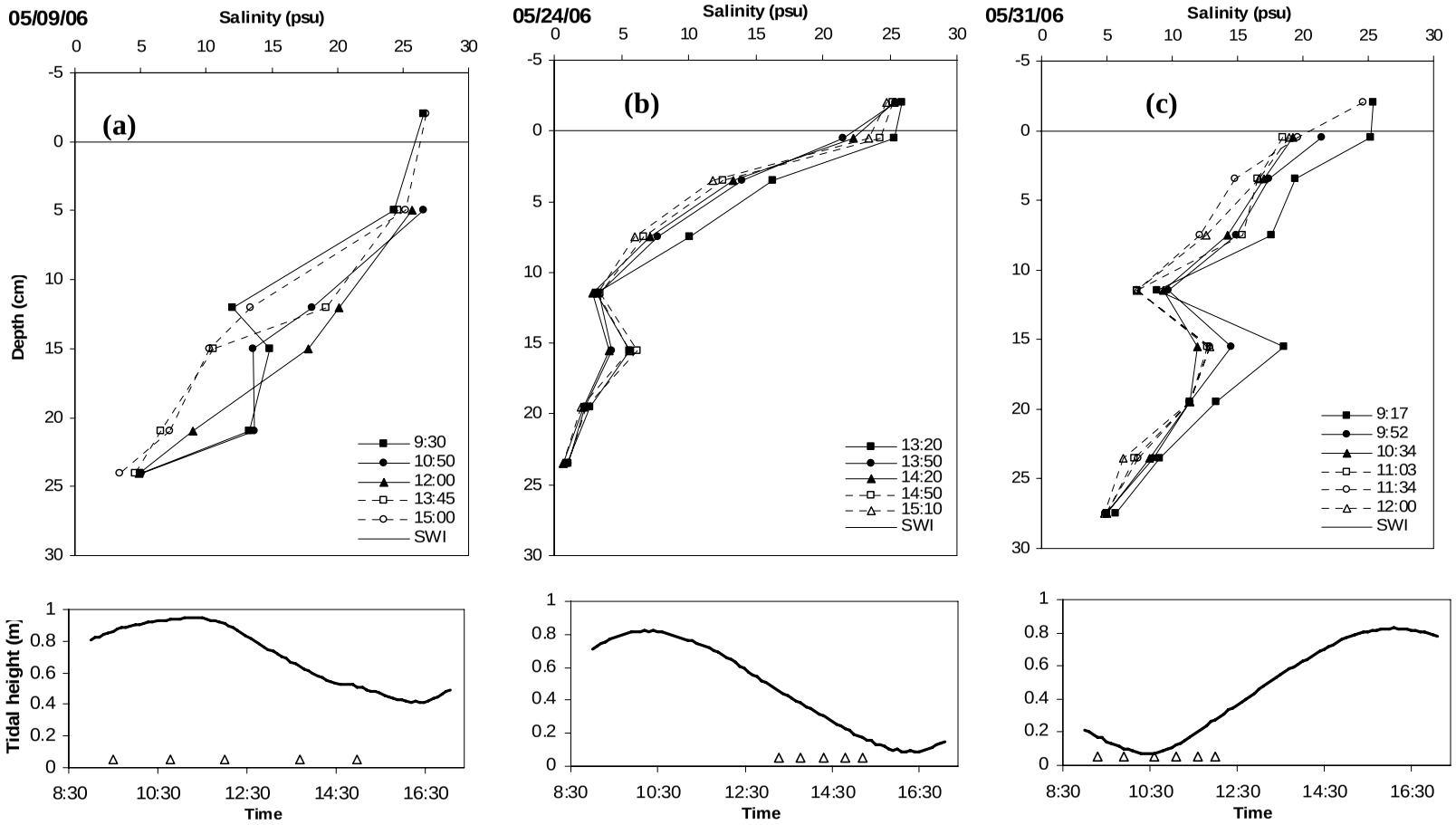

Figure V-4. Upper graphs show vertical salinity profiles taken at different times on the three sampling dates. Lower graphs show tidal curves over the sampling period; hollow triangular symbols indicate time points when profiles were sampled (see legends on upper graphs for exact times). (a) Profile taken 09 May 2006; (b) Profile taken 24 May 2006; (c) Profile taken 31 May 2006. Tide data from http://tidesandcurrents.noaa.gov (Station 8512735).

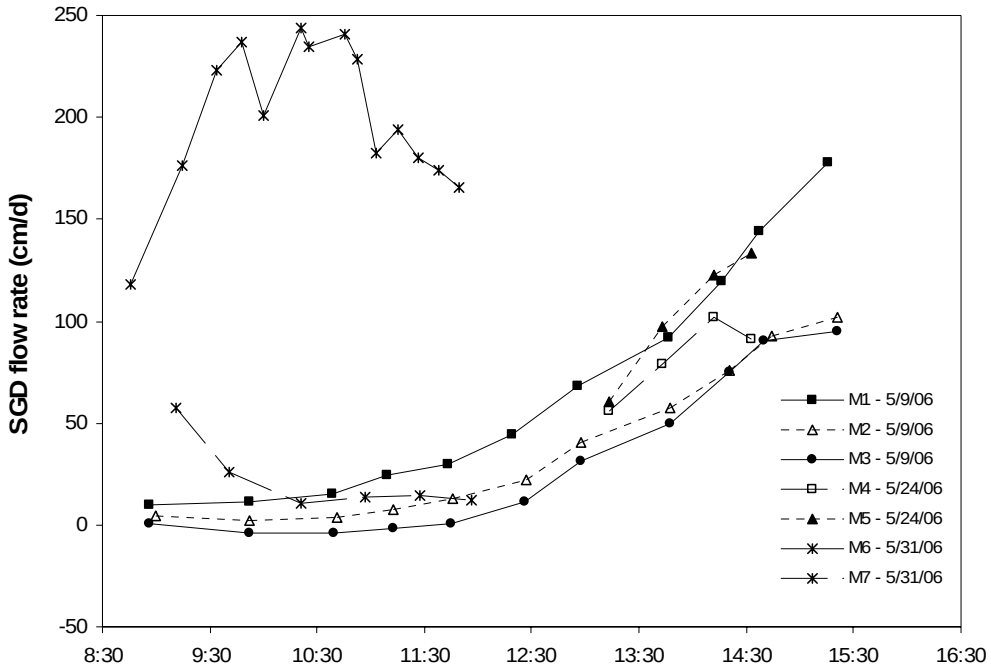

Figure V-5. SGD flow rate (cm d^{-1}, or m^3 m^{-2} d^{-1}) time series as measured by Lee-type seepage meters. The distinct change in flow with time is the result of tidal forcing, with highest flow rates occurring at low tide. Note that substantial differences in flow are evident between different meters, even though spatial separation was never more than a few meters. "M6" does not necessarily show different behavior than the other trends, low tide is simply offset during that sampling period relative to the other dates.

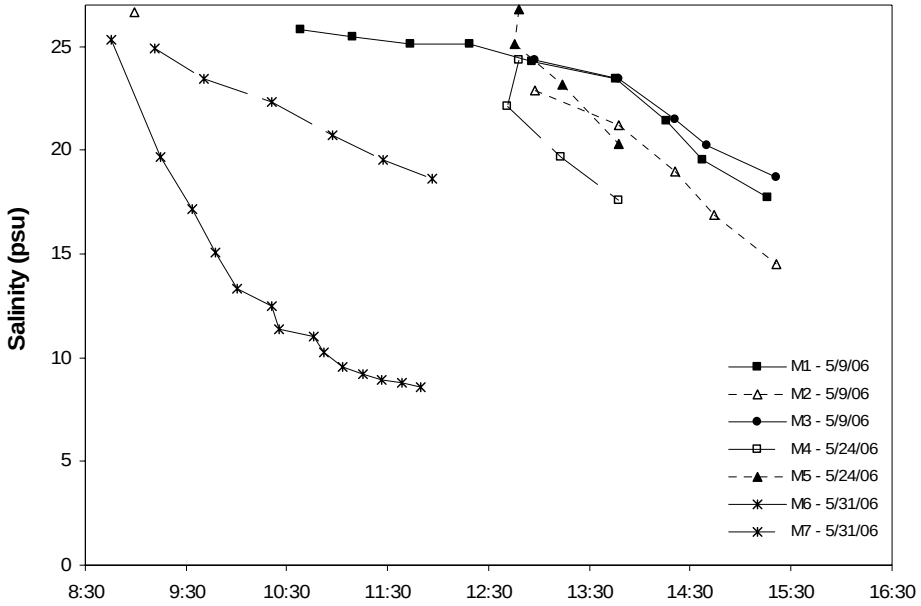

Figure V-6. Salinity of the water discharging from the seepage meters (i.e. the water in the bags). The salinity in the drum at the time of installation is the same as the ambient water. The rate of decrease, or slope delineated by adjacent points, is determined by the endmember salinity (the water entering the seepage meter) and the flow rate.

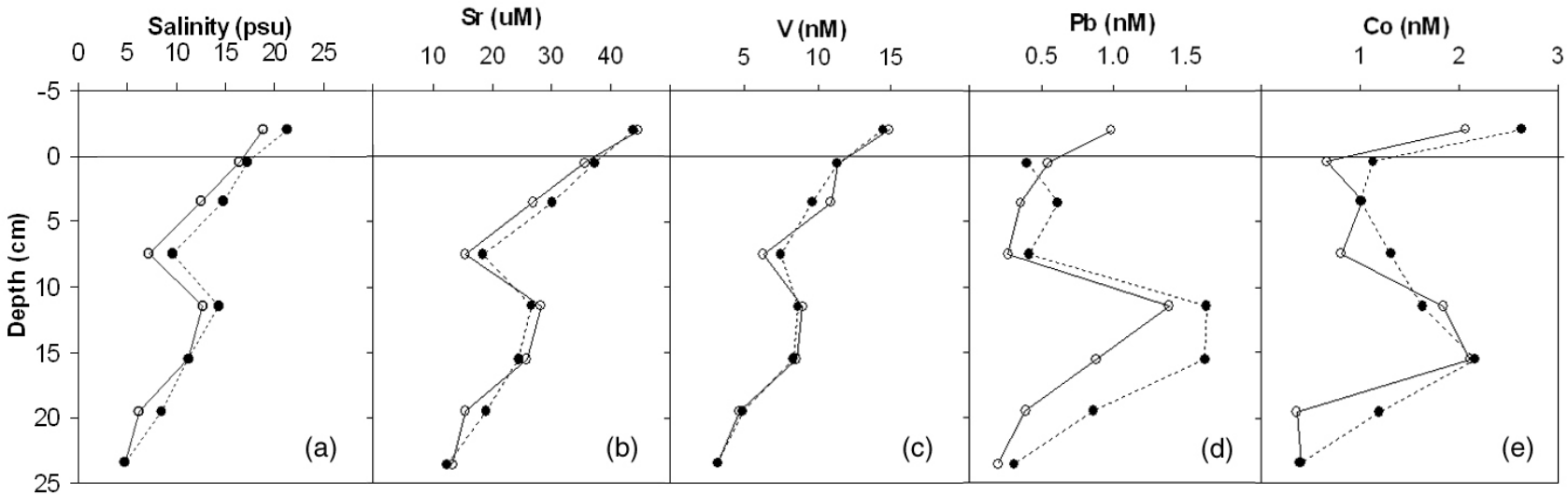

Figure V-7. Salinity and trace element profiles: (a) Salinity, (b) Sr, (c) V, (d) Pb, and (e) Co. The solid symbols represent a profile obtained at approximately 9:50, and the open symbols are a profile sampled at 12:00 on 05/31/06. This convention will be followed in all trace element plots. The horizontal solid line is the sediment-water interface. The sample above the sediment-water interface in the 9:50 profile (closed symbols) appeared to be contaminated for Pb (4.03 nM), and was removed to improve the clarity of the graph.

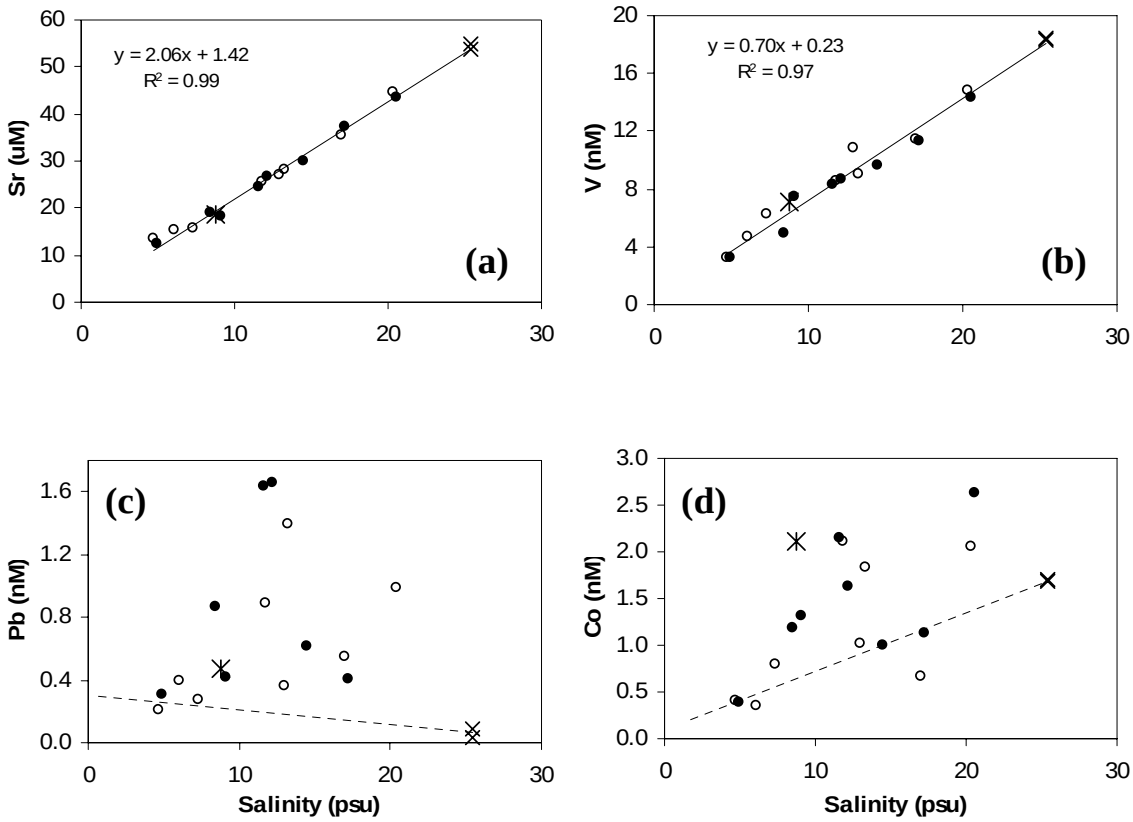

Figure V-8. Trace element distribution relative to salinity: (a) Sr, (b) V, (c) Pb, and (d) Co. The solid symbols represent a profile obtained at approximately 9:50, and the open symbols are a profile sampled at 12:00. Cross-shaped symbols represent surface water samples (not from the MPP), and asterisk-shaped symbols represent a sample obtained from seepage meter "M6" coincident with collection of the 12:00 piezometer profile. Solid lines in (a) and (b) represent linear regressions of all data points. Dashed lines in (c) and (d) represent conservative mixing between the observed high- and low-salinity endmembers.

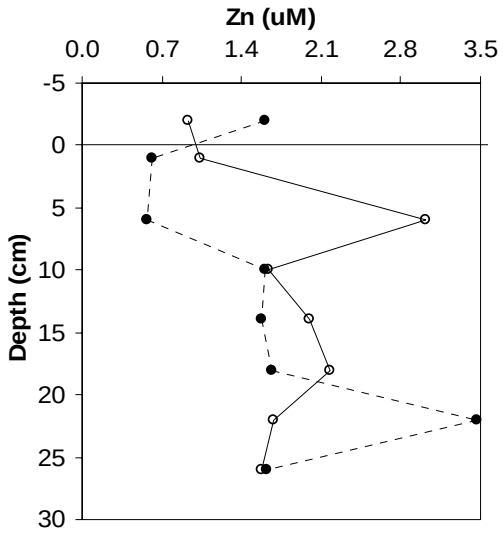

Figure V-9. Dissolved Zn profile. Symbols as in Fig. V-7.

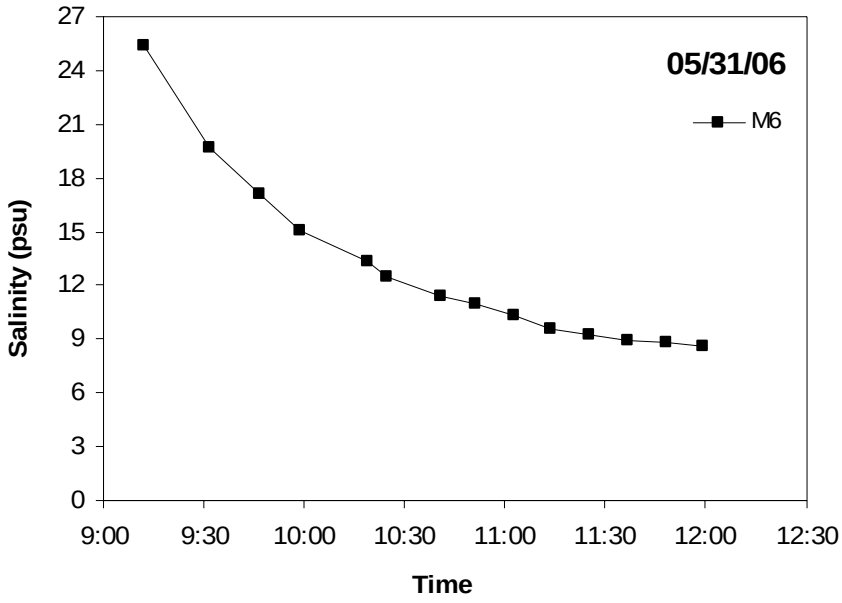

Figure V-10. Salinity of the water discharging from seepage meter "M6".

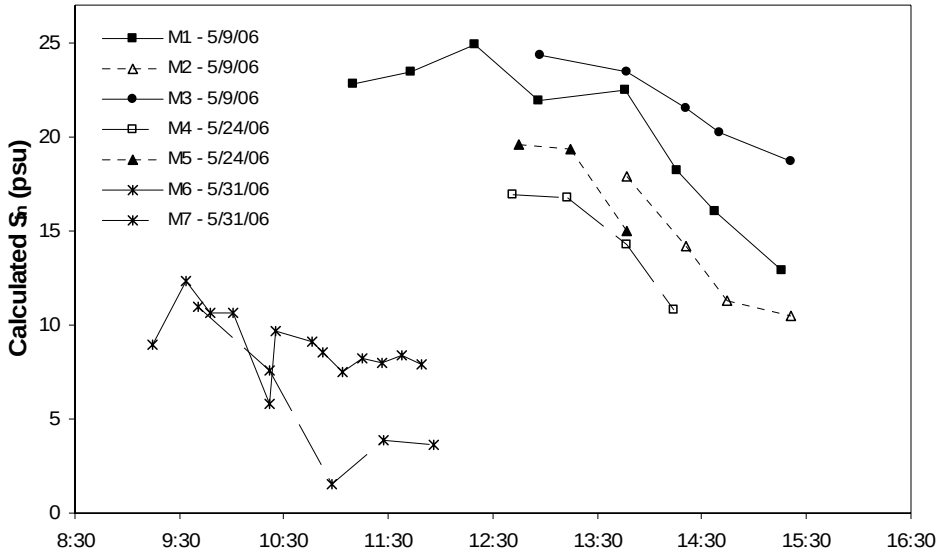

Figure V-11. Time evolution of the SGD endmember salinity as calculated by equation [5].

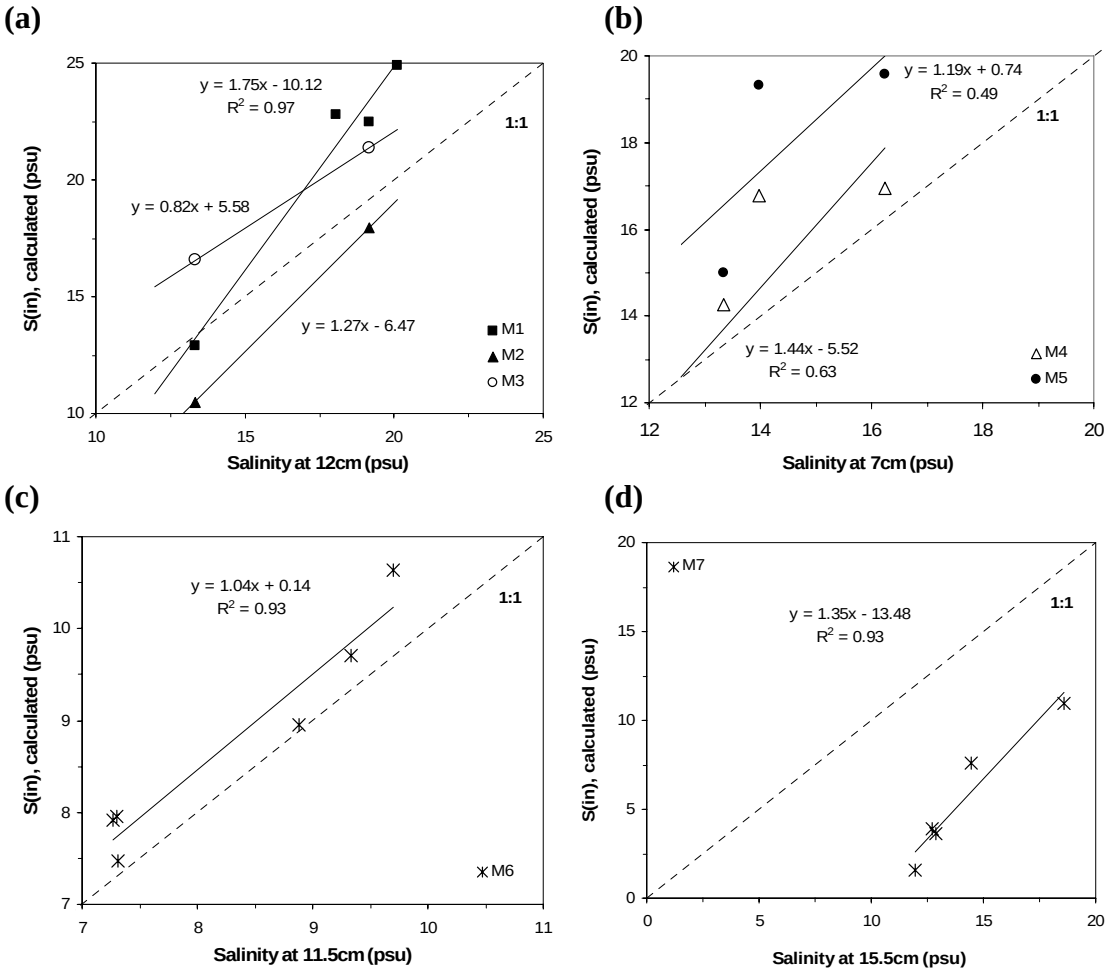

Figure V-12. Calculated S_{in} versus salinity measured at depth with the multi-port piezometer. The dashed line is the 1:1 relationship. (a) 09 May. S_{in} calculated for all three drums correlates best with the salinity measured at 12 cm depth. (b) 24 May. S_{in} calculated for both drums correlates best with the salinity measured at 7 cm depth. (c) 31 May. S_{in} calculated for the high flow drum "M6" correlates very well with the salinity at 11.5 cm depth. (d) 31 May. S_{in} calculated for drum "M7" correlates best with the salinity at 15.5 cm depth, but is far from the 1:1 relationship, suggesting that in this case the SGD endmember is close to 15.5 cm depth, but may be mixing with less seawater than the flowpath at 15.5 cm.

CHAPTER VI:

The distribution and speciation of trace metals in a shallow subterranean estuary

INTRODUCTION

The low organic content (< 0.1 wt. %) of permeable sediments led to the early presumption that such sedimentary environments were relatively unreactive, and thus of limited importance for geochemical cycling in the coastal ocean. A number of more recent studies have shown that the low organic content is due to rapid remineralization and flushing (e.g. Shum and Sundby, 1996; Huettel et al., 2003). Consequently, the role of permeable sediments in coastal biogeochemical cycling is being reevaluated, and all indications suggest that these sedimentary environments are vastly important to nearshore chemical budgets (Shaw et al., 1998; Portnoy et al., 1998; Basu et al., 2001; Windom et al., 2006; Charette and Sholkovitz, 2006; Kim et al., 2005).

At the same time, the processes of porewater advection through such permeable sediments are also beginning to be recognized (Moore, 1996). Not only does this submarine groundwater discharge (SGD; Burnett et al., 2003) represent a common and massive flux of water (although, not necessarily fresh) to the coastal ocean, but there is also a very large flux of associated chemical constituents (Moore, 1996, 1997; Basu et al., 2001; Shaw et al, 1998; Charette and Buesseler, 2004; Charette et al., 2001; Jahnke et al., 2003). Although there is substantial literature on nutrient flux due to SGD (Portnoy et al., 1998; Jahnke et al., 2003; Kim et al., 2005; Zimmermann et al., 1985; Lewis, 1987; Rutkowski et al., 1999; Ullman et al., 2003; Charette et al., 2001), less is known about the impact of SGD on trace metal fluxes. Trace elements studied thus far include Fe and Mn (Windom et al., 2006; Windom and Niencheski, 2003; Spitieri et al., 2006; Snyder et al., 2004; Charette and Sholkovitz, 2002, 2006; Testa et al., 2002), U (Charette and Sholkovitz, 2006; Duncan and Shaw, 2003), Mo (Windom and Niencheski, 2003), Sr

(Charette and Sholkovitz, 2006), As (Bone et al., 2006), Hg (Bone et al., in press), and rare earth elements (REE, Duncan and Shaw, 2003).

However, the fluxes of metals across the sediment water interface depend largely on their geochemistry, especially during early diagenetic cycling (Shaw et al., 1990). Consequently, the subsurface mixing zone of fresh groundwater and saline porewater, termed the "subterranean estuary" (Moore, 1999), is a highly dynamic zone which determines the composition of the advecting porewater (Charette and Sholkovitz, 2006; Bone et al., 2006; Bone et al., submitted). As noted above, studies of metal cycling in this zone have been limited to Mn, Fe, Hg, and Mo.

Thus, the objective of the current study is to examine the distribution and cycling of selected trace metals in a subterranean estuary. A shallow (< 1 m) subsurface zone has been chosen as the region of interest, in the assumption that being near the sediment-water interface, this is the region where biogeochemical processes are most likely to influence the composition of the discharging porewater. For comparison with the profile through the subterranean mixing zone, we include a profile collected in a nearby fully saline subsurface zone. There are likely different mechanisms regulating porewater flow between the two sites, and the comparison will be useful in examining geochemical processes unique to the different environments.

Study Site

The site chosen for this study is located in Great South Bay, NY, at the end of Roe Avenue in the town of Patchogue (Fig. VI-1). Great South Bay is a large, shallow lagoon on the south shore of Long Island, NY. Bottom sediments are permeable sandy

glacial outwash. These sediments are approximately 30 m in depth, and comprise the Upper Glacial Aquifer. As this is the source of the groundwater examined in this study, discussion of deeper aquifers is omitted here. The tidal range in the bay is small, less than 0.25 m. The salinity of the bay water is generally between 25 and 29, and is regulated primarily by two major rivers, the Connetquot and Carmans Rivers. These surface freshwater sources are approximately equidistant from the Roe Ave. study site, 10-15 km on either side.

The Roe Avenue site was chosen because good documentation exists for SGD rates at this location for the past ~25 years (Bokuniewicz, 1980; Bokuniewicz and Zeitlin, 1980; Bokuniewicz and Pavlik, 1990; Seplow, 1991; Bokuniewicz et al., 2004), and a shallow depth to fresh groundwater has been also been reported (Seplow, 1991; Bokuniewicz et al., 2004). SGD flow rates at this site range between about 1 and 11 cm d^{-1}, with averages of about 2 to 4 cm d^{-1} (Bokuniewicz and Zeitlin, 1980; Bokuniewicz et al., 2004). Vertical hydraulic conductivities range between ~2 and 25 m d^{-1}, declining bayward from shore, as do SGD flow rates (Bokuniewicz et al., 2004).

The surficial subterranean estuary has been identified and reported often at this location (Seplow, 1991; Bokuniewicz et al., 2004; A. Beck, upublished observation, Aug. 2005), although not by that name. The mixing zone is unstable, essentially an inverse estuary, with fresh water underlying more saline water (S = 28). The shallow mixing zone is presumably maintained by upward advection of fresh, terrestrial groundwater and downward dispersion of salt water. The mechanism for the latter process is unknown, although salt fingering and wave stirring are the most likely possibilities (Bokuniewicz, 1992; Bokuniewicz et al., 2004).

The first sampling device (Piezometer Fresh, or "Piez F") described in the current study was installed approximately 30 m from shore, in order to sample through the mixing zone (Figs. VI-1 and VI-2). The second device (Piezometer Saline, or "Piez S") was placed farther offshore, about 100 m, where much lower flow rates have been measured (Bokuniewicz et al., 2004). Here, rates of advection appear to be low enough to allow dispersion or diffusion of salt to depths greater than 76 cm (the deepest sample in the profile). Thus, two profiles are contrasted here: Piez F, which samples the salinity gradient from 0 to 29 (chloride: 0-390 mM; and Piez S, which samples only saline water at salinities between 25 and 29 (chloride: 310-390 mM; Fig. VI-2).

METHODS

The multi-port piezometers (MPP) used in this study have been described and tested in detail elsewhere (Beck et al., submitted; Chapter V). Briefly, the MPP was designed for collection of high-resolution, uncontaminated trace metal porewater profiles in permeable sediments. The body of the MPP was constructed of white PVC pipe. A pointed tip was cast from fiberglass resin, and attached to the bottom of the pipe by a PVC fitting molded into the resin at the time of casting. Rectangular ports are machined into the side of the MPP to accommodate porous plastic cylinders, which protrude in semi-circles from the face of the PVC pipe. Ports were spaced closer together (~ 2 cm between ports) in the top 30 cm of the MPP, and about triple farther apart below that depth. The length of each port was 2 cm, giving minimum sampling depth midpoints of ~ 4 cm intervals. Detailed discussion of sample overlap is provided by Beck et al. (submitted; Chapter V), but at the porewater volumes extracted for this study, it was

probably minor. The porous ports were connected to dedicated Teflon tubes with flexible C-flex tubing. The dead volume of the port with the longest tubing was less than 15 mL.

After machining, all components of the MPP were acid-washed separately for one week in 3N HNO_3, rinsed thoroughly with MilliQ water (MQ; 18.2 mega-ohm cm), and soaked for one week in 1N HCl. Following assembly and gluing, the MPP was soaked for one week in dilute HCl. The MPP was then rinsed 5 times with MQ, including the ports and tubing, and the entire apparatus was wrapped in 3-5 layers of heavy plastic sheeting for transport to the field site. Upon arrival at the site, a thin steel pole covered with white epoxy paint was inserted through the top of the MPP, behind the sample tubing, to contact the base of the resin tip. The plastic sheeting was then removed, and the MPP was driven to the desired depth in the sediment by hammering on the top of the steel pole with a slide hammer. The pole was the withdrawn, leaving approximately 20 cm of the MPP body standing free above the water surface with the sampling tubes. After ~1 hour, each tube was purged of ~30 mL of porewater using an acid-washed polypropylene syringe. Both MPPs were then allowed to equilibrate for ~36 hours, with the free sample tube ends sealed within double polyethylene bags.

After the equilibration period, the sample tubes were each attached to dedicated, acid-washed, all-polypropylene 60 mL syringes with short sections of acid-cleaned C-flex tubing. Each depth was purged of about 10-30 mL of porewater, and then samples were collected. Approximately 45-60 mL was pulled into the syringes; nearly simultaneous sampling was achieved by cocking the syringes in “fill” position with sections of rigid Teflon tubing (Huettel, 1990; Beck et al., submitted [Chapter V]).

Sample fill rates were ~ 50 mL min^{-1}, well below the 100 mL min^{-1} required for obtaining good trace metal samples (Creasy and Flegal, 1999; Sañudo-Wilhelmy et al., 2002).

Each syringe was left attached to the sample tubing after being filled to prevent exposure to oxygen. Each syringe, in turn, was detached, and connected to an acid-washed 25 mm, 0.2 micron pore size syringe filter. Approximately 5 mL of sample was purged through the filter to prevent oxidation artifacts (Bray et al., 1973; Lyons et al., 1979), and then 10-15 mL was collected in an acid-washed 30 mL LDPE bottle. The remaining sample was reserved for the chemical separations described below.

Samples for total metals determination were returned to the clean lab, acidified with 100 μL $QHNO_3$, and allowed to sit for 2 months to ensure that all metals were in solution. All metals samples, including the speciation fractions described below, were analyzed by ICPMS (ThermoFinnigan Element2) following 20-fold dilution. An In spike was used as an internal standard to correct for instrument variability during analysis. Samples were analyzed using standard addition techniques, a particularly important consideration given the variability in salinities of the samples. Analysis of two standard reference materials (NIST 1643d and SLRS-4) provided an accuracy check. Recoveries of all elements were within 10% of the reference value. Precision of metals analyses were dependent on the analyte concentration, but were generally better than 5%.

Metal Speciation

Metal speciation was operationally defined using the solid-phase extraction technique described by Beck and Sañudo-Wilhelmy (submitted). Separations were carried out in the field immediately following collection. Briefly, an initial aliquot of 10-

15 mL of sample was syringe-filtered (through acid-cleaned, 25 mm, 0.2 μm pore size polypropylene filters) directly through a column of Chelex-100 resin (ammonium form). This resin is used to extract the kinetically-labile fraction. Flow rate through the 1 mL resin bed was maintained at a constant flow rate of ~10 mL min^{-1}. The column was immediately rinsed with ultraclean ammonium acetate buffer (at pH ~8), sealed, and double-bagged in polyethylene bags.

A second 10-15 mL aliquot of sample was then passed through a second column of C-18 resin. This resin is a hydrophobic C-18 moiety bound to a silica support, and extracts the hydrophobic organic-metal complexes. This fraction has been referred to as "the most geochemically significant fraction" (Hanson and Quinn, 1983). The column was then rinsed with MilliQ water, capped, and double-bagged.

Columns were returned to the clean lab, where Chelex and C-18 columns were eluted with several aliquots of 2N $QHNO_3$ and Optima-grade methanol, respectively. An eluate volume of at least 3 column volumes was used. To the methanol fraction, 100 μL of concentrated $QHNO_3$ was added to oxidize the organic matter. Both eluate fractions were then taken to dryness at room temperature under a HEPA filtered flow hood. An additional 100 μL of $QHNO_3$ was added to the methanol fraction to ensure complete destruction of the organics, and redried. Both eluate residues were then redissolved in 2 mL of 1N $QHNO_3$, and allowed to sit for at least 1 month to ensure that all metals were in solution.

Salinity, pH, ORP, and dissolved O_2 were determined in the field on the remaining porewater sample using a YSI 556 multi-probe. Where insufficient volume remained, additional sample was withdrawn with the syringe for probe measurement. As

a check against the conductivity/salinity probe, chloride was analyzed as an entirely conservative tracer. Cl^- was determined using a Copenhagen Radiometer chloride titrator. Reproducibility for the Cl^- analyses was generally better than 2%.

RESULTS and DISCUSSION

Ancillary parameters

The discussion of trace element distribution in interstitial waters of permeable sediments is best begun with a description of the general geochemical characteristics of that environment. Figure VI-2 shows the distribution of four ancillary parameters which generally characterize the two profiles presented here. Chloride, analogous to salinity, presented here as an entirely unreactive, conservative tracer, shows the most striking contrast between profiles. Piez F samples saline water in the overlying water column, with chloride concentration of ~380 mM, corresponding to a salinity of about 28-29 (Pilson, 1998). The chloride concentration then decreases with depth to completely fresh water at about 30 cm. This 30 cm layer in the upper sediment column represents the subterranean estuary. Below 30 cm depth only fresh water is observed. In contrast, Piez S sampled only porewater with a chloride composition of ~310-390 mM, corresponding to salinities of 23-29. As discussed in the previous section, the presence or absence of a mixing zone provides a convenient contrast to examine processes unique to the subterranean estuary.

Both profiles show similar behavior of pH with depth (Fig. VI-2). The pH in the overlying water is 7.6-8, and stays above 7.5 in both profiles to a depth of about 15 cm. Piez S shows an increase during this interval to a maximum of 8.58. Below 15 cm, the

pH in both profiles drops sharply by nearly 1 pH unit. This decrease occurs over less than 15 cm. Below 24 cm, the pH in both profiles is approximately stable. In Piez F, the pH does increase slightly from 6.78 at 24 cm to 7.36 at 75 cm. The trends observed for pH do not seem to be driven by salinity differences (i.e. cannot be explained only by the mixing of fresh and saline porewaters).

The dissolved oxygen (DO) profile should be relied upon with caution, as the samples were exposed to the air during transfer into the probe measuring vessel. The oxygen content of the overlying water of Piez F appeared to be higher by nearly a factor of 2, as compared to overlying water of Piez S. The high dissolved oxygen (170-200 μM) immediately subsurface may be due to the activity of photosynthetic benthic algae. Oxygen in the profiles decreases to ~50 μM below 5 cm depth. Oxygen remains at this level to the bottom of Piez S, while it peaks to nearly 250 μM at 38 and 76 cm in Piez F. This feature may be real, as horizontal advection of O_2-rich porewaters has been previously reported (Testa et al., 2002). Non-local transport of surficial water to depth may also account for the peak (Aller, 2001). However, the O_2 peaks are not reflected in the vertical distribution of other parameters, suggesting that these increases may simply be artifacts of the of the O_2 measurements.

ORP, or Oxidation-Reduction Potential, as measured with an $Ag/AgCl_2$ electrode is a measure of the capacity of a solution to transfer electrons. (ORP can be reported against the normal hydrogen electrode, as Eh, by adding 240 mV to the values reported here. Ultimately, these ORP data are largely used as a qualitative indicator of reducing conditions to further strengthen the trace metal trends, and exact numeric values are not particularly important except for the Eh-pH diagrams described below.) ORP in these

profiles generally follows a trend similar to oxygen; Piez S had low O_2 in overlying water (100 μM), and has low ORP (-12.6 mV). Conversely, the higher oxygen levels in water overlying Piez F (190 μM) coincide with higher ORP (+65 mV). Both profiles show decreasing ORP with depth to 15 cm, the same depth at which pH dropped precipitously. Thus, the pH minima appear to coincide with ORP minima.

In summary, the two profiles are contrasted thus: Piez F samples through a salinity mixing zone from 29 to nil, while Piez S is fully saline (23-29). Both piezometers sample profiles with highest pH at the surface, a decrease to 15 cm, and relatively constant pH thereafter. Dissolved oxygen is high at the surface, and tends to follow the same trends as pH. The same behavior is observed for ORP, with more oxidizing conditions at the surface, and reducing conditions at depths below 15 cm. Piez F has a lower pH, but more DO and is less reducing.

These porewater samples lacked any smell of hydrogen sulfide, and other porewater samples we have collected in GSB (Beck et al., submitted; Chapter III) have also lacked significant indication of H_2S. Hines and Buck (1982) showed that the distribution of sulfate-reducing bacteria in the subterranean estuary fluctuates with sulfate concentrations. Consequently, we would not expect sulfate reduction to occur in the freshening zone of Piez F. Given the lack of sulfide smell in either profile, and the similarity in Fe profiles (described below), sulfate reduction is probably not significant. This is supported by the results of Slater and Capone (1987), who only observed sulfide production in specific layers of surficial sediment of Great South Bay. However, sulfur cycling cannot be definitively excluded as an important process governing trace metal cycling in these profiles.

Total dissolved trace metals

Figure VI-3 shows vertical profiles of the eight trace metals discussed in detail here. Profiles of the metals species are also shown in Fig. VI-3, but will be discussed in a second section.

Fe and Mn

Fe and Mn have well-characterized redox behavior which provides a useful segue from the ancillary parameters described aboved. In Piez F, there is a well-defined, sharp peak in Mn centered at 17 cm depth (Fig. VI-3a). Dissolved Mn reaches a maximum of 755 μM, although the peak only spans about 25 cm, and the depth resolution may not have been sufficient to capture the apex. Mn concentrations in the overlying water column were only ~1-2 μM, and concentrations below the peak were generally < 20 μM.

Fe in Piez F follows Mn in the expected diagenetic sequence (Fig. VI-3a). Mn begins to be released to solution at ~5 cm depth, reaches a maximum at 17 cm, and declines to nearly zero by 45 cm. Fe enters solution at 17 cm depth, reaches a maximum at 45 cm, and continues to decline at the base of the profile (76 cm). Dissolved Fe concentrations in the overlying water were less than 0.1 μM, much lower than those observed for Mn. The maximum observed Fe level (90 μM) was more than 2 orders of magnitude lower than the highest observed Mn concentrations. If absolute concentrations of the dissolved constituents indicate geochemical significance, then Mn may be a more significant determinant in metal cycling in this system than is Fe.

In Piez S, the trends of Mn and Fe were less clear (Fig. VI-3a). Mn entered solution immediately below the interface, reaching 400 μM by only 5 cm depth. A shallow peak is seen between the interface and approximately 24 cm, with maximum concentrations of 804 μM at 17 cm. From a minimum of 145 μM at 24 cm, dissolved Mn concentrations increased somewhat erratically to the highest observed levels (1125 μM) at the bottom of the 76 cm profile. Dissolved Fe trends in Piez S were also not as clear as in Piez F. Fe is first observed in solution at 13 cm depth, increasing slowly to about 1.4 μM at 38 cm. Concentrations below 38 cm are high and erratic, matching the variability observed for Mn, although Mn and Fe below 38 cm appear to vary inversely. As in Piez F, Mn concentrations were higher than dissolved Fe in Piez S, in this case, by more than two orders of magnitude.

The presence and removal of Fe in these profiles does not appear to be a function of oxygen penetration or redox conditions (as indicated by ORP). Instead, pH-dependent precipitation of Fe-oxides (probably amorphous oxyhydroxides), as described by Spitieri et al. (2006), appears to be the mechanism regulating the vertical distribution of Fe in these profiles. As shown in Fig. VI-4, there is an apparent pH threshold of approximately 7.5; Fe is more soluble in more acidic porewater, and is removed from solution at more basic pH.

Comparing the two profiles, the shallowest peak in Mn is observed at the same depth: ~15 cm. This suggests that the sharp peak observed in the salinity transition zone (STZ) is probably not a result of processes unique to the mixing zone. Instead, it is likely that both profiles reflect organic matter delivery (both dissolved and particulate) by seawater recirculation and infiltration. Oxidation of this organic matter results in the

removal of oxygen in the upper 5-10 cm of the sediments, and oxidation at deeper depths then proceeds with oxidants of decreasing energy yield during electron transfer. The Mn peak at 15 cm depth in both cores reflects the depth of organic matter delivery as well as the shallow depth of oxygen penetration.

The decline in dissolved Mn below the 15 cm peak in Piez F is not as easily explained. There are a number of possibilities, including: dilution from mixing with fresh groundwater, authigenic mineral formation (e.g. Mn-carbonate; Berner, 1980; Elderfield et al., 1981), adsorption onto Fe-hydroxides, or oxidation by NO_3 (Hulth et al., 1999). Because Fe enters solution as Mn declines, sorption of Mn^{2+} by Fe-oxides is not likely the cause for the decline. Lacking alkalinity data, precipitation of authigenic minerals cannot be conclusively evaluated. However, the lack of removal observed at the same depths in Piez S suggests that the removal is due to a process unique to the mixing zone sampled in Piez F. Simple dilution due to mixing may be the simplest (i.e. Ockham's) explanation for the decrease, as the data at salinities below that where the peak occurs (S = 12) are quite linear (Fig. VI-5).

However, the possibility of oxidation by nitrate is very interesting, and deserves mention as it has implications for the oft-cited SGD-derived nutrient flux. The scenario of denitrification by Mn^{2+} oxidation has been noted by Hulth et al. (1999), with the proposed reaction:

$5Mn^{2+} + 2NO_3^- + 4H_2O \Rightarrow 5MnO_2 + N_2 + 8H^+$

In the current sediments, Mn^{2+} is produced during the oxidation of organic matter (i.e. that delivered by seawater recirculation) by MnO_2 in surface sediments. NO_3^- is delivered by the advection of nitrate-contaminated groundwater. Fresh groundwater in

GSB has elevated levels of nitrate (100-270 μM; Slater and Capone, 1987); coupled with the observed high levels of dissolved Mn, this reaction will tend to proceed strongly towards the products. Thus, Mn cycling in the STZ in permeable sediments may result in substantial removal of NO_3 by denitrification.

In any case, it is clear that Mn and Fe are cycled very actively in these sediments. Dissolved Mn concentrations reach very high levels (exceeding 1 mM), while Fe is significantly lower (<0.1 mM). The strong geochemical cycling of both these elements will likely have a strong influence on other trace metals (Shaw et al., 1990), as shown below.

It is worth briefly discussing here the interaction between Fe and P in these profiles. The SGD-derived P flux can be the major input of P to coastal waters (Zimmerman et al., 1985), and differential input of N- or P-enriched groundwater can affect how coastal waters are nutrient limited (Slomp and Van Capellen, 2004). Phosphate in marine sediments is often cycled with Fe due to sorption by solid-phase oxides (Charette and Sholkovitz, 2002; Jahnke et al., 2003). In the current profiles, dissolved P (as total P, not phosphate) behaves quite differently between the two locations (Fig. VI-6). In Piez F, the trends are similar between P and Fe in the porewater. In Piez S, however, the two elements are strongly decoupled. It is possible that the order-of-magnitude higher levels of Fe in Piez F result in much stronger control on P movement in the porewater than in Piez S. Alternatively, the trends observed in Piez S may result from bacterial storage and release (Toerien et al., 1990). In the latter case, constant input of P-enriched groundwater (Clarke et al., 2006) at Piez F may relieve the

need for cellular storage by bacteria, therefore making Fe the dominant determinant of P distribution in the porewater.

Mo and V

Having discussed the redox-active metals Mn and Fe, our discussion turns to two other redox-sensitive transition metals, Mo and V (Fig. VI-3b). Both of these have been used as sedimentary indicators of ocean anoxia, as they are presumably insoluble under reducing conditions, either by scavenging of reduced forms (Wehrli and Stumm, 1989), co-precipitation with Fe-sulfides (Bertine, 1972), or direct precipitation of sulfide forms (Rivera-Duarte and Morse, 1992). Association of V with Fe-oxides has also been shown on surfaces of phytoplankton cells (Tang and Morel, 2006). Organic complexation may play a role in the removal of Mo from porewater under anoxic conditions (Malcom, 1985), but has also been implicated in improving Mo and V solubility (Brumsack and Gieskes, 1983; Shaw et al., 1990).

The dominant process regulating Mo distributions in these profiles appears to be cycling with Mn. (Cycling of Mo, Ni, and Co with Mn will be discussed at length here. To somewhat belabor the point and clarify the geochemical association, Fig. VI-7 shows the profiles of these metals side-by-side.) In Piez F, the dissolved Mo peak (300 nM) occurs at 15 cm depth, slightly above the Mn peak at 17 cm. This offset may reflect a non-steady state situation due to lag resulting from differences in the rate of remobilization of Mo versus Mn (Shaw et al., 1990), or may be the result of lower affinity of Mo for Mn-oxides re-precipitated at a higher pH (as shown for other metals by Sundby et al., 1986). The slight offset of these two elements is responsible for their poor

direct correlation in Piez F (r^2 = 0.27, Fig. VI-8). There is a much stronger correlation (r^2 = 0.90) between these two elements in Piez S. The difference in correlation between the two elements at the different locations may reflect a site-specific process, such as Mo input by fresh groundwater, but this is not conclusively discernible in the data.

The dissolved Mo trend with salinity (Fig. VI-9) shows that nowhere in either profile are Mo concentrations lower than would be predicted by mixing between low Mo groundwater and open ocean water (Bruland, 1983). This contrasts with the results from Jamaica Bay (discussed in Chapter IV), where Mo removal from the water column and porewater was observed. In fact, the concentrations of Mo in the present porewater profiles are substantially above the conservative mixing line. Furthermore, Mo concentrations at the surface of the overlying water column are 6% (Piez F) and 12% (Piez S) greater than conservative mixing would predict. This supports the results of Dalai et al. (2005), who observed substantial (~50 – 200%) excesses of Mo over conservative mixing predictions. They also showed a strong correlation of dissolved Mo with ^{228}Ra, and argued that porewater exchange (i.e. SGD) could be the mechanism transporting both constituents. The fact that Mo concentrations in porewater immediately subsurface are the same or lower than the overlying water suggests that preferential flow is the likely mechanism for transporting Mo past the sediment-water interface. Given that Mo and Ra both show affinity for Mn-oxides, the results of Dalai et al. (2005) and the current results suggest that preferential flow provides a common and important pathway for transporting reactive trace elements past surficial oxide layers.

The contrary results observed in Jamaica Bay give evidence that SGD probably does not represent a constant source or sink for Mo in the coastal ocean (Windom and

Niencheski, 2003); instead temporal changes in Mo remobilization in sediments, sedimentary oxide pools, and seawater recirculation through sediments can all affect the distribution of Mo in coastal surface waters. Seasonal variability in SGD patterns may be important for the Mo source/sink in permeable sediments.

The distribution of V in the current profiles is not explained as easily as was Mo. At Piez F, V levels in the overlying water were 65-70 nM (Fig. VI-3b), nearly 3-fold higher than would be predicted for that salinity by the conservative behavior of V in seawater. A high concentration (65 nM) was measured immediately below the sediment-water interface, with concentrations dropping to 35-40 nM between 5 and 17 cm depth. Below 17 cm, concentrations of dissolved V again increase, to 85 nM. Constant concentrations (85-103 nM) were measured between depths of 24 and 52 cm. V levels then increase to the bottom of the profile, reaching a maximum of 149 nM at 76 cm depth. In Piez S, dissolved V in the overlying water was again elevated (~50 nM), and concentrations in porewater were again high and variable (38-137 nM; Fig. VI-3b).

No correlation was observed between V and any of the other chemical parameters measured in this study. Thus, it is impossible to conclusively identify the process responsible for V cycling in these porewaters. It is interesting that the V minimum in Piez F coincided exactly with the Mo peak (Fig. VI-10). (A slight minimum in Piez S also seems to match with the uppermost peak in Mo.) At face value, this suggests that the process regulating Mo mobility (i.e. Mn-oxides) is having an inverse effect on V solubility. However, the mechanism resulting in this pattern is unclear.

Speculatively, it is possible that V mobility in the fresh and saline portions of the Piez F profile is due to complexation with DOC (Brumsack and Gieskes, 1983; Shaw et

al., 1990). Indeed, DOC concentrations in Great South Bay groundwater range between ~400 and 1600 μM, and range between ~200 and 800 μM in overlying water (Clark et al., 2006). These high concentrations of DOC may provide ligands for keeping V in solution, and a C-18 extractible fraction of V was indeed present in these profiles (see *Speciation* section below). To produce the observed distributions in Piez F, DOC would augment V mobility in the fresh and saline portions, but would be somewhat removed in the STZ. This allows for the constantly elevated levels of dissolved V observed in Piez S.

Certainly, this is a rather uncertain argument, and future work should examine V mobility in permeable sediments more rigorously. However, despite our inability to identify the mechanism for its enrichment, the consistently high V concentrations measured in porewater and overlying water suggest that SGD may be an important source of this element to Great South Bay, and SGD may perhaps explain the high (>35 nM) concentrations observed elsewhere (Caccia and Millero, 2003).

Co and Ni

Dissolved Co and Ni were similar to Mo in that both of these elements showed profiles suggestive of cycling with Mn (Figs. VI-3c and VI-8), consistent with previous reports (Shaw et al., 1990; Lienemann et al., 1997). Association with Mn appeared to be stronger for Co than Ni, consistent with previous reports (Shaw et al., 1990). As well, differences between Piez F and Piez S indicated that association with Mn was not a ubiquitous characteristic.

Co was enriched in porewater as much as 25-fold over water column values (75 nM vs. 3 nM, respectively). In Piez F, a strong peak was observed to levels of 73-75 nM

between depths of 17 and 24 cm. This peak coincided with that observed for Mn, but was less sharply defined, suggesting that Co is not responding to the Mn cycling as rapidly as Mn is solubilized or removed from solution (Shaw et al., 1990). The slow response of Co to apparent Mn phase (i.e. $Mn^{2/3+}$(aq) to MnO_x(s)) changes suggests that SGD could readily transport Co to the water column, even if Mn is precipitating at the sediment-water interface. This supports the positive Co:^{223}Ra correlation observed in Jamaica Bay (Chapter III). And indeed, dissolved Co levels in Great South Bay (3-11 nM) are highly elevated relative to Jamaica Bay (0.3-2 nM), despite a strong wastewater source of Co to the latter estuary.

In Piez S, a small peak (33 nM) in Co was observed between 5 and 17 cm depth, coincident with the uppermost Mn peak. However, below 24 cm, Co remained at low levels (4-12 nM) despite very high and variable dissolved Mn. Thus, Co at depth in Piez S was decoupled from Mn cycling. It is possible that the higher mobility of Co relative to Mn could allow the former element to be preferentially transported surfaceward by the slow advection of SGD. At this site, SGD rates are ~1.8 cm d^{-1} (Bokuniewicz et al., 2004), representing a porewater transit time in the sediments from bottom to top of the profile of ~2-3 weeks.

It is worth noting that fresh groundwater in this system does not seem to be a source of Co. As well, concentrations were higher at depth in Piez S than in Piez F, but the upper peak in Co concentration was higher in the latter profile. Thus, there appears to be greater trapping efficiency for Co in the subterranean estuary than in the fully saline porewaters. In addition, higher concentrations of Co were measured directly above the

sediment-water interface at Piez S (11 nM), indicating that the lower trapping efficiency of those porewaters did allow transport of Co to the water column.

Dissolved Ni trends were less clear than those for Co. Ni peaked at concentrations of 44 and 37 nM in Piez F and S, respectively (Fig. VI-3c). These peaks coincided with the uppermost peaks in Mn, but were broader than the sharp Mn and Co peaks. This pattern is consistent with the results of Tankere-Muller et al. (in press), and Shaw et al. (1990) have noted that Ni is mobilized more readily than either Mn or Co. This suggests that the broad peaks observed in the current profiles are due to relatively high mobility of Ni in solution, probably after input during Mn-oxide dissolution.

It is noteworthy that in Piez F, the maximum Ni concentrations are observed at 24 cm depth, where saline water is first observed (S = 6.3). Throughout the mixing zone, Ni appears to be mixing conservatively with respect to salinity (Fig. VI-11). Thus, it is difficult to identify if Ni input is due to the increase in salinity (i.e. giving an effective zero-salinity endmember of 52 nM vs. 14-32 nM actually observed in the fresh porewater), or if it is more dependent on Mn redox cycling. Certainly, the peaks observed for Ni in Piez S cannot be explained by a salinity effect. However, correlation of Ni with Mn (Fig. VI-8) is not especially good in either profile, and the large non-zero intercepts suggest that much of the Ni in the porewater is insensitive to Mn variability.

Concentrations of dissolved Ni in the Great South Bay water column (13-16 nM) are as high as those in Jamaica Bay (3-12 nM). As noted for Co, it is striking that an SGD source of Ni may be as strong in this system as wastewater is in Jamaica Bay.

Pb

Dissolved Pb levels (up to 4,250 pM; Fig. VI-3d) in these profiles are quite high compared to the Jamaica Bay water column (<350 pM), but are not that different from the Great South Bay water column (1,500 pM; Clark et al., 2006). The high Pb levels in the subterranean estuary at this Roe Avenue site are comparable also to levels measured at Mattituck (1,660 pM; Chapter V). In Piez F, Pb levels are highest in the fresh groundwater zone, ranging between 1,300 and 4,250 pM. At the first detection of saline water (S = 6.3), Pb levels drop by nearly an order of magnitude to 213 pM. Concentrations remain low throughout the brackish region, ranging between 64 and 213 pM. In Piez S, dissolved Pb is similarly low, with levels between 41 and 430 pM. This is consistent with the salinity patterns observed for Piez F.

In Piez F, the high Pb levels coincide with, and are moderately correlated with (r^2 = 0.67, Fig. VI-12), high concentrations of dissolved Al (up to 15 μM). This is consistent with the trends observed by Beck et al. (2007), although Pb and Al in the current samples are much higher. It is likely that Pb is kept in solution by association with an Al carrier phase (as argued by Beck et al., 2007). Thus, processes removing Al from solution will have a similar effect on Pb. It is possible that Al is being removed by precipitation of an Al-hydroxide solid (Kjoller et al., 2004) as a result of basification during mixing of fresh and saline groundwater. However, the pH in the uppermost (31 cm) fresh sample is 6.83, compared to the first saline sample (24 cm, S = 6.3), where pH was 6.78 (Fig. VI-2). Two points are certainly not enough to draw definitive conclusions, but this suggests that increased salinity, not pH, resulted in the Pb and Al removal (Fig. VI-13).

In the saline portion of Piez F and throughout Piez S, Al and Pb are completely decoupled. It is not clear what mechanism is regulating Pb cycling in saline groundwater. No correlation was observed with Fe, a common Pb carrier (Benjamin and Leckie, 1981; Wedepohl, 1995; Sañudo-Wilhelmy and Gill, 1999).

As mentioned in Chapter III, it may be possible to see the effect of metal transport by SGD in the elevated Pb patterns in surface waters reported by Clark et al. (2006). Highest dissolved Pb concentrations were measured in the rivers and perhaps at the inlet. These are the regions where we observed Ra enrichment, thus suggesting that SGD is a source of Pb to Great South Bay. Pb isotope analyses may be useful for definitively assessing this, as was shown in Jamaica Bay (Chapter IV).

Cu

Dissolved Cu profiles at this site are interesting because both piezometers show very similar trends (Fig. VI-3d). High (~30 nM) levels in surface waters declined in the sediment porewaters to <5 nM by 15 or 25 cm. Concentrations were then relatively constant, and increase in the bottommost samples to 8-17 nM. The distribution with salinity in Piez F shows that there is removal of Cu independent of simple endmember mixing (Fig. VI-14).

There is good correlation of Cu in both profiles with ORP (Fig. VI-15). As conditions in the porewater become more reducing, Cu is apparently removed from solution. The less reducing deep groundwater allows Cu to reenter solution. The correlation with reducing conditions suggests that precipitation of CuS(s) may be the removal mechanism (Cooper and Morse, 1998; Luther et al., 2002), although we have

argued earlier against the presence of sulfide in these profiles. It may be possible that very low levels of sulfide are produced without anoxic conditions (de Beer et al., 2005), out of sequence in the anticipated redox succession scheme (Froelich et al., 1979). Alternatively, sulfate reduction may be occurring in microsites (as noted by Shaw et al., 1990), and sulfide then diffuses into solution where it can complex dissolved Cu. More work is necessary to determine the role of sulfur cycling on metal mobility in these groundwaters.

Speciation of trace metals in surficial groundwater

To provide a first approximation of the specific metal complexes likely present in these samples, Fig. VII-17 shows Eh-pH diagrams for the different metals. These diagrams have been reproduced after Brookins (1988), and generally include systems of sulfur, carbon, oxygen, and hydrogen. The current samples are plotted on the stability fields to identify which chemical forms may dominate at the redox/pH conditions of the porewaters. All of the piezometer samples cluster near the origin, with near-neutral pH and either oxidizing or very mildly reducing conditions. It should be stressed that this provides only a very rough approximation of the possible geochemical speciation of these metals. The accuracy of these diagrams is only as good as the thermodynamic data used to construct them; as importantly, they were constructed using single metal activities (a_{metal} between 10^{-6} and 10^{-9}) and rather arbitrary activities of C and S (generally 10^{-3}). Without measurements of sulfur and carbon species in the porewater, this is probably the most reasonable approach. In natural environments, these diagrams may be quite inaccurate due to variable concentrations of the species considered, presence of other

elements (Garrels and Christ, 1965), or suspended colloidal matter (Langmuir, 1997). Furthermore, these plots include no consideration of chemical kinetics which may result in metastable intermediate species (Brookins, 1988). Nonetheless, they may provide some useful guidance for interpreting the Chelex and C-18 results, and will be discussed here with some reservation.

Three of the metals examined (Fe, Mn, and Mo) showed no evidence of organic complexation (discussed below), and these will be discussed first in the labile species section. Metals showing moderate organic association will be addressed next (Co, V, and Pb), followed by those metals with a substantial organic fraction (Cu and Ni).

C-18 extractible metals

A significant fraction of C-18 extractible species was only found for Cu (10-71%) and Ni (0-72%) (Fig. VI-3). The high percentage of Cu found in the C-18 fraction supports the low observed quantity of Chelex-labile Cu (see below; Shank et al., 2004; Shafer et al., 2004). Lesser amounts were measured for Co (1-22%), V (2-13%), and surprisingly, Pb (0-52%). It may be interesting to note that high C-18 extractible Pb values were measured in the water column immediately above the sediment-water interface in both piezometers (Fig. VI-3), suggesting that these compounds may potentially improve the mobility of Pb in this system. Generally though, this particular organic-metal fraction did not appear to be very important for metal mobility at this site, except for Cu and Ni. It is probable that soluble organic ligands would be more important in sediment porewater than hydrophobic complexes.

Chelex-labile species

Profiles of the metal species with depth are shown in Fig. VI-3. Substantial Chelex-labile fractions were observed for all metals except for Pb (detected in only 3 samples) and Cu (detected in 11 samples). These kinetically-labile complexes represented a generally constant proportion of the total dissolved pool (Fig. VI-16). This trend is strange considering that the total dissolved levels span a large concentration range (e.g. Mn: 2 - 1,125 μM). This pattern suggests that there is an excess of at least two ligand classes, one of which binds the metals in a way that they can rapidly be exchanged to the Chelex resin. However, the second ligand would have to bind the metal ions more strongly than Chelex resin, but yet could not remove the metals bound by the first ligand. It is unclear how this is possible, and application of additional speciation techniques may be useful in elucidating the mechanism in future studies.

Fe, Mn, Mo

The labile metal fraction was largest for Fe and Mn, representing 64 and 67% of the total dissolved pool, respectively. These percentages are less than Chelex-labile Mn and Fe reported for the Black Sea (Lewis and Landing, 1991), where the labile form represented approximately the entire total dissolved metal pool. Stability diagrams indicate that under the observed redox conditions, dissolved Mn should be present as reduced Mn^{2+} (Figure VI-17a). While this may support the large quantity of labile Mn measured, it does not explain why the Chelex-labile fraction occurs at such constant proportion (67%). The Fe diagram (Fig. VI-17b) indicates that Fe species in these porewaters should be dominated by solid-phase hematite (Fe_2O_3), or kinetically-hindered,

metastable iron oxyhydroxides (FeOOH). However, this rather contradicts the observed presence of high dissolved Fe levels; reducing the influence of C and S species allows the Fe^{2+} stability field to expand and encompass the samples (Geological Survey of Japan, 2005). It is therefore probable that the similar patterns observed for Chelex-labile Mn and Fe are determined by manganous and ferrous ion dominance.

Mo generally showed a constant labile percentage at ~20%. However, the three samples with the highest total dissolved Mo concentrations had exceptionally high amounts of labile Mo (38-45%). Nothing in the current dataset offers explanation for this trend. The Eh-pH diagram indicates that oxyanionic Mo(VI) should dominate (Fig. VI-17c), although it is not clear why some samples should be so clearly separated from the bulk. It is interesting that the 20% labile fraction observed here is similar that found in non-sulfidic porewater, while as much as 60% Chelex-labile Mo has been reported for sulfidic porewaters (Malcom, 1985). Perhaps these higher labile Mo samples in Piez S suggest the presence of local sulfate reduction.

Co, V, and Pb

Labile Co was high (68%) in Piez F, but lower (48%) in Piez S. This may reflect the greater amount of Co associated with Mn in Piez F relative to Piez S (Fig. VI-8). In this case, it suggests that cycling of Co with Mn results in a higher percentage of labile Co. The Eh-pH plot for Co (Fig. VI-17d) shows that the Piez F samples form two groups, one in the Co^{2+} stability field, and the other in the $CoCO_3$ (spherocobaltite) region. The former cluster represents the samples with higher labile, and % labile, Co. Therefore, it is possible that cycling with Mn oxides is maintaining ionic Co in solution,

and that this species is more labile than soluble carbonate complexes. As we note below, SGD transport of labile Co may be important in influencing the trace metal composition of the overlying water.

Relatively high proportions of labile V were observed, particularly in the saline region of Piez F and throughout Piez S, where labile V represented 20-50% of the total dissolved pool. In the fresh zone of Piez F, labile V dropped to less than 20%, and was generally closer to 10%. This is particularly interesting considering that the highest total dissolved V levels were measured in the fresh porewater. A salinity effect on all of the labile metals was observed only in this instance. Although all of the samples appear to fall within the range where oxidized V(V) should dominate, the freshwater samples are closest to the V(IV) field (Fig. VI-17e). As with Fe, uncertainty in the diagram construction may allow the V samples to fall into two distinct groups of species.

As previously noted, negligible labile Pb was detected. Although the Eh-pH diagram indicates a predominance of carbonate species (Fig. VI-17f), low levels of carbonate and sulfur would allow the Pb^{2+} field to expand greatly (Brookins, 1988). As with Ni (discussed below), the presence of C-18 extractible Pb without labile Pb indicates that most Pb is complexed. Given the particle-reactivity of Pb (Turekian, 1977), this suggests that nearly all dissolved Pb was bound by strong ligands, both aluminosilicate and organic in nature. It is also possible that colloidal association of Pb is important in this system, and future work may benefit from measuring colloids in the porewater.

Ni and Cu

Labile Ni was highly variable in both piezometers, ranging between 3 and 90% of the total dissolved Ni. The vertical distribution of labile species generally followed the total dissolved patterns, but clearly not at constant proportion. The Eh-pH diagram indicates that all of the dissolved Ni should be present as Ni^{2+} (Fig. VI-17g). However, the substantial organic fraction (up to 72%) suggests that most of the ionic Ni is associated with dissolved organic matter.

Chelex-labile Cu trends were the least clear of any of the metals. Labile Cu was only detected intermittently, and was often higher than the total dissolved levels, a physical impossibility. This suggests that the detection limit for labile Cu may have been higher than the blank levels indicated (3σ = 0.08 nM). The Eh-pH diagram indicates that both Cu(I) and Cu(II) may be present in these profiles (Fig. VI-17h), although this observation does little to explain the Chelex-extractible data.

The fact that almost all of the metals examined had high levels of labile species suggests that the surfaces of aquifer solids are generally unreactive. In other words, substantial dissolved metals would be expected only in the cases where soluble ligands exist which are stronger than the aquifer solid surfaces. Such may be true here, where the metals have a stronger affinity for the ligands than the sediment surfaces, but a lower affinity for the ligands than for the Chelex resin.

A useful comparison here is made with similar metal speciation performed in surface waters elsewhere. We have the fortunate opportunity to compare the speciation in these porewater profiles with samples processed in exactly the same manner from

surface and deep waters of the Long Island Sound, and surface waters of the open North Atlantic Ocean (S.A. Sañudo-Wilhelmy and A. Beck, 2005, unpublished data). This comparison is shown for the available metals in Table VI-1. For several of the metals, there is striking difference between the porewaters and surface waters: labile Fe is approximately 50% higher in the porewater, while labile Mo and V are between 2- and 10-fold lower. Labile Pb constituted a major fraction of the total dissolved pool in the water column (75%), but was not found in the porewater. Porewater labile Co was generally the same or higher than was observed in the two water columns. Labile Ni was variable in the porewater, but was largely below the 80-100% observed in the water column. Labile Cu was also variable in these profiles, and was either comparable to, or lower than, the water column.

Assuming that the Chelex-labile fraction is analogous to the bioavailable species (Buckley et al., 1985), these analyses suggest that only Fe and Co in SGD will be biologically relevant (i.e. only these select metals were more bioavailable in porewater than the water column). Certainly, transformations occurring in the water column may change the bioavailability of any metals with time, but an initial effect of SGD-input of labile metals will be observed rapidly in benthic organisms. An SGD input of labile Fe may also be important for brown tide blooms (Milligan, 1992; Gobler and Cosper, 1996). The low lability (compared to water column measurements) of Cu and Pb in this near-surface groundwater indicates that SGD input of these metals may not have an immediate detrimental effect on local ecology.

Importance of the subterranean estuary geochemistry to the SGD-associated trace metal flux to overlying waters

Armed with some knowledge of the geochemical cycling of trace metals in the near-surface subterranean estuary, we can begin to address the metal flux at the sediment-water interface. Without additional information on SGD water flux, it is not possible to quantitatively describe how the observed geochemical patterns may affect the resultant advective trace metal flux. However, we can qualitatively infer the pattern and significance of this transport from two lines of evidence which are addressed in this section.

First, concentrations of some trace metals (e.g. Mn, Mo, Co, Pb, Ni) were higher directly above the sediment-water interface than in either the water column surface or the surface sediment layer (Fig. VI-3). This pattern cannot be explained by simple mixing between surficial porewaters and the upper portion of the water column. In other words, this pattern could not be established if porewater flow was homogeneous across, and normal to, the sediment-water interface. It is more likely that this distribution is reflecting heterogeneous flow paths which deliver unmodified porewater from depth directly to the surface, bypassing many of the geochemical transformations observed with depth. This must be especially true for the redox-sensitive elements, such as Mn and Fe.

Dissolved Mn and Fe are advected toward the surface from reduced zones, where they exist in high concentrations (Fig. VI-3a). Upon reaching the near-surface, increasing oxygen penetration results in the precipitation of solid oxides of these metals (Froelich et al., 1979; Charette and Sholkovitz, 2002; Charette et al., 2005). This removal from solution is evident in the dissolved Fe and Mn profiles in Fig. VI-3a, as

concentrations in the upper 5 cm are nearly zero. Given the affinity of other dissolved metals for Mn-oxide (Loganathan and Burau, 1973; Murray, 1975) and Fe-oxide (Benjamin and Leckie, 1981; Benjamin et al., 1996) surfaces, concomitant removal should evident. This is particularly true for those metals previously discussed as correlating with Mn, such as Mo and Co. However, such removal contrasts with the high dissolved levels observed in the overlying water.

It is possible that there is heterogeneity in the thickness of the surface oxide layer; thinning of the oxic zone reduces its ability to completely scavenge constituents from solution as they diffuse or are advected out of the sediments (Aller, 1994b). Huettel et al. (1998) have shown very clearly that this can occur spatially on the order of centimeters or less, and oxygen penetration in those areas may be sufficiently reduced to allow dissolved Fe and Mn to be transported into the overlying water column.

Although the current dataset cannot specifically identify that such processes occur at the Roe Avenue site, we have observed related phenomena nearby. During ebb tide, large (~ 20 cm diameter) grayish spots develop at the sediment surface immediately above the waterline. These spots migrate with the falling tide line, and as they travel, the trailing edge of the spots changes color from the light gray-black to a dull orange-red. Scraping away the top few centimeters of sand reveals that the orange-red color is restricted to only the very surface sediment layer (e.g. Chapter IV: Fig. IV-2b). We assume that the changing color is due to varying redox conditions at the surface which allow reducing porewater to discharge in the zone delineated by gray color. As this discharge migrates with the tide line (i.e. the hydraulic boundary), oxygen diffuses into the now stagnant porewater at the trailing edge, and dissolved Fe and Mn are precipitated

as orange-red colored oxides. This color pattern matches previous observations of metal-oxide precipitation in permeable sediments (Huettel et al., 1998; Charette and Sholkovitz, 2002; Charette et al., 2005; Chapter IV). In fact, these observations are very close to reports of "Black Spots" in the German Wadden Sea (Freitag et al., 2003), although the mechanism there appears to be organic matter heterogeneity instead of tidally-forced advective "punch-through."

A migrating zone where reduced porewaters can escape the sediment surface is of paramount importance to our understanding of trace metal transport by SGD; instead of a uniform, highly reactive "Iron Curtain" (Charette and Sholkovitz, 2002), Fe and Mn precipitation is probably heterogeneous. These "black spots," where reducing porewater is discharged directly to the water column, may provide conduits through which dissolved constituents may flow unimpeded. Bio-irrigation may similarly allow advective flow to occur along preferential conduits. For surface-reactive metals which are enormously enriched in porewater compared to surface water (e.g. Mo, Co), this represents an efficient mechanism for transporting non-conservative trace metal signatures out of the sediments and into overlying waters (e.g. Chapter V).

CONCLUSIONS

In permeable marine sediments, a number of processes are active in maintaining concentrations of dissolved trace metals that are highly elevated relative to the overlying water. The processes appear to be primarily driven by organic matter remineralization, although changes in water chemistry associated with the mixing of fresh and saline porewaters are also important. Because metal cycling is very active near the sediment-water interface, the upper ~1 m of sediment is almost certainly the zone where SGD is imprinted with its dissolved trace metal signature. Although the current study did not address seasonal variability, the shallow subterranean estuary is probably highly subject to temporal variability in organic matter input, oxygen penetration, and SGD patterns and driving mechanisms.

Cycling of Mn during early diagenesis appears to be the dominant process regulating many of the trace metals examined in this study. Total dissolved Mn reached levels as high as 1 mM, and trends in dissolved Co, Mo, and Ni all generally matched Mn depth profiles.

Although Fe-oxides are the next most energetically-favorable oxidant after Mn-oxides, Fe cycling did not seem to be as significant at this study site as Mn. Dissolved Fe levels only reached 0.1 mM, and none of the metals studied correlated with Fe in the porewater. Dissolved Fe was higher in fresh groundwater than in saline groundwater by over an order of magnitude. This difference appeared to result from the lower pH of the fresh groundwater, and Fe trends with pH were consistent with pH-dependent precipitation.

Fe and Mn cycling appeared to have no impact on profiles of dissolved V, Cu, and Pb. The distribution of V in the subterranean estuary was almost exactly opposite that of Mo. The mechanism for this difference was unclear, but dissolved organic matter (DOM) may be responsible for maintaining high levels of dissolved V. A weak trend was observed between dissolved Pb and Al, consistent with previous reports, but was only evident in the subterranean estuary. Again, the process keeping Pb in solution was not readily identified, and DOM may be responsible. Positive correlation was observed between dissolved Cu and oxidation-reduction potential (ORP). Production of sulfide in more reducing porewaters may have resulted in the Cu removal, but regardless, mildly reducing conditions make these permeable sediments a likely sink for Cu.

None of the trace metal distributions appeared to be explicitly dependent on the salinity gradient of the subterranean estuary. Instead, trends occurring at the depth of the salinity transition zone were explained by pH or metal-oxide cycling. Dissolved Ni poses a possible exception to this, as highest concentrations were observed at the first depth of increased salinity. However, it may be more likely that Ni is cycled partially with Mn, and the distribution is otherwise simply due to mixing processes.

Chelex-labile metal species were prevalent for all metals except Pb and Cu. In general, the labile metal concentrations followed the total dissolved trends (i.e. represented a constant proportion). Compared to similar measurements made in the water column of the Long Island Sound and the North Atlantic Ocean, Chelex-labile species represented a smaller proportion of the total dissolved pool for Mo, V, Ni, Cu, and Pb. Labile Fe and Co represented a greater proportion of the total dissolved pool. If the Chelex-extractible fraction can be generally taken as the bioavailable portion, then

SGD may only influence coastal ecology by transporting Fe and Co. As noted above, an input of bioavailable Fe may have important implications for harmful algal blooms in coastal waters.

Hydrophobic organic-metal compounds appeared to be most significant for Cu and Ni, representing up to ~ 70% of the total dissolved pool. Lesser amounts (closer to 10-20%) were observed for Co, V, and Pb, and very little was found for Mo, Fe, and Mn. Although C-18 extractible compounds did not seem to be very important for metal cycling in these porewaters, this does not exclude the possibility of significant influence by hydrophilic organic species.

Dissolved trace metals in interstitial water of shallow permeable sediments reach very high concentrations, up to several orders of magnitude higher than surface water. Most trace metal distributions appear to be driven by Mn-cycling, and metal concentrations in the shallowest porewaters are generally very low. However, some anecdotal evidence for preferential flowpaths and discharge of reducing groundwater can be found at this site. Because of the high dissolved metal concentrations observed in these porewaters, SGD may represent a major source of some trace metals (e.g. V, Mo, Co, and Ni) to Great South Bay. Conversely, removal of Pb during mixing in the subterranean estuary may prevent Pb contamination from reaching the water column; in locations where this mixing zone does not exist (e.g. rivers), groundwater discharge may explain the high Pb levels in surface waters observed by other researchers. Non-conservative removal of Cu in reducing porewater suggests that seawater recirculation through the permeable sediments may be a sink for Cu in Great South Bay. More work is required to quantitatively assess the trace metal flux due to SGD; the development of a

seepage device which does not affect redox conditions in the overlying water and surficial porewaters may be necessary for collecting artifact-free samples of the discharging groundwater.

REFERENCES

Addy, K., A. Gold, B. Nowicki, J. McKenna, M. Stolt, and P. Groffman, 2005. Denitrification capacity in a subterranean estuary below a Rhode Island fringing salt marsh. Estuaries, 28 (6): 896-908.

Aller, R.C., 1994a. Bioturbation and remineralization of sedimentary organic matter. Effects of redox oscillation. Chemical Geology, 114 (3–4): 331–345.

Aller, R.C., 1994b. The sedimentary Mn cycle in Long Island Sound – Its role as intermediate oxidant and the influence of bioturbation, O2, and C(org) flux on diagenetic reaction balances. J. Mar. Res., 52: 259-295.

Aller, R.C., 2001. Transport and reactions in the bioirrigated zone. In: The Benthic Boundary Layer: Transport processes and biogeochemistry. B. Boudreau and B.B. Jorgensen, eds. Oxford University Press, Oxford. p 269-301.

Basu, A. R., S.B. Jacobsen, R.J. Poreda, C.B. Dowling, and P.K. Aggarwal, 2001. Large groundwater strontium flux to the oceans from the Bengal Basin and the marine strontium isotope record. Science, 293: 1470–1473.

Beck, A.J., and S.A. Sañudo-Wilhelmy, *submitted*. Impact of water temperature and dissolved oxygen on copper cycling in an urban estuary. Environmental Science and Technology.

Beck, A.J., Y. Tsukamoto, A. Tovar-Sanchez, M. Huerta-Diaz, H.J. Bokuniewicz, and S.A. Sanudo-Wilhelmy. 2007. Importance of geochemical transformations in determining submarine groundwater discharge-derived trace metal and nutrient fluxes. Applied Geochemistry, 22: 477-490.

Beck, A.J., J.P. Rapaglia, R. Coffey, J.K. Cochran, H.J. Bokuniewicz, and S.A. Sañudo-Wilhelmy, submitted. Simultaneous use of a new high-resolution Multi-Port Piezometer and seepage meters to characterize the physical and geochemical discharge of submarine groundwater. Limnology and Oceanography: Methods.

Benjamin, M.M., and J.O. Leckie, 1981. Multiple-site adsorption of Cd, Cu, Zn, and Pb on amorphous iron hydroxide. J. Colloid and Interface Sci., 79 (1): 209-221.

Benjamin, M.M., R.S. Sletten, R.P. Bailey, and T. Bennett, 1996. Sorption and filtration of metals using iron-oxide-coasted sand. Wat. Res., 30 (11): 2609-2620.

Berner, R.A., 1980. Early Diagenesis: A theoretical approach. Princeton. 241 pp.

Bertine, K.K., 1972. The precipitation of molybdenum in anoxic waters. Marine Chemistry, 1: 43-53.

Bokuniewicz, H, and B Pavilik. 1990. Groundwater seepage along a barrier island. Biogeochemistry 10: 257-276

Bokuniewicz, HJ, and Zeitlin, MJ. 1980. Characteristics of groundwater seepage into Great South Bay. MSRC, Special Report 35, SUNY, Stony Brook, NY, 30p.

Bokuniewicz, H.J., Pollock, M., Blum, J., and Wilson, R., 2004. Submarine groundwater discharge and salt penetration across the sea floor. Ground Water, 42: 983-989.

Bokuniewicz, H., 1980. Groundwater Seepage into Great South Bay, New York. Estuarine and Coastal Marine Science, 10 (4): 437-444.

Bokuniewicz, H.J. 1992. Analytical descriptions of subaqueous groundwater seepage. Estuaries 15, 458–464.

Bone, S.E., M.A. Charette, C.H. Lamborg, and M.E. Gonneea, 2007. Has Submarine Groundwater Discharge Been Overlooked as a Source of Mercury to Coastal Waters? Environmental Science and Technology, *In press*.

Bray, J.T., O.P. Bricker, B.N. Troup, 1973. Phosphate in Interstitial Waters of Anoxic Sediments: Oxidation Effects during Sampling Procedure. Science, 180 (4093): 1362-1364.

Brookins, D.G., 1988. *Eh-pH Diagrams for Geochemistry.* Springer-Verlag. New York, NY. 176 pp.

Bruland, K.W., 1983. Trace elements in seawater. Chemical Oceanography, Vol. 8, 2nd edn. (eds. J.P. Riley and R. Chester), Academic Press, New York. pp. 157–220.

Brumsack H. J. and Gieskes J. M., 1983. Interstitial water trace-metal chemistry of laminated sediments from the Gulf of California, Mexico. Mar. Chem., 14, 89–106.

Buckley, J.A., Yoshida G.A., Wells N.R., et al., 1985. Toxicities of total and Chelex-labile Cd to salmon in solutions of natural water and diluted sewage with potentially different Cd complexing capacities. Water Research, 19 (12): 1549-1554.

Burnett, W.C., H.J. Bokuniewicz, M. Huettel, W.S. Moore, and M. Taniguchi, 2003. Groundwater and pore water inputs to the coastal zone. Biogeochemistry, 66: 3-33

Caccia, V.G., and F.J. Millero, 2003. The Distribution and Seasonal Variation of Dissolved Trace Metals in Florida Bay and Adjacent Waters. Aquatic Geochemistry, 9: 111-144.

Capone, D.G., and M.F. Bautista, 1985. A groundwater source of nitrate in nearshore marine sediments. Nature, 313: 214 – 216.

Charette M.A., and K.O. Buesseler, 2004. Submarine groundwater discharge of nutrients and copper to an urban subestuary of Chesapeake Bay (Elizabeth River). Limnology and Oceanography, 49 (2): 376-385.

Charette, M.A., and E.R. Sholkovitz, 2002. Oxidative precipitation of groundwater-derived ferrous iron in the subterranean estuary of a coastal bay. Geophysical Research Letters, 29 (10), DOI: 10.1029/2001GL014512.

Charette, M.A., and E.R. Sholkovitz, 2006. Trace element cycling in a subterranean estuary: Part 2. Geochemistry of the pore water. Geochimica et Cosmochimica Acta, 70 (4): 811-826.

Charette, M.A., K.O. Buesseler, and J.E. Andrews. 2001. Utility of radium isotopes for evaluating the input and transport of groundwater-derived nitrogen to a Cape Cod estuary. Limnology and Oceanography, 46: 465-470.

Clark, L.B., C.J. Gobler, and S.A. Sanudo-Wilhelmy. 2006. Spatial and Temporal Dynamics of Dissolved Trace Metals, Organic Carbon, Mineral Nutrients, and Phytoplankton in a Coastal Lagoon: Great South Bay, New York. Estuaries and Coasts, 29(5): 841-854.

Cooper, D.C., and Morse, J.W., 1998. Biogeochemical controls on trace metal cycling in anoxic marine sediments. Environ. Sci. Technol., 32: 327-330

Creasey CL, Flegal AR. 1999. Elemental analyses of goundwater: demonstrated advantage of low-flow sampling and trace-metal clean techniques over standard techniques. Hydrogeology Journal, 7 (2): 161-167.

Dalai, T.K., K. Nishimura, and Y. Nozaki, 2005. Geochemistry of molybdenum in the Chao Phraya River estuary, Thailand: Role of suboxic diagenesis and porewater transport. Chemical Geology, 218: 189-202.

de Beer, D., F. Wenzhofer, T.G. Ferdelman, S.E. Boehme, Markus Huettel1, J.E.E. van Beusekom, M.E. Bottcher, N. Musat, and N. Dubilier, 2005. Transport and mineralization rates in North Sea sandy intertidal sediments, Sylt-Rømø Basin, Wadden Sea. Limnol. Oceanogr., 50 (1): 113–127.

Duncan, T., and T.J. Shaw, 2003. The Mobility of Rare Earth Elements and Redox Sensitive Elements in the Groundwater/Seawater Mixing Zone of a Shallow Coastal Aquifer. Aquatic Geochemistry, 9: 233–255.

Elderfield, H., R.J. McCaffrey, N. Luedtke, M. Bender, and V.W. Truesdale, 1981. Chemical diagenesis in Narragansett Bay sediments. American Journal of Science, 281: 1021-1055.

Froelich, P.N., G.P. Klinkhammer, M.L. Bender, N.A. Luedtke, G.R. Heath, D. Cullen, and P. Dauphin, 1979. Early oxidation of organic matter in pelagic sediments of the eastern equatorial Atlantic: Suboxic diagenesis. Geochim. Cosmochim. Acta, 43: 1075–1090.

Garrels, R.M., and C.L. Christ, 1965. *Solutions, Minerals, and Equilibria.* Jones and Bartlett Publishers, Inc. Boston, MA. p. 172-266.

Geological Survey of Japan, 2005. Atlas of Eh-pH diagrams: Intercomparison of thermodynamic databases. Geological Survey of Japan Open File Report No. 419. National Institute of Advanced Industrial Science and Technology. Research Center for Deep Geological Environments. Naoto, Takeno.

Gobler, C.G., E.M. Cosper, 1996. Stimulation of 'brown tide' blooms by iron. In: Yasumoto T, Oshima Y, Fukuyo Y (eds) Harmful and toxic algal blooms. Intergovernmental Oceanographic Commission of UNESCO, Paris, p 321–324

Hanson, AK, and Quinn, JG. 1983. The distribution of dissolved and organically-complexed copper in the Mid-Atlantic Bight. Can. J. Fish. Aquat. Sci., 40 (2): 151-161.

Hines, M.E., and J.D. Buck, 1982. Distribution of methanogenic and sulfate-reducing bacteria in nearshore marine sediments. Appl. Environ. Microbiol., 43: 447-453.

Huettel, M., 1990. Influence of the lugworm Arenicola marina on pore water nutrient profiles of sand flat sediments. Marine Ecology Progress Series, 62: 241-248.

Huettel, M., W. Ziebis, S. Forster, and G.W. Luther II, 1998. Advective transport affecting metal and nutrient distributions and interfacial fluxes in permeable sediments. Geochim. Cosmochim. Acta, 62 (4): 613-631.

Huettel, M., H. Røy, E. Precht, and S. Ehrenhauss, 2003. Hydrodynamical impact on biogeochemical processes in aquatic sediments. Hydrobiologia, 494: 231–236.

Hulth, S., R.C. Aller, and F. Gilbert, 1999. Coupled nitification/manganese reduction in marine sediments. Geochim. Cosmochim. Acta, 63 (1): 49-66.

Jahnke, R.A., C.R. Alexander, J.E. Kostka, 2003. Advective pore water input of nutrients to the Satilla River Estuary, Georgia, USA. Estuarine, Coastal and Shelf Science, 56: 641–653.

Kim, G., Ryu, J.W., Yang, H.S., Yun, S.T., 2005. Submarine groundwater discharge (SGD) into the Yellow Sea revealed by Ra-228 and Ra-226 isotopes: implications for global silicate fluxes. Earth and Planetary Science Letters 237 (1-2), 156–166.

Kjoller, C., D. Postma, and F. Larsen, 2004. Groundwater acidification and the mobilization of trace metals in a sandy aquifer. Environmental Science and Technology, 38: 2829-2835.

Langmuir, D., 1997. *Aqueous Environmental Geochemistry.* Prentice Hall. New Jersey. 600 pp.

Lewis, J.B., 1987. Measurements of groundwater seepage flux onto a coral reef: Spatial and temporal variations. Limnology and Oceanography, 32 (5): 1165-1169.

Lewis, B.L., and W.M. Landing, 1991. The biogeochemistry of manganese and iron in the Black Sea. Deep-Sea Research, 38 (2): S773-S803.

Lienemann, C.-P., M. Taillefert, D. Perret, and J.-F. Gaillard, 1997. Association of cobalt and manganese in aquatic systems: Chemical and microscopic evidence. Geochim. Cosmochim. Acta, 61 (7): 1437-1446.

Loganathan, P., and R.G. Burau, 1973. Sorption of heavy metal ions by a hydrous manganese oxide. Geochim. Cosmochim. Acta, 37: 1277-1293.

Luther III, G.W., S.M. Theberge, T.F. Rozan, D. Rickard, C.C. Rowlands, and A. Oldroyd, 2002. Aqueous copper sulfide clusters as intermediates during copper sulfide formation. Environ. Sci. Technol., 36: 394-402.

Lyons, W.B., H.E. Gaudette, and G.M. Smith, 1979. Porewater sampling in anoxic carbonate sediments: oxidation artefacts. Nature, 277: 48-49.

Malcom, S.J., 1985. Early diagenesis of molybdenum in estuarine sediments. Marine Chemistry, 16: 213-225.

Milligan, A.J., 1992: An investigation of factors contributing to blooms of the ‘brown tide’ *Aureococcus anophagefferens* (Chrysophyceae) under nutrient saturated (light limited) conditions. Masters thesis, SUNY, Stony Brook, NY.

Moore WS. 1996. Large groundwater inputs to coastal waters revealed by Ra-226 enrichments. Nature, 380 (6575): 612-614.

Moore, W.S., 1997. High fluxes of radium and barium from the mouth of the Ganges-Brahmaputra River during low river discharge suggest a large groundwater source. Earth and Planetary Science Letters, 150 (1-2): 141-150.

Moore, W.S., 1999. The subterranean estuary: a reaction zone of ground water and sea water. Marine Chemistry, 65 (1-2): 111-125.

Murray, J.W., 1975. The interactions of metal ions at the manganese dioxide-solution interface. Geochim. Cosmochim. Acta, 39: 505-519.

Pilson, M.E.Q., 1998. *An introduction to the chemistry of the sea*. Prentice Hall. p. 59.

Portnoy, J.W., B.L. Nowicki, C.T. Roman, and D.W. Urish, 1998. The discharge of nitrate-contaminated groundwater from developed shoreline to a marsh-fringed estuary. Water Resources Research, 34 (11): 3095-3104.

Rivera-Duarte, M.A., and J.W. Morse, 1992. Pyritization of trace metals in anoxic marine sediments. Geochim. Cosmochim. Acta, 56: 2681-2702.

Rutkowski, C.M., W.C. Burnett, R.L. Iverson, and J.P. Chanton, 1999. The effect of groundwater seepage on nutrient delivery and seagrass distribution in the northeastern Gulf of Mexico. Estuaries, 22 (4): 1033-1040.

Sañudo-Wilhelmy, S.A., F.K. Rossi, H. Bokuniewicz and R.J. Paulsen. 2002. Trace metal levels in uncontaminated groundwater of a coastal watershed: Importance of colloidal forms. Environmental Science and Technology, 36 (7): 1435-1441

Sañudo-Wilhelmy, S.A., and G.A. Gill, 1999. Impact of the Clean Water Act on the Levels of Toxic Metals in Urban Estuaries: The Hudson River Estuary Revisited. Environ. Sci. Technol., 33: 3477-3481.

Seplow, M.S. 1991. The influence of groundwater seepage on pore water salinity in Great South Bay. M.S. thesis, Marine Sciences Research Center, State University of New York, Stony Brook, New York.

Shafer M.M., Hoffmann S.R., Overdier J.T., et al., 2004. Physical and Kinetic Speciation of Copper and Zinc in Three Geochemically Contrasting Marine Estuaries. Environ. Sci. Technol., 38: 3810-3819.

Shank GC, Skrabal SA, Whitehead RF, et al., 2004. Strong copper complexation in an organic-rich estuary: the importance of allochthonous dissolved organic matter. Marine Chemistry, 88: 21-39.

Shaw, T.J., J.M. Gieskes, and R.A. Jahnke, 1990. Early diagenesis in differing depositional environments: The response of transition metals in pore water. Geochim. Cosmochim. Acta, 54: 1233–1246.

Shaw, T.J., W.S. Moore, J. Kloepfer, et al. 1998. The flux of barium to the coastal waters of the southeastern USA: The importance of submarine groundwater discharge. Geochimica et Cosmochimica Acta, 62 (18): 3047-3054.

Shum, K.T., and B. Sundby, 1996. Organic matter processing in continental shelf sediments - the subtidal pump revisited. Marine Chemistry, 53: 81-87.

Slater, J.M., and D.G. Capone, 1987. Denitrification in Aquifer Soil and Nearshore Marine Sediments Influenced by Groundwater Nitrate. Applied and Environmental Microbiology, 53 (6): 1292-1297.

Slomp, C.P., and P. Van Cappellen, 2004. Nutrient inputs to the coastal ocean through submarine groundwater discharge: Controls and potential impact. J. Hydrol., 295: 64-86.

Snyder, M., M. Taillefert, and C. Ruppel, 2004. Redox zonation at the saline-influenced boundaries of a permeable surficial aquifer: effects of physical forcing on the biogeochemical cycling of iron and manganese. Journal of Hydrology, 296: 164–178.

Spiteri, C., P. Regnier, C.P. Slomp, and M.A. Charette, 2006. pH-Dependent iron oxide precipitation in a subterranean estuary. Journal of Geochemical Exploration, 88: 399–403.

Sundby, B., L.G. Anderson, P.O.J. Hall, A. Iverfeldt, M.M. Rutgers van der Loeff, and S. F.G. Westerlund, 1986. The effect of oxygen on release and uptake of cobalt, manganese, iron, and phosphate at the sediment-water interface. Geochimica et Cosmochimica Acta, 50: 1281-1288.

Tankere-Muller, S., H. Zhang, W. Davison, N. Finke, O. Larsen, H. Stahl, and R.N. Glud, in press. Fine scale remobilization of Fe, Mn, Co, Ni, Cu, and Cd in contaminated marine sediment. Marine Chemistry, in press. DOI: 10.1016/j.marchem.2006.04.005

Testa, J.M., M.A. Charette, E. Sholkovitz, et al. 2002. Dissolved iron cycling in the subterranean estuary of a coastal bay: Waquoit Bay, Massachusetts. The Biological Bulletin, 203 (2): 255-256.

Toerien, D. F., A. Gerber, L.H. Lotter, and T.E. Cloete, 1990. Enhanced biological phosphorus removal in activated sludge systems. Adv. Microb. Ecol., 11: 173-230.

Turekian, K.K., 1977. Fate of metals in oceans. Geochim. Cosmochim. Acta, 41: 1139-1144.

Ullman, W.J., B. Chang, D.C. Miller, and J.A. Madsen, 2003. Groundwater mixing, nutrient diagenesis, and discharges across a sandy beachface, Cape Henlopen, Delaware (USA). Estuarine, Coastal and Shelf Science, 57: 539–552.

Wedepohl, K.H., 1995. The composition of the continental crust. Geochim. Cosmochim. Acta, 59 (7): 1217-1232.

Wehrli, B., and W. Stumm, 1989. Vanadyl in natural waters: adsorption and hydrolosys promote oxygenation. Geochimica et Cosmochimica Acta, 53: 69-77.

Windom, H., and F. Niencheski. 2003. Biogeochemical processes in a freshwater–seawater mixing zone in permeable sediments along the coast of Southern Brazil. Marine Chemistry 83: 121– 130

Windom, H.L., W.S. Moore, L.F.H. Niencheski, and R.A. Jahnke, 2006. Submarine Groundwater Discharge: a Large, Previously Unrecognized Source of Dissolved Iron to the South Atlantic Ocean. Marine Chemistry, 102: 252–266.

Zimmermann, C.F., J.R. Montgomery, and P.R. Carlson, 1985. Variability of dissolved reactive phosphate flux rates in nearshore estuarine sediments: Effects of groundwater flow. Estuaries, 8 (2B): 228-236.

TABLES and FIGURES

Chelex-labile metals, as a percent of the Total Dissolved pool

	Fe	Mo	V	Co	Ni	Cu	Pb
Roe Ave Piezometers	64	20	10-50	50-70	~50	0-30	0
Long Island Sound	40	60	75	57	78	23	76
North Atlantic Ocean	*	63	100	22	100	44	74

* >100%, Presumed contaminated

Table VI-1. Comparison of Chelex-labile metals in porewaters at the Roe Ave site, with the water column of Long Island Sound and the North Atlantic Ocean.

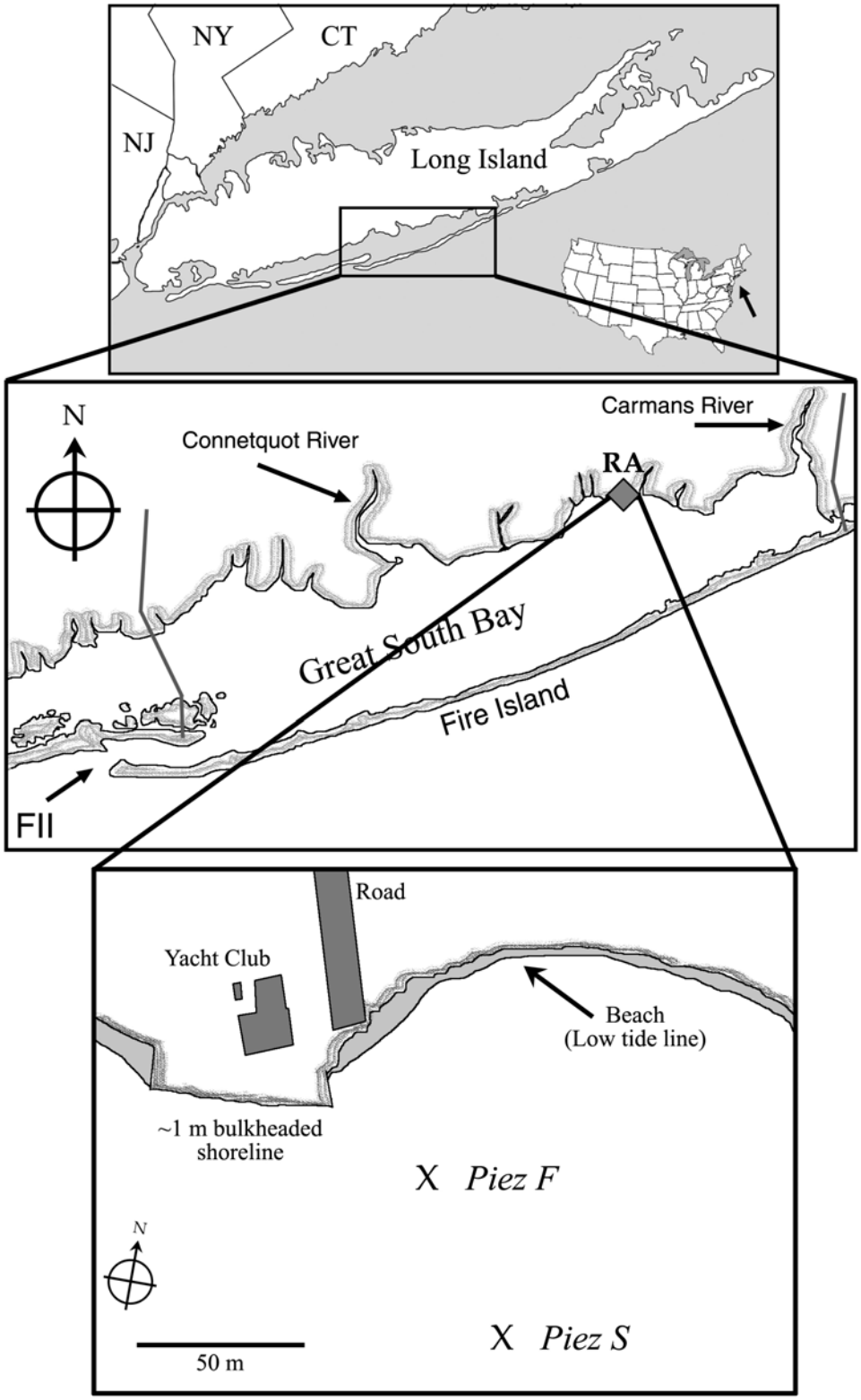

Figure VI-1. Sample site: Roe Avenue, Great South Bay, NY. Approximate locations of piezometer profiles are shown in the lower panel. Both are well below the low tide water level.

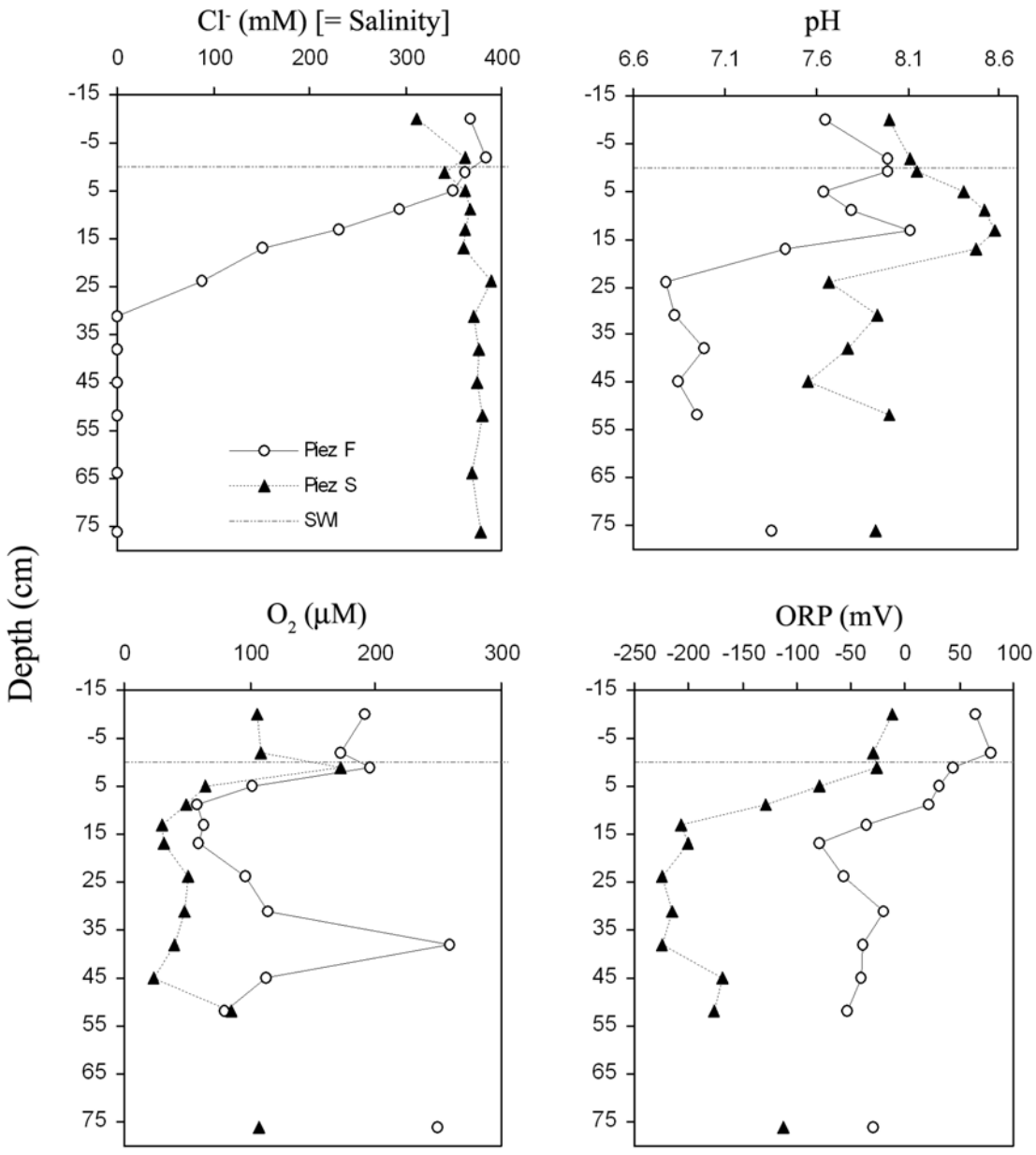

Figure VI-2. Ancillary parameters. The missing point at 64 cm depth was due to insufficient sample volume for probe measurement. In the upper left panel, chloride was determined to ensure that the salinity measurement was accurate.

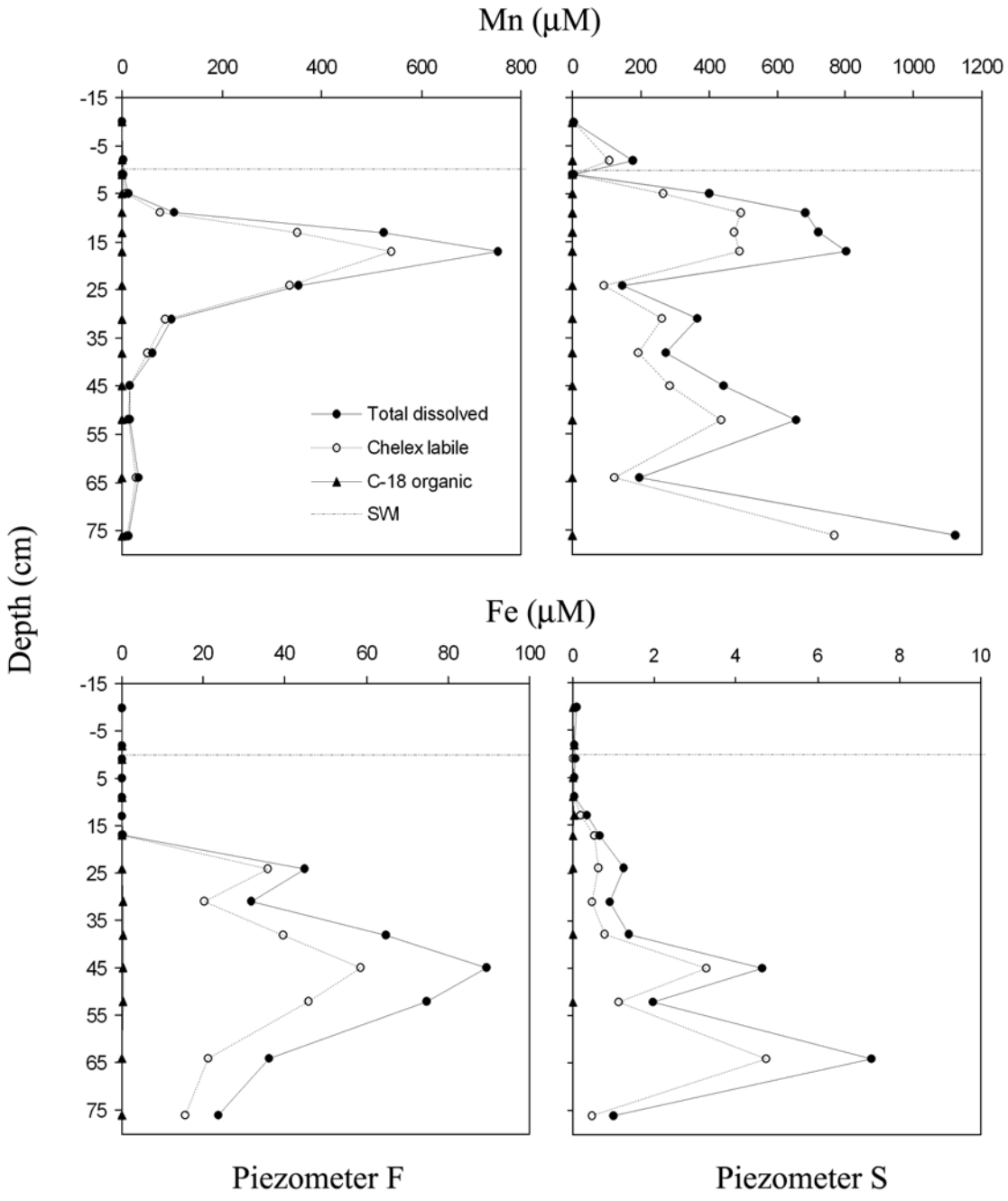

Figure VI-3a. Dissolved Mn and Fe in piezometer profiles. Solid circle symbols represent the total dissolved concentrations, hollow circles represent the Chelex-labile fraction, and solid triangles represent the metal fraction contained in C-18 extractible organic-metal complexes. Left-hand panels show the profile from Piezometer Fresh, or "Piez F"; right-hand panels show the profile from Piezometer Saline, or "Piez S." The design and layout conventions used here will be continued throughout Fig. VI-3. Note that the concentration scales may differ between the two piezometer graphs.

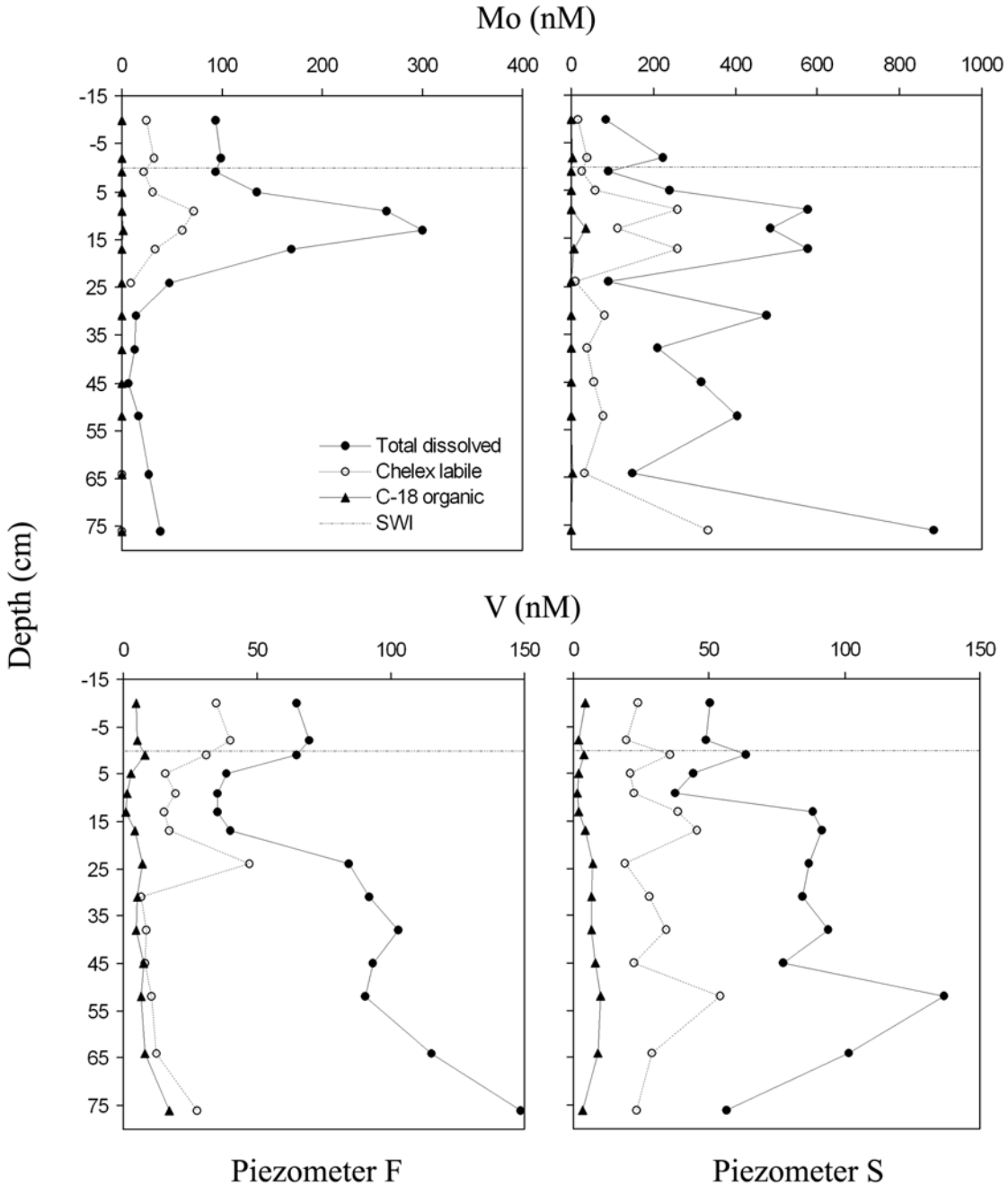

Figure VI-3b. Dissolved Mo and V profiles.

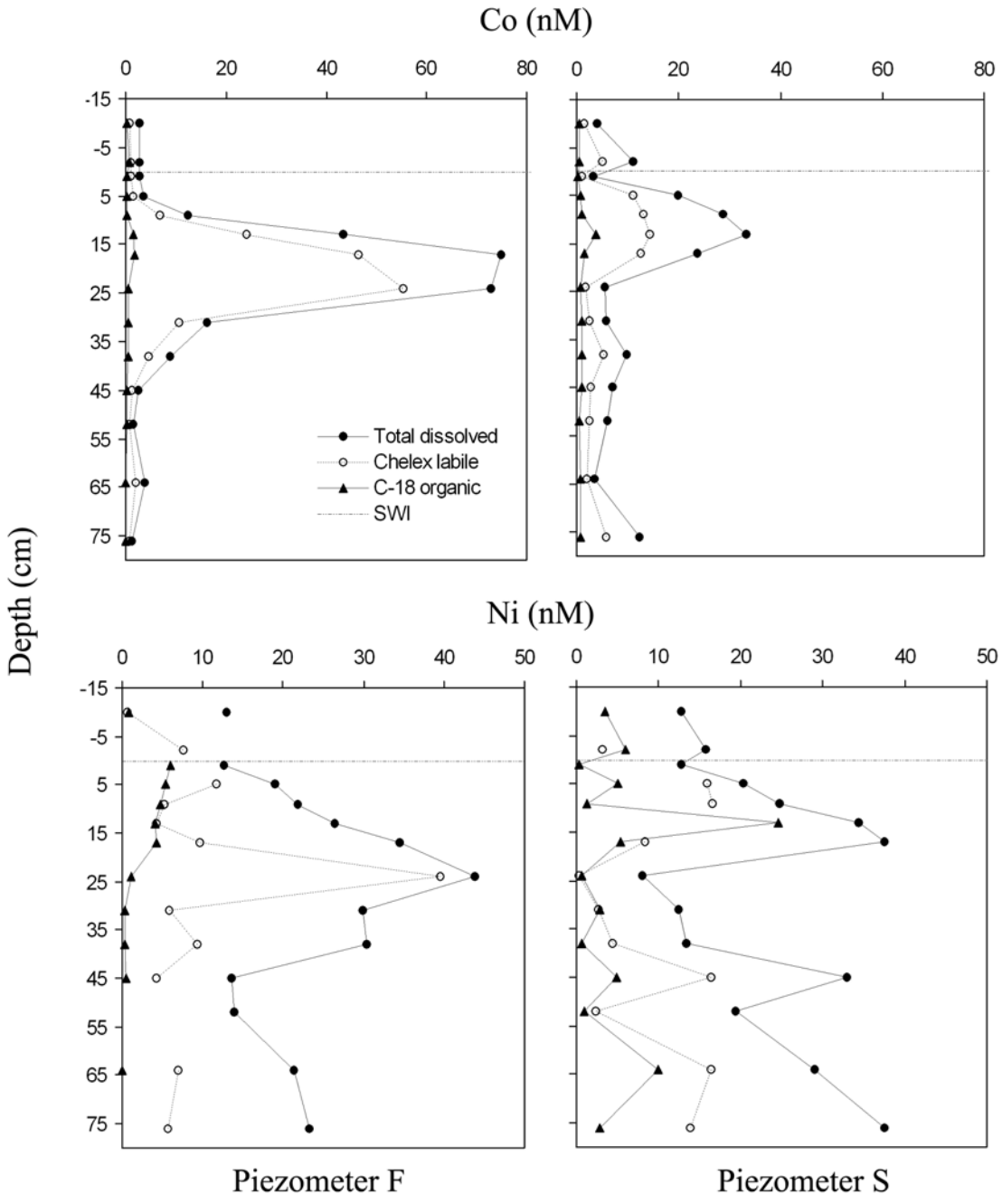

Figure VI-3c. Dissolved Co and Ni profiles.

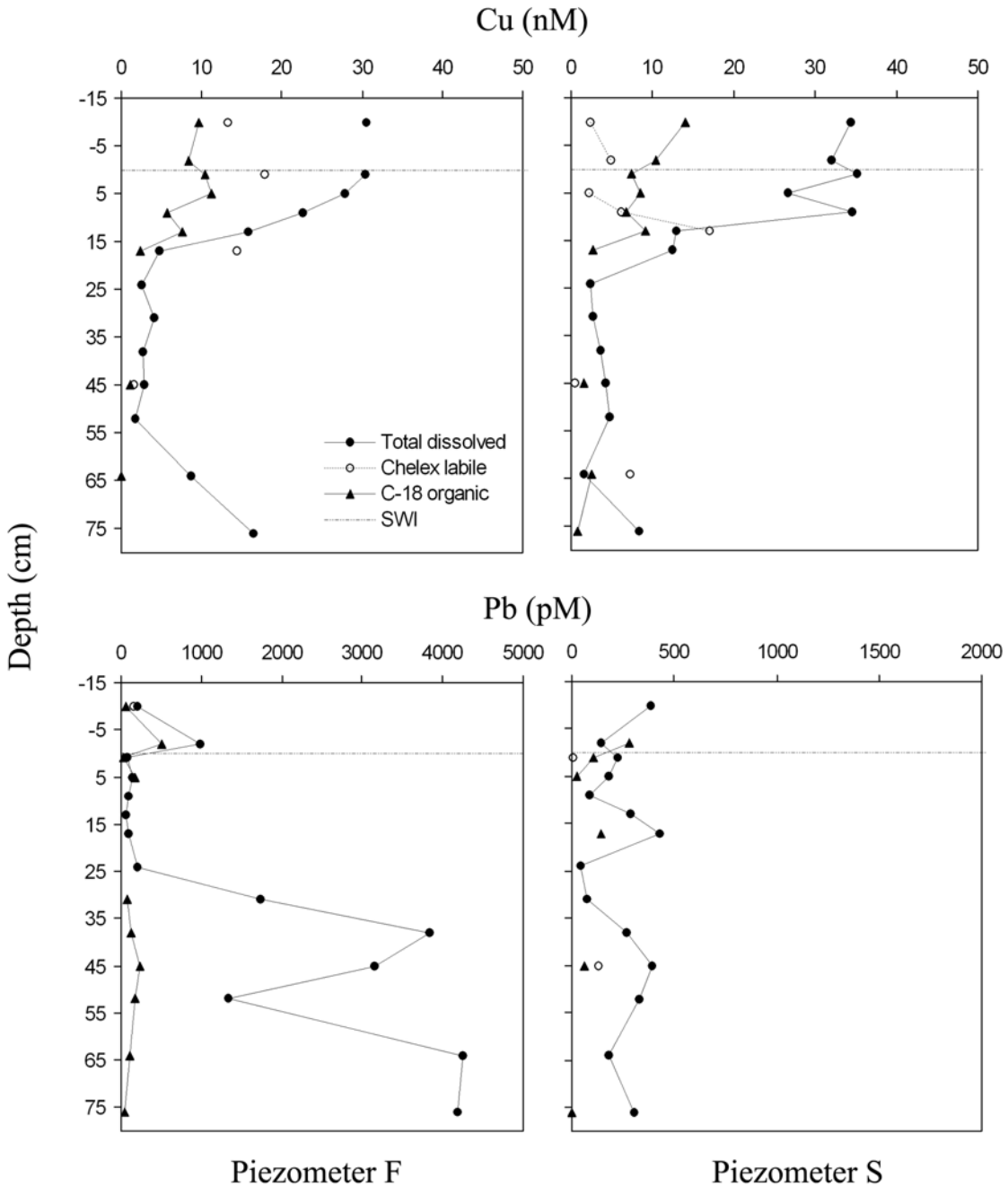

Figure VI-3d. Dissolved Cu and Pb profiles.

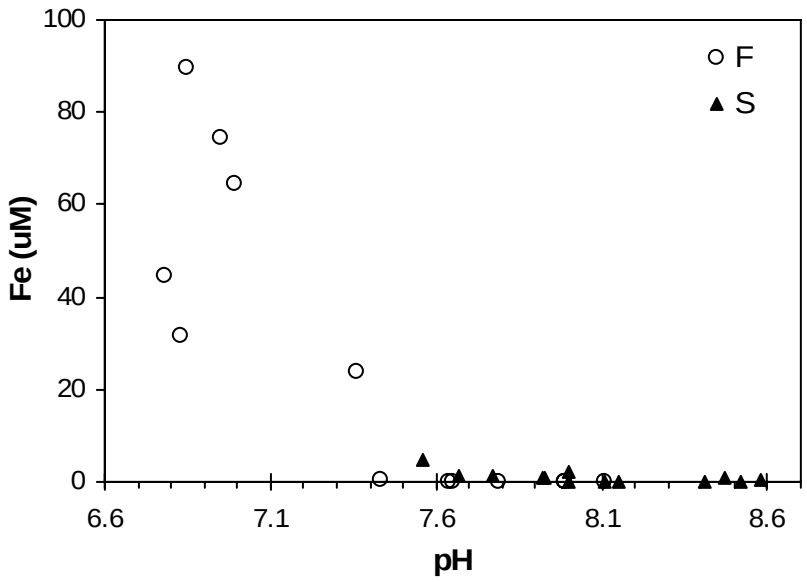

Figure VI-4. Dissolved Fe versus pH.

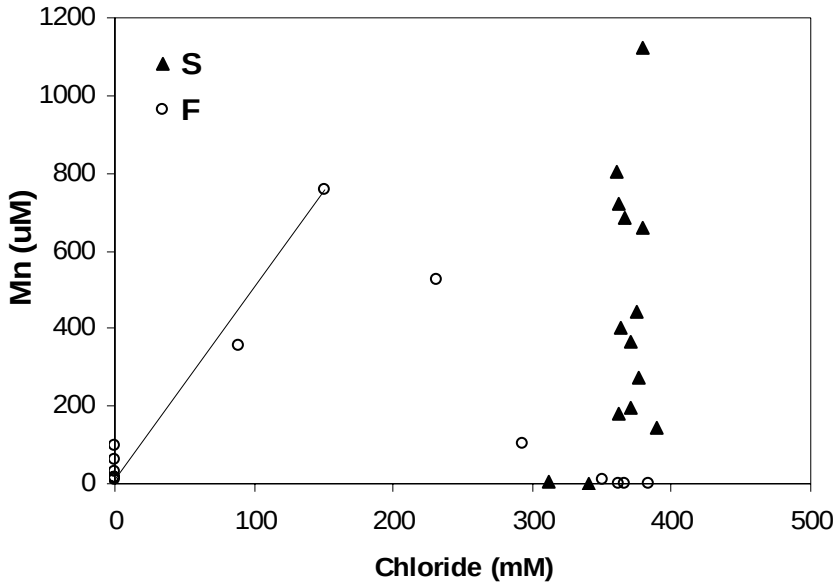

Figure VI-5. Dissolved Mn versus chloride. The solid line represents conservative mixing between the Mn peak and fresh porewater.

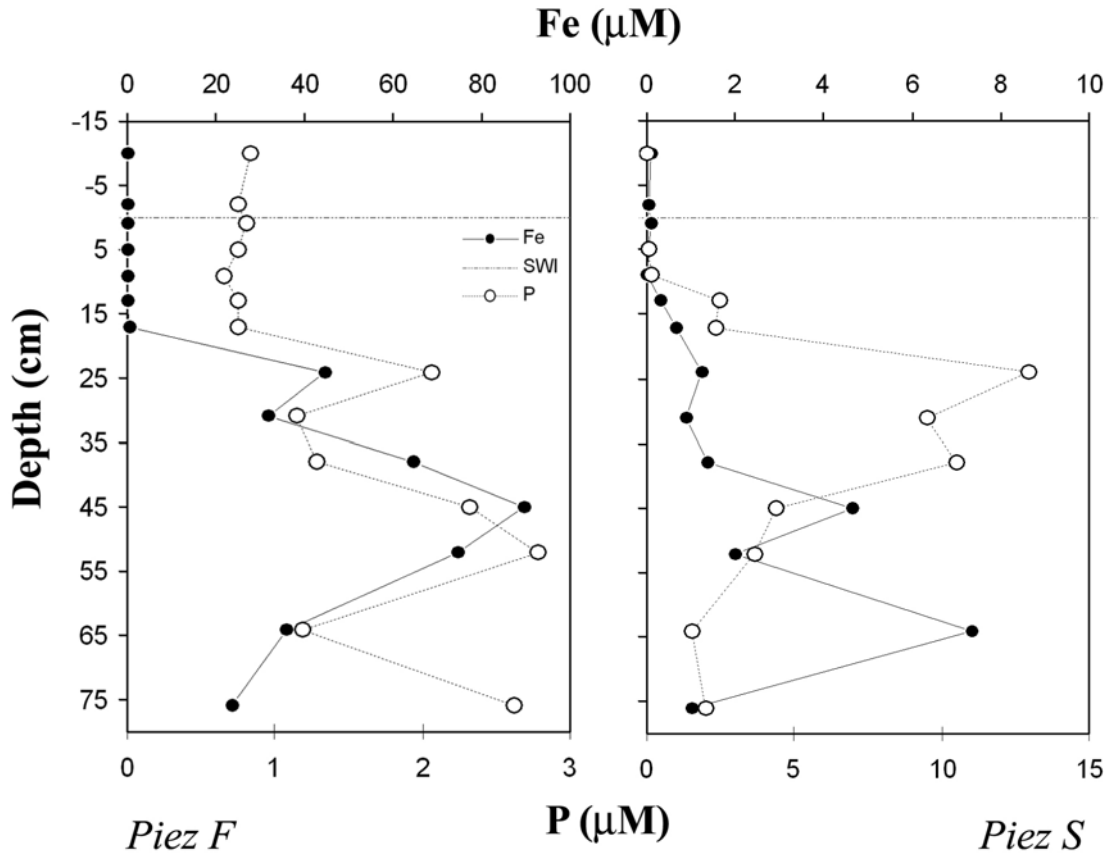

Figure VI-6. Porewater profiles of dissolved Fe and P. Note that the concentration scales are different between left-hand and right-hand graphs.

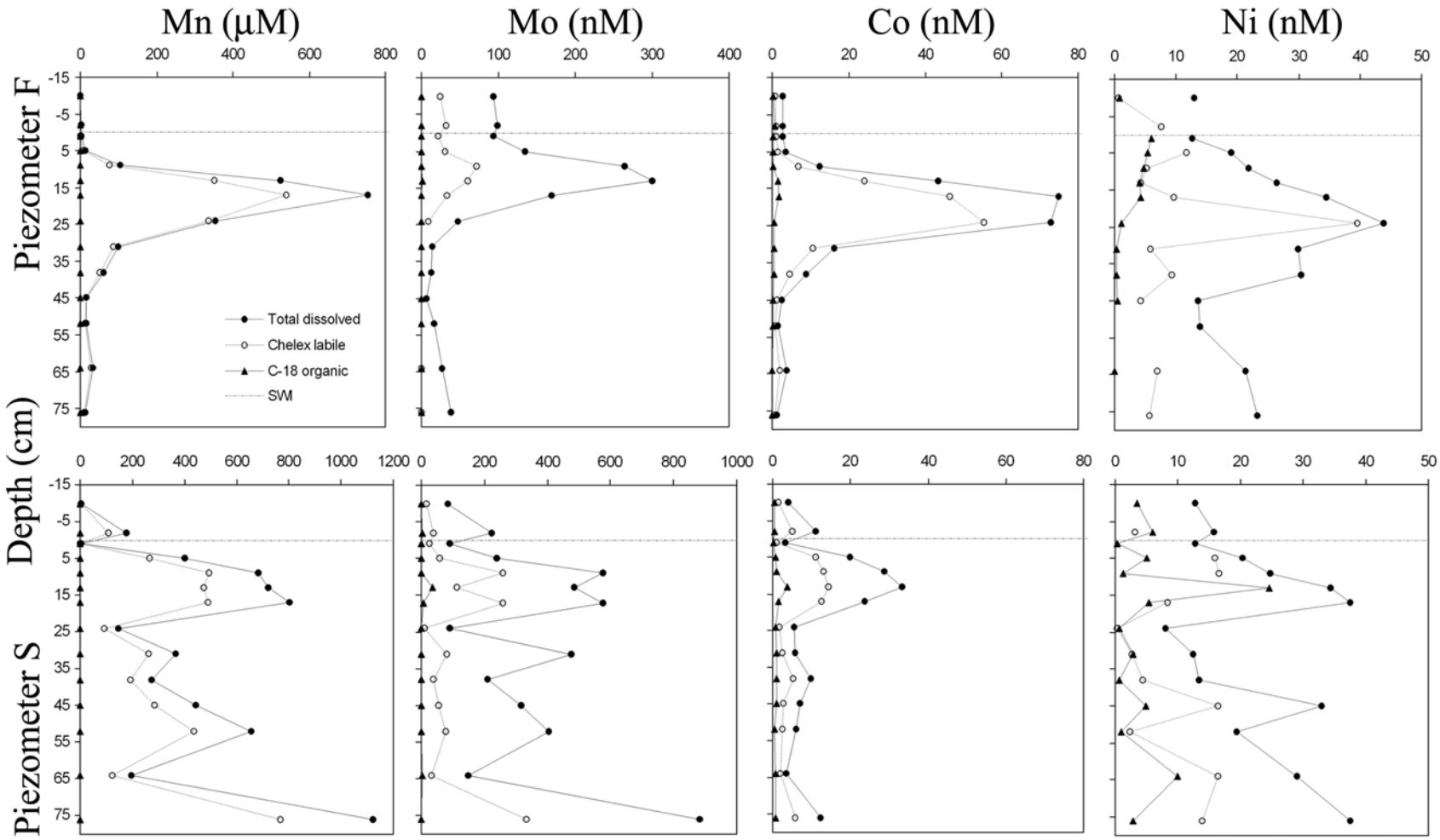

Figure VI-7. Side-by-side comparison of Mn, Mo, Co, and Ni depth profiles to show similarity in depths of dissolved metal maxima. Upper row shows Piez F, and lower row shows Piez S.

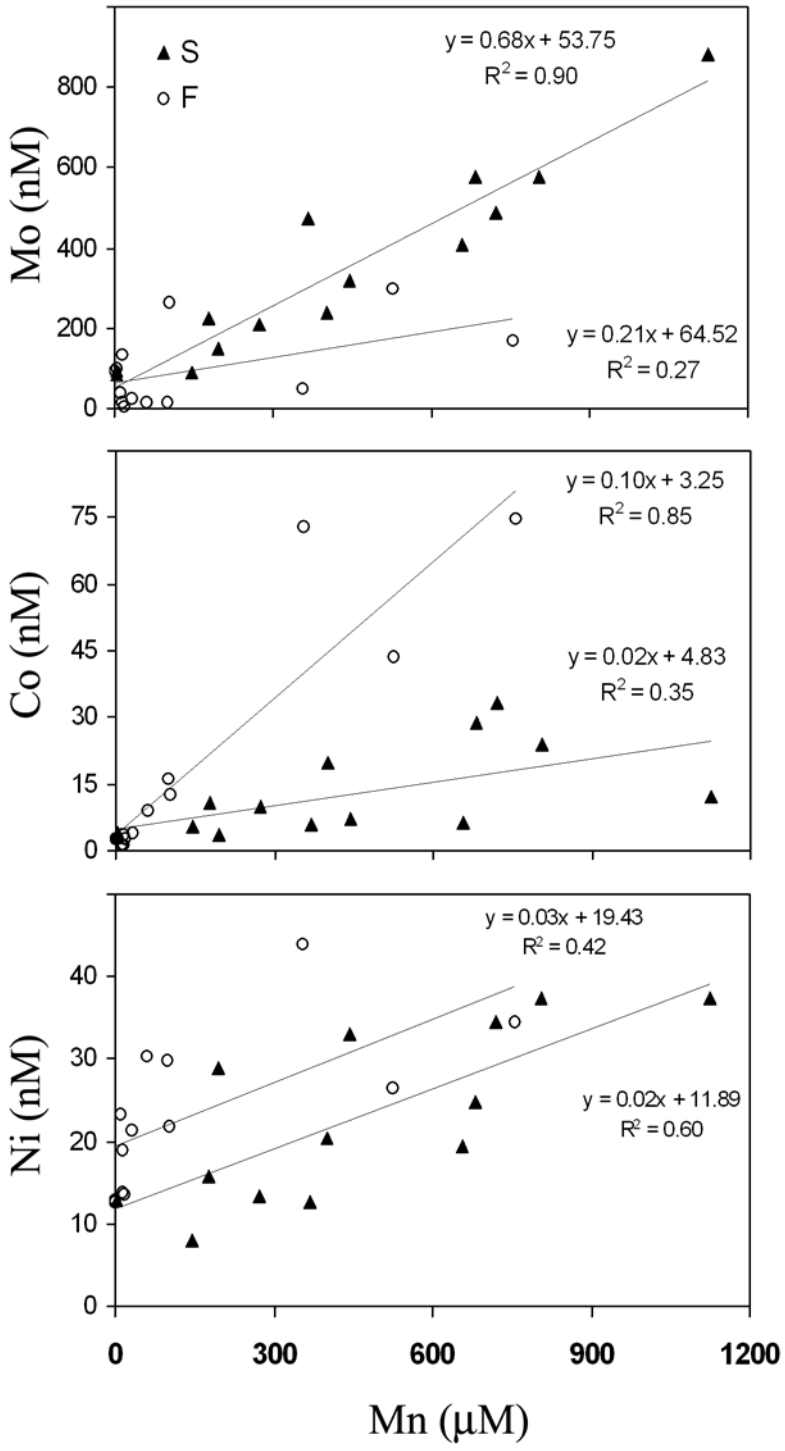

Figure VI-8. Correlations between Mn and Mo, Co, and Ni. Open circles represent Piez F, and solid triangles indicate Piez S. Solid lines, line equations, and correlation coefficients indicate linear regressions of the different piezometers.

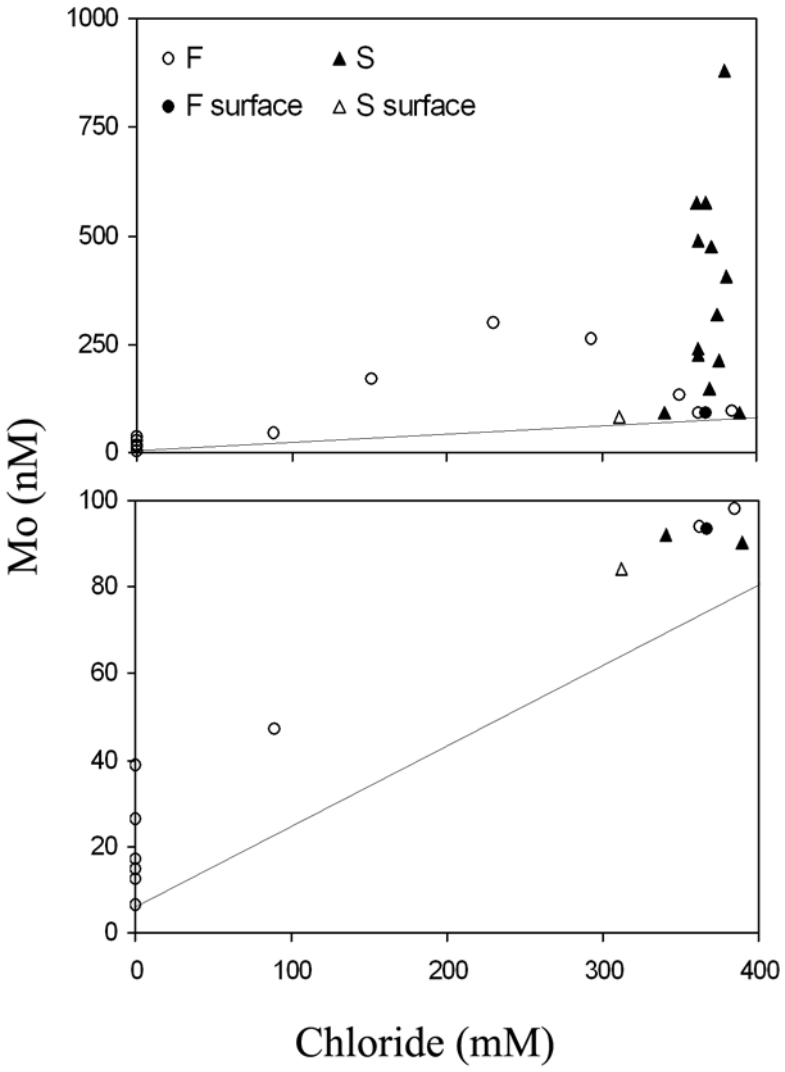

Figure VI-9. Dissolved Mo versus chloride. Symbols are the same as in Fig. VI-8, except note that the hollow triangle (at 312 nM Cl^-) and solid circle (at 367 nM Cl^-) indicate surface water column samples at Piez S and F, respectively. The lower graph shows an expanded view of the upper plot, where Mo is less than 100 nM.

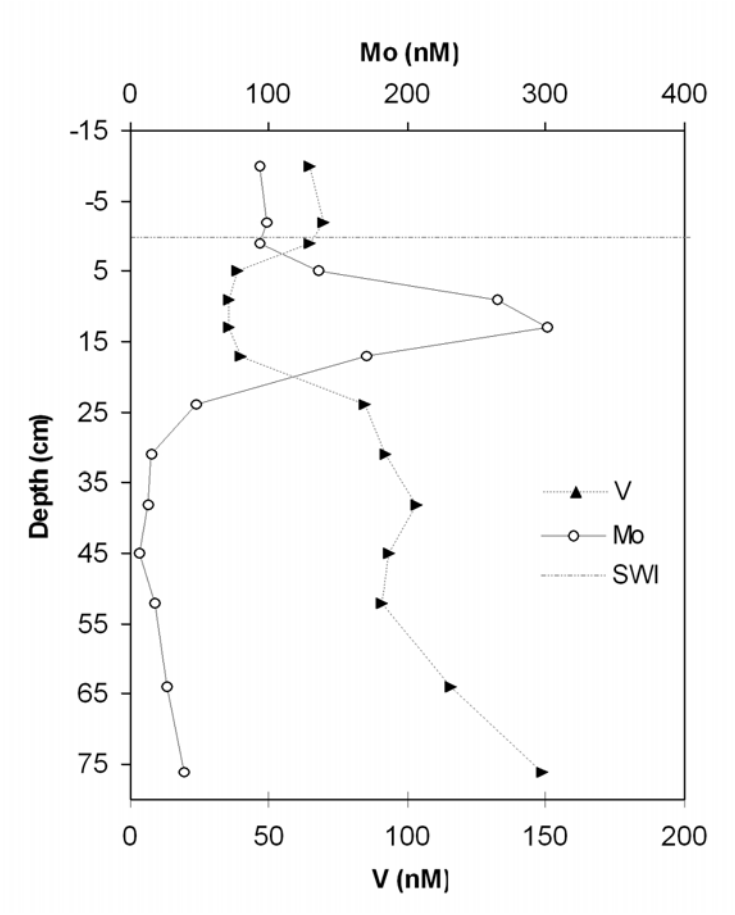

Figure VI-10. Dissolved Mo and V in Piez F.

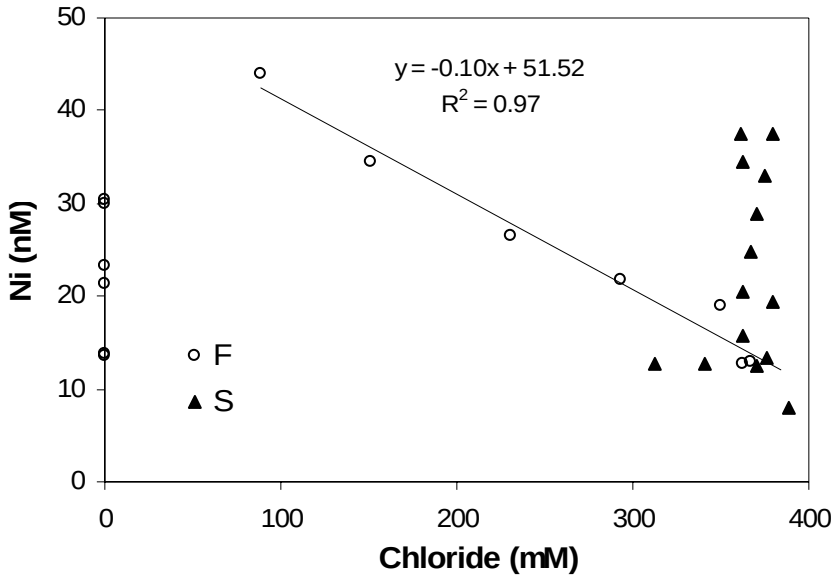

Figure VI-11. Dissolved Ni versus chloride. The solid line and equation represent a linear regression of the data from the saline portion of Piez F.

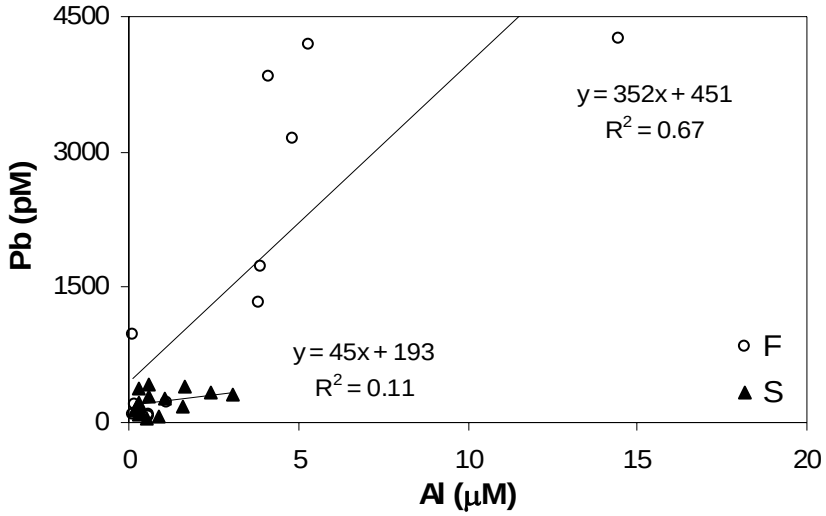

Figure VI-12. Dissolved Pb versus Al. The solid lines and equations represent linear regressions of the data from different piezometers.

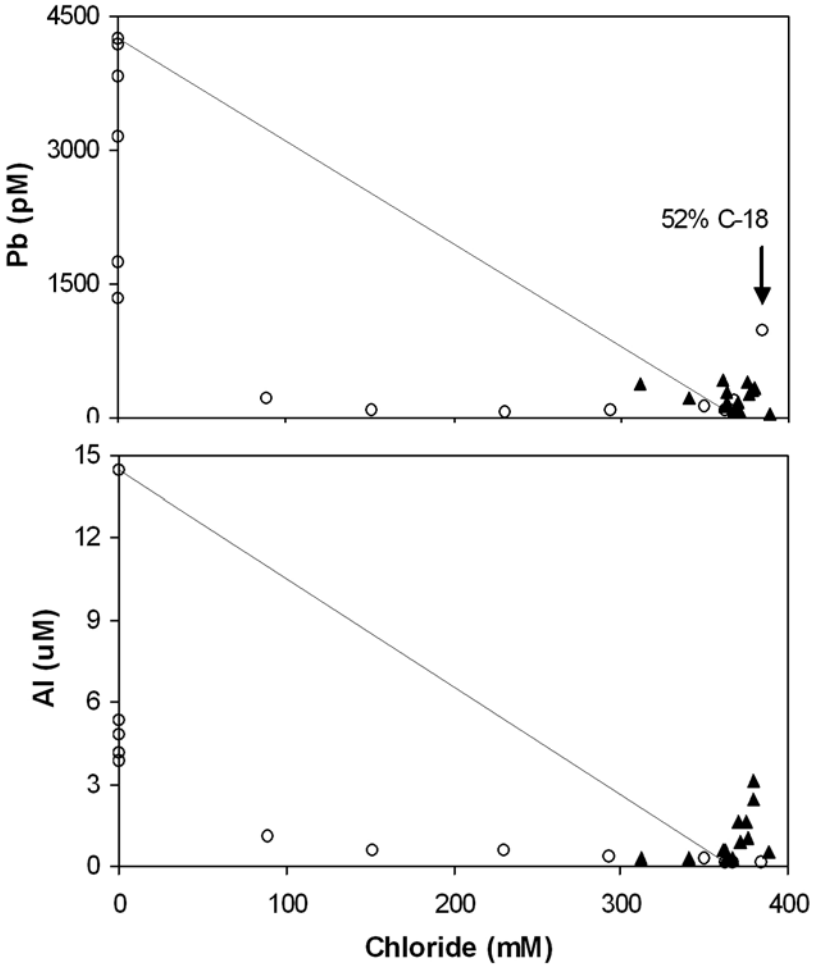

Figure VI-13. Dissolved Pb and Al versus chloride. The solid lines represent conservative mixing between the highest values measured in fresh groundwater and the shallowest porewater sample in Piez F. The arrow in the upper panel indicates a Pb sample from above the sediment-water interface in Piez F that had an unusually high proportion of C-18 Pb.

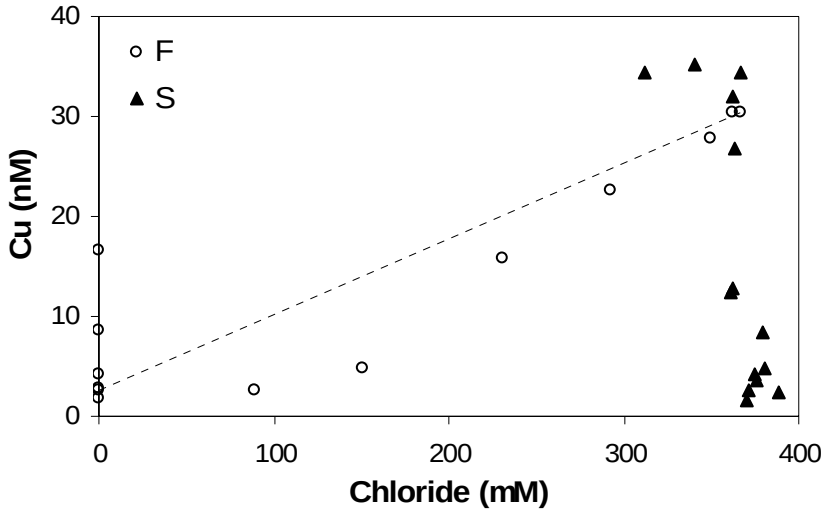

Figure VI-14. Dissolved Cu versus chloride. The dashed line represents conservative mixing between the samples with highest and lowest chloride.

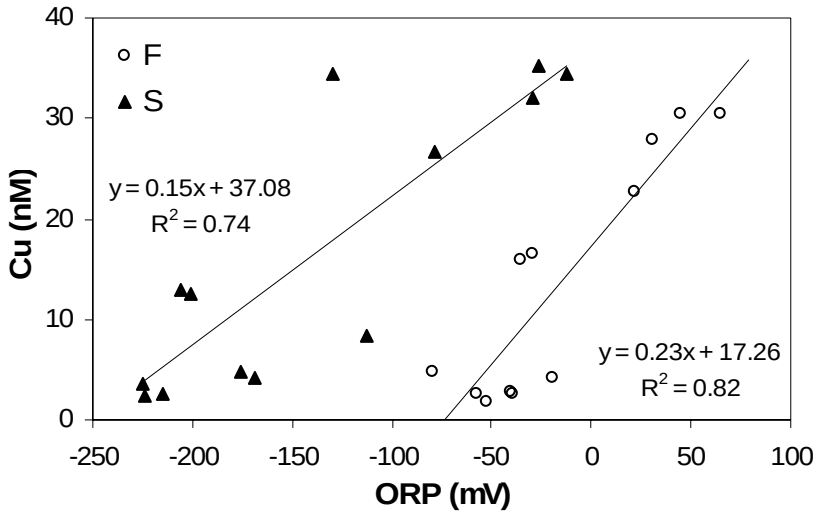

Figure VI-15. Dissolved Cu versus oxidation-reduction potential (ORP). The solid lines and equations represent linear regressions of the data from each piezometer.

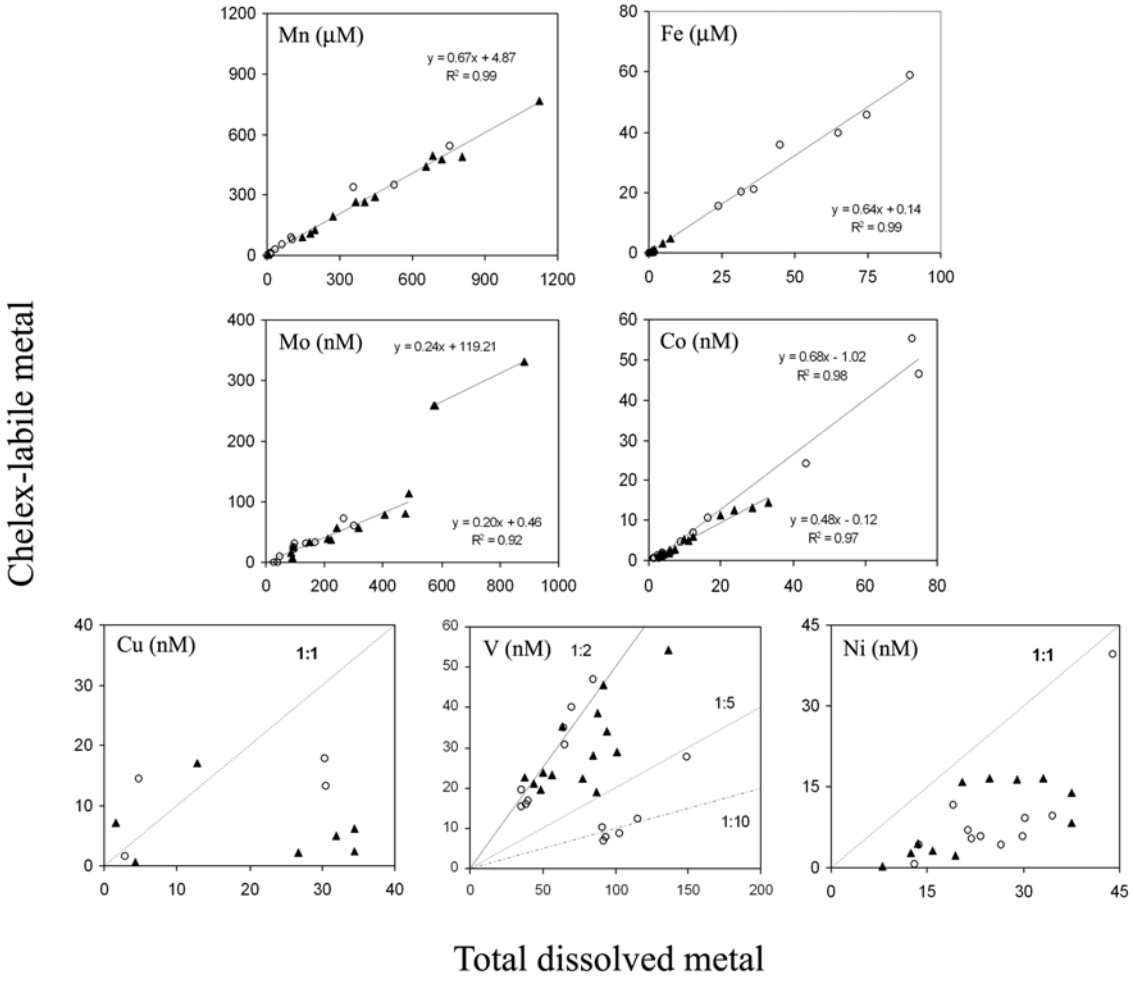

Figure VI-16. Chelex-labile metals versus total dissolved concentrations. Lines are used to estimate labile:total metal ratios. Lines accompanied by equations are drawn by linear regression of the data; lines labeled with ratios (in the lower three panels) were drawn to indicate the approximate ratios for data with substantial scatter.

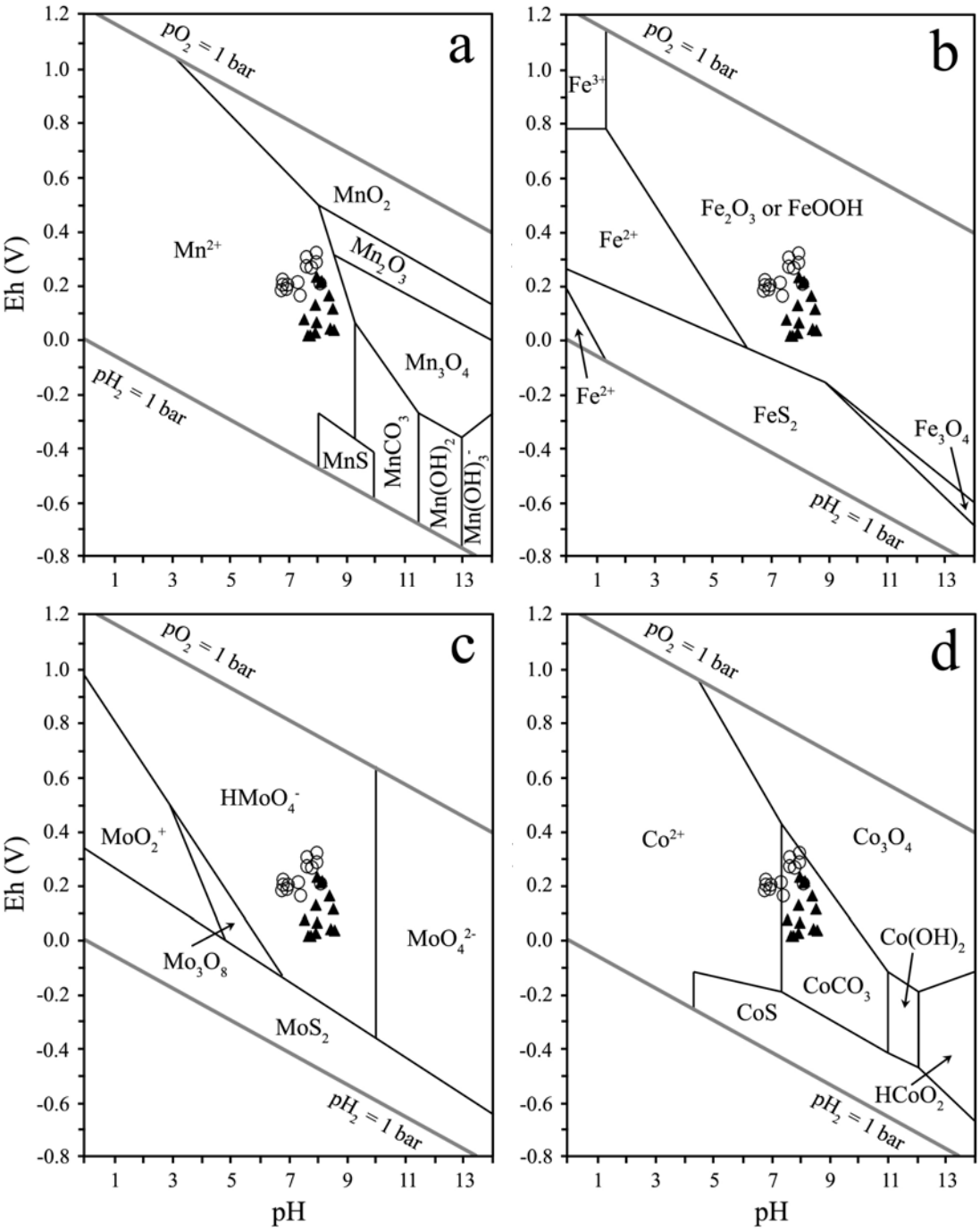

Figure VI-17. Eh-pH diagrams showing stability fields for different metal species. (a) Mn, (b) Fe, (c) Mo, (d) Co. The hollow circles and solid triangles indicate Piez F and Piez S samples, respectively. The upper and lower gray diagonals indicate the stability field of H_2O (O_2 and H_2, respectively). Graphs are drawn after Brookins (1988).

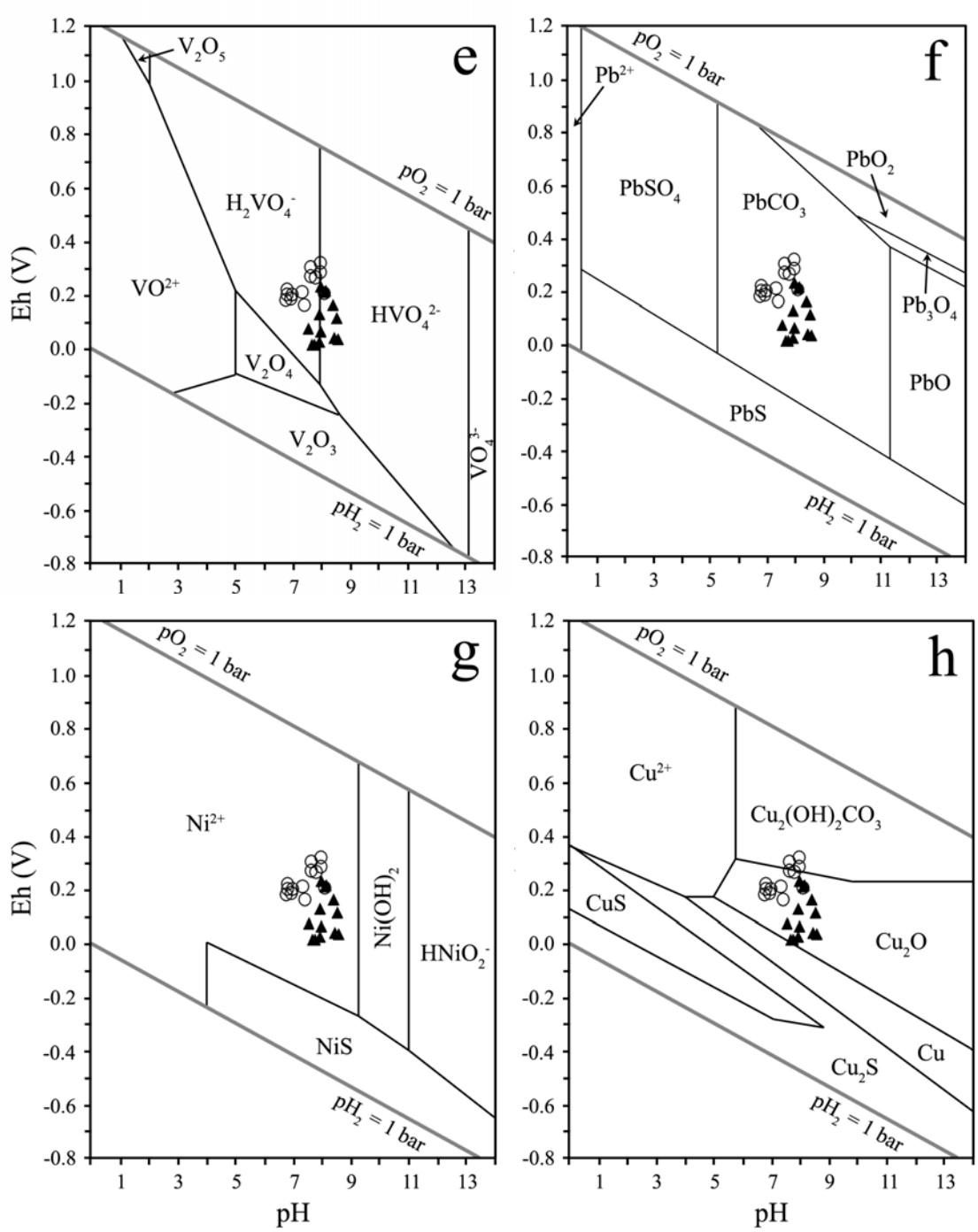

Figure VI-17, continued. Eh-pH diagrams showing stability fields for different metal species. (e) V, (f) Pb, (g) Ni, (h) Cu.

Chapter VII :
Summary and Future Work

Summary

The purpose of the current work is to provide new data on the distribution and cycling of trace metals in permeable coastal sediments. This dissertation seeks to identify the processes occurring in the subterranean estuary, the interface where fresh and saline groundwaters mix, and where chemical reactions imprint SGD with its trace metal signature. Combined with rigorous examination of Ra mass balance in two Long Island estuaries, information from trace metal distributions in the subterranean estuary can be used to better understand how SGD affects trace metal inputs and cycling in the coastal ocean.

Chapters II and III used Ra isotopes to estimate total SGD fluxes to two important embayments in Long Island, NY. SGD in Jamaica Bay varied seasonally, and during four cruises, SGD estimates were: $4.4 – 10.9 \times 10^9$ L d^{-1} (Sept. 2004), $2.1 – 7.0 \times 10^9$ L d^{-1} (Oct. 2004), $3.5 – 6.9 \times 10^9$ L d^{-1} (Sept. 2005), and $0.8 – 2.5 \times 10^9$ L d^{-1} (April 2006). In Great South Bay, data from one cruise in August 2006 indicated an SGD flux of $3.1 – 8.1 \times 10^9$ L d^{-1}. Given the massive amount of water represented by these SGD fluxes, even low concentrations of dissolved constituents in the discharging water may make SGD-derived chemical transport a major component of chemical budgets in these embayments.

In Chapter IV, it was shown that cycling of trace metals in Jamaica Bay groundwater clearly makes it difficult to identify the composition of the discharging

water, and this confounds attempts to quantify SGD-derived trace metal fluxes. Qualitatively, however, correlation of Fe, Ni, Zn, and Co with ^{223}Ra indicated that SGD was a probable source of these metals to the water column. The existence of this correlation, in spite of an enormous dissolved metal background from wastewater input, suggests that SGD is probably transporting a very large quantity of dissolved metals. In contrast, the water column distribution of Mo showed that nonconservative removal patterns matched the magnitudes of Ra-estimated SGD. In this case, recirculation of seawater through anoxic zones in permeable sediments acted to remove Mo from solution. Consequently, it is evident that SGD may act as either sink or source of different trace metals to the coastal ocean, depending on the geochemistry unique to individual metals. As well, metal transport by SGD is fundamentally dependent on the geochemical environment of the sediments through which SGD occurs.

Very crude estimates of SGD-derived metal flux were calculated using the average porewater concentration (i.e. not accounting for geochemical transformations before discharge from the sediments). The range of these fluxes was on the order of 10^{-1} mol d^{-1} (for Ag) to 10^{5} mol d^{-1} (for Fe). In general, SGD metal fluxes were closer to 1 – 10 mol d^{-1}. This exercise suggested that SGD could represent a trace metal source in Jamaica Bay as large as wastewater inputs.

Next, in Chapter V, the design and utility of a high-resolution sampling device (Multi-Port Piezometer, or MPP) was described for collecting porewater profiles through the shallow subterranean estuary. The MPP was tested at a site in Mattituck, NY. Multiple profiles were collected on different dates and at different tidal stages. The data showed that the depth of the subterranean estuary (~30 cm at this site) varied with tidal

stage and SGD flow rate. Flow rates reached very high levels at low tide, up to 250 cm d^{-1}; the persistence of a subterranean estuary in the face of such high flow rates suggests that the processes governing dispersion and mixing of salt water into the fresh interstitial waters are very strong indeed.

The water collected by seepage meters at Mattituck showed decreasing salinity as the headspace of the drums was replaced with fresher SGD. However, the salinity declined with time to a salinity asymptote of ~8, suggesting that the SGD endmember was brackish, not fresh. Mass balance calculations for water and salt in the seepage meters confirmed a brackish SGD endmember. Correlation between the calculated endmember variation with time and the change in salinity at depth in the sediment indicated that the discharging water was derived from 7-16 cm depth.

At this site, V and Sr were conservative in the subterranean estuary, while Pb and Co showed non-conservative excess at salinities between 5 and 15. Analysis of trace elements in water collected from the seepage meter showed that the source of the discharging water was derived from the location where non-conservative input was observed for Pb and Co. The nonconservative behavior for these metals occurred at the same depth indicated by endmember calculation based on salt mass balance. Thus, this chapter showed that non-local transport processes or preferential vertical flowpaths regulated the source of the discharging water, and provided a mechanism for SGD to bypass the surficial porewater layers. The characteristics of these apparent high-flow conduits were suggestive of a biological (macro-infaunal) origin. This chapter also highlighted the utility of combining porewater profiles with seepage meters to characterize a more accurate SGD-derived chemical flux.

Finally, in Chapter VI, dissolved trace metal distributions were examined in greater detail to elucidate mechanisms regulating the geochemical cycling of trace metals in the subterranean estuary. It was found that pH and redox cycling were probably the most influential factors affecting the distribution of the trace metals examined in this study.

Increasing pH by mixing slightly acidic fresh groundwater with slightly basic seawater resulted in the precipitation and removal from solution of Fe and possibly Al. Dissolved Pb levels in fresh groundwater were elevated, apparently due to association with Al (perhaps colloidal). Removal of Al from solution resulted in a concomitant reduction in dissolved Pb.

Redox-driven cycling of Mn appeared to have a greater influence on other trace metals than that of similar cycling by Fe, and was particularly important for the cycling of Co, Mo, and Ni. Peaks in dissolved Mn were observed from 5-25 cm depth, presumably due to reduction of solid oxides by microbial degradation of the organic matter delivered by recirculated seawater. Co, Mo, and Ni were presumably scavenged by Mn-oxides, and returned to solution when these oxides dissolved. Levels of trace metals in porewater were generally several-fold above the concentrations observed in overlying water, suggesting that SGD could be an important source of these metals to the water column. For Mo, levels in the overlying water were ~10% higher than would be expected from conservative mixing between fresh groundwater and seawater, indicating that SGD could indeed be transporting Mo-enriched porewater out of the sediments.

Cycling of Fe did not appear to influence the distributions of any of the metals studied here, although P and Fe were strongly coupled in the subterranean estuary. The

trends between Fe and P were completely offset in the fully saline profile. The lack of correlation between any of the trace metals and Fe may have been a result of absent sulfate reduction, as Fe-sulfides would certainly be expected to be important for trace metal mobility.

Processes regulating the distribution of dissolved Cu were unclear, although good correlation with oxidation-reduction potential was observed. As noted for Fe, complexation by sulfides would be the obvious and best explanation for this behavior, and the possibility of low sulfide levels or sulfide production in microenvironments cannot be ruled out.

An operationally-defined speciation technique using solid-phase extraction allowed separation of kinetically-labile metals and hydrophobic organic-metal complexes. A major fraction (> 50%) of labile species were observed for all elements except Pb and Cu. The high proportion of labile metals suggests that for the given porewater chemistry, most of the aquifer solid surfaces did not represent good binding sites.

Hydrophobic organic-metal complexes appeared to be relatively insignificant in this setting, although substantial proportions (up to 70%) of the total dissolved Ni and Cu were measured in this fraction. It is not clear how significant hydrophilic organic matter may be for determining metal solubility and mobility in these shallow groundwaters, but the distribution of dissolved V suggested that organic complexation may be important.

Implications for trace metal flux to the coastal ocean

There was clear evidence in Jamaica Bay that SGD supplied a significant portion of the Zn, Fe, Co, and Ni inventory in the bottom waters during Oct. 2004. SGD was also responsible for the substantial removal of dissolved Mo from bay waters. As well, Pb isotope trends indicated that while SGD was not a dominant source of Pb to the water column, it did supply isotopically-distinct Pb.

From these observations, there is little doubt that SGD is modifying the dissolved trace metal composition of the coastal ocean; however, the distribution of dissolved metals in the subterranean estuary in Jamaica Bay offered no clues how to accurately quantify this input. Results from an experiment combining piezometer profiles with seepage meter measurements at Mattituck, NY, indicated that heterogeneous flow patterns could be distinguished, and the dissolved metal flux could thereby be accurately quantified. Implementing similar methods in Jamaica Bay or Great South Bay may prove difficult, as SGD flow rates in the latter two estuaries are nearly two orders of magnitude lower than at Mattituck.

Nonetheless, qualitative or anecdotal evidence for heterogeneous flow was observed in both Jamaica Bay and Great South Bay. In Jamaica Bay, a large (~ 5-10 m diameter) groundwater seep was observed on Canarsie Pol. Precipitation of a rust-colored substance at the sediment surface in the seep indicated the presence of dissolved Fe. One can conjecture with relative confidence that dissolved Mn would also be present, as well as the trace metals that are dependent on Mn and Fe redox cycling (i.e. at least Mo, Ni, and Co). Slower sorption and precipitation kinetics for the latter trace metals than either Fe or Mn may allow these metals to disperse in the water column before Fe or

Mn are oxidized and precipitated out of solution. This would make SGD an effective conveyor of some trace metals, and would reduce the importance of a surface-layer metal-oxide "filter."

In Great South Bay, much smaller scale evidence was observed for discharge of reducing groundwater. In this estuary, ~20 cm "gray spots" appeared at the waterline at high tide, and migrated with the falling tide. Again, appearance of rust color in regions exposed to oxygen suggested the formation of Fe or Mn oxides. It is unknown how these features may influence the overall trace metal input to the water column. However, very high levels of dissolved metals were observed in porewater profiles in Great South Bay; if these measurements are characteristic of the water seeping from the beachface through the gray spots, then SGD could represent a very large trace metal source indeed.

Further evidence for trace metal input due to SGD could be found along two lines: first, a recent report of dissolved trace metals in Great South Bay (Clarke et al., 2006) found high levels of Pb in the Connetquot and Carmans Rivers. A Ra survey conducted in the current study revealed exceptionally high Ra activities in these locations compared to the rest of the bay, consistent with a greater SGD input (Bokuniewicz and Zeitlin, 1980). Second, when porewater profiles were collected, trace metals in bottom water were higher than surface bay water or surficial porewater, but were close in magnitude to the elevated concentrations measured at relatively shallow (~ 15 cm) depth in the sediments. Preferential vertical flowpaths similar to those observed at Mattituck could be responsible for these trends.

Without channelized flow through higher permeability conduits, SGD would probably not represent a large trace metal source to coastal waters. Very high porewater

concentrations of Mn were observed in both the saline and mixed profiles; in both profiles, dissolved Mn was reduced to nearly zero in the upper sediment layer, consistent with oxide precipitation in the zone of oxygen penetration. This surface layer would act as a chemical sieve for trace metals, scavenging them from solution before they enter the water column. Furthermore, changes in water chemistry associated with the fresh-saline interface of the subterranean estuary resulted in the removal of Fe, Al, and Pb. Thus, the subterranean estuary also seems to act as a filter for some fresh groundwater-borne trace metals. Similar removal, but from the seawater endmember, was observed for Cu. We have no knowledge of the change in solid-phase, sedimentary metal inventories associated with this removal, or whether it may vary temporally due to non-steady state conditions.

Ultimately, the results of the studies reported in this dissertation are in accordance with the conclusions of other researchers in strongly suggesting that SGD plays a major role in regulating the dissolved metal composition of the coastal ocean. It is interesting that SGD was observed to alternately represent a sink and source for dissolved Mo (Chapters IV and VI, respectively). Thus, processes regulating trace metal transport by submarine groundwater are not necessarily straightforward, and the role of porewater advection cannot *a priori* be designated a source or sink for a given metal. Future work in this field will benefit greatly from the development of a device for directly measuring an artifact-free advective trace metal flux.

Future work

Certainly, the development of a seepage meter-type device for collecting good SGD samples for trace metal analysis will be an enormous advance in this field. It may be possible to construct such a chamber with all metal-free components; redox and pH conditions could be kept constant following the oxygen diffusion coil and base injection procedure outlined by Westerlund et al. (1986), although doing this successfully while collecting discharging groundwater may be easier written than actually done. Even better would be a non-invasive approach similar to Windom et al. (2006) and Berg et al. (2003). Regardless of the approach, quantification of the flux is necessary, and heterogeneous flow renders 1-dimensional profiles somewhat unhelpful.

High resolution, simultaneous sampling of both "aquifer" solids and porewater may provide useful information on the net effect of trace metal transport by submarine groundwater. If SGD truly acts as significant a sink for Mo as the results of Chapter IV indicate, then it may be discernible in the solid phase. As well, solid phase analyses through the subterranean estuary may clarify whether the mixing zone is acting to remove substantial quantities of Pb, Fe, and Al from fresh groundwater.

The Pb isotope results from Chapter IV indicate that they can be used to successfully trace submarine groundwater input. It would be both fascinating and instructive to obtain high quality Pb-isotope analyses from shallow groundwater throughout Jamaica Bay; such data might indicate the source of the true SGD endmember.

If the chemical composition of the SGD endmember can be narrowed to reasonable uncertainty, then the refinements for Ra mass balance suggested in Chapter II

(e.g. focusing on constraining inlet exchange) may result in very precise estimates of SGD. Similar chemical behavior between trace metals and Ra makes the couple a very powerful tool in the coastal ocean. As our understanding of SGD flow patterns (and endmember identification) improve, groundwater flow to the ocean will undoubtedly be confirmed a significant component of coastal trace metal budgets.

References

Berg, P., H. Røy, F. Janssen, V. Meyer, B.B. Jørgensen, M. Huettel, and D. de Beer, 2003. Oxygen uptake by aquatic sediments measured with a novel non-invasive eddy-correlation technique. Mar. Ecol. Prog. Ser., 261: 75-83.

Bokuniewicz, H.J., and Zeitlin, M.J. 1980. Characteristics of groundwater seepage into Great South Bay. MSRC, Special Report 35, SUNY, Stony Brook, NY, 30 p.

Clark, L.B., C.J. Gobler, and S.A. Sanudo-Wilhelmy, 2006. Spatial and Temporal Dynamics of Dissolved Trace Metals, Organic Carbon, Mineral Nutrients, and Phytoplankton in a Coastal Lagoon: Great South Bay, New York. Estuaries and Coasts, 29 (5): 841-854.

Westerlund, S.F.G., L.G. Anderson, P.O.J. Hall, A. Iverfeldt, M.M. Rutgers van der Loeff, and B. Sundby, 1986. Benthic fluxes of cadmium, copper, nickel, zinc, and lead in the coastal environment. Geochimica et Cosmochimica Acta, 50: 1289-1296.

Windom, H.L., W.S. Moore, L.F.H. Niencheski, and R.A. Jahnke, 2006. Submarine Groundwater Discharge: a Large, Previously Unrecognized Source of Dissolved Iron to the South Atlantic Ocean. Marine Chemistry, 102: 252–266.

Appendix 1. Core Incubation

This core incubation experiment is designed to incubate undisturbed, high surface area, fine-grained sediment cores to examine the diffusion flux of Ra to the overlying water. The goal is to observe the Ra enrichment in the overlying water with time; the increase in Ra inventory occurs as the balance between input from diffusion and radioactive decay.

In order to obtain cores with the largest surface area possible, core tubes were constructed from 5-gallon buckets. The end of the bucket was cut off approximately 3-5 cm from the bottom, and saved for later use. In this way, the bucket barrel could simply be inserted into the sediment, acting as the core tube. After insertion into the sediment, a trough was dug around the outside, and a board inserted under the bucket. Lifting on the board removed the bucket, with its undisturbed sediment core, from the marsh surface. The bucket and sediment were slid off the board onto the inverted bucket-end. Short vertical slits were cut into the cut end of the bucket to facilitate the nesting of the inverted bucket-end and bucket barrel. The end was then cleaned of mud, dried, and sealed with duct tape. Strips of tape from the bottom of the core across the open top ensured that the bottom did not drop off during transport. The core could then be carried easily by the bucket handle.

In Jamaica Bay (JB), cores were obtained from a low intertidal region of a marsh creek immediately after the tide level had dropped to expose the mud surface. In Great South Bay (GSB), the tidal range was not sufficient for similar sampling, so cores were sampled under shallow water. In this case, it was necessary to drain the overlying water before transport to prevent disturbing or resuspending the sediment during transfer to the lab. When obtaining the cores, large volumes of bay water were also collected. Several 60 L barrels were filled with unfiltered water, while 2 barrels were filled with filtered water. The filtered water was obtained by pumping through cylindrical, polypropylene wound-fiber cartridges (1 micron).

Upon returning to the lab, three cores each were placed in two large, rectangular bins. Outside the cores, the bins were filled with unfiltered bay water to the same level as the overlying water inside the cores. Keeping the cores in this water bath during incubation helped to keep water temperature constant, and prevented artificially-

impressed flow of the porewater out the bottom of the core. Prior to filling the cores, two barrels (60 L each) were filled with filtered, Ra-free bay water. (The Ra was extracted by passing through Mn fiber at a flow rate less than 1 L per minute. It was important during preparation of this water that an excess of Mn-fiber was used. Furthermore, the initial effluent from the column had to be discarded to prevent contamination from dissolved or suspended particulate Mn.)

The cores were filled with about 5-10 L of Ra-free bay water. It was crucial to maintain a large volume of overlying water in order to more closely replicate natural conditions. Typical water column ^{224}Ra activities are on the order of 0.2 dpm L^{-1}, while porewater activities are approximately 4 dpm L^{-1}, an order of magnitude or more higher. Thus, as Ra diffuses into the overlying water in the cores, the concentration increases much more quickly than in the dilute natural water column. As a result, if too little overlying water is used, or if it is allowed to evaporate, the dissolved Ra will increase and the gradient driving diffusive flux will diminish. For this reason, inventories measured at long incubation times often appear to be the product of lower diffusion rates.

In any case, upon returning to the lab, the cores are filled with Ra-free water and allowed to incubate for about 24-48 hours. This allowed any artifacts of transport to diminish, and the cores to return to a more natural state (particularly allowing the benthic infauna to recover from the shock of transport). The overlying water in all the cores was aerated gently with aquarium pumps and airstones. This prevented alteration of the redox characteristics in the water and surface sediments, and helped keep the biological community alive. After the resting period, the overlying water was drained, and the cores were refilled with new Ra-free water. Cores were allowed to incubate for different periods of time: the first time point was obtained by filling a core and immediately draining the overlying water. The highest time resolution was required during the initial 100 h, and time points were sampled approximately every 12 hours. Incubations were continued for up to 460 h, although the best data appeared to be obtained at times less than 200 h. Beyond that time, the flux appeared to diminish, probably due to over-enrichment of the overlying water.

Each core was immediately refilled with new Ra-free water after draining. In this manner, additional time points could be obtained using a single core. The incubation

time was simply reset when the core was refilled. When a sample was obtained by draining the overlying water, the Ra was immediately extracted onto Mn-fiber. The initial effluent was again discarded, and the remainder was simply new Ra-free water, and could be returned to the large reservoir, homogenized, and used for subsequent incubations.

Appendix 2. Mn-fiber preparation for γ-counting

This section describes the use of a modified pellet press for compressing the Mn-fiber ash into a pellet that fits into the well-geometry gamma detector. The press itself was obtained from Parr Instruments. The pellet mold provided with the press was insufficient for our purposes, so all of the removable parts were taken off of the press, and substituted as described below. The substitute parts (e.g. nipple pipe and bolts) were obtained at a hardware store.

After delayed coincidence counting, Mn-fibers were ashed in a muffle furnace in Pyrex beakers at 475^{o}C for 8-16 hours. The length of time depended on the amount of fiber and the beaker size (i.e. the more tightly the fiber was packed in the beaker, the longer it needed to be ashed for complete combustion). After ashing, the fibers appeared to shrink slightly, but retained their general "fiber" appearance. However, the color changed from black to a light reddish-brown, and would crumble at a slight touch. The ash was very light, and would blow away without proper caution.

Each fiber was crushed and homogenized in its beaker with a glass stirring rod, yielding a fine powder. This powder was transferred quantitatively to a square piece of aluminum foil. The square was approximately 15 cm on each side; larger pieces occupied too much volume, while small pieces were not sufficient to completely seal the ash. The ash was poured in a line along one edge of the foil and rolled into a tight cylinder, much as one would roll a cigarette. The open ends of the cylinder were folded inward periodically, and ultimately, the ash was completely enclosed in 10-15 layers of aluminum foil. This procedure yielded a thin, 10-cm long, pliable cylinder of Al foil.

The cylinder was carefully inserted into a ¼" inner diameter, 5" length brass nipple pipe. This type of pipe is cast, and has a smooth interior. The foil-ash cylinder was approximately the length of the nipple pipe. Using a long, flat end bolt inserted into the nipple pipe, the cylinder was compressed from one end by hand. This generally yielded about a 30% compression. The nipple pipe was then inverted, and the foil-ash cylinder approached from the other side. Often, the initial compression would leave the foil-ash cylinder unyielding to manual pressure, and the hand pellet press was required. The pelleting apparatus of the pellet press (Parr Instruments) were removed, leaving only the lever and base. The nipple pipe (with foil-ash cylinder inside) could be placed under

the lever, and the flat-end bolt used as the compression tip. Initially, it was necessary to use short bolts that could fit under the lever, but as the pellet slid down the nipple pipe, progressively longer bolts could be used.

It was important to compress the pellet initially by hand and then invert the cylinder and compress from the other side; if one attempts to compress the pellet entirely from one end, it may swell so tightly against the nipple pipe walls that it cannot be removed from the pipe. In other words, compression from both ends ensured that the pellet was evenly compressed, whereas compression from one end usually left the other end only slightly compressed.

After being compressed to the proper cylinder height, the pellet could be removed from the nipple pipe. To do this, the pipe was inverted, and a long bolt inserted into the empty end (i.e. with the pellet at the top of the pipe). Lock-grip pliers were tightly locked onto the pipe, providing a hold for the pellet press lever. Then, pressing down on the pliers forced the pipe downwards, while the bolt prevented the pellet from moving, and it was forced out of the pipe. In the end, the procedure yielded a very tightly compressed cylinder that fit neatly into the small well g-detector.

Since ^{226}Ra is counted using a daughter nuclide (^{214}Bi), the pellets had to be aged for at least 3 weeks to allow the daughter to reach equilibrium. As ^{222}Rn is an intermediate in the decay chain, it was necessary to ensure that no Rn loss occurred from the compressed pellet (Dulaiova and Burnett, 2004). Although the pellets are very tightly compressed and are sealed within numerous layers of Al foil, Rn loss was examined by monitoring ingrowth in a standard. The standard was prepared from a liquid ^{226}Ra standard which was dripped onto some Mn-fiber. The fiber was ashed and prepared as described above. As shown in Fig. 1, the ^{214}Bi activity followed the expected ingrowth curve. This gave assurance that no ^{222}Rn was lost from the pellet.

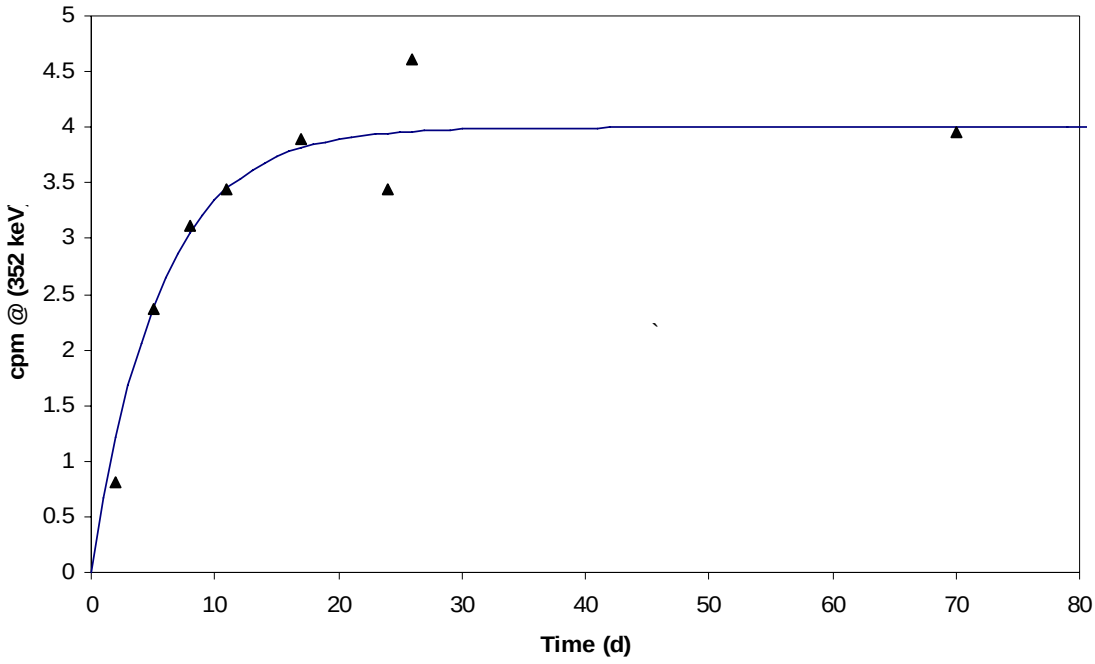

Appendix 2, Fig. 1. Increase in ^{214}Bi activity with time in a pelleted standard. The solid line describes the predicted ingrowth curve.